THE ROLE OF ARCHAEAL METHANOGENS IN BIOMINERALIZATION AND METAL CYCLING: FROM THE MICROSCOPIC TO THE GLOBAL SCALE

By

© 2010
Paul Alexander Kenward
B.S., University of Ottawa, 2003
M.S., University of Windsor, 2005

Submitted to the Department of Geology and the Faculty of the Graduate School of The University of Kansas in partial fulfillment of the requirements for the degree of Doctor of Philosophy

Advisory Committee:

_____
Jennifer A. Roberts, Chair

_____
David A. Fowle

_____
Robert H. Goldstein

_____
Luis A. Gonzalez

_____
Gwendolyn L. Macpherson

_____
Bryan L. Foster

Date defended:_____

The dissertation committee for Paul A Kenward certifies

that this is the approved version of the following dissertation:

THE ROLE OF ARCHAEAL METHANOGENS IN BIOMINERALIZATION AND METAL CYCLING: FROM THE MICROSCOPIC TO THE GLOBAL SCALE

Advisory Committee:

_____
Jennifer A. Roberts, Chair

_____
David A. Fowle

_____
Robert H. Goldstein

_____
Luis A. Gonzalez

_____
Gwendolyn L. Macpherson

_____
Bryan L. Foster

Date defended:_____

ABSTRACT

Paul A. Kenward, Ph.D.
Department of Geology, August 2010
University of Kansas

Archaea, including methanogens, comprise 20% of microbial biomass in global oceans. This study examines the role of Archaeal cell walls in primary low-temperature (30^{o}C) dolomite formation, the impact of biogenic methane generation on the diagenetic history of dolomite reservoirs, and the role of Ni and H_2 on methane production rates. Archaeal cell walls are fundamental in precipitating dolomite due to high carboxyl group density, which desolvate the Mg cation, facilitating nucleation. Therefore biogenic dolomite may be associated with methane production, which decreases effective hydraulic conductivity at high concentrations and is one means of preserving porosity in dolomite reservoirs. While Ni and H_2 are two controls on methane generation rates, Ni can be acquired from solid-phases and is not likely limited in modern or ancient environments. Archaea play a fundamental role in biomineralization and metal mobilization, linking these processes to carbon cycling through their metabolic production of an important greenhouse gas.

ACKNOWLEDGMENTS

While it is still debatable if it takes a village to raise a child, it has become very clear that it takes a department to graduate a PhD student. Or, at least it should. I have had a consistently enjoyable graduate journey within the Department of Geology in the pursuit of my doctorate. This is most certainly attributed in some part to having a good project, but mostly it was the people. To mention each individual's contributions to my success would put me into a second volume of my dissertation, and frankly, I cannot afford the extra binding fee. So I will have to lump some of them.

To start, I must thank my family, whose support throughout this process has been unending and whose faith in me has been unyielding. I will have to believe it is because they are just that fantastic, but the real reason for their faith may remain a mystery to me. They have given up much, mostly my time, by sending me far, far away for my PhD. I thank them immensely. Then I will say thank you to all of the faculty and staff who were not on my committee. Through your classes, advice and help around departmental intricacies I was able to navigate my research with greater ease. This includes all of the students who became my friends over the years, even those that graduated before me. Without these new found friends this would have just been work and not pleasure. Celina, Marina, Ezra, Pete, Natalie, Poteet, Rachel, Trish, Jesse, Kwan, Justin, Charity, Mark, Aimee, Bre, Sarah, Bekah and Carla have been around the longest and risked getting to know me very well over the years. There are many more than that too! I'd also like to thank Dunns Bros. coffee shop. Due to interesting computer difficulties the bulk of my dissertation was written there and I leave with many new friends. Admittedly they bought my friendship with coffee, donuts and wifi but the result is the same. I will truly miss my friends there, especially Adrienne.

I would like to thank my committee members. To say without them this would not have been possible would be an understatement. They all contributed knowledge, advice and support from there diverse backgrounds. Many of these chapters would be impossible to read, rather than just difficult, without their guidance. Luis Gonzalez, one of two department chairs on my committee over the years, has done much to support, and caffeinate, me over the years. Bob Goldstein has been especially supportive. From teaching me about carbonates, and dolomites in particular, to significantly contributing on each published paper to pointing out job opportunities to me as they cross his desk, Bob has done much to further my career. I cannot thank him enough. Along the line of insufficient thanks, I will tender more inadequate gratitude to David Fowle. Not only did he contribute to my writing, education and publication during my PhD, he did the same for my Masters degree before this. It was Dave's guidance that brought me here to do my PhD and he risked both love and his career by bringing me on board!

The phrase "last but not least" gets used a lot these days. Where my PhD advisor, Jennifer Roberts, is concerned this phrase is an understatement. While everyone mentioned above made indispensible contributions to my success, Jen did more than anyone could hope for. Displaying super human capacities of patience, support and scientific advice she guided me through the treacherous terrain that is grad school. She did more than graduate a student; she cultivated a mind and started me on the road to hopefully one day being a peer that she can collaborate with. Jen is unsatisfied with simple graduation and continues to work, and network, to help me find a future. Truly having gone above and beyond academic duty, there is not enough gratitude in any acknowledgement section written anywhere that could do her justice.

Thank you all!

TABLE OF CONTENTS

CHAPTER 1. INTRODUCTION

The study of biogeochemistry focuses on understanding the physical, geological, chemical, and biological controls on the Earth's natural processes. While all life on Earth influences global biogeochemical cycles, microorganisms are ubiquitous in aqueous geological environments and are integral to the geochemical cycling of trace metals, environmental nutrients, contaminants and greenhouse gases (Beveridge and Murray, 1980; Beveridge and Koval, 1981; Fein *et al.,* 1997; Fein *et al.,* 2001; Smith *et al.,* 2003). Microbial metabolism also regulates the saturation state, solubility and weathering of many important reservoir minerals such as dolomite and calcite (Roberts *et al.,* 2005; Kenward *et al.,* 2009). Both Archaea and Bacteria have lineages deeply rooted in the earliest origins of life on Earth, but while Bacteria are a well studied domain of life Archaea have received relatively less attention (DeLong, 2003). This is in part due to the difficulties associated with cultivating Archaea in controlled laboratory settings (Sowers and Anderson, 2007) as well as identifying Archaea using non-culture based techniques (Sowers and Anderson, 2007). Many Archaea thrive in mesophilic environments (25 to 40 °C) but also include a number of extremophiles and persist in ecosystems with extreme ranges of temperature, pH or salinity (Madigan and Martinko, 2005). It is this wide range of environments that Archaea inhabit and thrive in that allow them to make up such a large proportion of the Ocean's biomass and make them critical players in many geochemical cycles. This study investigates how the unique physiology of Archaea and their metabolic activity can affect geochemical cycles at many scales. At the microscopic scale, methanogenic Archaea supersaturate dolomite in solution and are key in overcoming kinetic barriers to precipitation on the cell surface. At the reservoir scale methanogenic Archaea can produce methane gas in sufficient quantities to alter the hydrologic qualities of carbonate systems, which may result in

porosity preservation and the formation of oil and gas reservoirs at depth. At the largest scale, understanding the controls on methane generation rates of Archaea during the Great Oxidation Event (Konhauser *et al.*, 2009) may help to explain the environmental conditions present at that time.

Archaea and Microbial Dolomite

Using a multidisciplinary approach is necessary to constrain the processes controlling the formation of low temperature dolomite (>30^{o}C). The mineral dolomite, $MgCa(CO_3)_2$, is notoriously difficult to synthesize under laboratory conditions at low temperature (less than 30ºC) and, despite its abundance in the ancient rock record, scarcely forms, occurring only in a limited range of modern environments (Land, 1985). This apparent departure from the geologists' guiding principle that the "present is the key to the past" established by Hutton's principle of uniformitarianism, is at the heart of the "Dolomite Problem" (McKenzie, 1991). It is this inconsistency that this study explores with special consideration to the role of Archaea, both methanogenic and halophilic, in promoting the formation of low-temperature dolomite.

There are two parts to the dolomite problem. The first is the relative scarcity of massive dolomites in modern settings, despite in many cases being saturated in solution, as compared to the ancient rock record where they are found in abundance. The second aspect of the dolomite problem is the difficulty in synthesizing primary dolomite, whereby dolomite precipitates directly from aqueous solution, at low temperature. Despite supersaturated conditions favoring the formation of dolomite and ample time for precipitation, researchers have been unsuccessful in synthesizing dolomite abiotically under laboratory conditions (Land, 1998). This lack of success is attributed to kinetic inhibitors such as temperature, pH, Mg:Ca ratio, concentration of

carbonate and ion complexing with water and sulfate (Goldsmith and Graf, 1958; Kitano, 1962; Folk, 1974; Folk and Land, 1975; Katz and Matthews, 1977; Baker and Kastner, 1981; Land, 1985; Gonzaález and Lohmann, 1985; Sibley *et al.*, 1987; Hardie, 1987; Zhong and Mucci, 1989; Slaughter and Hill, 1991; Arvidson and Mackenzie, 1997; Wright and Wacey, 2004). Recent research has supported long-held assertions (Nadson, 1928; Neher, 1959) that microorganisms play a fundamental role in the formation of primary dolomite at low-temperature.

It is only recently that investigators have explored the role of microorganisms, ubiquitous in water rock interactions, that significant progress has been made in understanding low-temperature dolomite formation. Vasconcelos *et al.* (1995) successfully synthesized ferroan dolomite in the presence of a native microbial consortium collected from a modern dolomite-precipitating environment, ushering in extensive scrutiny of microorganisms and microbial processes that facilitate dolomite formation. Modern dolomite forming environments are isolated and those that have been extensively studied have been found to be microbially active. These include the Coorong region of Australia in coastal lakes (Wright, 1999; Wright and Wacey, 2005), Lagoa Vermelha, Brazil, a hypersaline coastal lagoon (Vasconcelos and McKenzie, 1997), and the Persian Gulf sabkhas, evaporitic saltpans (Barbieri *et al.*, 2006). Evidence of primary dolomite precipitation from shallow and deep sea marine sediments, soils and groundwater has been documented (e.g., Hardie *et al*., 1987; Lumsden, 1988; Whipkey *et al.*, 2002; Roberts *et al.*, 2004; Kenward *et al.,* 2009). While the volume of dolomite in these settings is typically minor, forming as thin beds or nodules, all of these studies and their native microbial communities give insight into the mechanisms by which microorganisms mediate dolomite formation.

A wide variety of microorganisms have been implicated in dolomite formation. The best documented metabolic guild is dissimilatory sulfate-reducing bacteria. These bacteria utilize organic carbon coupled to sulfate as a terminal electron acceptor for energy, removing sulfate and generating alkalinity under anaerobic conditions (Vasconcelos and McKenzie, 1997; Warthmann *et al.*, 2000; Wright and Wacey, 2005). Other types of bacterial metabolic pathways have been shown to mediate low-temperature dolomite formation. The first, moderately halophilic aerobic heterotrophs, produce dolomite under laboratory conditions (Sánchez-Román *et al.*, 2008) utilizing nitrogenated organic matter coupled to oxygen as a terminal electron acceptor consuming acidity and producing alkalinity. The other bacterial metabolic guild that has been observed in dolomite precipitation is the sulfide oxidizers, which oxidize H_2S producing sulfate and acidity (Moreira *et al.*, 2004). This dolomite forming process has been inferred from geochemical and isotopic data from Lagoa Araruama, Lagoa Vermelha, and Brejo do Espinho, Brazil. Members of the Archaeal domain have also been linked with the formation of low-temperature dolomite, involving the generation or consumption of methane. While anaerobic methane oxidizers, which utilize methane and generate alkalinity, are found in concert with methanogens controlling low temperature dolomite formation in deep-sea sediments (Moore *et al.*, 2004) this study will focus exclusively on those Archaea that generate methane.

Isotopic signatures from a range of ancient sediments indicate that the activity of methanogens is linked to dolomite formation (Mazullo, 2000). Additionally, recent studies have linked methanogenesis to precipitation of dolomite in shallow groundwater (Roberts *et al.*, 2004; Kenward *et al.* 2009). Laboratory experiments indentified two methanogenic metabolic pathways associated with dolomite formation, acetoclastic and autotrophic. Acetoclastic methanogens cleave acetate forming methane and carbon dioxide, while autotrophic

methanogens combine carbon dioxide and hydrogen to form methane. These pathways were associated with *Methanosaeta sp.* and *Methanobacterium sp.,* respectively (Kenward *et al.*, 2009).

In this study we will look at the role of methanogenic Archaea in shallow groundwater environments (*Methanosaeta sp.* and *Methanobacterium sp.*) and in the lab (*Methanobacterium formicicum*) along with a strain of halophilic Archaea (*Haloferax sulfurifontis*) in promoting dolomite formation. While it is clear that the presence of some microorganisms promotes dolomite precipitation there is still debate as to the mechanisms (different metabolisms and surface nucleation) involved in this process. The most important criterion for the precipitation of dolomite is that supersaturated conditions exist. Many of the microbial guilds discussed previously are capable of driving supersaturation of dolomite as a result of their metabolic pathways (Vasconcelos and McKenzie, 1997; Warthmann *et al.*, 2000; Van Lith *et al.*, 2003; Moreira et al., 2004; Roberts *et al.,* 2004; Wright and Wacey, 2005; Sánchez-Román *et al.,* 2008; Kenward *et al*., 2009).

Achieving supersaturation, while necessary, is insufficient to precipitate low-temperature dolomite under abiotic conditions (Land, 1998). Therefore microorganisms must do more than drive dolomite saturation, they must help to overcome kinetic inhibitors to dolomite formation. For example, both autotrophic and acetoclastic methanogens will drive supersaturation, and will promote dolomite formation at low Mg:Ca ratios (>0.7) which is considered to be a key kinetic inhibitor to low temperature dolomite formation. Additional kinetic barriers, include ion complexation, hydration spheres and sulfate ions which form neutral complexes with Mg, thereby inhibiting the formation of low temperature dolomite (Baker and Kastner, 1981; Hardie, 1987; Zhong and Mucci, 1989; Slaughter and Hill, 1991; Arvidson and Mackenzie 1997; Wright

and Wacey, 2004). For example, one model for biogenic dolomite formation with sulfate-reducing bacteria (SRBs) is that the bacteria produce alkalinity, achieving dolomite saturation, while removing sulfate considered the kinetic barrier to precipitation. The role of a natural population of methanogenic Archaea in driving supersaturation and overcoming kinetic barriers to dolomite formation will be addressed in Chapter 2 of this study. This study involves the precipitation of dolomite at low temperature (30^{o}C) mediated by a mixed anaerobic microbial consortium composed of dissimilatory iron-reducing bacteria (DIRB), fermenters, and methanogens.

One common observation in modern microbial dolomites is the intimate association between the precipitated dolomite and the cell wall of the microorganism or exopolysaccharide (EPS) produced by the microorganisms. These observations, in combination with evidence of cell associated mineral nucleation (Schultze-Lam *et al.*, 1996; Fortin *et al.*, 1997; Douglas and Beveridge, 1998) have led to the hypothesis that these biological surfaces are involved in the nucleation of dolomite. Laboratory experiments, including those within this study, analyzing the charge character of the cell wall or structure have implicated nucleation directly onto the cell wall (van Lith *et al.*, 2003a; Bosak and Newman, 2003; Roberts *et al.*, 2004; Kenward *et al.*, 2009).

Archaeal cell wall structures and their role in nucleating dolomite

Archaeal cell walls and surface layers are chemically and morphologically distinct from bacteria. Some Archaea have polymers unique to their genus or species serving as a rigid cell wall. This includes Archaea from the genus *Methanosarcina,* which have a cell wall composed of methanochondroitin, which is similar to chondroitin sulfate, a polymer found in vertebrate

connective tissue. The extremophilic species *Halococcus morrhuae*, an extreme halophile, and the alkaliphilic *Natronococcus occultus* possess rigid cell walls composed of a sulfated heteropolysaccharide, and a unique glycoconjugate respectively. However a more common cell wall type (includes three genera) is one composed of a thick pseudomurein cell wall, including the methanogen *M. formicicum*. Pseudomurein chemically differs (L-talosaminuronic acid instead of muramic acid, and its peptide moiety lacks D-amino acids) from the peptidoglycan found in bacterial cell walls but performs similar morphological, functional, and structural roles (Kandler and König, 1993; Kandler and König H 1998). However, the cell wall of *H. sulfurifontis* is a proteinaceous S-layer with a consistent pattern of repeating subunits. This structure encapsulates the majority of Archaea (>90%). The S-layer is a paracrystalline structure with repeating protein or glycoprotein subunits. These ordered proteins and glycoproteins create a repeating pattern at the nano-scale. The model organism, *H. sulfurifontis*, used in this study has a hexagonal (p6) lattice symmetry (Supplemental Figure E1). This structured outer layer may be crucial in providing a nucleation template (e.g. Chan *et al*., 2004) for the formation of ordered dolomite. The S-layer is a paracrystalline structure enveloping the majority of Archaeal species (Kandler and Konig, 1998) and is embedded with a high density of carboxyl functional groups (Fowle *et al.,* 2011 in review).

Carboxyl groups are capable of removing water molecules from the hydration spheres around Mg^{2+} (Kluge and Weston, 2005; Tommaso and de Leeuw, 2010) and may be critical to the nucleation of dolomite. Carboxyl functional groups are present on all microbial cells and EPS, but at varying site densities. Therefore the third chapter of this study concerns itself with the role of the cell surface, and characterization of carboxyl functional group density, in both metabolizing and non-metabolizing Archaea (*M. formicicum* and *H. sulfurifontis*) in the

formation of dolomite. These Archaea are compared against a number of non-Archaeal controls, *Bacilus subtilis* and *Shewenella putrefaciens*, both well characterized with respect to their geochemical reactivity (e.g. Fein *et al.*, 1997; Daughney *et al.*, 2000; Sokolov *et al.*, 2001; Ngwenya *et al.*, 2001; Fein *et al.*, 2004). This allows the distinction to be drawn between the roles of live microorganisms in a solution supersaturated with respect to dolomite and the role of passive precipitation on the various cell surfaces of their non-metabolizing equivalents. It is possible that dehydration of Mg^{2+}, by carboxyl functional groups, may be a universal mechanism in promoting dolomite nucleation and that knowing the density of these sites (and the density of these organisms in a system) on a given organism or EPS may determine if dolomite can be precipitated. This would serve to further explain why some environments will form biogenic dolomite while others will not, despite similar geochemical conditions. Because the Earth's biosphere was predominantly micro-organisms and their extruded biofilms prior to a decline in stromatolite morphotype diversity and reefal microbial carbonate abundance preceding the Phanerozoic (Riding, 2006), it is possible that microbially precipitated dolomite was much more abundant in the ancient Earth. This biogenic dolomite could have been precipitated in ordered crystalline phases as a result of the increased ordering of carboxyl functional groups provided by the S-layers of Archaeal cell walls. Additionally, these more stable crystals would resist dissolution and persist longer as sites for overgrowths when geochemical conditions again became favorable for dolomite precipitation. The evolution of grazing and burrowing organisms would have disrupted the continuity of microbial EPS (Garrett, 1970; Awramik, 1972; Awramik and Sprinkle, 1999). Prior to these disruptions in EPS continuity we would expect the development of larger surface areas of dolomite and proto-dolomite nano-crystals to serve as nucleation sites for massive and wide spread dolomite units.

Biogenic Methane and Reservoir Quality

As well as facilitating the formation of dolomite nano-crystals, methanogenic Archaea are of particular interest due to their ability to generate large quantities of methane. Biogenic methane has already been associated with economic methane gas reservoirs (Dai *et al.* 1996; Noble and Henk jr. 1998; Shurr and Ridgely, 2002; Zhang *et al.* 2005) and may play a larger role in the evolution of porosity in carbonate reservoirs. Dolomitized rocks resist physical and chemical alteration as a result of compaction due to their superior structural properties as compared to limestone. This allows dolomite to retain more primary porosity with depth (Schmoker and Halley 1982, Benson et al 1984, Benson 1985, Schmoker et al 1985). The resistance to compaction does not prevent porosity loss due to dolomite cementation from overdolomitization (Murray and Lucia, 1976; Lucia, 1997; Jones and Xiao, 2005). Large quantities of biogenic methane produced by methanogenic Archaea can limit fluid flux and we propose may also serve to limit the cementation of primary porosity.

Being a relatively insoluble gas (1.2×10^{-3} mol/L seawater), methane rapidly saturates solutions and generates methane bubbles which then become nucleation sites for larger methane bubbles and eventually form large pockets of methane (Noble and Henk 1998; Zhang *et al.* 2005). Two phase flow regimes resulting from gas phases have been shown to reduce effective hydraulic conductivity across a range of sediment grain sizes (Mualem 1976; Van Genuchten 1980; Gerke and Van Genuchten 1993). If biogenic methane can reduce effective hydraulic conductivity, and sustain this reduction with increasing depth, then porosity loss due to cementation in these systems would be greatly reduced.

There are two controls on cementation in aqueous systems, diffusion and advection. Both of these processes control the availability of the ions necessary for the precipitation of cements. The diffusion gradient regulates the availability of ions for carbonate precipitation via diffusive flux. This process is up to two orders of magnitude slower than advection and controls ion availability for cementation (Fetter, 1999). Unlike diffusion, cementation from advection requires fluid flow through the porous media, and is therefore regulated by hydraulic conductivity within the substrate. As filling pore spaces with methane gas can create a two-phase flow regime, a subsequent lowering of effective hydraulic conductivity is expected. A loss of effective hydraulic conductivity would then diminish the transport of an aqueous liquid phase supersaturated saturated with respect to carbonates and reduce porosity loss via cementation.

In Chapter 4 of this volume, methane generation rates are modeled and their ability to create two-phase flow and reduce effective hydraulic conductivity on a geologically relevant time scale is assessed. Methane generation rates are calculated from natural settings, taken from both the literature and generated in the lab. Also examined is how a methanogenic two-fluid-phase carbonate system retains diminished effective hydraulic conductivities with depth, and thus, is protected from cementation that other associated stratigraphic units might experience.

Ni-limitation and Methanogenic Archaea During The Great Oxidation Event

Methanogenic Archaea, by virtue of their metabolism, can also impact methane flux on a global scale. As previously stated, methanogens generate prodigious quantities of methane capable of exsolving from solution. The final chapter of this dissertation (Chapter 5) investigates parameters that potentially controlled methanogenic Archaea and their role in the development of Earths' oxygenated atmosphere during the Great Oxidation Event.

The progressive rise of atmospheric oxygen, 2.7 Gya is believed to have been preceded by a decrease in atmospheric methane, from up to 1000 ppmv in the Archean to 1.79 ppmv in the modern atmosphere (Kasting 2005, Zahnle *et al.*, 2006). An increase in ocean sulfate levels from <1 mM prior to the Great Oxidation Event to 28 mM in modern oceans (Canfield and Farquhar, 2009) due to increased weathering of terrestrial sources causing the proliferation of sulfur reducing bacteria (SRB) is one proposed mechanism for this drop in atmospheric methane (Zahnle *et al.*, 2006). However, increased weathering is not supported by the rock record for that time interval. Molybdenum is a redox sensitive transition element found in sulfidic black shales in concentrations that are controlled by its concentration in seawater. An increase in oxidative weathering of the continents prior to the GOE would increase the concentration of molybdenum in sea water. Low concentrations of authigenic molybdenum found in sulfidic black shales prior to 2.2 Gyr ago suggest that there was minimal weathering over the period of the GOE. This contradicts the hypothesis that there was a flux of sulfur in the ocean due to continental weathering (Scott *et al.*, 2008). Another study has suggested that a Ni-famine preceding the great oxygen event may have contributed to diminishing the generation of biogenic methane (Konhauser *et al.* 2009). This study proposes that cooling mantle temperatures, resulted in less Ni-rich ultramafic rocks, which supplied dissolved Ni, than was provided by the hotter Archaean mantle. Since nickel has been largely considered a critical micro-nutrient necessary for methane generation, depletion in available aqueous Ni may have indeed had this effect. Ni-bearing hydrogenases, such as [NiFe]-hydrogenase, are necessary to catalyze the cleaving of the strong covalent bond of H_2 (436 $kJmol^{-1}$) in order to autotrophically synthesize methane (Jaun and Thauer, 2007). Studies have shown that concentrations of nickel below 100nM significantly affect methanogenesis, and that a concentration of 150nM is necessary to see significant

increases in biomass (Schonheit *et al.*, 1979). However, over the period of the Great Oxidation Event, aqueous Ni concentrations were as high as 200nM, more than enough for both methanogensis and growth (Konhauser *et al.*, 2009). Additionally, in the modern oceans those Archaeal methanogens that do require Ni-bearing hydrogenases are capable of reproducing and metabolizing with only 9nM of aqueous Ni available (Drever, 1988), though at a rate that is diminished compared to Ni-rich conditions.

While Ni-limitation may have reduced methanogensis prior to the Great Oxidation Event 2.7 Gyr ago, rates of autotrophic methanogenesis are more sensitive to parameters other than Ni availability. In this study it is proposed that H_2 gas, a critical part of autotrophic methanogenesis, could have controlled methane generation rates to a greater extent than Ni. In Chapter 5 the effect of Ni and H_2 limitation on methane generation rates of *Methanobacterium thermoautotrophicum* are compared. *M. thermoautotrophicum* is an autotrophic methanogenic Archaea that has been well studied and has been shown to depend on [NiFe]-hydrogenases for methane generation. *M. thermoautotrophicum* can thrive in a broad range of temperatures and salinities, 40 to 75 ^{o}C and 0.01 to 0.65 M NaCl, respectively, (Zeikus and Wolfe, 1973; Ciulla *et al.*, 1994) and has been used in previous studies as a model organism for Archaean studies of methane generation and [Ni] (Schonheit *et al*., 1979; Diekert *et al.* 1980; Speece *et al.*, 1983). By varying the concentration of Ni and H_2 available for methanogenesis in controlled batch reactors the effect of limitation of these nutrients on metabolism can be quantified. Additionally, data suggests that not only can Ni-dependent methanogens thrive under the conditions estimated to represent the Precambrian oceans but they are also potentially capable of utilizing Ni co-precipitated and sorbed to minerals such as iron oxides. If this is the case then it is much more likely that decreasing H_2 (g) concentrations controlled the generation of methane. The decrease

in atmospheric H_2 is due to Jeans escape of H_2 gas from the top of the Earth's atmosphere into space (Hunten, 1993) and mantle cooling (Arndt *et al.,* 2008). The latter process, mantle cooling, is the same mechanism cited to explain the loss of available Ni in solution. Hydrogen generation in this case is a product of serpentinization of the mantle according to the following reaction (Barley *et al.*, 1998; Barley *et al.*, 2005):

$$2Mg_{1.8}Fe_{0.2}SiO_4 + 2.933H_2O = Mg_{2.7}Fe_{0.3}Si_2O_5(OH)_4 + 0.9Mg(OH)_2 + 0.033Fe_3O_4 + \mathbf{0.033H_2}$$

As the mantle temperatures decreased, this H_2 generating process also decreased, a parameter much more sensitive in methanogen metabolism than Ni, though coincident in its change in relative abundance. As such, both the cooling mantle and H_2 escape into space over this period would combine to deprive methanogenic Archaea of this critical reductant over a period when biogenic methane in the atmosphere was on the decline. Determining the relative contributions of Ni-loss and H_2-loss on decreased biogenic methane will help to understand the controls on the development of the early Earths oxygenic atmosphere.

Due to their unique cell wall structures, Archaea can control micron scale precipitation and dissolution reactions at the cell surface. Additionally Archaeal methanogens can influence large scale reservoir quality by saturating solutions with methane gas and exsolving into solution. By developing a two-phase flow regime this way methanogenic Archaea reduce hydraulic conductivity and preserve primary porosity by inhibiting cementation. The controls on the productivity of methanogenic Archaea may have also played a significant role in the development of an oxygenic atmosphere and the evolution of multi-cellular organisms. The productivity of methanogens continues to play a role in the evolution of our modern atmosphere and plays a role in current carbon cycling and global climate. In order to understand and predict how methanogenic Archaea will continue to alter the Earths global geochemical cycles, (mineral

formation, reservoir development, nutrient cycling and atmospheric evolution) we need to elucidate the role they have already played in the development of these environments in the past 4.5 billion years.

CHAPTER 2. PRECIPITATION OF LOW-TEMPERATURE DOLOMITE FROM AN ANAEROBIC MICROBIAL CONSORTIUM: THE ROLE OF METHANOGENIC ARCHAEA

Published as a separate article:
Kenward PA, Goldstein RH, Gonzalez LA, and Roberts, JA (2009) Precipitation of low-temperature dolomite from an anaerobic microbial consortium: the role of methanogenic Archaea: Geobiology, v. 7, p. 556–565.

ABSTRACT

Here we report precipitation of dolomite at low temperature (30 °C) mediated by a mixed anaerobic microbial consortium composed of dissimilatory iron-reducing bacteria (DIRB), fermenters, and methanogens. Initial solution geochemistry is controlled by DIRB, but after 90 days shifts to a system dominated by methanogens. In live experiments conditions are initially saturated with respect to dolomite (Ω_{dol} = 19.40) and increase by two orders of magnitude (Ω_{dol} = 2 330.77) only after the onset of methanogenesis, as judged by the increasing [CH_4] and the detection of methanogenic micro-organisms. We identify ordered dolomite in live microcosms after 90 days via powder X-ray diffraction, while sterile controls precipitate only calcite. Scanning electron microscopy and transmitted electron microscopy demonstrate that the precipitated dolomite is closely associated with cell walls and putative extra-cellular polysaccharides. Headspace gas measurements and denaturing gradient gel electrophoresis

confirm the presence of both autotrophic and acetoclastic methanogens and exclude the presence of DIRB and sulfate-reducing bacteria after dolomite begins forming. Furthermore, the absence of dolomite in the controls and prior to methanogenesis confirm that methanogenic Archaea are necessary for the low-temperature precipitation of dolomite under the experimental conditions tested.

INTRODUCTION

Despite its abundance in ancient rock modern dolomite is much less common, and at particularly low temperatures (<50 °C), a poorly constrained process. Modern dolomite is usually found in association with marine influenced and other saline environments such as coastal sabkhas (Müller *et al.*, 1990) or hemipelagic mud (Middleburg *et al.*, 1990), hypersaline evaporative lakes such as the Coorong region, Australia (Alderman and Skinner, 1957), and Deep Springs Lake, California (Jones, 1965). The formation of dolomite in non-marine, aqueous systems has also been documented but its occurrence is rare. Freshwater dolomite formation typically occurs when DIC (dissolved inorganic carbon)-rich meteoric water mixes with Mg-rich groundwaters. Magnesium can be sourced from brackish groundwaters (El-Sayed *et al.*, 1991; Humphrey and Radjef, 1991), lake brines (Land and Hoops, 1973;Colson and Cojan, 1996) or as a result of the dissolution of Mg-bearing rocks such as basalt (e.g. Capo *et al.*, 2000; Whipkey *et al.*, 2002).

Reproducing the nucleation and precipitation of dolomite at low temperature under laboratory conditions has been a notoriously difficult endeavor using traditional geochemical techniques and is the subject of much debate (McKenzie, 1991; Land, 1998). Limited precipitation of modern dolomite has been largely attributed to kinetic barriers at low

temperature (<50 °C). While all minerals are subject to kinetic controls on mineral composition and distribution, dolomite is particularly susceptible. These constraints include saturation state, temperature, kinetics, pH, Mg:Ca ratio, concentration of carbonate, ion complexing, hydration spheres and sulfate (Goldsmith and Graf, 1958; Kitano, 1962; Folk, 1974; Folk and Land, 1975; Katz and Matthews, 1977; Baker and Kastner, 1981; Land, 1985; Hardie, 1987; González and Lohmann, 1985; Zhong and Mucci, 1989; Slaughter and Hill, 1991; Arvidson and Mackenzie, 1997; Wright and Wacey, 2004). As such, understanding the factors that control the precipitation of dolomite in both the laboratory and natural settings is an important step in understanding how dolomites formed in the past. Along with the above mentioned geochemical controls the role of live micro-organisms in overcoming the kinetic barriers to dolomite precipitation has been extensively studied (Vasconcelos *et al.*, 1995; Warthmann *et al.*, 2000; Van Lith *et al.*, 2003; Moreira *et al.*, 2004; Roberts *et al.*, 2004; Wright and Wacey, 2004, 2005; Rivadeneyra *et al.*, 2006; Sánchez-Román *et al.*, 2008).

A number of metabolic pathways have been implicated in promoting dolomite precipitation under conditions that may not be considered geochemically favored (i.e. low-temperature, low Mg:Ca and low saturation state), including both sulfate-reducing bacteria (SRBs) and methanogenic Archaea (Vasconcelos *et al.*, 1995; Van Lith *et al.*, 2003; Moreira *et al.*, 2004; Roberts *et al.*, 2004). A great deal of this work has focused on the role of SRBs in promoting dolomite formation (Vasconcelos and McKenzie, 1997; Warthmann *et al.*, 2000; Van Lith *et al.*, 2003; Wright and Wacey, 2005). Ways in which SRB may promote dolomite precipitation include the removal of sulfate, which can form a neutral complex with Mg and inhibit dolomite formation and other kinetic inhibitors (Baker and Kastner, 1981; Slaughter and Hill, 1991; Wright and Wacey, 2004). SRBs also increase DIC through their metabolism and

have demonstrated the ability to promote the formation of proto-dolomite minerals, often associated with cells or extra-cellular polysaccharides (EPS), which are assumed to mature into ordered dolomite over time (e.g. Vasconcelos and McKenzie, 1997; Van Lith *et al.*, 2003).

Methanogens are another group of micro-organisms shown to facilitate the formation of low-temperature dolomite; however, the controls on methanogenic dolomite remain poorly constrained. Previous research by Roberts *et al.* (2004) demonstrated that methane-generating Archaea are critical in overcoming kinetic barriers and driving the precipitation of dolomite in dilute aqueous systems both in the laboratory and in the field. These data suggest that in methanogenic environments neither extreme supersaturation with respect to dolomite nor high Mg: Ca ratios are required in the bulk solution to precipitate dolomite at low temperatures.

Methanogens are members of the domain Archaea and are obligate anaerobes known to persist in a wide variety of extreme and mesophilic environments. Methanogens employ a number of metabolic pathways for subsistence, and several of these pathways are capable of promoting carbonate saturation (Roberts *et al.*, 2004; Madigan and Martinko, 2005). Acetoclastic methanogens generate DIC through their metabolic pathway while autotrophic methanogens consume CO_2, driving up solution pH with their metabolism. Because both of these mechanisms could facilitate carbonate mineral precipitation, it is necessary to study this process in greater detail to determine the roles each metabolic guild might have in precipitation of dolomite.

Considering the highly variable biogeochemistry found in natural environments and the potential for microbially induced dolomite formation, it is essential to be able to isolate the contribution of the different metabolic guilds in a variety of these systems to understand how they promote dolomite precipitation. To accomplish this, a natural consortium of microbes from

a freshwater aquifer near Bemidji, Minnesota was incubated in native groundwater in small microcosms to study a low sulfate, low Mg:Ca, fresh water system as an end-member in beginning to isolate variables for low-temperature dolomite formation.

Although evaluating this chemical system is counter to the paradigm that seawater and seawater-derived fluids are ultimately most important in formation of low-temperature dolomite (Land, 1985; Hardie, 1987), precipitation of dolomite from this system would serve as an important control on conditions conducive to precipitation of low-temperature dolomite in natural systems. By re-examining the work by Roberts *et al.* (2004) over time this study demonstrates that dolomite can be formed in such systems and that the Archaeal methanogens may be necessary for the precipitation of dolomite in this low ionic strength environment ($I < 0.01$ m). Dolomite precipitation occurs subsequent to the end of dissimilatory iron reduction (DIR) and both metabolic guilds of methanogenesis, acetoclastic and autotrophic, are involved in its formation. The precipitate is ordered, leading to the possibility of compositional and textural preservation that may allow analogs to be recognized in the rock record.

MATERIALS AND METHODS

Field description and sample collection

The field site from which groundwater and native microbes were collected was a petroleum spill site approximately 16 km northwest of Bemidji, Minnesota, part of the USGS Toxic Substances Program. This site was chosen for its geochemical makeup, where solutions are near equilibrium or slightly supersaturated with respect to dolomite, and ongoing microbial succession fueled by the presence of free-phase petroleum. Calcite and dolomite precipitation

has been reported in the anaerobic zone, where active methanogenesis takes place (Baedecker *et al.*, 1993; Bennett *et al.*, 2001; Roberts *et al.*, 2004). We collected samples from the same location as Roberts *et al.* (2004); a highly anaerobic, reducing zone, down-gradient of the floating pool of oil, which is coincident with high concentrations of dissolved methane. Groundwater in the organic carbon rich zone is anaerobic, with a pH of 6.74; 3.4 mm dissolved organic carbon, 0.66 mm Fe^{2+}, 0.74 mm CH_4 and 1.2 mm Si. The water also contains 4.58 mm Ca^{2+}, 1.35 mm Mg^{2+} and 12.4 mm HCO_3^-. Other constituents, including Al, K, Na, SO_4, NO_3 and PO_4 are present at concentrations <0.01 mm (e.g. Roberts *et al.*, 2004). The anaerobic zone is dominated by dissimilatory iron-reducing bacteria (DIRB), fermenting bacteria and methanogens, which occur only in discrete zones (Bekins *et al.*, 1999). Groundwater used in batch microcosm experiments was pumped using a vacuum pump and polyethylene tubing into sealed 60 mL anaerobic pre-vacuumed sterile serum vials. To isolate native micro-organisms, a 1.98-m core was taken next to well location 9014, over the interval of 8.07–10.21 m below land surface, which is consistent with isolated zones of methanogenesis as determined by Bekins *et al.* (1999). Core sampling was done using sterile technique, in an anaerobic glove bag in the field immediately after sampling. Sections of <20 cm were sampled and homogenized. Core material and groundwater were maintained at 4 °C for no longer than 48 h until batch microcosms were completed.

Batch microcosms

Here, we utilize batch laboratory microcosm experiments as a simplified artificial ecosystem representing conditions in the petroleum-contaminated aquifer near Bemidji, MN. Replicate microcosms were constructed using sterile glass bottles filled with 5 g of dry sterilized

Columbia River Basalt (>0.5-mm size fraction) (Hooper and Hawkesworth, 1993) as a source of Mg, Fe and P for microbial activity (e.g. Roberts *et al.*, 2004), 40 mL of anaerobic groundwater and 5 μL of petroleum from the core as the sole source of organic carbon. Whole rock geochemistry indicates that the basalt composition is 51.0% SiO_2, 13.7% Al_2O_3, 14.1% Fe_2O_3, 8.9% CaO and 4.5% MgO, with a total P concentration of 3000 ppm that occurs as chlorapatite (Bennett *et al.*, 2001). Native microbial populations were extracted from 10 g of aquifer sediment that was suspended in 30 mL of filtered groundwater and 0.5 mL of a non-ionic surfactant, Tween 80, shaken and left to react for 3 h, then sonicated with low power sonication for 1 min to remove cells from sediment surfaces. One mL of the resulting suspended microbial native consortium obtained in this manner was injected into each batch microcosm containing the filtered native groundwater for a final concentration of 1.3–2.5 $\times 10^5$ cells mL^{-1}.

To mimic aquifer conditions, it was necessary to buffer pH, DIC, Ca^{2+} and Mg^{2+} concentrations as well as maintain saturation with respect to calcite and dolomite. This was accomplished by using sterile chips of dolomite and calcite (0.5 cm^3) (Wards Scientific), contained in regenerated cellulose dialysis tubing (Nominal MWCO = 3500), that were added to each batch microcosm. The dialysis tubing prevented direct microbial interaction with the carbonate mineral surfaces but allowed solutions to equilibrate rapidly with calcite and dolomite and allow a detectable (using XRD) mass of minerals to accumulate. Sterile controls were constructed by autoclaving microcosms, created in an identical manner to those above, for 20 min at 120 °C.

Twenty replicate microcosms and two sterile controls were constructed. Live microcosms were killed (wholly deconstructed) approximately every 30 days and measurements were taken

to monitor temporal changes in biomass and microbial community as well as changes in aqueous, headspace (the gas phase of each individual microcosm) and solid phase geochemistry.

Aqueous geochemistry

Prior to killing, headspace gas concentrations were determined using an Agilent Technologies Network GC System 6890N with a Thermal Conductivity Detector. CH_4 and CO_2 phases in the headspace were separated by running 250 µL samples through an Alltech Hayesep Q 80/100 Packed Column at 90 °C (analytical error for headspace gas measurements was 0.5%).

Sampling for aqueous geochemistry was performed in an anaerobic chamber as well as measurements of pH, alkalinity and dissolved iron. Alkalinity was determined using a 0.2-µm filtered, un-acidified sample by a manual titration to pH = 3 and endpoint determination. Titrated alkalinity was confirmed by modeling alkalinity based on the partial pressure of dissolved carbon dioxide and pH using Geochemists Workbench 6.0 (Bethke, 2008). The ferrozine method, with an analytical error of 1%, at a wavelength of 562 nm was employed to determine aqueous Fe(II) and Fe(T) concentrations (Stookey, 1970). Changes in aqueous iron concentration were tracked to monitor the activity of DIRBs and population succession in each microcosm. Filtered (0.2 µm) and acidified (100 µL of 10% ultrapure HNO_3 to a pH below 3) samples were analyzed for cation concentrations using a PerkinElmer Optima 5300 DV Inductively Coupled Plasma-Optical Emission Spectrometer, which has an analytical error of 5%. Speciation of solutions and calculation of mineral saturation states were accomplished using Geochemists Workbench 6.0 (Bethke, 2008).

Five milliliters aliquots was taken for stable isotope measurements. These were filtered into pre-vacuumed nitrogen purged air-tight microcosms, poisoned with mercuric chloride and acidified with 100% H_3PO_4. The $\delta^{13}C$ of DIC was measured by extraction of 10–50 µL of the gas phase using a CombiPal with subsequent injection into a Thermo Finnigan GASBENCH II and interface to a ThermoFinnigan MAT253 Isotope Ratio Mass Spectrometer (IRMS) operating in continuous flow mode (CF-IRMS). Isotope values are reported relative to V-PDB.

Mineral characterization

The remaining solution was filtered to remove the solid phase and used for four different solid phase analyses. Samples for scanning electron microscopy (SEM) were prepared by using the chemical critical point drying technique (CCPD) (Nation, 1983; Vandevivere and Bevaye, 1993). These samples were stub-mounted and sputter-coated with gold for 90 s before analysis with SEM. Samples were examined using a LEO 1550 Field Emission SEM equipped with an energy dispersive spectroscopy detector (EDS; EDAX Phoenix detector). Samples for transmission electron microcopsy (TEM) were fixed with gluteraldehyde to a final concentration of 2.5%, embedded in a polymer and cryo-microtomed to create thin sections. Samples were analyzed at the Guelph Regional Integrated Imaging Facility for analysis using a Philips CM 10 with an EDAX sapphire X-ray system for EDS. Diffraction was performed using a Philips EM 400 TEM at 100 kV. Secondary mineral precipitates were identified with X-ray powder diffraction (XRD) on a Bruker AXS D8 Advance X-ray diffractometer and a xyz stage with Cu-Kα beam. Carbonate precipitates were also analyzed for $\delta^{13}C$ and $\delta^{18}O$ values for both the calcium carbonate fraction as well as the dolomite fraction. These measurements were done to delineate metabolic pathways, and specific contributions to carbonate precipitation. Replicate

samples were treated with 1% acetic acid solution for 1 h to remove calcite, air-dried in a laminar flow hood and analyzed by reaction with 100% H_3PO_4 in a Thermo Finnigan KIEL III interfaced to a dual inlet Thermo Finnigan MAT 253 IRMS. Isotopic values are reported relative to V-PDB.

Biomass and identification of microbial population

Population growth was monitored via direct counts. Cells were stained with 4',6-diamindino-2-phenylindole (DAPI) (10 mg L^{-1}) and 20 random fields were counted to ensure statistically robust results (Yu *et al.*,1995). Cell counts from sterilized controls were also measured and subtracted from the live microcosms to account for the initial population (as DAPI stains dead cells as well as live). Characterization of microbial communities and their individual members was accomplished using denaturing gradient gel electrophoresis (DGGE; Microbial Insights, Inc., Rockford, TN) from only those microcosms testing positive for the presence of dolomite. Only those micro-organisms constituting at least 1–2% of the overall population formed bands (Fig. 3), which were then excised, sequenced and identified based on DNA sequences found in the Ribosomal Database Project.

RESULTS

Batch microcosms were killed over time to obtain temporal data pertaining to changes in biomass, aqueous and head-space geochemistry as well as solid phase geochemistry and composition within the experimental microcosms. Changes in solution geochemistry allow us to infer the microbial succession and its impact on dolomite supersaturation and precipitation.

Dissolved iron was initially high (0.098 mm) in the Bemidji groundwater used in the experimental microcosms, but diminished greatly 90 days after initial inoculation (0.023 mm)

and was almost entirely removed from solution by 166 days, although the microcosms remained completely anaerobic (Fig. 1). Methane in solution increased rapidly to 0.23 mm after 90 days, reaching an average concentration of 0.28 mm after 166 days and increased slightly to 0.38 mm by the end of the experiment (305 days). Aqueous CH_4 was calculated using Henry's Law on headspace measurements for individual batch microcosms. The aqueous CH_4 from the sterile controls (due to the fact that the groundwater contained an initial concentration of CH_4) was subtracted from the live microcosms to track the change in CH_4 concentration (Fig. 1).

Microcosms were inoculated to a final concentration of $<3 \times 10^5$ cells mL^{-1} after which sterile control microcosms were autoclaved to render them sterile. There was no geochemical indication of microbial metabolism in the sterile controls. Microbial populations within the live batch microcosms increased steadily reaching exponential phase after 112 days. After 166 days microbial populations no longer increased exponentially and reached stationary phase at 3.9×10^7 cells mL^{-1} (Fig. 2).

We sampled three replicate microcosms well after the onset of dolomite formation (270 days) to assay the dominant micro-organisms and potential metabolic pathways that were present during these events. Using DGGE, a profile of amplified DNA from a portion of the 16S rRNA gene was generated to identify the dominant species in the sampled microcosms (Fig. 3). Only those microbes with an excellent similarity index (>0.900) were considered. Autotrophic methanogens, members of the family *Methanomicrobiaceae*, and acetoclastic methanogens, from the genus *Methanosaeta*, were identified. Several fermenting bacteria (*Smithella spp*., *Spirochaeta spp*. and *Azoarcus spp*.) were identified along with these methanogens (Table 1). Neither DIRB nor SRB were detected in these samples.

A number of geochemical changes occurred in solution over the course of the experiment (Table 2). The pH of the live experimental solutions increased from 7.42, initially, to 8.01 at the end of 305 days. Concentrations of Ca, Mg and Si increased in the live experimental solutions relative to controls. Calcium exhibited the greatest increase from 2.48 mm initially to 4.54 mm after 305 days, while Mg only increased from 1.62 to 2.04 mm over the duration of the experiment. Subsequently, the Mg:Ca molar ratio decreased from 0.71 to 0.45 over this period. The concentrations of dissolved CO_2 and HCO_3^- increased significantly during the course of the experiment, from 2.42 to 4.97 mm and from 2.16 to 4.48 mm, respectively. Also observed over the course of the experiment was an increase in the $\delta^{13}C$ of the DIC, from 6.3‰ initially to 9.11‰ at 166 days. Precipitate abundance was below the detection limit for measurement of solid phase stable isotopic composition.

These changes to the solution geochemistry result in radical changes in the saturation states of all carbonate mineralogies including dolomite (Table 3), yet there were no significant changes detected in controls. Increases in pH and DIC yielded even greater increases in the saturation state of carbonate mineral phases within the experimental microcosms. Over the course of the experiment saturation state (Ω = ion activity product Ksp^{-1}; example $\Omega_{dolomite} = [Ca^{2+}][Mg^{2+}][CO_3^{2-}]^2 \times 10^{17.1}$) for both magnesite and aragonite increased by an order of magnitude. Dolomite saturation state showed a two order of magnitude increase from Ω = 19.40 to 2330. The saturation state of calcite only increased from Ω = 1.27 to 24.76. Siderite was the only carbonate mineral to decrease in saturation state, changing from Ω = 6.35 to 1.32 by the end of the experiment.

Dolomite was not detected in the sterile controls but was observed as early as 90 days into the live experiments. Ordered dolomite (2.88 Å) was detected in the live experimental microcosms (Fig. 4) (ordering peaks are present at 4.03, 2.53, 2.19 and 2.07 Å), as were high-Mg calcite (3.02 Å), siderite (2.79 Å) and disordered dolomite (2.89 Å). Calcite (3.03 Å) was present in all microcosms, including controls, while magnetite (2.53 Å) and hematite (2.69 Å) were absent in all microcosms including controls.

Preparation for TEM probably removed most EPS but SEM images preserved both microbes and their putative EPS, showing a widespread mineral encrustation of these surfaces. Samples imaged using SEM revealed a wide range of morphologically diverse microbes including cocci (not shown), cylindrical rods and blunt-ended rods (Fig. 5). Minerals are observed attached to (i.e. encrusting) the cell walls as well as in close proximity to the cells and basalt surfaces. We observed continuous carbonate surfaces closely associated with putative EPS on top of basalt surfaces, as well as individual carbonate crystals (<50 nm diameter) growing off of cell walls (Fig. 5). The continuous carbonate surfaces appeared as a thin (>0.5 μm) veneer coating the basalt grains, as is indicated by the EDS signals for Si, Fe and Al detected by excitation through and below the carbonate precipitates. Individual planar carbonate crystals appeared to be rhombic and grew together to form somewhat circular aggregates. EDS of these planar carbonates indicate the presence of Mg, Ca, O and C. This suggests that these carbonate crystals are either dolomites or very high-Mg calcite. Other EDS analyses (data not shown) targeting only biomass-coating basalt grains showed similar elemental values but lacked Mg. Therefore, the Mg is contributed by neither the basalt nor the biomass and must be sourced from the planar crystal rhombs.

Transmission electron microcopsy coupled with EDS was used to examine the precipitates in greater detail. Figure 6(A,B) shows such images along with the targeted elemental analysis. All copper and silica signatures observed are artifacts of the preparation. EDS scans of minerals attached to the surfaces of rods (Fig. 6A) were relatively rich in Mg, Ca, O and C while being very low in Fe and Si. Phosphorous sourced from the cell was also observed in these scans. Other minerals appear to have replaced several microbes leaving cross-sections (circles derived from cocci or rods) of the mineralized microbes in their stead. These minerals contained Mg, Ca, O and C but were almost completely devoid of Fe, Si and P (Fig. 6B). Other EDS analyses on biomass only (data not shown) gave peaks only for C, O, Fe, Si and P with neither Mg nor Ca present.

DISCUSSION

The initial high Fe(T) concentration, coupled with a relatively low methane concentration suggest that metabolism of dissimilatory DIRB control the aqueous geochemistry early in the experiment (e.g. Lovley *et al.*, 1997; Vargas *et al.*, 1998; Coates *et al.*, 1999). The coincidence of significantly diminished total aqueous Fe after 90 days with an order of magnitude increase in methane (Fig. 1) and a radical exponential increase in biomass (Fig. 2) indicates that the generated methane is biogenic in origin, consistent with a shift from a DIRB-driven system to one controlled by anaerobic methane production (e.g. Froelich *et al.*, 1979; Lovley and Phillips, 1987; Roden and Wetzel, 1996). It is only after there has been a shift in community structure at 90 days, that dolomite is detected. DGGE analysis confirms that methane-generating Archaea are present and numerous in dolomite-producing microcosms (Fig. 3), therefore, we infer these micro-organisms are responsible for the production of methane. While methanogenic Archaea

that utilize both autotrophic and acetoclastic metabolic pathways were found in the natural consortium, *Methanosaeta spp*., an acetoclastic methanogen was only positively identified in one of the three microcosms sampled. *Methanomicrobiaceae*, a family of the order *Methanomicrobial*, which are strictly autotrophic in nature, were found in all three microcosms sampled. Acetoclastic methanogens were likely present in the other two microcosms but were below detection levels for band excision and identification (see Fig. 2). The universal absence of DIRB and SRB during the periods following the first observed formation of dolomite is significant. This supports geochemical data indicating DIRBs cease to play a role in the microcosms early on, and are important only before dolomite is precipitated, while SRB are completely absent from the system. This result is consistent with the findings of Roberts *et al.* (2004), but here we conclusively identify only methanogens after the onset of dolomite precipitation, rather than infer their presence based on geochemistry and isotopic signatures.

The shift from a system dominated by DIR to an Archaeal methane-generating system has a number of impacts on the microcosms over time. Most notable among these changes were the increase in initial pH and alkalinity during methanogenesis (Table 2). The early increase in alkalinity (within the first 90 days) can be explained by DIRB and the acetoclastic methanogens, *Methanosaeta spp.*, which generate bicarbonate as an end product of their metabolism at near neutral pH (equations 1 and 2; Madigan and Martinko, 2005).

$$CH_3COO^- + 8Fe^{3+} + 4H_2O = 2HCO_3^- + 8Fe^{2+} + 9H^+ \quad (1)$$

$$CH_3COO^- + H_2O = CH_4 + 2HCO_3^- \quad (2)$$

After DIR ceases, the acetoclastic methanogens continue to drive up alkalinity, while pH increases via removal of aqueous CO_2 by the autotrophic Archaeal methanogens (equation 3; Thauer, 1998).

$$CO_2 + 4H_2 = CH_4 + 2H_2O \quad (3)$$

These metabolic activities increase dolomite saturation by almost 2500-fold (Table 3). While supersaturation with respect to dolomite does not guarantee its precipitation (e.g. Land, 1998), XRD analysis of our live samples confirms that dolomite precipitates in our live experimental microcosms and does not precipitate in the sterile controls. Ordering peaks (at 4.03, 2.53, 2.19 and 2.07 Å) for dolomite confirm that the dolomite precipitated is ordered. In addition to dolomite, high-Mg calcite peaks are also present in the products of the live experimental microcosms. The siderite present in the live experimental microcosms is the most probable sink for the iron in solution (Fig. 1).

While the DIRB did not contribute directly to the precipitation of dolomite their activity may affect the geochemistry of the microcosms sufficiently to facilitate later precipitation of dolomite. They accomplished this by raising alkalinity and inducing siderite precipitation removing Fe from solution. Other studies have demonstrated that the precipitation of methanogenic dolomite is preceded by DIRB-promoted siderite formation followed by the alteration of siderite to pyrite by SRB. In the absence of sulfate, as in our microcosms, the process proceeds to dolomite precipitation and leaves the siderite unaltered (e.g. Coleman, 1985;Curtis *et al.*, 1986). In the Coleman (1985) and Curtis *et al.* (1986) studies, ferroan dolomite was interpreted to have precipitated under both methanogenesis and DIR. These authors, however, considered only acetoclastic methanogenesis, which they believed lowered

pH, concluding that ongoing DIR was necessary to raise pH and saturate with respect to ferroan dolomite. This is in contrast to our experimental system, in which autotrophic methanogenesis raises pH and drives dolomite saturation in the absence of DIR.

In the experiments, autotrophic methanogenesis was important in raising pH and was likely responsible for the increase in $\delta^{13}C$ of the DIC (6.3–9.11‰). The DGGE profile indicates the predominance of autotrophic methanogens in the native consortium relative to acetoclastic methanogens. Thus it is likely that, while both metabolic guilds are present, the autotrophic methanogens play the dominant role in controlling solution geochemistry and dolomite saturation state.

While both disordered dolomite and ordered dolomite were detectable via XRD within the first 90 days of the experiment, the abundance of disordered dolomite relative to ordered dolomite (disordered-dolomite:ordered-dolomite) decreases from a high of 2.5:1 at 90 days to a low of 0.9:1 at 166 days. Moreover $\Omega_{(siderite)}$ decreases (i.e. < siderite equilibrium) within 166 days. This suggests that siderite and disordered dolomite precipitation were early processes, while the formation of ordered dolomite persisted and may have increased after 90 days.

Scanning electron microscopy and TEM imageries confirm that minerals associated with cell walls and putative EPS of the consortium are Mg-bearing carbonate minerals. EDS of the planar carbonate surfaces indicate the presence of Mg, Ca, O and C (data not shown). Using TEM we see a similar elemental spectrum for carbonate crystals attached to the cell wall (Fig. 6A). EDS of the cell wall alone (data not shown) shows Si and Fe and no coincident Ca or Mg, which suggests that these elements are not part of the carbonate minerals. Furthermore, we assert that Si and Fe associated with the cell wall are largely artifacts of passive cation sorption,

which may precipitate amorphous Si and Fe oxides from solution. This conclusion is supported by the contrast between carbonate-encrusted cell walls (Fig. 6A) and a cell wall (in cross-section) that has been completely replaced by dolomite nano-crystals (Fig. 6B). EDS analyses reveal that the carbonate-encrusted cell wall (Fig. 6A) has abundant phosphate with Fe and Si present, but the dolomite nano-crystal replaced cell wall (Fig. 6B) lacks phosphate, Fe and Si, indicating that none of the original micro-organism remains.

Although we observe different crystal sizes and structures, all dolomite was observed in close association with cell walls or EPS of the consortium. The ability of EPS and the bacterial cell wall to sorb metals and nucleate minerals has been widely observed. Direct cellular and EPS nucleation has been observed with both calcite and dolomite on a number of bacterial surfaces (Takeshi *et al.*, 2000; Van Lith *et al.*, 2002; Bosak and Newman, 2003; Van Lith *et al.*, 2003; Roberts *et al.*, 2004). Mineral nucleation on cell walls is not limited to carbonate minerals and has been demonstrated with Fe-silicates (ferrihydrite and non-tronite), Mn-oxides and other silicate minerals (Konhauser and Ferris, 1996; Douglas and Beveridge, 1997; Fortin *et al.*, 1998). Here we demonstrate dolomite nano-crystals intimately associated with Archaeal cell walls (Fig. 5) and similar to Roberts *et al.* (2004), the dolomite precipitated in this study appears to be ordered, and we observe individual dolomite crystals as small as 50 nm in diameter as well as planar carbonate surfaces (<0.5 μm thick) unlike other studies using SRB in which dumbbell and cauliflower-like morphologies (e.g. Warthmann *et al.*, 2000; Van Lith *et al.*, 2003) are observed.

Our results suggest that both the cell wall and EPS are important in controlling the dolomite crystals and structures formed. We hypothesize that initial nucleation and dolomite formation of ordered dolomite takes place on the Archaeal cell wall with its paracrystalline

structure serving as a template (e.g. Schultze-Lam *et al.*, 1996). When cells are associated with EPS we suspect that subsequent dolomite precipitation is directed by EPS structure, forming thin layers of planar carbonates. Because these precipitates are ordered and found encrusting cells, they may have a high preservation potential allowing us to recognize both compositional and textural evidence of this microbial process in the modern rock record.

The results of this research demonstrate that methanogenic Archaea may play an essential role in precipitating low-temperature dolomite in systems where they represent the dominant metabolic pathway. By precipitating dolomite from a freshwater environment with low sulfate and Mg:Ca ratios (<1), we reveal that this sort of microbial mediation can overcome the least favorable conditions for dolomite precipitation. It is likely that Archaeal methanogens accomplish this by not only increasing dolomite saturation through their metabolic processes, but also overcome kinetic barriers (hydration spheres and neutral complexation of Mg, e.g. Slaughter and Hill, 1991; Wright and Wacey, 2005) to ordered dolomite formation through interactions with their cell wall structure and, possibly associated EPS.

While the dolomites observed herein are very small, this mechanism can still indirectly yield widespread dolomitization by seeding environments otherwise incapable of precipitating dolomite due to kinetic barriers (e.g. Burns *et al.*, 2000; Rao *et al.*, 2003). For example, if a freshwater dominated portion of a marine mixing zone, which may not produce massive dolomites, is seeded with enough dolomite micro-crystals or planar dolomites, we may expect pervasive dolomitization to occur after marine-dominated conditions (and supersaturation of dolomite) are reinstated. This mechanism not only applies to modern systems, but may have also contributed to the formation of ancient massive dolomites. Because Archaeal methanogenesis

was more abundant in the past this could explain why dolomites are more abundant in the ancient rock record than in the modern.

ACKNOWLEDGEMENTS

This research was funded by Shell International Exploration and Production. The authors would like to acknowledge Brad Prather for his contributions to funding, the late Terry Beveridge and his laboratory for TEM analysis of dolomites, and David Moore for assistance with SEM imaging and EDS mapping. The manuscript was greatly improved by reviews from David Fowle, two anonymous referees, and Kurt Konhauser.

Band	Similar Genus	Similarity Index
1.2	*Methanomicrobiaceae*	0.97
1.5	*Spirochaeta spp.*	0.99
2.2	*Methanosaeta spp.*	0.98
2.3	*Methanomicrobiaceae*	0.96
2.4	*Azoarcus spp.*	0.96
2.5	*Smithella spp.*	0.96
3.1	*Methanomicrobiaceae*	0.97
3.4	*Smithella spp.*	0.96

Table 1 Sequence results from bands excised from Fig. 3. Identifications are based on DNA sequences in the Ribosomal Database Project

Microcosm[a]	Days[b]	pH	Ca	Mg	Mg:Ca	Si	K	Fe(T)	HCO_3	$\delta^{13}C_{(DIC)}$	$CO_{2(aq)}$
MC1	0	7.42	4.44	1.72	0.70	0.75	0.01	0.10	9.40	6.3	2.42
MC2	188	7.25	4.53	1.52	0.60	0.69	0.01	>0.01	9.66		2.52
M1	60	7.37	4.63	1.91	0.41	0.76	0.02	0.10	12.40	8.3	3.29
M2	90	7.18	4.52	1.90	0.42	0.84	0.01	0.08	13.80	8.15	4.24
M3	112	7.24	5.03	2.05	0.41	0.82	0.01	0.02	15.67	7.97	4.06
M4	166	8.13	4.51	2.07	0.46	0.86	0.02	0.02	13.33	9.11	3.99
M5	188	7.24	4.00	1.97	0.49	0.80	0.02	>0.01	14.50		4.24
M6	234	7.92	4.02	1.93	0.48	0.95	0.02	>0.01	15.29		4.24
M7	268	7.96	4.83	2.06	0.43	0.83	0.01	>0.01	14.38		5.71
M8	305	8.01	4.54	2.04	0.45	0.93	0.02	>0.01	15.14		4.97

[a]Reactors are designated RC for reactor controls and R for live reactors.

[b]Days to sacrifice of reactors.

Table 1. Chemical composition of reactor solutions

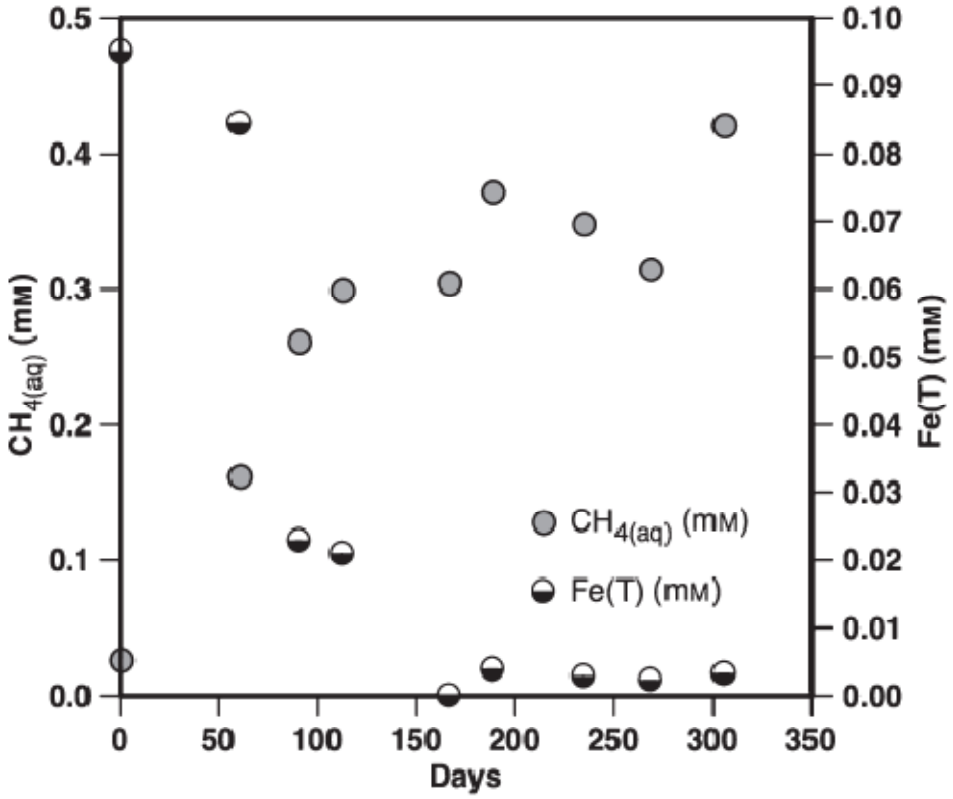
0.5
0.4
0.3
0.2
0.1
0.0
$CH_{4(aq)}$ (mM)
0.10
0.09
0.08
0.07
0.06
0.05
0.04
0.03
0.02
0.01
0.00
Fe(T) (mM)
0
50
100
150
200
250
300
350
Days
$CH_{4(aq)}$ (mM)
Fe(T) (mM)

Figure 1

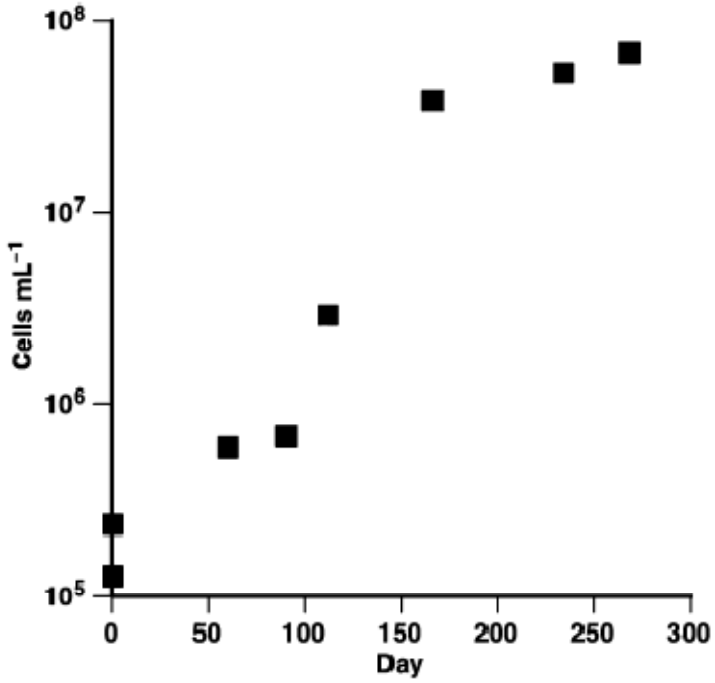

Figure 2

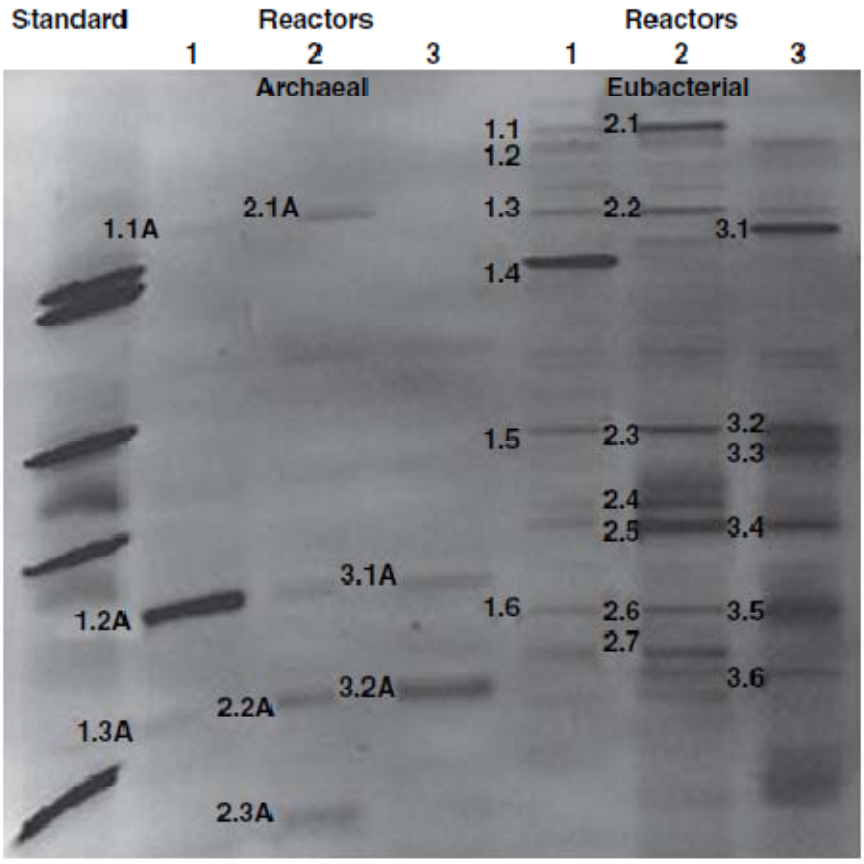
Standard
Reactors
1
2
3
Archaeal
Reactors
1
2
3
Eubacterial
1.1A
2.1A
1.2A
3.1A
2.2A
3.2A
1.3A
2.3A
1.1
1.2
1.3
1.4
1.5
1.6
2.1
2.2
2.3
2.4
2.5
2.6
2.7
3.1
3.2
3.3
3.4
3.5
3.6

Figure 3

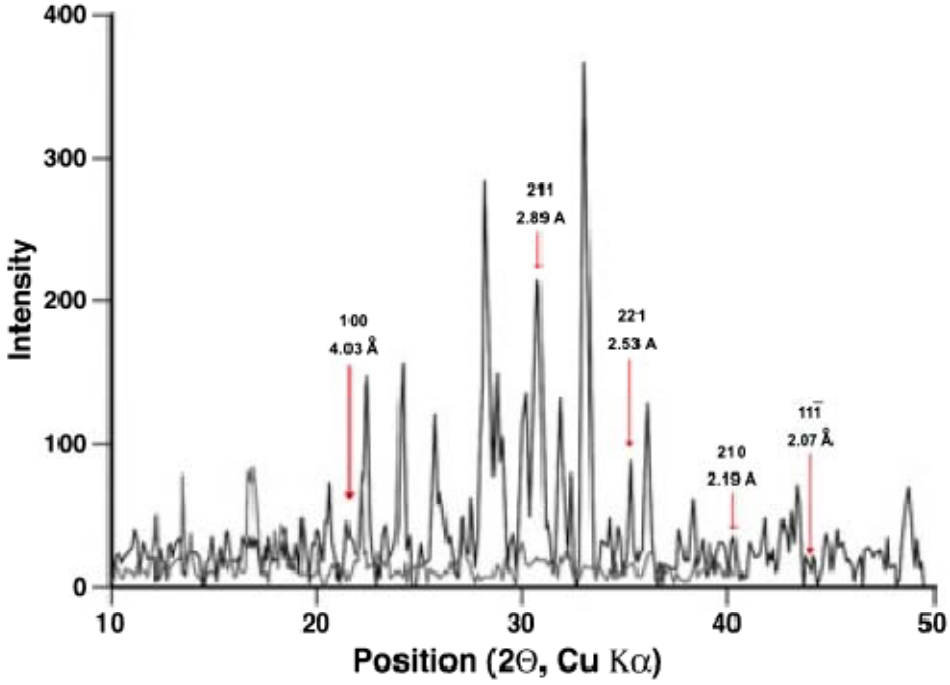
400
300
200
100
0
Intensity
211
2.89 A
100
4.03 Å
221
2.53 A
210
2.19 A
111
2.07 Å
10
20
30
40
50
Position (2Θ, Cu Kα)

Figure 4

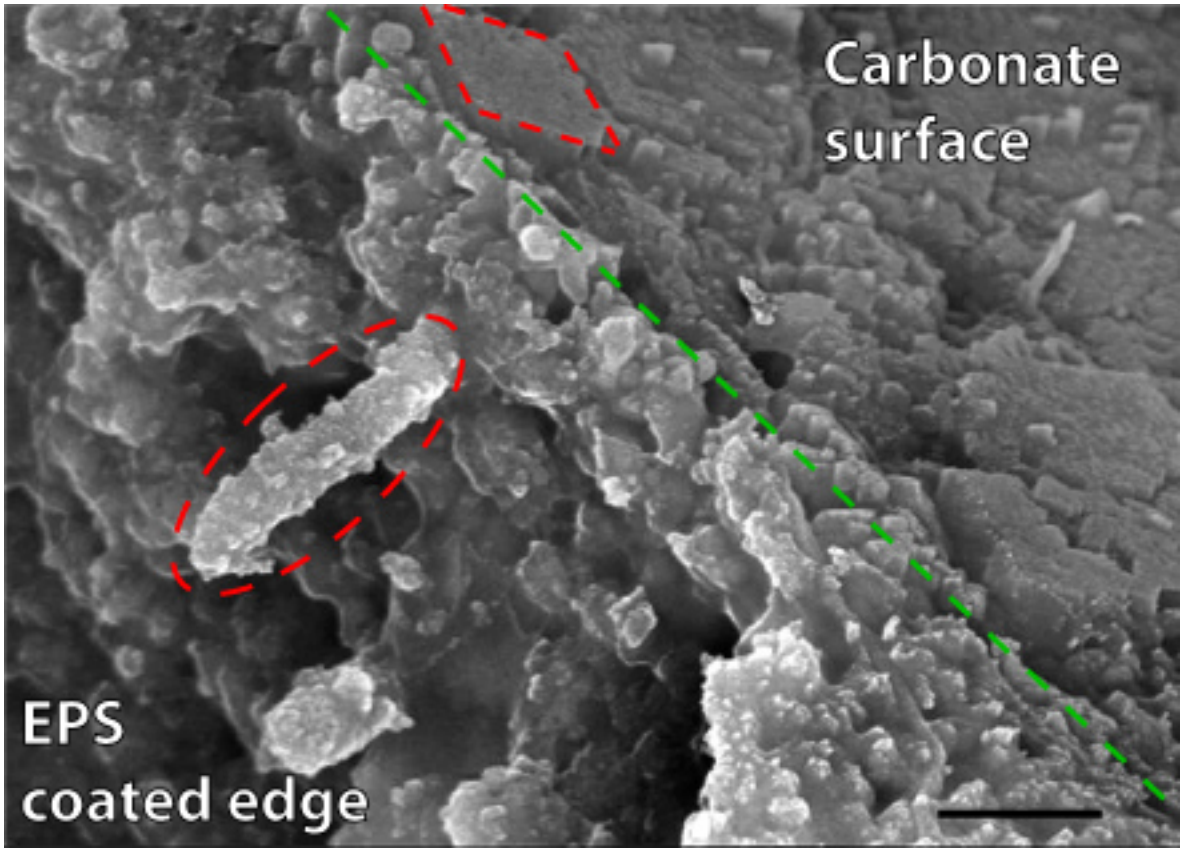

Figure 5

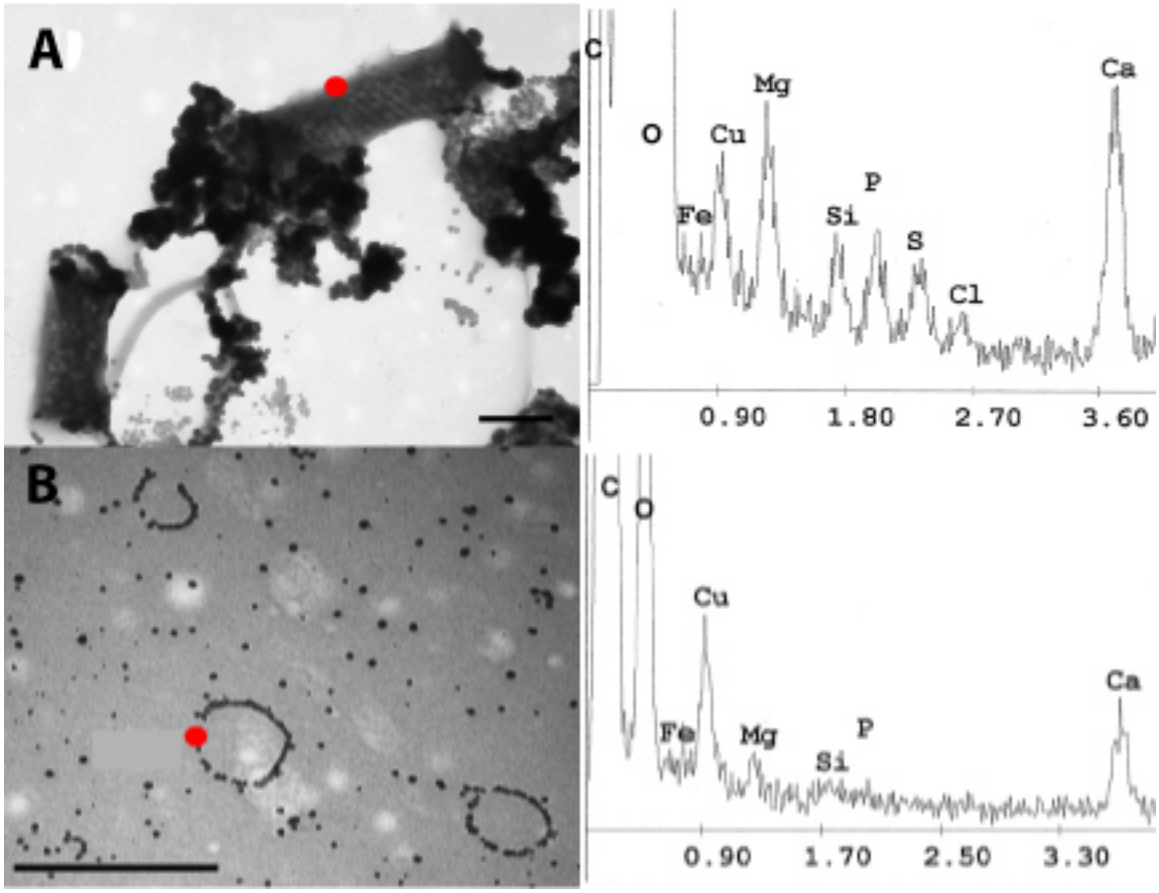
A
B
C
O
Cu
Mg
Fe
Si
P
S
Cl
Ca
0.90
1.80
2.70
3.60
C
O
Cu
Fe
Mg
Si
P
Ca
0.90
1.70
2.50
3.30

Figure 6

Figure 1. Dissolved iron (half-filled circles) and methane (shaded circles) for batch microcosms as a function of time. The analytical error for the ferrozine method was1% and the analytical error for methane measurements was 0.5%.

Figure 2. Changes in biomass (cells mL^{-1}) in batch microcosms as a function of time. Initial biomass was accounted for by subtracting dead biomass from autoclaved controls.

Figure 3. DGGE profile of amplified DNA from a portion of the 16S rRNA gene. Banding patterns and relative intensities of the recovered bands provide a means of comparing the communities. Micro-organisms must constitute at least 1–2% of the total microbial community to form a visible band. Labeled bands were excised and sequenced. This information is provided in Table 1.

Figure 4. Powder X-ray diffraction plots of intensity in counts per second (cps) as a function of position (2h). Comparing scans after a 234-day reaction period with live consortia (solid black line) and an autoclave-sterilized control (grey line). Arrows indicate ordered dolomite (2h = 30.85; d-spacing = 2.88) including ordering peaks for the products of the live experimental microcosms. None of the dolomite peaks are present in the sterilized control. The prominent peaks at 2h = 27.45 and 2h = 33.10 are quartz and halite, respectively.

Figure 5. SEM photomicrograph depicting putative EPS in close association with planar carbonate surfaces and encrusted cells. The EPS-coated edge (lower left of dashed green line) is encrusted with nanometer-sized minerals and contains a microbe (dashed red circle) encrusted in the same. Rhombohedral minerals, many of which have grown together, populate the planar carbonate surface (top right of dashed green line). EDS scan of one rhomb (dashed red

rhombohedron) indicates that the mineral contains C, O, Ca and Mg consistent with dolomite mineralogy (spectra not shown). Scale bar = 1 μm.

Figure 6. TEM photomicrographs of prepared samples from the live batch microcosms after 234 days. The TEM images (A) depict two blunt-ended rods associated with nano-crystals that are consistent in composition with dolomite according to EDS spectrum (immediate right of image), and (B) depict circles of Mg-bearing carbonate minerals (according to EDS spectrum at immediate right of image) that had encrusted the cell wall (in cross-section), which no longer remains. Red dots indicate the sites targeted for EDS scans. Cu and Si peaks in EDS scans are artifacts of TEM preparation and grid-mounting. Scalebars = 1 μm.

CHAPTER 3. ARCHAEAL CELL WALLS FORM ORDERED DOLOMITE AT LOW-TEMPERATURE DUE TO HIGH DENSITY OF SURFACE FUNCTIONAL GROUPS

ABSTRACT

Pervasive in the ancient rock record, primary dolomite remains scarce in modern systems at low temperatures (< 50^{o}C), even those systems supersaturated with respect to dolomite. This scarcity is attributed to a number of kinetic inhibitors, including ion complexation , Mg:Ca ratio, and dolomite saturation state. The precipitation of low-temperature dolomite, at one time considered a purely geochemical problem, has been reevaluated to include the impact of microorganisms. Here we report precipitation of primary, ordered dolomite at 30^{o}C, facilitated solely by the cell walls of two non-metabolizing Archaea from saline solutions (I = 0.66 & 0.99 mol kg^{-1}) with Mg:Ca ratios ranging from 1:1, 5:1 and 10:1 and slightly saturated with respect to dolomite ($\Omega_{dolomite}$ = 3.4 to 4.7). Control experiments utilizing *Bacillus subtilis*, *Shewanella putrefaciens* and *functionalized microspheres* did not precipitate dolomite. Cell wall functional groups were characterized and quantified, and Archaeal cell walls possess carboxyl group densities 8.12 x 10^{-4} (*M. formicicum)* to 1.26 x 10^{-3} (*H. sulfurifontis*) mol g^{-1}. Published values for Bacteria and spheres used in this study are approximately one order of magnitude lower than for Archaea. Because carboxyl groups play a critical role in removing hydration spheres from Mg^{2+}, we propose that high site densities on cell walls and EPS may overcome kinetic barriers associated with Mg hydration spheres and facilitate dolomite nucleation under supersaturated conditions. Structural ordering of these groups, as found in S-layers, may lead to precipitation of more

ordered phases at lower Mg:Ca ratios. These data explain precipitation of low-temperature dolomite associated with numerous metabolic guilds, including Bacteria and Archaea, and often reported in association with EPS or cell wall surfaces, and a identifies a key and widespread mechanism in the formation of disordered dolomite and ordered primary phases of dolomite at low temperature.

INTRODUCTION

The synthesis of low-temperature dolomite (less than 50ºC) in the laboratory is a markedly difficult process despite being abundant in the ancient rock record. The prevalence of massive dolomites in the ancient rock record cannot be reconciled with their striking absence from modern environments. This irregularity is compounded by the difficulty with which primary dolomite (passive precipitation of the mineral into pore space) is synthesized at low temperature. Despite conditions favoring its formation (1000x saturation) and extended reaction periods (32 years), researchers have been unsuccessful in synthesizing dolomite abiotically under laboratory conditions (Land, 1998). This failure has been attributed to reduced reaction kinetics by inhibitors including low Mg:Ca ratio, ion complexing, hydration spheres and the formation of neutral complexes with sulfate (Goldsmith and Graf, 1958; Kitano, 1962; Folk, 1974; Folk and Land, 1975; Katz and Matthews, 1977; Baker and Kastner, 1981; Land, 1985; Hardie, 1987; González and Lohmann, 1985; Zhong and Mucci, 1989; Slaughter and Hill, 1991; Arvidson and Mackenzie, 1997; Wright and Wacey, 2004; Hardie, 1987, Sibley et al., 1987).

Modern studies have ascertained that microorganisms play a fundamental role in the formation of dolomite at low-temperatures. The majority of this research has targeted bacterial metabolism, surfaces, and their extra-cellular polysaccharides (EPS). Principle among these

include sulfur reducing bacteria (SRBs; Vasconcelos et al., 1995; Vasconcelos and McKenzie, 1997; Warthmann *et al.*, 2000; Van Lith *et al.*, 2003; Wright and Wacey, 2005), sulfide oxidizers (Moreira et al., 2004) and moderately halophilic aerobic heterotrophs (Sánchez-Román *et al.,* 2008). These organisms have been shown to promote the formation of dolomite via their metabolism, which generate alkalinity, reduce acidity and, in the case of SRBs, remove sulfate, a well recognized kinetic inhibitor (Baker and Kastner, 1981). In the case of SRBs the formation of disordered phases of dolomite (proto-dolomite) minerals is often directly associated with cells or (EPS). These proto-dolomites may then mature into ordered dolomite over time (Vasconcelos and McKenzie, 1997; Van Lith et al., 2003). In addition to bacteria, previous studies have demonstrated ordered dolomite precipitation at low-temperature (30 ^{o}C) linked to the activity of Archaeal methanogens from solutions with various Mg:Ca ratios (as low as 0.4) (Roberts *et al.*, 2004; Kenward *et al.*, 2009). Similar to studies with SRB, these precipitates are found associated with cell surfaces and putative EPS.

Archaeal cell wall surfaces differ considerably from those found in association with the more commonly studied domain of bacteria. Wheareas there is some diversity in composition and cell wall architecture in Archaea, there are two common types. First, pseudomurein cell walls, found in organisms across three genera, are similar to murein structures found in gram positive bacteria. These cell walls differ considerably in chemistry (L-talosaminuronic acid instead of muramic acid, and its peptide moiety lacks D-amino acids) and chirality of the interactive surfaces. Second, most Archaea (>90%), instead of a cell wall, have a single surface layer (S-layers). These are paracrystalline structures with repeating protein or glycoprotein subunits creating a repeating pattern at the nano-scale, occurring as oblique (p1, p2), square (p4) and hexagonal (p3, p6) lattice symmetry (Kandler and König, 1993; Kandler and König, 1998).

Little is known about the geochemical reactivity of these Archaeal cell surfaces, unlike many gram-negative and gram-positive Eubacterial cell walls, which have been extensively characterized for their functional group distribution and density, their ability to sorb metals and their role as heterogeneous nucleation sites. Metal sorption onto microbial surfaces has been demonstrated as an initial step in nucleation of some biogenic minerals (e.g. Chan *et al.*, 2004).

Here we investigated the effect of different Archaeal cell surfaces, *M. formicicum* which possesses a pseudomurein cell wall and *H. sulfurifontis*, which possesses an S-layer, in precipitating ordered dolomite as a function of Mg:Ca ratio and presence of sulfate in slightly supersaturated solutions at 30ºC. Numerous control experiments were performed to isolate the contribution of the cell wall in precipitating dolomite and to deconvolute the contribution of metabolic activity in dolomite formation.

METHODS

Batch Reactors

Batch reactors were created using sealed 60ml serum vials containing either a single strain Archaea (*M. formicicum or H. sulfurifontis*), a single strain bacteria (*B. subtilis or S. putrafaciens*) or polystyrene microspheres coated with carboxyl, R-COO- functional groups at 10^5 cells (spheres) mL^{-1}. To these solutions were added NaCl, Na_2CO_3, $MgCl_2$, and $CaCl_2$ (See Table 1 for solution compositions). Replicate experiments were created with identical geochemistry as those in Table 1, but with the addition of 0.028 M of Na_2SO_4 , to test the effects of marine levels of sulfate on dolomite formation. $MgCl_2$ and $CaCl_2$ were added to create three Mg:Ca ratios in solution: 10:1, 5:1 and 1:1. The final solutions were set to pH 7.2 to obtain

$\Omega_{dolomite}$ ranging from 3.4 to 4.7 (calculated using Geochemists workbench, Table 1). A range of $\Omega_{dolomite}$ was a result of keeping other carbonate species undersaturated under the diverse geochemical conditions. All reactors remained undersaturated with respect to calcite, aragonite, siderite and magnesite. Ionic strength was set to 0.66 mol kg^{-1} for all experimental systems, except for those with *H. sulfurifontis,* in order to represent systems closer to marine conditions (~0.7 mol kg^{-1}). Reactors containing *H. sulfurifontis* had a metahaline ionic strength of 0.99 mol kg^{-1} to maintain cell integrity.

All media recipes are detailed in Appendix B. Microbial cultures were grown to stationary phase under the following conditions. *S. putrefaciens* and *B. subtilis* were cultured aerobically in tryptic soy broth with 0.5% yeast at 37 ^{o}C in a shaker incubator. *M. formicicum* was obtained from ATCC (#33274) and cultured, in an anaerobic incubator, using Methanobacteria medium (ATCC medium #1045) at 30 ^{o}C under an 80%H_2, 20% CO_2 atmosphere. *H. sulfurifontis* was obtained from ATCC (BAA 897) and cultured aerobically at 37 ^{o}C in a halophilic growth medium (ATCC medium #2448). Archaeal and eubacterial cells were harvested from stationary phase and washed via centrifugation and rinsing five times with a 0.66 M or 0.99 M NaCl solution, depending on the desired ionic strength. Afterward the microbial cultures underwent one of three preparations before being injected into the prepared dolomite reactors. These treatments were live, lysed and non-metabolizing. For live reactors concentrated cells were added to dolomite reactors untreated. Lysed cells were treated by passing centrifuged cultures through a French Press (Garen and Echols, 1962) three times, leaving only cell walls. For the final treatment the addition of a powerful mitochondrial uncoupling agent, carbonyl cyanide m-chlorophenylhydrazone (CCCP), rendered cells metabolically inactive while keeping the cells intact (Heytler, 1980). Live and non-metabolizing cells were injected into reactors to a

final concentration of 10^5 cells ml^{-1}, while the cell wall fragments were derived from lysed cells of the same concentration of live cells. The functionalized polystyrene microspheres were added to reactors under solutions and treatments identical to those experienced by both Archaeal microorganisms, including ionic strength, temperature, the addition of CCCP, and dolomite saturation, but the cell wall fragment treatment was excluded. Additionally, completely abiotic reactors were created for the same geochemical conditions listed above in which no cells, cell wall fragments or microspheres were added.

Batch reactors containing cells (live and metabolically inactivated by CCCP) or cell wall fragments of *M. formicicum* were sacrificed every 7 days for a 42 day period at 30°C to monitor changes in the geochemistry leading to the formation of dolomite. Because dolomite was only found in reactors that equilibrated for the full six week period, subsequent reactors were equilibrated for six weeks (42 days) at 30°C prior to being sacrificed.

Mineralogy and imaging

At the end of the six week period, solutions were extracted and filtered for cation, alkalinity and pH measurements. Unfiltered solutions were treated with 2% gluteraldehyde at this time to preserve samples for transmission electron microscopy (TEM). Reactors were then opened under anaerobic conditions to obtain precipitated phases. A 30 mL volume of fluid was filtered on 0.2 micron filters, which air dried in the anaerobic chamber and was then mounted and analyzed using X-ray powder diffraction (XRD) on a Bruker AXS D8 Advance X-ray diffractometer with Cu-Kα beam. Samples were characterized with TEM on whole-mount grids to visualize and identify dolomite precipitates and their association with cell surfaces. Preserved fragments and any associated precipitates were washed twice with ultra-pure water and

centrifuged at 17,000 × g, 20°C for 30 minutes. After centrifugation, the pellets were directly deposited on Formvar-coated 200 square mesh Cu grids (Electron Microscopy Sciences). Excess water was removed via sterile filter paper and the grids were then allowed to air-dry in a fume hood for 1 hour.

TEM observations were operated at a 200 kV accelerating voltage using a TECNAI X-Twin G2 transmission electron microscope equipped with a double-tilt stage. Selected area electron diffraction was conducted to understand crystallography of minerals attached to bacteria. EDS analyses were performed with an EDAX (operated at 200 kV) using scanning transmission electron microscopic (STEM) mode with a spot size of 300 nm.

Characterization of Archaeal Cell Walls

Deprotonation constants and surface site concentrations were determined from acid-base titrations carried out under an N_2 atmosphere at 298 K (e.g., Fein et al., 2004) on suspensions of *M. formicicum* in a background electrolyte of 0.01 M NaCl, to buffer ionic strength. The site density of carboxyl functional groups was determined by analyzing the data using PROTOFIT 2.1 software (Turner and Fein, 2006). Carboxyl group site densities for *B. subtilis* (Daughney *et al.*, 2000), *S. putrefaciens* (Sokolov *et al.*, 2001), *H. sulfurifontis* (Fowle *et al.*, in review) and EPS (*Desulfovibrio sp.)* (Braissant *et al.*, 2007; Konhauser et al., 2010) were taken from the literature. Carboxyl group site density on the functionalized polystyrene microspheres is 1.40 x 10^{-4} mol g^{-1}(Bangs Laboratories Inc. certified). The results from this study and the carboxyl group site densities obtained from the literature and Bangs laboratories are listed in Table 1.

Competitive cation sorption experiments were conducted in triplicate batches with varying initial concentrations of Mg^{2+} and Ca^{2+} added as $MgCl_2$ and $CaCl_2$. These batches were

set at an initial Mg:Ca ratio of either 0.1:1, 0.5:1, 1:1, 2:1, 3:1 or 5:1 and allowed to equilibrate with the non-metablozing cells of *M. formicicum* for two hours (Data displayed in Appendix E2). Kinetic sorption experiments showed that Mg^{2+} and Ca^{2+} sorption to the cell walls of these species was a rapid process equilibrating after 30 minutes (Appendix E3). After this period the solutions were filtered through 0.2 μm filters to remove the microorganisms and the cations attached to their cell walls. The filtrate was then acidified with 100 μL of 10% ultrapure HNO_3 to a pH below 3. These aliquots were then analyzed for cation concentration using a PerkinElmer Optima 5300 DV Inductively Coupled Plasma-Optical Emission Spectrometer, which has an analytical error of 5%. From this data the cations sorbed to the cell wall were calculated and Mg:Ca ratios were determined for the cell surface.

RESULTS

Only batch reactors with live, metabolizing cells of *M. formicicum* experienced any significant change in solution chemistry over the six-week period of the experiment. In these, solution pH increased from 7.2 to 8.1 after the first week and remained at that value for the remainder of the experiment. The increased pH resulted in a significant increase in calculated saturation state (Ω) for dolomite, increasing from 3.4, 3.7 and 4.7 to 79.9, 87.4 and 102.0 for 1:1, 5:1 and 10:1 Mg:Ca ratios respectively. No other batch reactors for the Archaea, bacterial controls, or abiotic controls experienced any noticeable changes in pH, alkalinity or Mg:Ca ratio after the six week equilibration period. No change to solution chemistry was detected for any of

the reactors that precipitated dolomite, due to the high initial concentration of Mg, Ca and CO_3^{2-} in these reactors.

Dolomite (stoichiometric, ordered, and disordered) was only detected in reactors containing cell walls or metabolically inactive *M. formicicum* and *H. sulfurifontis*. Dolomite was absent from live reactors of the Archaeal strains, as well as all treatments containing *Bacillus subtilis* and *Shewanella putrefaciens*, and polystyrene microspheres (Table 1) after 42 days of incubation (Table 2). Dolomite formation was not detected in the presence of sulfate for any of the experimental conditions.

H. sulfurifontis precipitated dolomite in reactors containing metabolically inactive cells and cell wall fragments. Dolomite and protodolomites (high Mg-Calcite) were observed at all Mg:Ca ratios for both treatments. Differences in precipitate mineralogy are observed between cell fragments and inactivated cells. For the cell wall fragment of *H. Sulfurifontis* we observe high-Mg calcite at 1:1 Mg:Ca ratios while both high-Mg calcite and ordered dolomite is observed at 5:1 Mg:Ca ratios and only ordered dolomite is observed for Mg:Ca of 10:1. By contrast, intact non-metabolizing cells precipitated ordered dolomite at all Mg:Ca ratios (1:1, 5:1 and 10:1).

Powdered XRD analysis confirms that the dolomite precipitated is ordered with a primary peak at d-spacing = 2.89Å with the presence of ordering peaks at 4.03Å and 2.53Å for both *M. formicicum* and *H. sulfurifontis* (Fig. 1).

After the 42 day reaction period, dolomite was detected for *M. formicicum* cultures that were either metabolically inactive (10:1 Mg:Ca ratio only) or present only as cell wall fragments (5:1 Mg:Ca ratio only). Also present were peaks for NaCl (largest peak if Fig 2b), calcite and

high-Mg calcite. TEM identified mineral crystals in contact with cell wall fragments of *M. formicicum* (5:1 Mg:Ca ratio), forming as nano-sized crystals (Fig. 2a). Energy dispersive spectroscopy (EDS) identifies C, O, Mg and Ca in the minerals associated with cell surface material, which is consistent with the observed dolomite mineralogy identified using XRD (Fig. 2b). Other elements detected with EDS (K and P) are attributed to the organic matter and the Cu is a product of the preparation process for TEM. Powdered XRD confirmed that neither protodolomite nor disordered phases were present in the sample analyzed in cell wall fragments of *M. formicicum* at 5:1 Mg:Ca ratio run, indicating that ordered dolomite was the initial phase. TEM analysis of the intact cells of *M. formicicum* revealed mineral precipitates directly on the cell wall surface (Fig. 3). Selected area electron diffraction of these minerals provide a unit cell with a, b axis lengths equal to 4.9 Å at an angle of $\gamma = 120^{o}$ from each other. Dolomite along this same surface should be a, b = 4.84 Å and $\gamma = 120^{o}$. The calcite unit cell should be a, b = 4.989 Å. These data indicate that the mineral is dolomite rather than calcite.

Titration experiments using *M. formicicum* yielded reversible sorption data (Figure 5). Modeling using PROTOFIT 2.1 provided a site density of 8.13×10^{-4} moles g^{-1} (Table 2). This is higher than carboxyl group site densities on the polystyrene microspheres (1.40×10^{-4} moles g^{-1}) and those values taken from the literature on *B. subtilis* and *S. putrefaciens,* which were 1.20×10^{-4} and 4.50×10^{-4} respectively. The site density of carboxyl groups on both *H. sulfurifontis* (1.62×10^{-3} moles/g) and the EPS of *Desulfovibrio sp.* (1.64×10^{-3} to 2.39×10^{-3} mol g^{-1}) are greater than those observed on *M. formicicum*. The concentration of carboxyl groups from another microbe's EPS, that of *Hymenobacter aerophilus*, was taken from the literature and yielded a concentration of carboxyl groups of 2.39×10^{-3} moles g^{-1}(Konhauser *et al.*, 2010) but has not yet been tested for its ability to promote precipitation of dolomite. Competitive sorption

between Mg and Ca in solution yielded a greater Mg:Ca ratio on the cell wall than was initially in solution (Appendix E2). At a relatively low Mg:Ca ratio in solution of 1:1, a 25% increase in Mg:Ca ratio is observed on the cell wall (1.25:1). At higher solution Mg:Ca ratios, the preferential sorption of Mg is amplified. A Mg:Ca ratio of 2:1 originally in solution produces a 5:1 ratio on the cell wall and 5:1 ratio in solution produces a 14:1 ratio on the cell wall.

DISCUSSION

The Archaeal cell wall, either intact and non-metabolizing or fragmented, is the reaction surface for dolomite formation for these experimental vessels. No dolomite precipitated in vessels in the absence of cellular material, with metabolizing microbial cells or in any experiment with sulfate. Dolomite precipitation on the surface of M. formicicum required high Mg:Ca ratios; 5:1 and 10:1 for cell wall fragments and intact non-metabolizing treatments respectively. *H. sulfurifontis* precipitated dolomite at all three Mg:Ca ratios while intact and non-metabolizing and at 5:1 and 10:1 Mg:Ca ratios on its cell wall fragments. Runs with cell wall fragments precipitated high-Mg calcite at 1:1 Mg:Ca ratios. Furthermore, the supersaturated solutions did not produce dolomite in the absence of Archaeal cells. Considering that all of the reactors were modestly supersaturated with respect to dolomite, $\Omega = 3.4$ to 4.7, but not all precipitated dolomite we must conclude that Archaeal biomass facilitated the formation of dolomite by overcoming kinetic barriers.

Supersaturation with respect to dolomite is necessary to precipitate dolomite and a number of studies have looked at the potential for microbes to drive dolomite supersaturation (Vasconcelos and McKenzie, 1997; Warthmann *et al.*, 2000; Van Lith *et al.*, 2003; Roberts et al., 2004; Wright and Wacey, 2005; Kenward et al., 2009). However, it has already been

demonstrated that supersaturation alone is insufficient to precipitate dolomite (Land, 1998). In order to deconvolute the role of microbially generated supersaturation from the role of the microbial cell wall, reactor solutions were set to be slightly supersaturated with respect to dolomite. Live reactors of *M. formicicum* drove saturation higher by raising pH from 7.2 to 8.1. However, as with the reactors with live *H. sulfurifontis*, reactors with live *M. formicicum* did not precipitate dolomite. One potential mechanism for preventing the precipitation on these surfaces is the generation of H^+ at the cell surface via the proton motive force. This has two effects; the first is the observation that the generation and storage of H^+ in their cell walls by metabolizing microbes may yield a cell wall with a relatively lower pH than its environment (Koch, 1986). This would decrease carbonate saturation at the surface. The second is that due to the generation of H^+ while metabolizing, the cell wall of *B. subtilis* was found to be positively charged, thereby decreasing its ability adsorb cations, such as Ca^{2+} and Mg^{2+} (Kemper et al., 1993).

The ratio of magnesium relative to calcium in solution would represent another major kinetic control on dolomite formation. Mg^{2+} is the most abundant divalent cation in microbial cells at cellular concentrations ranging from 15−25 mM in prokaryotic cells (Maguire and Cowan, 2002; Moomaw and Maguire, 2008). To accommodate this high demand for Mg^{2+} microborganisms have evolved specific binding sites (CorA Mg^{2+} channel) for Mg sorption and intake that are in the cell wall of about half of all Archaea and bacteria (Szegedy and Maguire, 1999; Warren et al., 2004; Maguire, 2006; Moomaw, 2010). In this study it was observed that non-metabolizing cells of *M. formicicum* preferentially adsorbed Mg over Ca (Appendix E2). These findings suggest that Mg:Ca ratios on the cell wall can be higher than those observed in solution, and this may reduce the effect of low Mg:Ca ratio in solution as a kinetic inhibitor. However, if high Mg demand and preferential sorption over Ca was the only controlling factor

for precipitating dolomite then all of the organisms would have precipitated dolomite and this is not what was observed. In this study we tested three solution Mg:Ca ratios (1:1, 5:1 and 10:1) and can conclude that while low solution Mg:Ca ratio was not the limiting factor for dolomite formation it did impact the nature of the dolomite precipitated under certain conditions. High Mg:Ca ratios were necessary to precipitate dolomite from non-metabolizing (10:1) and cell wall fragments (5:1) for *M. formicicum*. Runs with cell wall fragments of *H. sulfurifontis* were impacted by lower Mg:Ca ratios, precipitating only high-Mg calcite at 1:1 Mg:Ca and both high-Mg calcite and dolomite at 5:1 Mg:Ca. Only at the highest Mg:Ca ratio, 10:1, did cell wall fragments of *H. sulfurifontis* precipitate only ordered dolomite. High solution Mg:Ca ratios were not required to precipitate dolomite in all cases, however. The non-metabolizing *H. sulfurifontis* precipitated ordered dolomite down to Mg:Ca ratios as low as 1:1. This is consistent with the literature that also shows that precipitation of dolomite is possible at low Mg:Ca ratios (Kenward *et al.*, 2009, 0.4:1, Mg:Ca; Wright and Wacey, 2004, 1:1, Mg:Ca).

The formation of neutral complexes with sulfate is another way in which Mg^{2+} can be removed from solution and limited for dolomite formation (Equation 1):

$$Mg^{2+}(aq) + SO_4^{2-}(aq) \rightarrow MgSO_4^{0}(aq) \qquad \text{(Equation 1)}$$

Sulfate has, however, been presented as a kinetic inhibitor to (Baker and Kastner, 1981) as well as a promoter (Siegel, 1961; Brady *et al.,* 1996) for dolomite precipitation. The function of sulfate as a catalyst is limited to sulfate-rich environments with up to 200 times the sulfate as modern seawater (Jones, 1966) or highly evaporative environments (Brady et al., 1996). The proposition of sulfate as an inhibitor at concentrations closer to but lower than seawater (4mM as compared to 28 mM in modern seawater) was more appropriate to hydrothermal systems with

temperatures ranging from 215 to 225 ^{o}C (Morrow and Ricketts, 1988). The study by Baker and Kastner (1981) also identified sulfate at low concentrations as a dolomite inhibitor under hydrothermal conditions and then extrapolated that back to surface temperatures. A more recent study by Sanchez-Roman in 2009 considered low temperature marine conditions more appropriate to those found at the Earth's surface than the study by Baker and Kastner and included a microbial component. In this study the precipitation of dolomite by moderately halophilic aerobic bacteria occurred at 25 and 35 ^{o}C in the presence of sulfate concentrations of 0, 14, 28 and 56 mM. These studies combine to present conflicting roles for sulfate in the formation of dolomite. In this study none of the experimental conditions containing 28mM of SO_4^{2-} precipitated dolomite, including those similar experimental conditions that precipitated dolomite in the absence of sulfate. This is consistent with the rock record which show changes from dolomite-calcite seas to aragonite seas coincident with rising SO_4^{2-}:Ca ratios despite coincident increases in Mg:Ca ratios (Mackenzie *et al.,* 2008). These results are also supported by numerous studies on SRB promoting dolomite formation while removing sulfate in reducing environments (Vasconcelos and McKenzie, 1997; Warthmann *et al.*, 2000; Wright and Wacey, 2005).

As previously discussed the observed microbial demand for Mg and competitive sorption (Appendix E2) should result in a higher ratio of Mg to Ca on the cell wall surface. However because this process is universal to Archaea and Bacteria it would not explain why the Archaea precipitated dolomite while the bacteria did not. In aqueous environments, such as dolomite-forming environments Mg^{2+} is hydrated by 6 H_2O molecules and as such the mechanism by which hydrated Mg^{2+} is adsorbed to the cell wall may control the formation of dolomite in this study.

The hydration of Mg cations is a critical kinetic inhibitor in all dolomite forming environments. Because calcite grows readily, even at low temperatures, the dehydration and carbonation of Ca is thought to be a rapid process (Brady *et al.*, 1995). Conversely, $MgCO_3$ is considerably more difficult to grow under laboratory conditions at low temperatures (Sayles and Fyfe, 1973). Therefore the rate-limiting steps for dolomite growth can be envisioned as the dehydration and carbonation of Mg cations (Lippman, 1973). Previous work with organic macro-molecules have shown that they can increase the quantity of Mg included in calcite by breaking down hydration spheres around divalent cations such as Ca^{2+} and Mg^{2+}, favoring the dehydration of Mg over Ca (Stephenson *et al.*, 2009). It is also possible that the surface functional groups, such as carboxyl groups, can also break down the hydration spheres around Mg^{2+} and stabilize it on the cell wall. This is critical since Figure 4 depicts one way in which carboxyl groups can accomplish the dehydration and promote the carbonation of Mg and subsequent formation of $MgCO_3$ as a building block for dolomite. Initially in solution as $[Mg(H_2O)_6]^{2+}$ the hydrated form of Mg is drawn to the negatively charged surface of the cell wall (Fig 4a).

The dehydration and binding of $[Mg(H_2O)_6]^{2+}$ to a carboxyl functional group on the cell wall is an energetically (ΔH = -199.8 kcal mol^{-1}) favorable process (Fig 4b, Equation 2) resulting in the ejection of a water molecule and the formation of a $[Mg\ (H_2O)_5(RCO_2)]^+$ complex (Kluge and Weston, 2005; Tommaso and de Leeuw, 2010).

$$[Mg(H_2O)_6]^{2+} + RCO_2^- \rightarrow [Mg\ (H_2O)_5(RCO_2)]^+ \ (\Delta H = -199.8 \text{ kcal mol}^{-1}) \quad \text{(Equation 2)}$$

In this form the energy required to break off another water molecule with CO_3^{2-} in order to create $MgCO_3(H_2O)_4(RCO_2)$ on the cell wall (Fig 4c, Equation 3) is much more favorable (ΔG is 13.6 kcal mol^{-1} lower) (Katz *et al.*, 1998).

$$[Mg\ (H_2O)_5(RCO_2)]^+ + CO_3^{2-} \rightarrow MgCO_3(H_2O)_4(RCO_2) \qquad \text{(Equation 3)}$$

The ΔH_f^o (kcal mol^{-1}) for $MgCO_3$ = -265.52 while the ΔH_f^o (kcal mol^{-1}) for $CaCO_3$ is -288.43 kcal/mol, therefore the decrease in energy from one carboxylate bond will narrow the energy gap between the two alternatives. Surface carboxyl functional groups adsorb Mg^{2+} allowing them to create a $MgCO_3(H_2O)_4(RCO_2)$ complex under these conditions and create a template for the attachment of a Ca^{2+} and a second CO_3^{2-} to create a thin dolomite template for further precipitation.

Neither of the bacterial surfaces, representing typical Gram positive and Gram negative surfaces, nor the functionalized polystyrene microspheres, charged colloids used to approximate the charged cell (Harvey, 1989), were able to precipitate dolomite. However, both bacterial strains and the polystyrene microspheres have the same carboxyl groups distributed across their surface. To explain why these controls do not precipitate dolomite we must consider the effect that carboxyl site density could play in the nucleation of dolomite. The considerably higher concentration of carboxyl sites on the Archaeal cells could, using this mechanism, explain why dolomite is not observed on the surface of bacterial cells or the functionalized microspheres. The development of a thin $MgCO_3^-$ layer will be greatly affected by the proximity of R-$CO_2MgCO_3^-$ complexes to each other. In the cases of bacterial cells and micro-spheres used in this study, the carboxyl groups are too sparse and R-$CO_2MgCO_3^-$ complexes are more likely to be isolated than those on the surfaces of either *H. sulfurifontis* and *M. formicicum* with 2 to 10 times their site densities. The higher density of carboxyl groups, in moles g^{-1}, leads to a smaller parking area (2.15 and 1.09 $Å^2$ $group^{-1}$ for *M. formicicum* and *H. sulfurifontis* respectively), and therefore a tighter assemblage of R-$CO_2MgCO_3^-$ complexes as compared *B. subtilis*, *S. putrefaciens* or the functionalized microspheres (14.70, 3.92 and 6.20 $Å^2$ $group^{-1}$ respectively).

The Archaeal cell walls in this study are not the only organic surfaces in nature with very high densities of carboxyl functional groups potentially capable of dehydrating and binding Mg. Titrations of the EPS produced by *Desulfovibrio sp.* reveal carboxyl group site densities ranging from 1.64 x 10^{-3} to 2.39 x 10^{-3} moles g^{-1}. Functional groups embedded in the EPS of SRBs have already been implicated in carbonate mineral formation with regards to Ca sorption (Braissant et al., 2007). This mechanism can be used to explain dolomites observed to be associated with the EPS of SRBs, including *Desulfovibrio sp.* (Bontognali *et al.*, 2010; Bontognali *et al*., 2008; Vasconcelos *et al*., 2006). SRBs already drive saturation with respect to dolomite and remove another critical kinetic inhibitor, SO_4^{2-}, which forms a neutral complex $MgSO_4^0$ to remove Mg^{2+} from solution. These mechanisms coupled with the high density of carboxyl functional groups could be cause of precipitation of dolomite in these studies. The additional role of overcoming an additional kinetic barrier, hydration spheres, to dolomite formation would further the role EPS can play in the promotion of dolomite formation. This would also explain why the dolomite produced in these systems is seen associated with the EPS rather than the cells themselves. High carboxyl group concentration in EPS is not limited to *Desulfovibrio sp*. *Hymenobacter aerophilus*, for example, possesses 2.39 x 10^{-3} moles g^{-1} carboxyl groups, which suggests this mechanism of Mg dehydration and dolomite nucleation via high carboxyl group density may be widespread. In order to isolate the role of the cell wall as the reactive surface in this study all of the cells were washed and shaken five times in an NaCl solution (0.66 or 0.99 M), prior to experimentation to remove any continuous biofilm that may have formed during growth of the cultures to stationary phase. There was no visible continuous EPS coating the cells of those reactors that formed dolomite. Additionally neither the live culture of *M. formicicum* or *H. sulfurifontis* precipitated dolomite, despite the continued formation of fresh EPS. These

observations make it very unlikely that EPS is the critical surface of dolomite formation in these reactors.

Additionally dolomite precipitation is observed over a larger range of conditions (Mg:Ca ratio and whole cell versus fragmented cells) for *H. sulfurifontis* than *M. formicicum*. This could be due to the even higher concentration of carboxyl groups in *H. sulfurifontis* (1.62×10^{-3} g/mole) than in *M. formicicum* (8.13×10^{-4}). Furthermore, the nature of the S-layer of *H. sulfurifontis* may explain the discrepancy between the formation of ordered dolomite on H. sulfurifontis at all Mg:Ca ratios and the formation of ordered dolomite only at high (10:1) Mg:Ca ratios only on *M. formicicum.* Additionally the absence of an S-layer may explain why there is only the formation of disordered dolomite (high-Mg calcite, low-Ca dolomite) on the EPS of SRB (Vasconcelos and McKenzie, 1997; Van Lith et al., 2003). The reason dolomites associated with EPS of *Desulfovibrio sp.* tend to be protodolomites, is likely due to the variable constituents that make up EPS. EPS have been shown to include polysaccharides, proteins, glycoproteins, nucleic acids, phospholipids, and humic acids along with cell wall fragments of the native microorganisms (Geesey, 1982). As a result microbial EPS lacks the continuous ordered distribution of functional groups that is observed in the paracrystalline S-layer of most Archaea. *M. formicicum* is a gram positive Archaea with a thick pseudomurein cell wall. Pseudomurein chemically differs from Eubacterial peptidoglycan, but is morphologically, functionally, and structurally similar (L-talosaminuronic acid instead of muramic acid, and its peptide moiety lacks D-amino acids; Kandler and König H, 1993; Kandler and König H 1998). The cell wall of *H. sulfurifontis* is a proteinaceous S-layer with a consistent pattern of repeating subunits that can further facilitate the initial nucleation and formation of ordered dolomite, with its paracrystalline structure serving as a template (e.g., Schultze-Lam *et al.*, 1996).

CONCLUSIONS

Microbial surfaces are implicated in facilitating the nucleation and precipitation of numerous minerals, including carbonates (Schultze-Lam *et al.*, 1996; Fortin *et al.*, 1997; Douglas and Beveridge, 1998; Bosak and Newman, 2003; van Lith *et al.*, 2003; Roberts *et al.*, 2004; Kenward *et al.*, 2009). Besides serving as surface sites for nucleation, the carboxyl functional groups abundant on the cell walls of *H. sulfurifontis* and *M. formicicum* may also help to overcome kinetic barriers to dolomite nucleation. Desolvation of Mg^{2+} is a powerful kinetic inhibitor to dolomite formation under all aqueous conditions (Wright and Wacey, 2004). Here we demonstrate that Archaeal surfaces are more reactive than bacterial surfaces due to their high carboxyl group density, which facilitates the dehydration of $Mg(6H_2O)^{2+}$ complexes. S-layers, composed of protein or glycoprotein subunits, while not unique to Archaea are a very common feature of Archaeal cell envelopes, representing the majority of all Archaea (Kandler and König, 1998; Sleytr and Messner, 1988). Archaeal cell walls and surfaces are comparatively less characterized than those of Eubacteria, and here we demonstrate that their unique compositions and structures result in enhanced reactivity to mineral precipitation. However, we assert that these characteristics of Archaea are not exclusive and that carboxyl site density and ordering of these functional groups in proteinaceous microbial materials are broad mechanisms for mineral templating and specifically low-temperature dolomite formation. This model explains microbial dolomite facilitated by numerous metabolic guilds and provides more quantitative guiding principles for evaluating dolomite-precipitating environments.

The dolomite surfaces precipitated by the cells of Archaea and the proto-dolomites from EPS at low temperature are not responsible for abundant precipitation, in this case producing nano-scale crystals. These crystals, however, may be indirectly responsible for widespread

dolomitization by seeding environments otherwise incapable of precipitating dolomite due to kinetic barriers (e.g., Burns *et al.*, 2000; Rao *et al.*, 2003).

Organism	Mg:Ca Ratio	Mg (mM)	Ca (mM)	HCO_3 (mM)	NaCl (M)	pH	I	Ω_{dol}
Haloferax sulfurifontis	10:1	5.0	0.5	13.0	0.98	7.2	0.99	3.9
	5:1	10.0	2.0	7.0	0.98	7.2	0.99	3.7
	1:1	2.0	2.0	10.0	0.98	7.2	0.99	3.7
Methanobacterium formicicum	10:1	10.0	1.0	5.0	0.65	7.4	0.66	4.7
	5:1	10.0	2.0	4.0	0.65	7.4	0.66	3.7
	1:1	5.0	5.0	3.0	0.65	7.4	0.66	3.4

Table 1: Initial geochemical conditions of reaction vessels for dolomite precipitation by *H. sulfurifontis* and *M. formicicum* for live cells, non-metabolizing cells and cell wall fragment treatments. All biological and abiotic controls, including carboxylated microspheres, were run in vessels under the initial geochemical conditions of both *H. sulfurifontis* and *M. formicicum.* Saturation states of dolomite are not identical for all Mg:Ca ratios in order to keep the solutions initially undersaturated with respect to calcite for those experimental conditions.

Reactor	$\Omega_{dolomite}$*	Mg:Ca ratio†	pH
M. formicicum (live)	3.4-4.7	None	7.4
M. formicicum (cell wall fragments)	3.4-4.7	5:1	7.4
M. formicicum (non-metabolizing)	3.4-4.7	10:1	7.4
H. sulfurifontis (live)	3.7-3.9	None	7.2
H. sulfurifontis (cell wall fragments)	3.7-3.9	5:1 and 10:1	7.2
H. sulfurifontis (non-metabolizing)	3.7-3.9	1:1, 5:1 and 10:1	7.2
Microspheres (R-COO-), *S. putrefaciens* and *B. subtilis*	3.4-4.7	None	7.2
Abiotic	3.4-4.7	None	7.2

*Ω= ion activity product Ksp^{-1}

†Only Mg:Ca ratios in which dolomite is detected are listed

Table 2: Geochemistry and precipitation results of experimental dolomite reactors. Saturation state of dolomite reported to include the range as a result of varying Mg:Ca ratio. Only Mg:Ca ratios that resulted in dolomite formation are listed and where no dolomite is observed, none is listed. Geochemistry of each system, including pH and ionic strength remained constant over the 42-day intervals, except for the vessels containing live M. formicicum which showed increased pH (to 8.1) and Ω_{dol}.

Substrate	Carboxyl site density (moles g^{-1})	Parking area ($Å^2$ $group^{-1}$)	Mineral precipitate
B. subtilis	**1.20×10^{-4}** (Daughney *et al.*, 2000)	**14.70**	**No dolomite[1]**
S. putrefaciens	**4.50×10^{-4}** (Sokolov *et al.*, 2001)	**3.92**	**No dolomite[1]**
Microspheres	**1.40×10^{-4}** (This study)	**6.20**	**No dolomite[1]**
M. formicicum	**8.13×10^{-4}** (This study)	**2.15**	**Ordered dolomite and Mg-calcite [1]**
H. sulfurifontis	**1.62×10^{-3}** (Fowle *et al.*, in review)	**1.09**	**Ordered dolomite[1]**
EPS (*Desulfovibrio sp.)*	**1.64×10^{-3} to 2.39×10^{-3}** (Braissant *et al.*, 2007)	**Unknown**	**Disordered dolomite, Mg-calcite and Ca-dolomite[2]**
EPS (*Hymenobacter aerophilus.)*	**2.39×10^{-3}** (Baker *et al.*, 2010)	**Unknown**	**Unknown capacity**

[1] Results from this study

[2] Results from Bognotoli *et al.,* 2008 and Vasconcelos *et al.,* 2006

Table 3: Carboxyl site densities, in moles g^{-1}, for the Bacterial and Archaeal strains used in this study and the references for those values. Also included are the carboxyl site densities for the EPSs of *Desulfovibrio sp* and *Hymenobacter aerophilus*. The capacity for precipitation of dolomite (ordered and disordered phases), results from this study as well as Bognotoli *et al.*, 2008 and Vasconcelos *et al.*, 2006, are included.

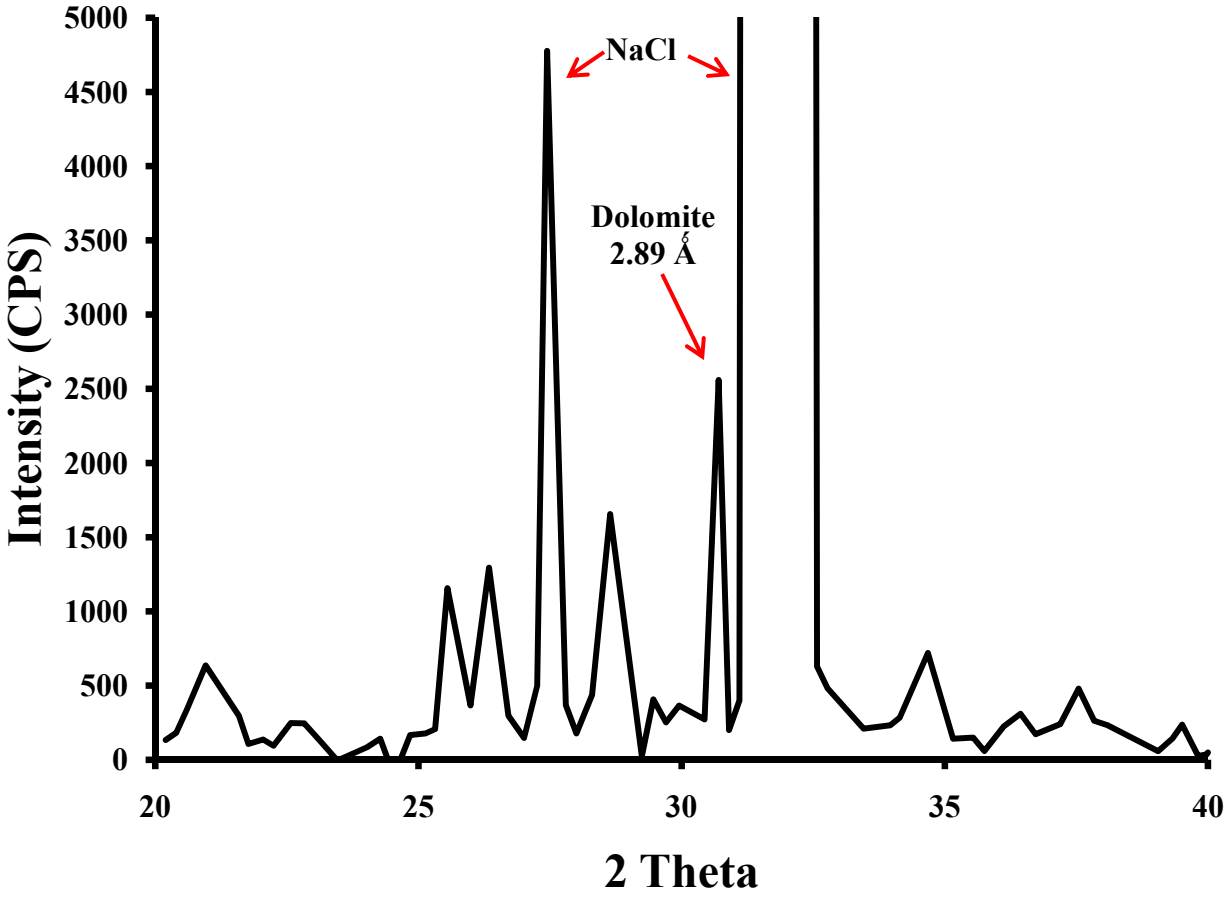
5000
4500
4000
3500
3000
2500
2000
1500
1000
500
0
Intensity (CPS)
NaCl
Dolomite
2.89 Å
20
25
30
35
40
2 Theta

Figure 1

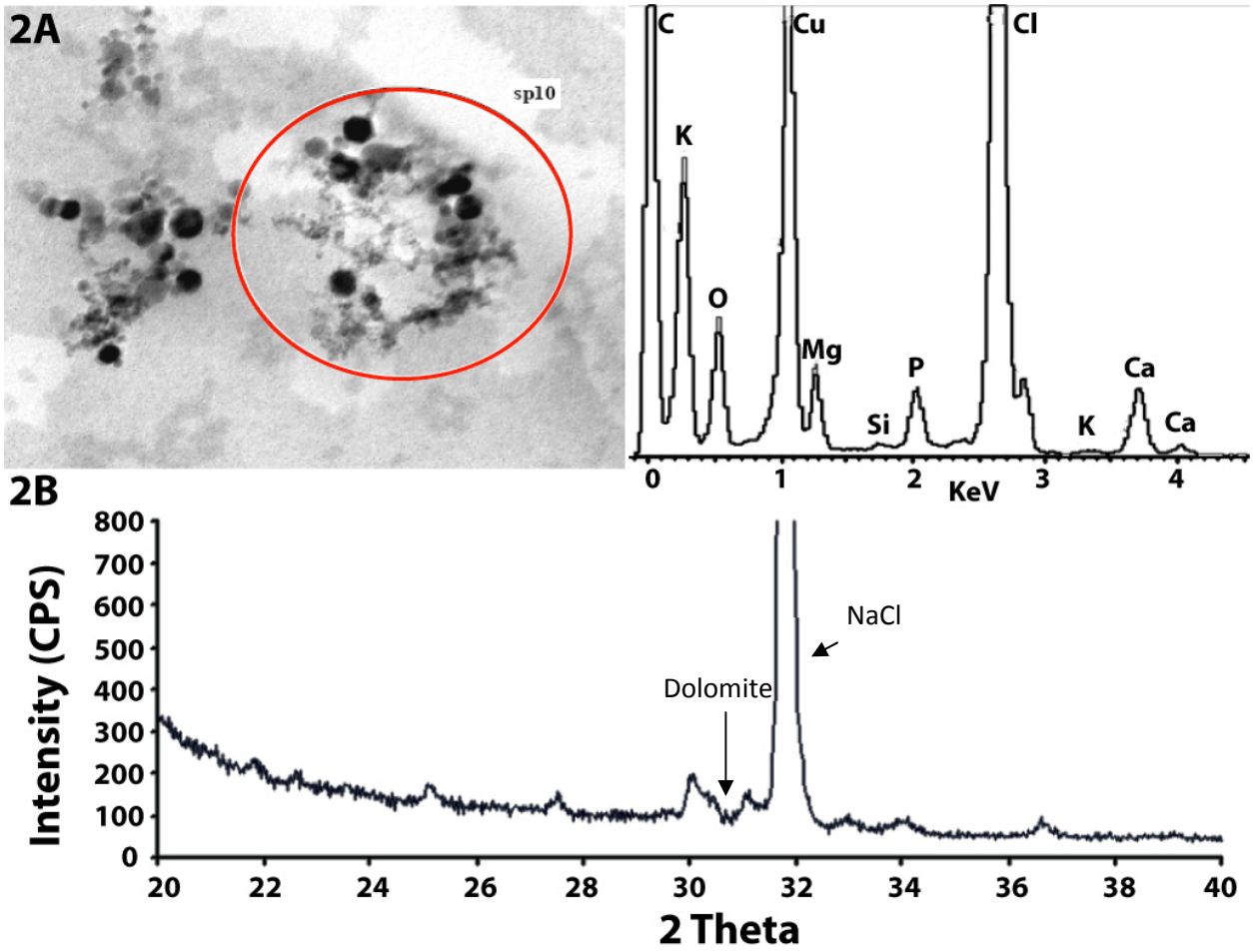
2A
sp10
C
Cu
Cl
K
O
Mg
P
Si
K
Ca
Ca
0
1
2
KeV
3
4
2B
Intensity (CPS)
800
700
600
500
400
300
200
100
0
NaCl
Dolomite
20
22
24
26
28
30
32
34
36
38
40
2 Theta

Figure 2.

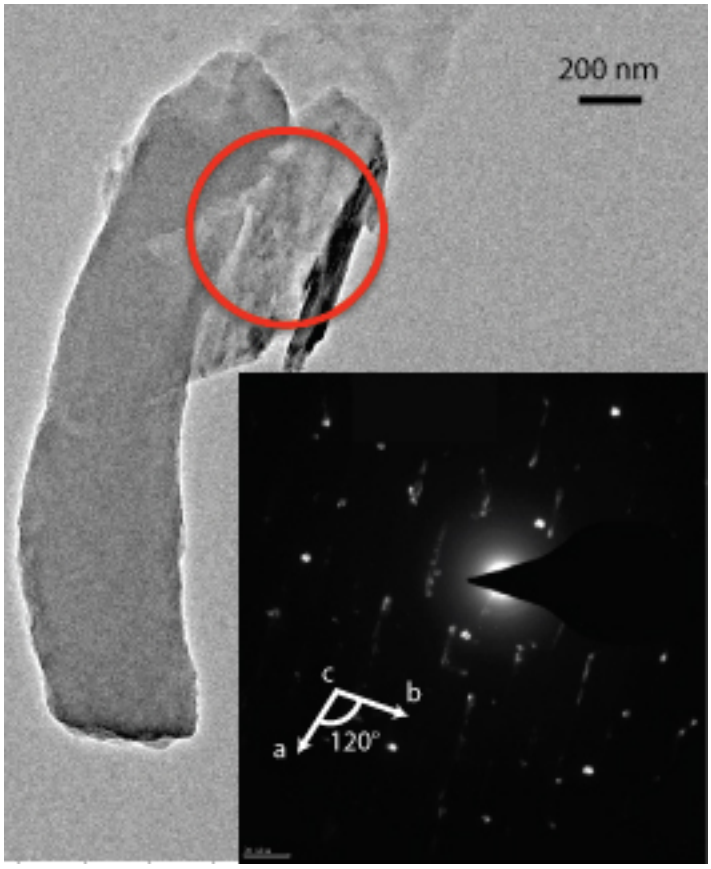

Figure 3

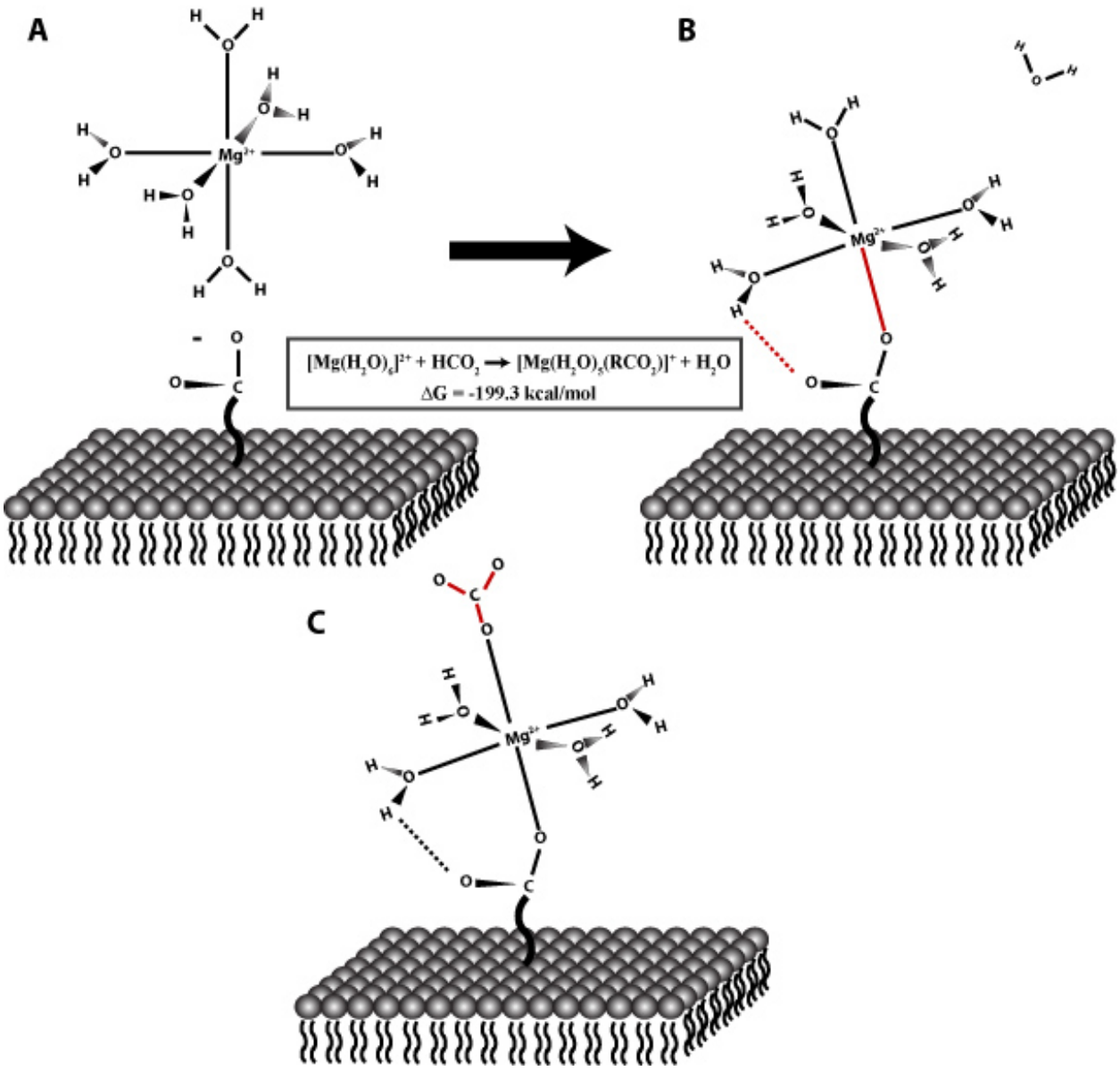
A
B
C
$[Mg(H_2O)_6]^{2+} + HCO_2^- \rightarrow [Mg(H_2O)_5(RCO_2)]^+ + H_2O$
$\Delta G = -199.3$ kcal/mol

Figure 4.

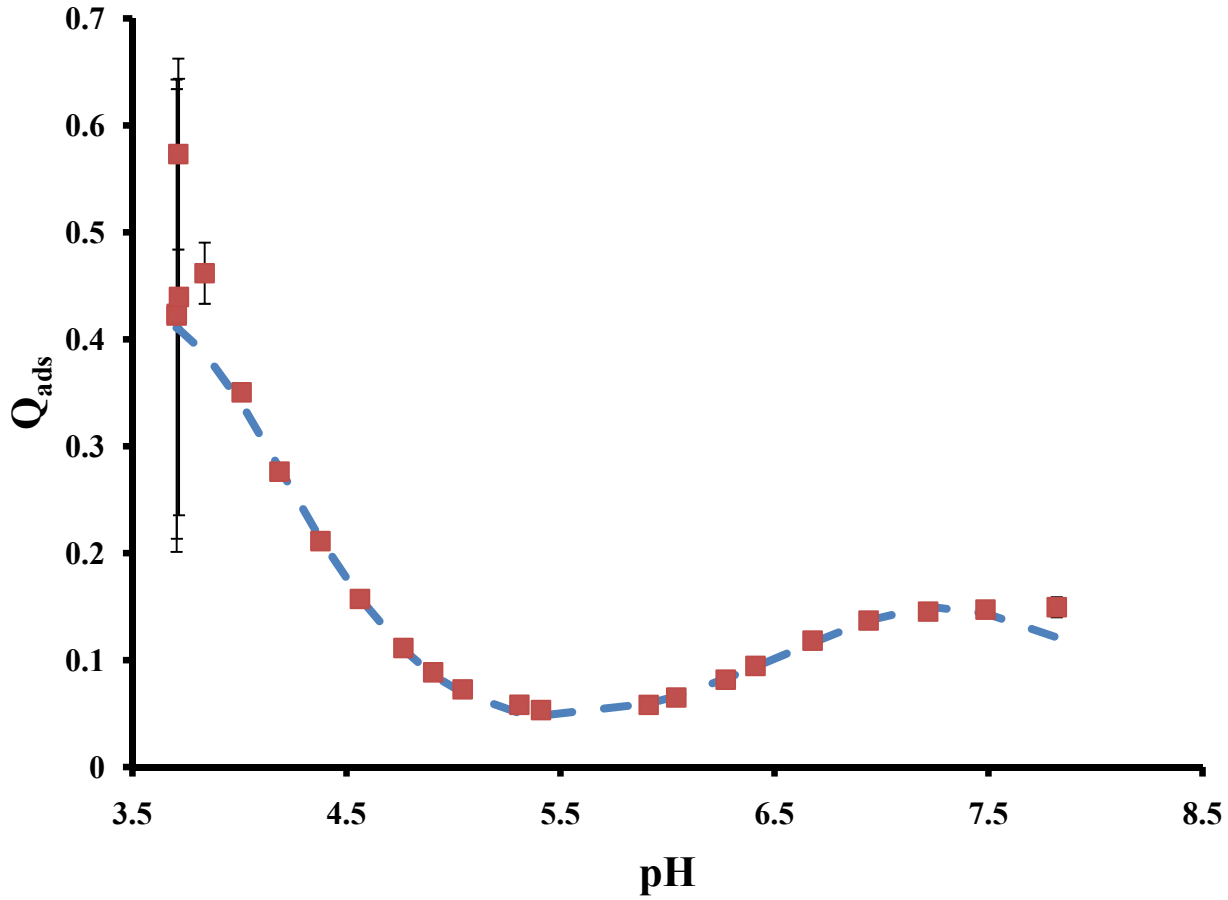

Figure 5

Figure 1: Powder X-ray diffraction plot of intensity in counts per second (cps) as a function of position (2-theta). Scan after a 42-day equilibration period with metabolically inactive cells of *H sulfurifontis.* Arrow indicates ordered dolomite (2-theta = 30.89; d-spacing = 2.88). The prominent peak at 2-theta = 33.10 is halite.

Figure 2: Dolomite precipitated in association with cell wall fragments of *M. formicicum* with a Mg:Ca ratio of 5:1. Transmitted Electron Microscopy (TEM) photomicrograph of spheriodal to hexagonal nano-sized minerals attached to cell wall fragments of *M. formicicum* along with the associated elemental spectrum for the targeted area represented by the red circle (A). Powdered X-ray diffraction pattern of minerals isolated from reactor from which the TEM sample (above) was taken showing the dolomite main peak at d-spacing = 2.89 (B). The prominent peak at 2-theta = 33.10 is halite.

Figure 3: TEM micrograph of negatively stained, whole mounted *Methanobacterium formicicum.* Diffraction pattern for attached mineral is shown (insert). Looking from the c axis the, a, b plane is 4.9 Å and the angle γ being 120^{o} corresponds to dolomite (a, b = 4.84 Å, $\gamma = 120^{o}$). Scale bar is 200 nM.

Figure 4: Modeled behavior of aqueous $[Mg(H_2O)_6]^{2+}$ and a negatively charged carboxyl functional group on a microbial cell wall (A). The aqueous Mg^{2+} will readily eject an H_2O in order bind to the carboxyl functional group (B) in an energetically favorable reaction (inserted equation). The new $[Mg\ (H_2O)_5(RCO_2)]^{+}$ complex carries a residual positive charge which is satisfied by the inclusion of aqueous carbonate (CO_3^{2-}) (C) or bicarbonate ($H\ CO_3^{2-}$).

Figure 5: Q_{ads} (the number of protons exchanged with the adsorbent, normalized to adsorbent mass) of titrated cells of M. formicicum as a function of pH (red squares). Also plotted is the

modeled average of Qads (dashed blue line), derived from modeling the data using PROTOFIT 2.1 software (Turner and Fein, 2006).

CHAPTER 4. MODEL FOR HOW ARCHAEAL METHANOGENESIS CAN PRESERVE EARLY POROSITY IN DOLOMITE AND LIMESTONE RESERVOIRS

ABSTRACT

In some dolomite and limestone hydrocarbon reservoirs, protection from cementation is a primary factor in porosity preservation. We present a model in which methanogens produce CH_4 that exsolves in porespace, creating a two-phase system that reduces effective hydraulic conductivity (K), protecting pore space from cementation. Methanogens have been implicated in dolomite formation and generate methane to fill pore space of a model near-surface carbonate sediment (37.5% primary porosity) with $CH_{4(g)}$ in 180—4,650 years, depending on nutrient levels. This results in occlusion of the aqueous phase from pore spaces and throats, creating a two-phase flow regime, reducing the effective hydraulic conductivity of model marine carbonate sand by about 50% (from 2.8 to 1.2 cm/day) in as little as 55 years, therefore reducing aqueous fluid flow necessary for cementation. Despite rapid burial and complete cessation of methanogenesis, effective hydraulic conductivity could take >100,000 years to return to its original value. If methanogenesis continues with burial the effective hydraulic conductivity is reduced to zero (after 250 years). Dolomites can preserve more primary porosity with depth than other carbonates, due to increased resistance to mechanical reduction of porosity. We propose that in addition to increased structural resistance that there is a biogenic model for porosity preservation in dolomites linked to the activity of methanogens.

INTRODUCTION

Dolomite and limestone are both effective hydrocarbon reservoirs. Dolomites contain 80% of North America's oil and gas reserves (Zenger *et al.,* 1980). Globally carbonates account for approximately 50% of oil and gas production with a slightly greater percentage of world hydrocarbon reserves being produced from dolomites over limestones (Mazzullo, 2004). It has been suggested that this is due, in part, to greater porosity and permeability typically, but not always, found in dolomites (Schmoker and Halley, 1982). Despite being abundant throughout the rock record, dolomite is uncommon in modern settings. Since dolomites can help form excellent reservoirs, and have not yet been abiotically synthesized at low temperatures (< 50 ^{o}C), there has been a great deal of research into the origin of massive dolomites. Studies of modern dolomite have found dolomites in association with marine or marine influenced environments. These environments include coastal sabkhas (Muller *et al.,*1990) and hemipelagic mud (Middleburg *et al.,*1990). Dolomite has also been associated with hypersaline evaporative lakes such as the Coorong region Australia (Alderman & Skinner, 1957), and Deep Springs Lake, California (Jones, 1965). Other than marine environments dolomite has formed in regions where DIC (dissolved inorganic carbon)-rich meteoric waters mix with Mg-rich groundwaters (Land & Hoops, 1973; El-Sayed *et al.,* 1991; Humphrey and Radjef, 1991; Colson and Cojan, 1996; Capo *et al.,*2000; Whipkey *et al.,* 2002).

The limited quantity and restricted environments of modern dolomite precipitation largely have been attributed to kinetic barriers that need to be overcome at low temperatures. These kinetic barriers include solution saturations state with respect to dolomite, temperature, pH, Mg:Ca ratio, concentration of carbonate, and ion complexation with both water and sulfate (Goldsmith and Graf, 1958; Kitano, 1962; Folk, 1974; Folk and Land, 1975; Katz and Matthews, 1977; Baker and Kastner, 1981; Land, 1985; Hardie, 1987; González and Lohmann, 1985;

Zhong and Mucci, 1989; Slaughter and Hill, 1991; Arvidson and Mackenzie, 1997; Wright and Wacey, 2004).

Recent studies, however, have shown that microorganisms such as sulfate reducing bacteria (SRB) and methanogenic Archaea can act to overcome these barriers. They do this through removing kinetic inhibitors and driving dolomite to supersaturation by raising alkalinity, reducing sulfate concentrations (SRB only), and possibly by concentrating Mg^{2+} relative to Ca^{2+} on cell wall or exopolysaccharide (EPS) material (e.g., Vasconcelos *et al.,* 1995; Van Lith *et al.,* 2003; Moreira *et al.,* 2004; Roberts *et al.,* 2004; Kenward *et al.,*2009). As Archaeal methanogenesis is common in marine carbonate sediments from the sediment-water interface and down to burial depths of 1, 100 meters - (Reed *et al.,*2002; Newberry *et al.,*2004), it is possible that many dolomitized reservoir rocks had an early history of low-temperature dolomitization in the presence of this process, followed by later diagenesis.

Whereas numerous metabolic guilds have been associated with low-temperature dolomite formation, methanogenic Archaea do more than simply promote the precipitation of dolomite. Methanogenic Archaea are capable of generating great quantities of biogenic methane (Noble and Henk, 1998; Zhang *et al.,* 2005), which we hypothesize to impact the preservation of early porosity in these dolomites. Populations of methanogenic Archaea generate large quantities of CH_4 gas as a product of their metabolism, as has been observed in the Qaidam basin, the large biogenic gas province in China with 2937.6×10^8 m^3 of biogenic gas reserves (Dai *et al.,* 1996). When rates of biogenic methane generation are high, aqueous pore fluids become supersaturated with the dissolved gas and methane gas exsolves. Methane gas occupies pore spaces and becomes trapped in pore throats and attached to mineral grain surfaces. These methane bubbles become nucleation sites for even larger methane bubbles that eventually can form large pockets

of methane (Noble and Henk 1998; Zhang *et al.,* 2005). Two-phase flow regimes resulting from a gas and aqueous liquid phase are known to decrease the effective hydraulic conductivity across a range of sediment grain sizes (Mualem 1976; Van Genuchten 1980; Gerke and Van Genuchten 1993).

It has been observed that dolomites tend to preserve more primary porosity with depth than other carbonates (Schmoker and Halley, 1982; Benson *et al.*,1984; Benson, 1985; Schmoker et al.,1985). The primary argument for this phenomenon has been the increased resistance to mechanical and chemical compaction, compared to limestone, at depth (Schmoker and Halley, 1982). Despite resistance to compaction, however, a great deal of porosity is lost to dolomite cementation from flux of aqueous fluids (overdolomitization) (Murray and Lucia, 1976; Lucia, 1997; Jones and Xiao, 2005). If biogenic methane can reduce effective hydraulic conductivity and sustain this reduction over time, porosity loss due to cementation in these systems could be greatly reduced.

Both diffusion and advection control carbonate cementation. Diffusive flux of ions for carbonate precipitation is controlled by the diffusion gradient and is a process up to two orders of magnitude slower than the advective flux of ions (Fetter, 1999). Unlike diffusion, cementation from advection requires fluid flow through the porous media, which is controlled by the effective hydraulic conductivity of the system. We suggest that methanogenic microbes could, by filling pore spaces with CH_4 gas, create a two-phase flow regime, which would lower the effective hydraulic conductivity. This reduction in effective hydraulic conductivity would result in decreased transport of the aqueous fluid phase, and therefore, decreased cementation in carbonate sediments. This also suggests that methanogen-promoted dolomites are more likely to retain their primary porosities at depth and serve as hydrocarbon reservoirs. If methanogenic

dolomites serve as the nuclei for dolomite crystals in dolomite reservoirs, then it is likely that such a system experienced a period of *in situ* methane generation. The methane could have decreased effective hydraulic conductivity, and therefore, decreased the rate of cementation in relation to strata lacking a methane-gas phase. In this study we explore the extent to which methanogens can generate sufficient methane to create two-phase flow and reduce effective hydraulic conductivity on a geologically relevant time scale. We will also examine how a methanogenic two-fluid-phase carbonate system can retain diminished effective hydraulic conductivities with depth, and thus, be protected from cementation that other stratigraphic units might experience.

MODEL PARAMETERS

Hypothetical System

All of the models considered were derived initially using the same theoretical unconsolidated shallow marine carbonate, one cubic meter (m^3) in volume. It is modeled as a closed system and all fluids are considered saturated with respect to carbonate minerals. The textural properties of this sediment were derived using the Rosetta program on the USDA (U.S. Department of Agriculture) website for initially water-saturated sediment with sand-sized grains. All of the variables provided by Rosetta were calculated from the averages of 308 actual sediments with sand-sized grains (Table 1). The model was filled with marine water and a population of methanogens that had already reached stationary phase. Because the population density (in cell ml^{-1}) is an important factor determining the rate of methanogenesis it is important to properly estimate a conservative poplution size to use in these models. Research comparing

five geographically distinct areas of the Pacific Ocean has observed consistent microbial populations (always more than 10^4 cells ml^{-1}) with depths greater than 500m (Parkes *et al.,* 1994). In the a site in the Japan Sea an initial biomass of 10^9 cells ml^{-1} at the water-sediment interface decreased to 10^7 cells ml^{-1} at 518 meters below the water-sediment interface. Also at 518 meters below the water-sediment interface there is also a spike in pore water methane concentration (Parkes *et al.,* 1994). The same study has modeled that these populations will continue to even greater depths, being limited only by temperature. This is supported by other studies that show microbial populations of 10^4 cells ml^{-1} down to depths of 800 meters beneath the sediment-ocean water interface (Reed *et al.,* 2002; Wellsbury *et al.* ,2002). Methanogenesis has also been observed at even greater depths (1, 100 meters). Therefore a population of methanogens as low as 10^4 cells ml^{-1} would be a conservative estimate (Reed *et al.,* 2002; Newberry *et al.,* 2004).

Methane Generation Rates

In an effort to consider the range of environments and nutrient concentrations in which methanogenesis occurs, rates of methane generation were taken from the literature to represent the end members of methane generation in natural systems. To represent the lower end member of methane generation rates (0.06 $fmolcell^{-1}day^{-1}$), nutrient-starved methanogens found in deep ocean systems were considered (personal communication, Colwell). To establish an upper end member of methane generation rates (108-135 $fmolcell^{-1}day^{-1}$), we used data from a consortium of methanogens grown in an anaerobic digester, under ideal temperature and abundant nutrient conditions for methanogenesis (Li and Noike, 1992). Between these end members we considered methane generation rates that represent more common natural conditions from two specific environmental controls. The first was a native consortium of microbes collected from a

petroleum spill site approximately 16 km northwest of Bemidji, Minnesota, part of the USGS Toxic Substances Program. This consortium was extracted from cores taken from the methanogenic zone of the groundwater (Bekins *et al.,* 1999). These were cultured in their native groundwater, in 60ml anaerobic reactor vessels; they contained both acetoclastic and autotrophic methanogenic Archaea (Roberts *et al.,* 2004; Kenward *et al.,* 2009). The second was derived from a pure strain culture of the autotrophic methanogen *Methanobacterium formicicum* (ATCC # 33274) grown at 30 ^{o}C in a dilute pre-reduced anaerobic media with CO_2 as the terminal electron acceptor. *M. formicicum* was cultured in 60ml serum vials with 15 ml anaerobic headspace. Headspace samples were taken with an airtight syringe during exponential and stationary phases and analyzed using an Agilent Technologies Network GC System 6890N with a Thermal Conductivity Detector. The CH_4 phase in the headspace was separated by running 250 µL samples through an Alltech Hayesep Q 80/100 Packed Column at 90 °C, which had an analytical error of 0. 5%. The results of these studies yielded methane generation rates of 0.97 fmolcell^{-1}day^{-1} for the consortium and 31.7 fmolcell^{-1}day^{-1} for the pure strain. The rate determined experimentally for *Methanobacterium formicicum* in this study compares well to a batch culture experiment using methanogens taken from sediments of Lake Izunuma, in Japan. This lake had been contaminated by wastewater and the resulting consortium of methanogens generated methane at a rate of 31.5 fmolcell^{-1}day^{-1} (Lay *et al.,* 1996). Thus, a range of metabolic activities within the population was modeled from data in the literature, with methane generation rates of 0.06, 0.97, 31.5 and 108 fmolcell^{-1}day^{-1} (Table 2).

Methane Solubility

Methane solubility for all models were determined via a phase equilibrium calculation for a ternary, H_2O-CH_4-NaCl, system constrained by temperature, pressure and the concentration of

NaCl (Duan and Mao, 2006; Duan and Sun, 2006; Sun and Duan, 2005). Average ocean salinity, 0.6 M NaCl, was used along with temperature and pressure to constrain methane solubility. Temperature and pressure, used in the phase equilibrium calculation, were controlled by burial depth using the following formulas:

$$T = 298.15 + (0.02 * D) \quad \text{(Equation 1)}$$

$$P = 101.325 + (10.2 * D) \quad \text{(Equation 2)}$$

Where T is temperature in Kelvin, P is pressure in kPa and D is depth in meters. This data was used to constrain the aqueous methane solubility for the hypothetical aqueous phase. For biogenic methane bubbles to form, the capacity for soluble methane must be overcome (Duan and Mao, 2006; Duan and Sun, 2006; Sun and Duan, 2005).

After methane becomes supersaturated in the solution, the volume of methane (g) was determined using the ideal gas law formula:

$$V = (nRT)/P$$

(Equation 3)

Where V is the volume of methane gas; P is the pressure as determined in Eq. 1; T is the temperature as determined in Eq. 1; n is the number of moles of methane gas and R is the gas constant 8.314 J K^{-1} mol^{-1}.

Effective Hydraulic Conductivity

In order to constrain the impact of biogenically generated methane bubbles on effective hydraulic conductivity, the following equations were used: (van Genuchten, 1980)

$$K = K_s \times S_e^{L}[1-(1-S_e^{n/(n+1)})^{1-1/n}]^2$$

(Equation 4)

Where,

$$Se = (\Theta - \Theta_r)/(\Theta_s - \Theta_r)$$

(Equation 5)

K_s represents the water-saturated hydraulic conductivity, and is controlled by the relative pore water-saturation, S_e (Equation 5) along with the parameter L which is an empirical pore tortuosity/connectivity parameter that is normally assumed to be 0.5 (Mualem, 1976). The residual pore water-saturation (Θ_r), water saturation (Θ_s) and n (porosity) are known values provided by the Rosetta database. The relative water saturation varies with Θ representing the amount of pore space occupied by biogenic methane gas.

MODEL RESULTS

In order for methane bubbles to occupy pore space, a solution must achieve supersaturation with respect to methane. Several factors control the rate at which saturation was reached for methane in equilibrium with the modeled seawater, and rate of subsequent generation of methane gas. A hypothetical model of what exsolvation of gas would look like is given in Figure 1. Initially (Figure 1a), the solution will become supersaturated with respect to CH_4 and small bubbles will form. These bubbles will continue to grow and block pore throats where they may become trapped (Figure 1b). Finally as more methane gas collects smaller bubbles will accumulate into larger bubbles further hindering flow of water by blocking pore throats or by locally wetting the grain surface with the gas phase (Figure 1c). In the model, methane

generation rate (Table 2) has the greatest impact on the rate of generation of methane gas at all depths (Table 3). This modeled range of methane generation rates varies by nearly 4 orders of magnitude. In nature this would be controlled by variations in nutrient availability, geochemistry, temperature, and population size, which could be very low (10^1 to 10^2 cells ml^{-1}) or enriched (10^9 cells ml^{-1}) (Kendall and Boone, 2006).

Effect of Methane Generation Rate

In the model, taking the conservative population (10^4 cells ml^{-1}) of methanogenic Archaea with a high generation rate (31.6 $fmolcell^{-1}day^{-1}$) in a freshly deposited shallow marine carbonate unit, the aqueous phase would reach saturation with respect to methane (10.1 years) followed by significant methane gas generation occupying 50% of the available pore space in only 180 years (Table 3). Even under lower methane generation rates (0.97 $fmolcell^{-1}day^{-1}$) 50% of the available pore space would be replaced by methane within 5,820 years. At the other end of the spectrum, a nutrient starved population of cells with very low methane generation rates (0.06 $fmolcell^{-1}day^{-1}$) would take 8,380 years to reach methane saturation and 133,380 years to occupy 50% of the available pore space in a near-surface shallow marine sediment.

Effect of Burial Depth

Given sustained microbial methanogenesis during burial, which has been observed in the formation of large methane reservoirs (Noble and Henk, 1998) and to depths of 1,100 m (Newberry *et al.,*2004), methane saturation and exsolvation are controlled by pressure and temperature, which is in turn controlled by depth (Table 3, Equation 1 and Equation 2). The effect of temperature and pressure on methane solubility is most pronounced between 10 and 100m depth. In the modeled results, a change of one order of magnitude in depth (from 10m to

100m) results in an order of magnitude increase in the time necessary to saturate the aqueous solution. However, a similar one order magnitude change in depth, from 1m to 10m or from 100m to 1000m, results in a two or three fold increase in the time required to saturate the solution with respect to methane, respectively. The effect of depth on the time it takes to fill 50% of the pore space with methane bubbles is most pronounced at depths greater than 100m (Table 2). The time it takes to occupy 50% of available pore space with methane bubbles approximately doubles from 1m to 10m in depth and takes five times longer going from 10m to 100m in depth. Increasing depth by another order of magnitude to 1000m in depth has a proportional order of magnitude increase in the time necessary to fill 50% of the available pore space.

Coupled Model of Methanogenesis and Effective Hydraulic Conductivity

A quantitative analysis of the effect of formation of two fluid phases within the pore system of the sediment was conducted using the formula for unsaturated effective hydraulic conductivity (Equation 4), modified from van Genuchten (1980). The system was modeled at a constant depth of 1 m using the average population of 10^4cells ml^{-1}, and for methane generation rates of 0.06, 0.97, 31.5, and 108 fmol$cell^{-1}day^{-1}$Results are depicted in Figure 2. The initial decline in effective hydraulic conductivity as a result of the development of two-phase flow is relatively rapid. In order to reduce effective hydraulic conductivity by 50% only 17% of the available pore space needs to be occupied by methane bubbles (Figure 2). This takes between 16 and 28,000 years depending on the methane generation rate assumed. The model results show that effective hydraulic conductivity can decrease rapidly in closed systems with biologically feasible rates of methanogenesis.

A model can also be created for the dissolution of exsolved methane during burial, to evaluate the duration of the methane's effect on effective hydraulic conductivity. Given the same carbonate sand previously discussed, average microbial population (10^4 cells ml^{-1}), surface pressure, 25 ^oC, and rapid rate of methanogenesis of 31.5 $fmolcell^{-1}day^{-1,}$ 52% of pore space is occupied by methane in ~160 years (Figure 3). After this period of methane buildup, the model simulates complete cessation of methanogenesis, followed by burial, at a rate of twenty centimeters every 1000 years. Burial rate used is based on long term deposition along the progradational margin of the Great Bahama Bank (McNeill, 2005). In the model, after 52% of the pore space is filled with CH_4 gas, effective hydraulic conductivity has decreased from 2.28 to 0.31 cm day^{-1}, 13% of the original value. Once the system has reached this condition, methanogenesis is cut off in the model, and the system is buried. The increase in pressure and temperature during burial leads to dissolution of methane, but requires more than 240, 000 years (48 meters depth) to return to the original 2.28 cm day^{-1} (Figure 3). The model results demonstrate that even a short pulse of methanogenesis can lead to a long-lived decrease in effective hydraulic conductivity in closed systems.

A model can also be created for continuous methanogenesis during burial. The model assumes a slow rate of methane production of 0.06 fmol/cell/day, burial of 20 cm per 1000years, the conservative population of 10^4 cells ml^{-1}, standard temperature and pressure (stp) at the surface, and a geothermal gradient of 25 ^oC km^{-1}. The model is allowed to run for 5 million years to achieve a burial depth of 1 km (Figure 4). If methanogenesis continues during burial, methane gas will occupy all of the pore space except the residual pore water-saturation (Θ_r). As a result effective hydraulic conductivity will be reduced to zero. The modeled results show that given continuous but slow methanogenesis during 5 million years of burial, this two-phase system is

sustained. This condition will severely limit the degree of fluid flux, and thus limit further dissolution or precipitation.

DISCUSSION

Effect of Decrease in Effective Hydraulic Conductivity

Empirical modeling has shown that methane generation to occupy 17% of the pore space in a carbonate sand would decrease effective hydraulic conductivity by 50% (Fig. 2). For typical moderate nutrient closed systems, this effect can take only 55 and 1,800 years to develop (Figure 2b, c).

Cementation has been established as a major cause of porosity reduction in carbonates (Choquette and Pray, 1970; Ginsberg *et al.*, 1971; Folk *et al.,* 1973; Murray and Lucia, 1976; Mazzullo, 1977; Lucia, 1997; Choquette and Pray, 1970). Cementation relies heavily on fluid flux to deliver ions for precipitates (Badiozamani *et al.*, 1977; Wood and Hewett, 1982; Skolasińska, 2006). Rates of ion movement through diffusion are commonly low (1×10^{-9} to 2×10^{-9} m^2/s; Fetter, 1999) in comparison to rates of ion flux from fluid flow in the shallow subsurface. Thus, any decrease in effective hydraulic conductivity in the shallow subsurface could have a profound effect on decreasing the rate of porosity loss due to cementation. Moreover, any areas of sediment that are wet by the gas phase, might be protected from cementation altogether. This preserves the primary or early pores. It should be noted, alternatively, if aqueous fluids are undersaturated with respect to carbonate minerals, decrease in flow of aqueous fluids also limit enhancement of pore space (Murray, 1960).

The longer the sediment contains a separate gas phase, the longer the rate of aqueous fluid flow can be decreased relative to surrounding strata. The modeling efforts reported herein

show that methane bubble accumulation can be relatively rapid and that even after methanogenesis has ceased, it may take hundreds of thousands of years of burial for methane bubbles to dissolve and compress. In a system in which methanogenesis continues during burial, it is clear from the modeling that the two-phase system can persist easily for millions of years during the upper kilometer of sediment burial, thus providing long-lived reduction in the rate of aqueous fluid flux, and potentially, decrease in the rate of cementation relative to surrounding units.

Some extant gas fields provide support for the idea that early presence of a gas phase (whether biogenic or thermogenic in origin) protects original porosity from cementation. The first such example can be found in the Puguang Gas Field located in the northeast Sichuan Basin, China. This dolomite reservoir has preserved primary porosity with depth (up to 3,000m) and was filled with methane early on; it represents one of the largest gas resources in China (YongSheng *et al.,* 2008). The natural gases of the Puguang Gas Field are dry with methane concentrations between 72% and 80%. The porosities of the dolomites in the Feixianguan and Changxing Formation reservoirs, which represent the majority of the methane resource, range from 8% to 14%. A limestone unit, located between two dolomite units, however, has a porosity of only 2%. In fact three units, one limestone and two dolomite, were classified as having good primary porosity prior to burial and only the two dolomite units retained their porosity to become good reservoirs (YongSheng *et al.,*2008). The authors of this study identified early stage gas-filling along with rapid burial were the keys to the preservation of primary porosity. Only the dolomites which experienced rapid hydrocarbon filling retained their primary porosity with burial.

Another study, by Al-Aasm and Packard (2000), compared two dolomite fields with similar initial conditions but different diagenetic histories. The first, the Debolt Formation of the Dunvegan Field (NW Alberta), has high porosity (average of 15%) and remains relatively unaltered despite burial up to 4,000 meters. In contrast the second dolomite unit, the Mount Head Formation of the Shell Waterton Field (SW Alberta), shows signs of significant alteration with burial and a loss of porosity due to recrystallization of earlier-formed dolomite. Despite similar origins and facies the Debolt Formation preserved greater porosity resulting from hydrodynamic isolation (Al-Aasm and Packard, 2000). One mechanism of isolation presented by the authors was the early introduction of methane in the system, potentially biogenic in origin prior to deep burial.

Link Between Dolomite and Porosity Preservation

In both examples, one from China and one from Canada, dolomite units with exposure to methane early during burial retained a greater degree of primary porosity than closely associated dolomites and limestones that underwent similar burial histories. Methanogenic Archaea are known to encourage the formation of dolomite, even at low temperature (e.g., Vasconcelos *et al.,*1995; Mazullo, 2000; Van Lith *et al.,*2003; Moreira *et al.,*2004; Roberts *et al.,* 2004; Kenward *et al.,*2009). Thus, methanogenic activity may be one of the important reasons why some dolomite reservoirs preserve porosity. Methanogens produce the separate gas phase that can cause two-phase fluid flow and decrease the rate of aqueous fluid flow and cementation. They can also precipitate dolomite nuclei, which can affect the distribution of dolomite as opposed to limestone reservoir rock.

Predicting Reservoirs

Microbial methanogenesis and exsolvation should be common in marine carbonate sediments, especially those with high nutrient levels, temperature between 4 and 60 ^{o}C, anaerobic conditions and high microbial biomass (Noble and Henk, 1998; Suess et al. 2001; Newberry *et al.,*2004; Zhang et al. 2005). Methane exsolvation is even known in low nutrient marine systems with small populations of methanogens, such as Hydrate Ridge (700-900m below the surface), with a population of 10^1 to 10^2 cells ml^{-1} (Suess et al. 2001).

If near-surface methanogenesis aids porosity preservation in dolomite and other carbonate reservoirs, then predicting the distribution of such preserved porosity may require understanding conditions of microbial methanogenesis. Given the proper temperature and anaerobic conditions, microbial methane generation by microorganisms is largely controlled by nutrient availability (Table 2), varying by over four orders of magnitude from as low as 0.06 $fmolcell^{-1}day^{-1}$ for nutrient starved systems and as high as 108-135 $fmolcell^{-1}day^{-1}$ given an excess of nutrients.

CONCLUSIONS

1. This model predicts that methanogens are capable of rapidly generating sufficient $CH_{4(g)}$ to reduce effective hydraulic conductivity of sand sized carbonate sediments by 50% needing only 17% CH_4 gas occluding pore spaces. With conservative estimates of metabolic rates (0.97 to 31.5 $fmolcell^{-1}day^{-1}$) and population density (10^4 $cellsml^{-1}$) this reduction of effective hydraulic conductivity can take place in a short period of time (55 to 1, 800 years).

2. If methanogenesis ceases and is followed by rapid burial, it would take more than 400,000 years to restore the initial effective hydraulic conductivity in the system.

3. Continued methanogenesis during burial could reduce effective hydraulic conductivity to zero after 250 years and remain that way for millions of years until methanogenesis ceases.

4. The two-phase fluid flow system, which reduces the effective hydraulic conductivity, can reduce cementation by reducing transport of necessary cations (Ca, Mg and Si) into the model system. This may explain preservation of porosity in some carbonate reservoirs.

5. While methanogenesis can, and likely does occur, during the early stages of formation of both dolomite and limestone units, there remains a connection between the presence of methanogens and the formation of dolomite. This may explain why, in concert with increased structural resistance to mechanical porosity loss, dolomites in many systems retain more porosity than limestone.

6. Because this mechanism of porosity preservation has potential as a predictive tool, more field work should be conducted to explore what variables control development of two-phase systems due to microbial methanogenesis.

CHAPTER 5. Ni-BEARING IRON OXIDES AS A NUTRIENT SOURCE FOR ARCHAEAL METHANOGENESIS PRIOR TO THE GREAT OXIDATION EVENT AND THE ROLE OF H_2 ON METHANE GENERATION

ABSTRACT

The rise of atmospheric oxygen approximately 2.4 billion years ago has generated a great deal of conjecture as to the geochemical events that preceded such a global event. A dramatic fall in atmospheric methane is an oft-cited cause of this early oxygenation event and the activity of methanogenic microbes is intrinsically tied to the concentration of atmospheric methane. As such, factors affecting the rate of biogenic methane production are consequential to the rise of oxygen during this period. Studies have suggested that a Ni-famine due to cooling mantle temperatures preceding the decrease in methane generation allowed for the Great Oxidation Event. This study uses a model organism, *Methanobacterium thermoautotropicum*, to test the impact of proposed Ni depletion on methane generation rates. Our data demonstrate that varying aqueous Ni concentration (400, 200, 50 and 9 nM Ni) had little impact on methane generation rates (2.86, 2.82, 3.27 and 3.29 mM $cell^{-1}$ $hour^{-1}$ respectively). Furthermore, *M. thermoautotrophicum* was able to generate methane in the presence of Ni-bearing Fe-oxides (400 and 200nM Ni bound in solid Fe-oxides), abundant during this period of oxidation preserved as

Banded Iron Formations. Under these conditions methane was generated at a rate significantly higher than (50-70%) that which was observed in Ni-free controls and total methane generated was comparable (85% of total methane) to cultures with equivalent concentrations of Ni in solution. Hydrogen depletion, also due to mantle cooling as well as diminished volcanic sources of H_2 gas coupled with loss to space is another hypothesis for diminished methanogenesis. Decreasing H_2 concentrations in this study (1.7, 1.4 and 0.3 μM H_2) led to dramatically reduced methane generation rates (1.05×10^{-8}, 7.77×10^{-9} and 2.86×10^{-9} mM $cell^{-1}$ $hour^{-1}$ respectively) for *M. thermoautotrophicum*. These data indicate that a decrease of the vital reductant H_2 is a plausible explanation for the subsequent decrease in biogenic methane in the atmosphere immediately preceding the oxidation of the Earth's atmosphere.

INTRODUCTION

The onset of the Great Oxidation Event (GOE), approximately 2.4 Gyr ago, is one of the most significant events in Earth history, shaping subsequent biogeochemistry and organismal diversity (Sleep and Bird; 2008). Constraining the controls on the increase in oxygen at this time has been a subject of great interest. Modern oxygenic photosynthesis generates oxygen far in excess of modern O_2 sinks and sustains our atmosphere above equilibrium with crustal and mantle rocks (Lovelock, 1979). Molecular fossils of biological lipids confirm the existence of both cyanobacteria and eukaryotes by 2.7 Ga (Brocks *et al.*, 1999; Summons *et al.*, 1999), requiring oxygenic photosynthesis, by cyanobacteria, prior to this time. The discrepancy between the onset of oxygen generating microorganisms and the GOE (~300 million years) can be explained by the presence of O_2 sinks. These sinks include ferrous iron in continental crusts,

reduced submarine volcanic and metamorphic gases and methane in the atmosphere (Kump and Barley, 2007; Sleep and Bird, 2008). The progressive rise of atmospheric oxygen in the atmosphere is believed to have been preceded by a decrease in atmospheric methane (Zahnle *et al.*, 2006). Given the highly reactive relationship between oxygen and methane, removal of atmospheric methane would diminish a significant sink for atmospheric O_2. Biogenic methane would have resulted in an atmospheric methane concentration as high as 10^3 ppmv, as compared to the modern value of 1.7 ppmv (Catling, 2001; Kasting 2005, Zahnle *et al.*, 2006). Modern marine methanogenesis in the low-sulfate zones of the ocean is primarily autotrophic in nature as indicated by having isotopically lighter $\delta^{13}C$ (−110 to −600‰) (Whiticar *et al.*, 1998). Only *Methanosarcina acetivorans* and *Methanosarcina siciliae*, have been isolated from marine environments (Elberson and Sowers, 1997; Ferry and Lessner, 2008). Autotrophic methane is generated as follows:

$CO_2 + 4H_2 \rightarrow CH_4 + 2H_2O$ (Equation 1)

Concentrations of H_2 in the anoxic early atmosphere are thought to be at least of the order of 1000 ppm (Kasting, 1992) as compared to 0.55ppmv today. CO_2 concentrations were also higher than today and sulfate concentrations were lower (>1 mM) (Canfield *et al.*, 2000; Kasting and Siefert, 2002). Due to this excess of H_2 it is likely that the autotrophic mode of methanogenesis was prevalent in the period prior to the oxidation of the Earth. The mechanism by which biogenic methane in the atmosphere diminished prior to the GOE is still a matter of debate. However, a combination of loss due to photolysis (reaction with UV light in the atmosphere)

$CH_4 + CO_2 + h\nu \rightarrow 2CO + 2H$ (Equation 2)

and a reduction in the generation of biogenic methane remains the most probable cause.

Explanations for diminished biogenic methane include an increase in ocean sulfate levels and the resulting proliferation of sulfur reducing bacteria (SRB) (Zahnle *et al.*, 2006). However, an increase in weathering is not supported by the rock record (Scott *et al.*, 2008), including sulfur isotopic data (Papineau *et al.*, 2007), it has been suggested that a significant fall in aqueous Ni concentrations is the cause (Konhauser *et al.*, 2009). Konhauser *et al.* (2009) hypothesized that the Archaean mantle ceased producing the same volume of abundant Ni-rich komatiites and olivine-rich basalts due to mantle cooling and that this cooling resulted in a depletion of aqueous Ni (Nisbet, 1982; Arndt *et al.*, 2008). The same study by Konhauser *et al.* (2009) used experimentally derived Ni- iron oxide co-precipitation coefficients along with banded iron formations (BIFs) ranging from 0.55 to 3.8 Gyr in age as a proxy for aqueous Ni during the Archaean and Proterozoic. Using the concentration of Ni in the ancient BIFs (a sink for aqueous Ni) they were able to approximate the aqueous Ni content of the ocean during this period. They observed a fall off in Ni concentrations over the Archaean-Proterozoic boundary (2.5 Gyr ago) from values as high as 400nM to values as low as 200nM. After this period ocean Ni concentrations continued to decrease to less than 50nM 0.7 Gyr ago, attaining modern values of 9nM (Drever, 2007) at about 0.55 Gyr ago (Konhauser *et al.*, 2009).

While nickel can be toxic to bacteria and fungi in high concentrations (>5 ppm), it is also a critical trace element used by autotrophic methanogens in a number of enzymes including, [NiFe]-hydrogenases, carbon monoxide dehydrogenase, acetyl-CoA synthase/decarbonylase, and methyl-coenzyme M reductase (Jaun and Thauer, 2007). The role of [NiFe]-hydrogenases is to

catalyze the breaking of the strong covalent bond of H_2 (436 $kJmol^{-1}$) in order to autotrophically synthesize methane (Equation 1).

This important first step to methanogenesis is impacted by Ni-limitation with diminished growth and metabolic rates. Limitation, however, has only been demonstrated with Ni(aq) concentrations below 100nM (Schonheit *et al.*, 1979) and over the period of the GOE aqueous Ni concentrations were as high as 200nM (Konhauser *et al.*, 2009). In fact, methanogen populations, though significantly diminished in the modern ocean compared to the ancient, continue to reproduce and metabolize today with only 9nM of aqueous Ni available. If 200nM Ni is sufficient for continued methanogenesis during the GOE it is likely that methane generation rates were controlled by another factor. Because autotrophic methanogenesis consumes four moles of H_2 for every mole of methane generated, a significant decrease in H_2 potentially catastrophic for methane generation prior to the GOE. Therefore in this study we test the hypothesis that the concentration of H_2 is the controlling factor for the rapid loss of atmospheric methane.

Modern atmospheric concentrations of 0.55 ppmv are considerably less than the estimates of H_2 concentration in the Archaean which ranges, with a great deal of contention, from 1000-300000 ppmv (Kasting, 1993; Tian *et al.*, 2005; Catling, 2006; Tian *et al.*, 2006). Loss in atmospheric H_2 is due to a number of reasons including the loss of H_2 gas into space (Hunten, 1993), a shift towards subaerial volcanism rather than submarine, and also includes the same mechanism cited for the reduction in aqueous Ni, mantle cooling (Arndt *et al.,* 2008). Mantle cooling affects hydrogen generation in this case by reducing high temperature serpentinization of the mantle (Barley *et al.*, 1998; Barley *et al.*, 2005):

$2Mg_{1.8}Fe_{0.2}SiO_4 + 2.933H_2O = Mg_{2.7}Fe_{0.3}Si_2O_5\ (OH)_4 + 0.9Mg(OH)_2 + 0.033Fe_3O_4 + \mathbf{0.033H_2}$

(Equation 3)

As mantle temperatures decreased there was decrease in dissolved H_2 for methanogenesis, which coincident with the loss in aqueous Ni.

Jeans escape of H_2 gas from the top of the Earth's atmosphere into space (Hunten, 1993) and a transition from submarine to subaerial volcanism are other factors contributing to a decrease in atmospheric and dissolved H_2. While Jeans escape reflects the loss of H_2 from the atmosphere, and therefore from the system, decreasing submarine volcanism and serpentinization would have had a more immediate effect on autotrophic methanogenesis. Both of these processes not only generate hydrogen but they generate hydrogen in the aqueous phase. Hydrogen generation in the ocean would have eventually migrated excess H_2 to the atmosphere, but would result in more available dissolved H_2 in the ocean. With the cooling mantle and a transition to aerial volcanism that vented its H_2 (g) directly into the atmosphere, autotrophic methanogens came to rely more and more on an overall decreasing flux of dissolved H_2. As such, diminished submarine H_2 production and H_2 to Jeans escape loss over this period would serve to limit H_2 available to methanogens over a period when biogenic methane in the atmosphere was on the decline.

In order to compare the affects of diminished H_2 and Ni on methane generation rates we ran controlled batch experiments using *Methanobacterium thermoautotrophicum*. *M. thermoautotrophicum* is an autotrophic methanogenic Archaea that has been well studied and has been shown to depend on [NiFe]-hydrogenases for methane generation. In the study by Konhauser *et al.* 2009, *M. thermoautotrophicum* was the model organism used in many of the references cited for the Ni-dependence of methanogenesis. *M. thermoautotrophicum* is well

suited for this study because of the broad range of temperature and salinities in which it can thrive, 40 to 75 ^{o}C and 0.01 to 0.65 M NaCl respectively (Zeikus and Wolfe, 1973; Ciulla *et al.*, 1994).

To delineate the role of Ni and H_2 concentrations on the methanogenic productivity over a period of decreasing aqueous nickel and dissolved hydrogen we ran batch reactor experiments with *M. thermoautotrophicum.* In these batch reactors we varied aqueous Ni and dissolved H_2 concentrations while holding the other constant in order to determine their respective effects on methane generation rates. Additionally we added Ni-bearing iron oxides to certain batches as the sole source of Ni. This was to determine if the iron oxides that were used to estimate the concentration of aqueous Ni in the Proterozoic oceans could also be a source of Ni for methanogenesis during periods of Ni-starvation. We expect that despite the proportionately large decrease in aqueous Ni, from 400nM to 50-200nM over the period of the GOE, that methanogenesis will be more inhibited by H_2 concentration. While there is some debate as to the actual atmospheric concentration of H_2 over the GOE, it is certain that during that period a number of conditions contributed to decrease in dissolved H_2, potentially limiting methanogenic metabolism.

METHODS AND MATERIALS

Batch Reactors

Batch reactors were constructed of anaerobic 500ml serum vials with 450ml of headspace, 50 mL of media with varying Ni contents and inoculated with *M. thermoautotrophicum*. All reactors and media were made in glassware cleaned with 20% nitric

acid in order to remove all metal contaminants including Ni and Fe. Initially, cultures of *M. thermoautotrophicum* were grown in a standard Ni-rich (841 nM $Ni_{(aq)}$) autotrophic medium (Appendix B) at 60 ^{o}C. After reaching stationary phase (after 36 hours) these organisms were centrifuged and rinsed (four times) with a Ni-free solution composed of the same formulation as the culture medium but lacking aqueous Ni. The isolated culture pellet was then re-suspended in a medium with a known concentration of Ni to a concentration of 10^8 cells ml^{-1}. These solutions of isolated *M. thermoautotrophicum* and medium were aseptically added to the batch reactors.

In order to test the effects of aqueous Ni concentrations on methane generation by *M. thermoautotrophicum*, reactors were designed as described above with constant H_2 concentration of 0.3 μM and a variety of aqueous Ni concentrations. Concentrations of 9 nM, 200 nM and 400 nM were selected to represent Ni concentrations for modern seawater, Stage 2 and Stage 1 Oceans (as per Konhauser *et al.*, 2009) respectively. In order to test the effect of changing H_2 concentrations on methane generation by *M. thermoautotrophicum*, batch reactors were designed in the same way but with constant $Ni_{(aq)}$ of both 200 and 400 nM and different dissolved H_2 concentrations. These concentrations were 1.7, 1.4 and 0.3 μM H_2.

To determine the ability of *M thermoautotrophicum* to utilize Ni in Ni-bearing iron oxide, batch reactors were designed with Ni-bearing iron oxides as the sole source of Ni and compared to vessels with 841 nM aqueous Ni and control reactors with no aqueous Ni. These Ni-bearing iron oxides were created by mixing 0.01 mM of $FeCl_3$ for every 0.005 mM of $NiCl_2$ x $2H_2O$ and titrated to a pH of 7.5. The resulting precipitate was centrifuged and rinsed 5x with distilled and deionized water, then placed in dialysis tubing and allowed to soak in distilled and deionized water for 2 weeks while refreshing the water solution every 48 hours. The final precipitate was centrifuged and re-suspended in a final solution of distilled and deionized water. In all cases

Methanobaterium thermoautotrophicum was added to a final concentration of 10^8 cell ml^{-1} after headspace equilibrium was reached.

All reactors were incubated at 60 ^oC with agitation until methanogenesis reached stationary phase. Headspace was sampled and analyzed for gas composition every 2 hours. Solutions were analyzed for microbial biomass after 48 hours.

Geochemical analysis

Headspace gas concentrations were assayed using an Agilent Technologies Network GC System 6890N with a Thermal Conductivity Detector. CH_4, H_2 and CO_2 phases in the headspace were separated by running 250 μL samples through an Alltech Hayesep Q 80/100 Packed Column at 90 °C (analytical error for headspace gas measurements was 0.5%).

Biological analysis

Aliquots of 5ml and 10ml of reactor solution were taken for cell counting and dry weight measurements respectively. These were taken at the completion of the methane generation period and compared with the initial concentration of 10^8 cells ml^{-1} of *M. thermoautotrophicum*.

RESULTS

After each experimental reactor reached stationary phase the resulting biomass was compared to the initial biomass. These results identified that under no geochemical conditions was there any observed change in biomass.

The effect of varying $Ni_{(aq)}$ concentrations on methane generation over time with a fixed initial headspace concentration of H_2 at 0.3 μM is illustrated in Figure 1. Under all conditions there is an initial lag phase of approximately 9 hours, followed by a period of exponential

methane generation (from 16 hours to 30.5 hours). Stationary phase is reached after 44 hours generating a net of 1.10 to 1.15 mM methane. Methane generation rates (mM $cell^{-1}$ $hour^{-1}$), calculated from early exponential to late exponential phase (14.5 hour period), are listed in Table 1. There is no noticeable decrease in methane generation rates when the concentration of aqueous Ni decreases from 400 nM to 200 nM, (2.86 and 2.82 mM $cell^{-1}$ $hour^{-1}$ respectively) nor is there a decrease in methane generation rates going from 50 nM or 9 nM (3.27 and 3.29 mM $cell^{-1}$ $hour^{-1}$ respectively). There is a slight increase (15%) in methane generation rate at these lower $Ni_{(aq)}$ levels. This may be a result of an initial addition of slightly higher concentration of H_2 gas in these vessels, 0.35 μM (50 nM and 9 nM $Ni_{(aq)}$) as compared to 0.3 μM H_2 (400 nM and 200 nM $Ni_{(aq)}$). In all cases, cultures metabolizing with aqueous Ni in solution generate methane significantly faster (approximately 3x) than the zero-Ni control, which generated methane at a rate of 1.05 mM $cell^{-1}$ $hour^{-1}$ (Table 1).

Data for methane generation by *M. thermoautotrophicum* in the presence of a Ni-bearing Fe-oxide and 0.3 μM H_2 is shown in Figure 2. The lag phase for *M. thermoautotrophicum* in these batches is closer to that observed for the Ni-free control reactors (approximately 20 hours) followed by an exponential phase from 32.5 hours to 61.5 hours. After reaching stationary phase, after 76 hours, the net generation of methane was approximately 0.91 mM. Data for methane generation rates over the 29 hour exponential phase is given in Table 1. In addition to a longer lag phase (Fig. 2), the rate at which methane was generated was also slower than their non-solid phase counterparts. At 400 nM of Ni present in the solid Fe-oxides, methane generation rates are 55% of those with 400 nM $Ni_{(aq)}$ and for 200 nM Ni in Fe-oxides methane generation is 60% the rate of 200 nM $Ni_{(aq)}$. However methane generation rates over this 29 hour period, using solid phase Ni are considerably higher, 50 to 70% more, than what is observed in

the control, where no Ni is provided either in aqueous or solid phase (Table 1). Additionally while the rate of methane generation is only slightly more than half of that of the aqueous Ni experiments, the Ni-bearing Fe-oxide batches produced a total of approximately 0.91 mM of methane (Figure 2), which is 85% of the total methane generated with 400 and 200 nM of aqueous Ni. These reactor experiments suggest that *M. thermoautotrophicum* can obtain Ni from solid phase Fe-oxides in the absence of aqueous alternatives.

Figure 3 and Table 2 depict the effects of varying headspace hydrogen concentrations on methane oxidation rates. Methane generated over time is illustrated in Figure 3 and shows that after a lag phase similar to that observed in the aqueous Ni batch experiments (approximately 9 hours). *M. thermoautotrophicum* reaches early exponential phase (after 10.5 hours) and continues to generate methane at this rate until late exponential phase (after 28.5 hours) for H_2 concentrations of 1.70 (squares) and 1.40 (circles) μM H_2. Data for 0.3 mM H_2 at 400 nM and 200 nM $Ni_{(aq)}$ from Figure 1 are also plotted (diamonds) for comparison. Unlike increasing $Ni_{(aq)}$ concentrations, increasing $H_{2(g)}$ yielded a significant increase in methane generation rates (Table 2). Similar to the results observed in Figure 1, there is almost no difference between the reactors run with 200 nM $Ni_{(aq)}$ and 400 nM $Ni_{(aq)}$ within the different H_2 concentrations. However, increasing H_2 concentrations from 0.3 μM to 1.4 μM results in methane generation rates increasing from 2.86×10^{-9} to 7.77×10^{-9} mM $cell^{-1}$ $hour^{-1}$ (at 400nM Ni) and from 2.82×10^{-9} to 7.8×10^{-9} mM $cell^{-1}$ $hour^{-1}$ (at 200 nM Ni). A further increase to 1.70 mM H_2 increases the methane generation rates further to 1.05×10^{-8} mM $cell^{-1}$ $hour^{-1}$ (for both 400 and 200 nM Ni). The difference in the total methane generated is clearly visible in Figure 3. Reactors with H_2 concentrations of 0.3 μM, 1.4 μM and 1.70 μM generate 1.1 mM, 1.7 mM and 2.9 mM methane respectively.

DISCUSSION

Methane generated in the absence of any source of Ni in the control batches can be explained by residual Ni-bearing hydrogenases within the culture while initially grown in Ni-rich media. Despite care to use nitric acid washed glassware and nickel free reagents, small amounts of contamination may also be responsible for the methane generation in the control vessels. Even with the residual Ni we observe a significantly lower methane generation rate (1.05×10^{-9} mM $cell^{-1}$ $hour^{-1}$) in the control as compared to any of the experimental vessels. This situation is similar to the supposed evolution from a Ni-rich ocean (400 nM Ni) to one that was somewhat less Ni-rich (50 to 200 nM Ni) over the period of the Great Oxidation Event. The lack of impact on methane generation rate caused by varying aqueous Ni concentrations suggests that that while Ni is necessary for significant methanogenesis, 9 nM of aqueous Ni may be as effective as 400 nM. Mantle cooling, yielded a transition from 400 nM Ni, 2.7 Gyr ago, to 200nM Ni, 2.5 Gyr ago, was rapid on a geologic time scale (~200 Mya). However given generation times measured in hours or days this is an exceptionally long period on the evolutionary scale of microorganisms (Brocks *et al.*, 1999). It may also be argued that over the time period of mantle cooling and the development of a possible Ni-famine, that methanogens which could thrive on limited aqueous Ni were selected over those requiring high concentrations of $Ni_{(aq)}$. This is one explanation for the observation that *M. thermoautotrophicum* is able to adapt to limited Ni concentrations (9 nM) despite Ni-rich growth conditions (840 nM) immediately prior to this transition. There are numerous modern studies that demonstrate that Archaeal methanogens are highly adaptive to a number of changing conditions including temperature, metal concentrations, salinity and nutrient availability (Kotsyurbenko *et al.*, 1996; Schulz *et al.*, 1996; Kawashima *et al.*, 2000; Bruno *et*

al., 2005). As such it is possible that methanogens were able to adapt to limited Ni concentrations which continue to the present day. These results also suggest that H_2 gas may have a more significant impact than the concentration of $Ni_{(aq)}$ on methane generation rates for *M. thermoautotrophicum*, if aqueous Ni is necessary at all.

The novel technique of using molar Ni/Fe ratios preserved in banded iron formations used by Konhauser *et al.*, suggest an alternate source of Ni for methanogens. Prior to lithification Ni-bearing iron oxides could have been high surface area sources of Ni on the ocean floor for methanogenic Archaea. The data in this study indicates that the presence of Ni-bearing iron oxides as the only source of Ni, increases the methane generation rate of *M. thermoautotrophicum* by 50% to 70% above the Ni-free control. Certainly the significantly longer lag period, 10 hours longer than the aqueous Ni vessels, suggest that *M. thermoautotrophicum* required more time to adapt to Ni being available from a solid source. This data also clearly identifies aqueous Ni as a preferred source of Ni for methanogens, generating methane up to twice as fast as their solid-phase counterparts. However, in the complete absence of aqueous Ni, solid-phase Ni present in iron oxides, can provide enough Ni to generate a comparable quantity of methane. Solid phase Ni batch reactors generated 85% of the total methane generated in the batch reactors with an identical concentration of Ni in aqueous phase. Certainly a 15% drop in methane would not explain the significant catastrophic collapse of atmospheric methane observed over the period leading up to the Great Oxidation Event approximately 2.4 Gyr ago.

The effect of changing H_2 concentrations on net methane generation (Fig. 3) and on methane generation rates (Table 2) is striking. Changing the reactor $Ni_{(aq)}$ concentration from 400 nM to 200 nM to simulate what occurred 2.5 Gyr ago, immediately preceding the GOE

(Konhauser *et al.*, 2009), we only see a very small decrease in methane generation (2.86×10^{-9} to 2.82×10^{-9} respectively). However, changing the concentration of H_2 at those concentrations of Ni has a pronounced effect. Increasing from 0.3 to 1.7 mM dissolved H_2 yields a greater than 3-fold increase in methane generation rate. Isotopic studies have demonstrated that methane generated by methanogens is sourced from dissolved H_2 gas (Daniels *et al.*, 1980). Hydrogen gas is highly insoluble (solubility constant = 7.8×10^{-4}) so dissolved hydrogen would be greatly influenced by changes in atmospheric concentrations. Given that the Archaean-Proterozoic atmosphere was CO_2 rich, H_2 gas is the most likely limiting reagent in the autotrophic generation of methane (Equation 1). There is great debate as to whether the Archaean atmosphere contained 30% or 0.3% H_2 gas, based on rates of H_2 generation and whether escape from the thermosphere was energy or diffusion limited (Tian *et al.*, 2005; Catling, 2006; Tian *et al.*, 2006). However, there is little debate that decreasing volcanic flux of H_2 (from an Archaean high of 3×10^{10} cm^{-2} s^{-1} modern levels of 2×10^9 cm^{-2} s^{-1}) and H_2 sourced from mantle serpentinization decreased as the mantle cooled (Barley *et al.*, 1998; Pavlov and Kasting, 2002; Barley *et al.*, 2005; Sleep *et al.*, 2005). Another factor controlling the availability of aqueous H_2 for methanogenesis is the transition observed as volcanism changed from predominantly submarine in the Archaean to submarine/subaerial in the Paleoprotorozoic (Kump and Barley, 2007). H_2 ejected directly into the atmosphere would be limited for submarine methanogenesis by diffusion as opposed to being "bubbled" into the ocean.

CONCLUSIONS

Considering the importance of H_2 as the reductant for methanogenic metabolism and as the source of hydrogen in the methane generated, it is more likely that changes to atmospheric H_2 concentration prompted the dramatic fall of atmospheric methane concentrations. Nickel

limitation as a result of similar mechanisms to reduced H_2 availability (cooling mantle) no doubt exacerbated the situation. However, methanogens continue to thrive today on lower aqueous Ni concentrations than observed during the Great Oxidation Event. Data from this study also suggest that not only could methanogens have adapted to lowered concentrations of aqueous Ni, but can acquire Ni from Ni-bearing iron oxides. Understanding the sources and sinks of dissolved H_2 and how they have changed over time is especially important to understanding the fall of atmospheric methane and rise of oxygen over 2.5 Gyr ago.

M. thermoautotrophicum **10^8 cells ml^{-1}**	**Concentration of aqueous Ni (nM)**	**Concentration of H_2 (μM)**	**Methane generation rate (mM $cell^{-1}$ $hour^{-1}$)**
Control	**0**	**0.3**	**1.05×10^{-9}**
Aqueous Ni	**400**	**0.3**	**2.86×10^{-9}**
Aqueous Ni	**200**	**0.3**	**2.82×10^{-9}**
Aqueous Ni	**50**	**0.3**	**3.27×10^{-9}**
Aqueous Ni	**9**	**0.3**	**3.29×10^{-9}**
Ni in solid iron oxide	**400nM**	**0.3**	**1.56×10^{-9}**
Ni in solid iron oxide	**200nM**	**0.3**	**1.73×10^{-9}**

Table 1. Methane generation rates as a function of Ni concentration and phase. Rate determined from methane generation over a period over early to late exponential phase (see Figure 1 and 2) by populations of M. thermoautotrophicum (10^8 cell ml^{-1}).

M. thermoautotrophicum **10^8 cells ml^{-1}**	**Concentration of aqueous Ni (nM)**	**Concentration of $H_{2(g)}$ (μM)**	**Methane generation rate (mM $cell^{-1}$ $hour^{-1}$)**
Aqueous Ni	**400**	**0.3**	**2.86×10^{-9}**
Aqueous Ni	**200**	**0.3**	**2.82×10^{-9}**
Aqueous Ni	**400**	**1.4**	**7.77×10^{-9}**
Aqueous Ni	**200**	**1.4**	**7.80×10^{-9}**
Aqueous Ni	**400**	**1.7**	**1.05×10^{-8}**
Aqueous Ni	**200**	**1.7**	**1.05×10^{-8}**

Table 2. Methane generation rates as a function of H_2 concentration. Ni is available in aqueous phase. Rate determined from methane generation during early to late exponential phase (see Figure 3) by populations of *M. thermoautotrophicum* (10^8 cell ml^{-1}).

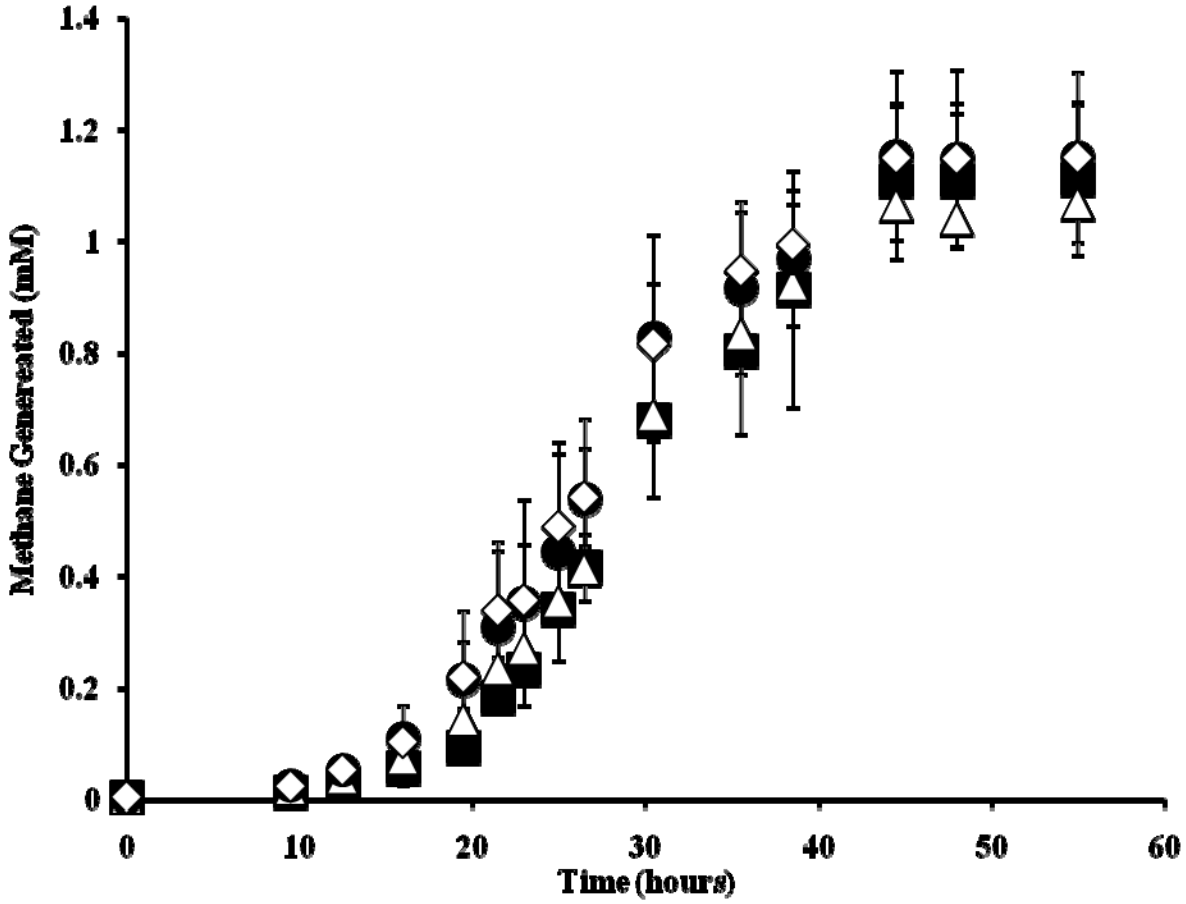
Methane Generated (mM)
1.4
1.2
1
0.8
0.6
0.4
0.2
0
0
10
20
30
40
50
60
Time (hours)

Figure 1.

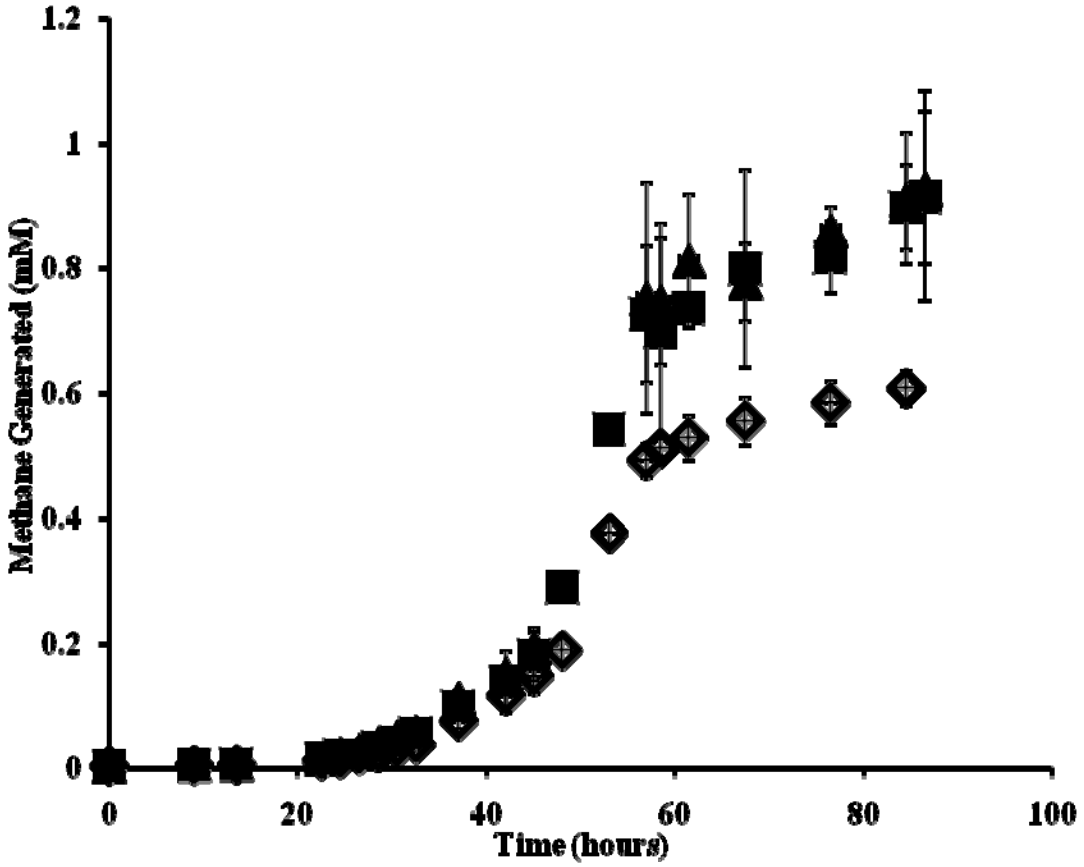
1.2
1
0.8
0.6
0.4
0.2
0
Methane Generated (mM)
0
20
40
60
80
100
Time (hours)

Figure 2.

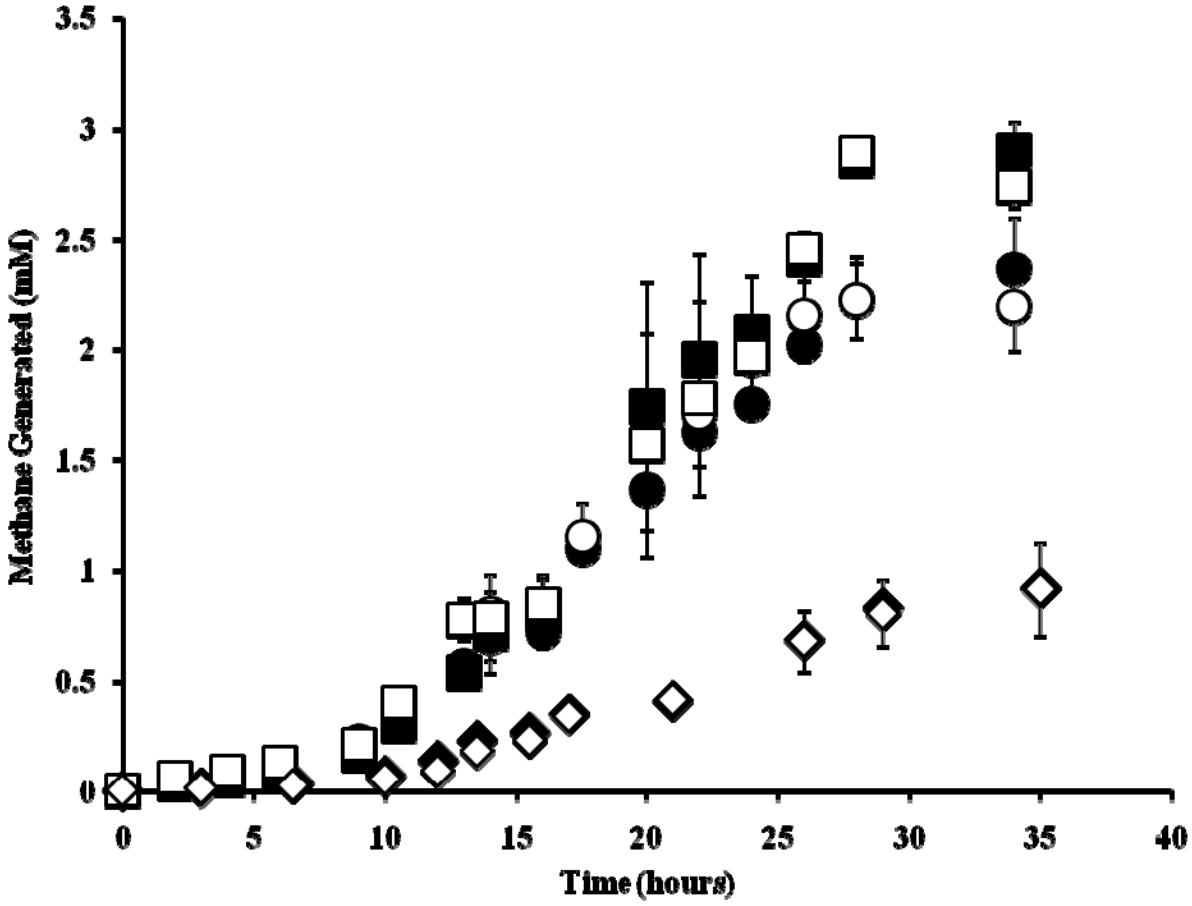
Methane Generated (mM)
3.5
3
2.5
2
1.5
1
0.5
0
0
5
10
15
20
25
30
35
40
Time (hours)

Figure 3.

Figure 1. Total methane generated (mM) as a function of time (hours) and aqueous Ni content by *M. thermoautotrophicum*. Ni concentrations varied from 400 nM (squares), 200 nM (triangles), 50 nM (diamonds) and 9 nM (circles).

Figure 2. Total methane generated (mM) as a function of time (hours) and solid phase Ni content by *M. thermoautotrophicum*. Ni concentrations were either 400 nM (squares) or 200 nM (triangles) available as Ni-bearing Fe-oxides. Control batches were conducted with no Ni provided in aqueous or solid phase (white diamonds).

Figure 3. Total methane generated (mM) as a function of time (hours), aqueous Ni content and H_2 in solution by *M. thermoautotrophicum*. Ni concentrations were either 400 nM (white) or 200 nM (black) while H_2 concentration ranged from 1.7 μM (squares), 1.4 μM (circles) and 0.3 μM (diamonds).

CHAPTER 6. CONCLUSION

Archaeal microorganisms are abundant throughout the Earth and comprise 30% of the microbial biomass in the global oceans (Karner *et al.*, 2001). In this study we have observed how the metabolic processes and cell wall chemistry, especially carboxyl functional group density, of Archaea can supersaturate solutions with respect to dolomite and break down hydration spheres to precipitate high-Mg calcite, disordered dolomite and ordered dolomite. Higher site densities of carboxyl functional groups on the cell wall, particularly the s-layer of certain Archaea like *H. sulfurifontis*, can release and bind Mg^{2+} for the formation of dolomite from $Mg(H_2O)_6$ hydration spheres. Unlike other kinetic inhibitors, such as neutral complexation with SO_4^{2-}, temperature and Mg:Ca ratios, the formation of hydration spheres around Mg^{2+} is ubiquitous in all dolomite forming environments. Therefore the role of carboxyl functional groups in removing these hydration spheres is of universal importance in low-temperature biogenic dolomite nucleation. The role of carboxyl functional groups in overcoming hydration sphere complexation of Mg^{2+} is not limited to Archaea, but may also apply to the exopolymeric substances secreted by other microbes (i.e. sulfur reducing bacteria) associated with dolomite formation. However, it is the ordered structure of the repeating subunits in the s-layer that likely resulted in the observed ordered dolomite in our studies. These ordered dolomite crystals have a greater potential for preservation in their environments and later serve as seed crystals for volumetrically significant dolomite precipitation.

Besides mediating low temperature dolomite precipitation reactions, Archaea are also responsible for producing large volumes of biogenic methane. This large-scale generation of methane can have both regional and global scale impacts on Earth's geochemical cycles. The generation of enormous quantities of biogenic methane has already been identified in a number

of economic methane reservoirs. The effect of copious gas in a porous reservoir is a decrease of effective hydraulic conductivity and a resulting decrease in diagenetic alteration. Because post depositional cementation, along with compaction, is a major factor in the loss of primary porosity with burial, decreasing effective hydraulic conductivity due to 2-phase flow dynamics created by biogenic methane could contribute to the preservation of primary or other early forms of porosity. This study demonstrates that Archaeal methanogens are capable of generating the methane necessary to saturate and exsolve from solution, rapidly occupying pores and pore throats (in 160 years) over a geologically significant timescale with continued methanogenesis (5 million years). The resulting 2-phase flow regime results in loss of effective hydraulic conductivity (87% decrease) and subsequent cementation, which relies heavily on solution transport of ions for mineral precipitation. This loss of effective hydraulic conductivity is resilient with burial, even with the total cessation of further methanogenesis, requiring more than 240, 000 years to recover 100% of the original hydraulic conductivity.

The propensity for methanogenic Archaea to generate copious amounts of CH_4 (g) had a greater impact in the Archaean, potentially inhibiting the oxygenation of the Earth's atmosphere prior to 2.5 billion years ago. The onset of the Great Oxidation Event (GOE) was immediately preceded by a substantial decrease in atmospheric biogenic methane. While a proposed Ni-famine prior to the GOE is unlikely to have had the suggested impact on autotrophic methanogenesis, H_2 limitation over the same period is likely to have resulted in a dramatic reduction in methanogenesis. This suggests that Archaea maintain the ability to seriously alter the atmosphere and life on Earth, if geochemical conditions change to favor their metabolism.

Archaeal microorganisms still represent a largely understudied domain of life, which can have and has had a profound impact on the development of life and mineralogy on Earth.

Important mechanisms, including the chemistry of their cell walls and metabolism, can both actively and passively modify their immediate environment. The results of these changes may persist for millions, even billions, of years either as massive dolomitic mountains, dolomite reservoirs and even the air we breathe.

REFERENCES

Al-Aasm, I.S. and Packard, J.J. (2000) Stabilization of early-formed dolomite: a tale of divergence from two Mississippian dolomites. Sedimentary Geology, 131, 97–108

Alderman, A.R. and Skinner, H.W.C. (1957) Dolomite sedimentation in the south-east of South Australia. American Journal of Science, 255, 561–567.

Arndt, N.T. (1991) High Ni in Archean tholeiites. Tectonophysics, 187, 411–420.

Arvidson, F.S. and Mackenzie, F.T. (1997) Tentative kinetic model for dolomite precipitation rate and its application to dolomite distribution. Aqueous Geochemistry, 2, 273–298.

Badiozamani, K., Mackenzie, F.T. and Thorstenson, D.C. (1977) Experimental carbonate cementation: Salinity, temperature and vadose-phreatic effects: Journal of Sedimentary Petrology, 47, 529-542.

Baedecker, M.J., Cozzarelli, I.M., Siegel, D.I., Bennett, P.C., Eaganhouse, R.P. (1993) Crude oil in a shallow sand and gravel aquifer-III. Biochemical reactions and mass balance modeling in anoxic groundwater. Applied Geochemistry, 8, 569–586.

Baird, A.J. and Waldron, S. (2003) Shallow horizontal groundwater flow in peatlands is reduced by bacteriogenic gas production. Geophysical Research Letters, 30:2043, DOI:2010.1029/2003GL018233

Baker, P.A. and Kastner, M. (1981) Constraints on the formation of sedimentary dolomite. Science, 213, 214–216.

Baker, M.G., Lalonde, S.V., Konhauser, K.O., and Foght, J.M. (2010) Role of extracellular polymeric substances in the surface chemical reactivity of *Hymenobacter aerophilus*, a psychrotolerant bacterium. Applied and Environmental Microbiology, 75, p. 102–109.

Banfield, J.F., Welch, S.A., Zhang, H., Thompsen-Ebert, T., and Penn, R.L. (2000) Aggregation based crystal growth and microstructure development in natural iron oxyhydroxide biomineralization products. Science, 289, 751-754.

Barbieri, R., Stivaletta, N., Marinangeli, L, and Ori, G.G. (2006) Microbial signatures in sabkha evaporite deposits of Chott el Gharsa (Tunisia) and their astrobiological implications. Planetary and Space Science, 54: 726-736.

Barley, M.E., Krapezˇ, B., Groves, D.I. and Kerrich, R. (1998) The Late Archaean bonanza: metallogenic and environmental consequences of the interaction between mantle plumes, lithospheric tectonics and global cyclicity. Precambrian Research, 91, 65–90.

Barley, M.E., Bekker, A. and Krapež, B. (2005) Late Archean to Early Paleoproterozoic global tectonics, environmental change and the rise of atmospheric oxygen. Earth and Planetary Science Letters, 238, 156-171.

Beckwith, C.W. and Baird, A.J. (2001) Effect of biogenic gas bubbles on water flow through poorly decomposed blanket peat. Water Resources Research, 37, 551-558.

Bekins, B.A., Godsy, E.M., and Warren, E. (1999) Distribution of microbial physiologic types in an aquifer contaminated by crude oil. Microbial Ecology, 37, 263–275.

Bennett, P.C., Rogers, J.R., Hiebert, F.K. and Choi, W.J. (2001) Silicates, silicate weathering, and microbial ecology. Geomicrobiology Journal, 18, 3–19.

Benson, R.H., Chapman, R.E. and Deck, L.T. (1984) Paleoceanographic events and deep sea ostracodes. Science, 224, 1334–1336.

Benson, D.J. (1985) Diagenetic controls on reservoir development and quality, Smackover Formation of southwest Alabama. Gulf Coast Association of Geological Societies Transactions, 35, 317-326.

Bethke, C.M. (2008) Geochemical and Biogeochemical Reaction Modeling. Cambridge University Press, Cambridge, UK, 543 p.

Beveridge, T.J. and Murray, R.G.E. (1980) Sites of metal deposition on the cell wall of *Bacillus subtilis*. Journal of Bacteriology. 141, 1438-1448.

Beveridge, T.J. and Koval, S.F. (1981) Binding of metals to cell envelopes of *Escherichia coli* K-12. Applied Environmental Microbiology. 42, 325-335.

Bontognali, T.R.R., Vasconcelos, C., Warthmann, R.J., Dupraz, C., Bernasconi, S.M., and McKenzie, J.A. (2008) Microbes produce nanobacteria-like structures, avoiding cell entombment. Geology, 36, 663-666.

Bosak, T. and Newman, D.K. (2003) Microbial nucleation of calcium carbonate in the Precambrian. Geology, 31, 577-580.

Brady, P.V., Krumhans, J.L., and Papenguth, H.W. (1996) Surface complexation clues to dolomite growth. Geochimica et Cosmochimica Acta, 60, 727-731.

Braissant, O., Decho, W., Dupraz, C., Glunk, C., Przekop, K.M. and Visscher, P.T. (2007) Exopolymeric substances of sulfate-reducing bacteria: Interactions with calcium at alkaline pH and implication for formation of carbonate minerals. Geobiology, 5, 401-411.

Bruno, M.S. Young, J.T. Moghaddam, O. Wongb, H., and Apps J.A. (2005) Thermal treatment, carbon sequestration, and methane generation through deep-well injection of biosolids. Developments in Water Science, 52, 2005, 587-604.

Burns, S.J., McKenzie, J.A., Vasconcelos, C. (2000) Dolomite formation and biochemical cycles in the Phanerozoic. Sedimentology, 47, 49–61.

Butler, R.F., Hervé, F., Munizaga, F., Beck, M.E., Burmester, R.F. and Oviedo, E. (1991) Paleomagnetism of the Patagonian Plateau basalts, southern Chile and Argentina. Journal of Geophysical Research, 96, 6023-6034.

Canfield, D.E., Habicht, K.S., and Thamdrup, B. (2000) The Archean sulfur cycle and the early history of atmospheric oxygen. Science, 288, 658-661.

Canfield D.E. and Farquhar J. (2009) Animal evolution, bioturbation, and the sulfate concentration of the oceans. Proceedins of the National Academy of Science, 106, 8123–8127.

Capo, R.C., Whipkey, C.E., Blachère, J.R., and Chadwick, O.A. (2000) Pedogenic origin of dolomite in a basaltic weathering profile, Kohala peninsula, Hawaii. Geology, 28, 271–274.

Catling, D.C., Zahnle, K.J., and McKay, C.P. (2001) Biogenic methane, hydrogen escape, and the irreversible oxidation of early Earth, Science, 293, 839-843.

Catling, D.C. (2006) Comment on "A Hydrogen-Rich Early Earth Atmosphere". Science, 311, 38.

Chafetz, H.S., and Folk, R.L. (1984) Travertines: depositional morphology and the bacterially constructed constituent. Journal of Sedimentary Petrology, 54, 289-316.

Chan, C.S., De Stasio, G., Welch, S.A., Girasole, M., Frazer, B.H., Nesterova, M.V., Fakra, S., and Banfield, J.F. (2004) Microbial polysaccharides template assembly of nanocrystal fibers. Science, 303, 1656-1658.

Choquette, P.W. and Pray, L.C. (1970) Geologic nomenclature and classification of porosity in sedimentary carbonates. American Association of Petroleum Geologists Bulletin, 54, 207-250.

Ciulla, R. Clougherty, C., Belay, N., Krishnan, S., Zhou, C., Byrd D. and Roberts, M.F. (1994) Halotolerance of *Methanobacterium thermoautotrophicum* delta H and Marburg. Journal of Bacteriology, 176, 3177-3187.

Coates, J.D., Ellis, D.J., Gaw, C.V., and Lovley, D.R. (1999) *Geothrix ferrnentans* gen. nov., sp. nov., a novel Fe(III)-reducing bacterium from a hydrocarbon-contaminated aquifer. International Journal of Systematic Bacteriology 49, 1615–1622.

Coleman, M.L. (1985) Geochemistry of diagenetic nonsilicate minerals, Kinetic considerations. Philosophical Transactions of the Royal Society of London, 315, 39–56.

Colson, J., and Cojan, I. (1996) Groundwater dolocretes in a lake-marginal environment: an alternative model for dolocrete formation in continental settings (Danian of the Provence Basin, France). Sedimentology, 43, 175–188.

Curtis, C.D., Coleman, M.L., and Love, L.G. (1986) Pore water evolution during sediment burial from isotopic and mineral chemistry of calcite, dolomite and siderite concretions. Geochimica et Cosmochimica Acta, 50, 2321-2334.

Dai, J., Song, Y., and Zhang, H. (1996) Main factors controlling the foundation of medium-giant gas fields in China. Science in China Series D: Earth Sciences, 40, 1-10.

Daniels, L. Fulton, G., Spencer, R.W. and Orme-Johnson, W.H. (1980) Origin of hydrogen in methane produced by *Methanobacterium thermoautotrophicum*. Journal of Bacteriology, 141, 694-698.

Daughney, C.J., Fowle, D.A. and Fortin, D. (2001) The effect of growth phase on proton and metal adsorption by *Bacillus subtilis*. Geochimica et Cosmochimica Acta, 65, 1025–1035.

DeLong, E.F. (2003) Oceans of Archaea. American Society for Microbiology News, 69, 503-511

Diekert, G., Weber, B., and Thauer, R.K. (1980) Nickel dependence of factor F430 content in *Methanobacterium thermoautotrophicum*. Archives of Microbiology, 127, 273-277.

Douglas, S. and Beveridge, T.J. (1997) Mineral formation by bacteria in natural microbial communities. FEMS Microbiology Ecology, 26, 79–88.

Drever, J. I. (1988) The Geochemistry of Natural Waters 2nd edn. Prentice Hall, Englewood Cliffs, N.J.

Duan, Z., and Mao, S. (2006) A thermodynamic model for calculating methane solubility, density and gas phase composition of methane-bearing aqueous fluids from 273 to 523 K and from 1 to 2000 bar. Geochimica et Cosmochimica Acta, 70, 3369-3386.

Duan, Z. and Sun, R. (2006) A model to predict phase equilibrium of CH_4 and CO_2 clathrate hydrate in aqueous electrolyte solutions. American Mineralogist, 91, 1346-1354.

Elberson, M.A., and Sowers, K.R. (1997) Isolation of an aceticlastic strain of Methanosarcina siciliae from marine canyon sediments, and emendation of the species description for Methanosarcina siciliae. International Journal of Systematic Bacteriology, 47, 1258-1261.

Elhadj, S., DeYoreo, J.J., Hoyer, J.R. and Dove, P.M. (2006) Role of molecular charge and hydrophobicity in regulating the kinetics of crystal growth. Proceedings of the National Academy of Science, 103, 19237-19242.

El-Sayed, M.I., Fairchild, I.J. and Spiro, B. (1991) Kuwaiti dolocretes: petrology, geochemistry and groundwater origin. Sedimentary Geology 73, 59–75.

Fein, J.B., Daughney, C.J., Yee, N. and Davis, T. (1997) A chemical equilibrium model for metal adsorption onto bacterial surfaces. Geochimica et Cosmochimica Acta, 61, 3319-3328.

Fein, J.B., Martin, A.M. and Wightman, P. G. (2001) Metal adsorption onto bacterial surfaces: development of a predictive approach. Geochimica et Cosmochimica Acta, 65, 4267-4273.

Fetter, C.W. (1999) Contaminant Hydrology, second edition. Prentice Hall, Upper Saddle River, NJ.

Ferry, J.G., and Lessner, D.J. (2008) Methanogenesis in Marine Sediments. In Wiegel, J., R. Maier and M. W. W. Adams (eds.), Incredible Anaerobes: From Physiology to Genomics to Fuels, Annals of the New York Academy of Science, New York, NY. 1125, 147-157.

Folk, R.L., Roberts, H.H., and Moore, C.H. (1973) Black phytokarst from Hell, Cayman Islands, British West Indies. Geological Society of America Bulletin, 84, 2351-2360.

Folk, R.L. (1974) The natural history of crystalline calcium carbonate: effect of magnesium content and salinity. Journal Sedimentary Petrology, 44, 40–53.

Folk, R.L. and Land, L.S. (1975) Mg/Ca ratio and salinity: two controls over crystallization of dolomite. American Association of Petroleum Geologists Bulletin, 59, 60–68.

Fortin, D.F., Ferris, G.F. and Scott, S.D. (1998) Formation of Fe-silicates and Fe-oxides on bacterial surfaces in samples collected near hydrothermal vents on the Southern Explorer Ridge in the northeast Pacific Ocean. American Mineralogist, 83, 1399–1408.

Fowle, D.A. and Fein, J.B. (2001) Quantifying the effects of *Bacillus subtilis* cell walls on the precipitation of copper hydroxide from aqueous solution. Geomicrobiology Journal, 18, 77-91.

Fowle, D.A., Kinnebrew, N., Kenward, P.A., and Roberts, J.A. (in Review) Heavy metal sorption onto a halophilic Archaea. Aquatic Geochemistry.

Froelich, P.N., Klinkhammer, G.P., Bender, M.L., Luedtke, N.A., Heath, G.R., Cullen, D., Hammond, D., Hartman, B. and Maynard, V. (1979) Early oxidation of organic matter in pelagic sediments of the eastern equatorial Atlantic: suboxic diagenesis. Geochimica et Cosmochimica Acta, 43, 1075–1090.

Garen, A., and Echols, H. (1962) Genetic control of induction of alkaline phosphatase synthesis in *E. Coli*. Proceedings of the National Academy of Science, 48, 1398-1402.

Gerke, H.H. and van Genuchten, M.T. (1993) A Dual-Porosity Model for Simulating the Preferential Movement of Water and Solutes in Structured Porous Media. Water Resources Research, 29, 305-319.

Ginsburg, R.N., Marszalek, D.S. and Schneidermann, N. (1971) Ultrastructure of carbonate cements in a Holocene algal reef of Bermuda. Journal of Sedimentary Petrology, 41, 472-482.

Glaser, P.H., Chanton, J.P., Morin, P., Rosenberry, D.O., Siegel, D.I., Ruud, O., Chasar, L.I. and Reeve, A.S. (2003) Surface deformations as indicators of deep ebullition fluxes in a large northern peatland. Global Biogeochemical Cycles, 18, doi:10.1029/2003GB002069

Goldsmith, J.R. and Graf, D.L. (1958) Structural and compositional variations in some natural dolomites. Journal of Geology, 66, 678–693.

González. L.A. and Lohmann, K.C. (1985) Carbon and oxygen isotopic composition of Holocene reefal carbonates. Geology, 13, 811–814.

Hardie, L.A. (1987) Dolomitization: a critical view of some current views. Journal of Sedimentary Petrology, 57, 166–183.

Harvey, R.W., George, L.H., Smith, R.L. and LeBlanc, R.D. (1989) Transport of microspheres and indigenous bacteria through a sandy aquifer: results of natural- and forced-gradient tracer experiments. Environmental Science and Technology, 23, 51-56.

Heytler, P.G. (1980) Uncouplers of oxidation phosphorylation, Pharmacology and Therapeutics, 10, 461-472.

Hooper, P.R. and Hawkesworth, C.J. (1993) Isotopic and geochemical constraints on the origin and evolution of the Columbia River basalts. Journal of Petrology, 34, 1203–1246.

Humphrey, J.D. and Radjef, E.M. (1991) Barbados, West Indies: sedimentary geology, dolomite stoichiometric variability resulting from changing aquifer conditions. Sedimentary Geology, 162, 219–238.

Hunten, D.M. (1993) atmospheric evolution of the terrestrial planets. Science, 259, 915-920

Jones, B.F. (1965) The hydrology and mineralogy of Deep Springs Lake, California. U.S. Geological Survey Professional Paper, 502-A, 56.

Jones B. F. (1966) Geochemical evolution of closed basin water in western Great Basin. Proceedings of the Second Symposium on Salt sponsored by the Northern Ohio Geological Society, 1, 181-200.

Jones, G.D. and Xiao, Y. (2005) Dolomitization, anhydrite cementation and porosity evolution in a reflux system: Insights from reactive transport models. American Association of Petroleum Geologists Bulletin, 89, 577-601.

Jaun, B. and Thauer, R.K. (2007) Nickel and its Surprising Impact in Nature. In Metal Ions in Life Sciences Vol. 2 (eds. Sigel, A., Sigel, H. and Sigel, R.K.O.) Wiley and Sons, 323–356

Kandler, O. and König, H. (1993) Cell envelopes of Archaea: structure and chemistry. In The Biochemistry of Archaea (Archaebacteria) (eds. Kates, M., Kushner, D. J. and Matheson, A.T.). Elsevier, Amsterdam, 223–259.

Kandler, O. and König, H. (1998) Cell wall polymers in Archaea (Archaebacteria). Cellular and Molecular Life Sciences, 54, 305–308.

Kandianis, M.T., Fouke, B.W., Johnson, R.W., Veysey, J. and Inskeep, W.P. (2008) Microbial biomass: A catalyst for $CaCO_3$ precipitation in advection-dominated transport regimes. Geological Society of America Bulletin, 120, 442-450.

Karner, M. B., DeLong, E.F. and Karl, D.M. (2001) Archaeal dominance in the mesopelagic zone of the Pacific Ocean. Nature, 409, 507–510.

Kasting, J.F., and Siefert, J.L. (2002) Life and evolution of Earth's atmosphere. Science, 296, 1066-1068.

Kasting, J.F. (2005) Methane and climate during the Precambrian era. Precambrian Research, 137, 119-129.

Katarzyna, S. (2006) Clogging microstructures in the vadose zone - laboratory and field studies. Hydrogeology Journal, 14, 1005-1017.

Katz, A. and Matthews, A. (1977) Oxygen isotope fractionation during the dolomitization of calcium carbonate. Geochimica et Cosmochimica Acta, 41, 1431–1438.

Katz, A.K., Glusker, J.P., Beebe, S.A. and Bock, C.W. (1996) Calcium ion coordination: a comparison with that of beryllium, magnesium, and zinc. Journal of the American Chemical Society, 118, 5752–5763.

Kawashima, T., Amano, N. Koike, H., Makino, S., Higuchi, S., Kawashima-Ohya, Y., Watanabe, K., Yamazaki, M., Kanehori, K., Kawamotoi, T., Nunoshiba, T., Yamamoto, Y., Aramaki, H., Makino, K., and Suzuki, M. (2000) Archaeal adaptation to higher temperatures revealed by genomic sequence of *Thermoplasma volcanium*. Proceedings of the National Academy of Science, 97, 14257–14262.

Kellner, E. and Waddington, J.M. (2004) Dynamics of biogenic gas bubbles in peat: Potential effects on water storage and peat deformation. Water Resources Research, 41, doi:10.1029/2004WR003732.

Kendall, M.M. and Boone, D.R. (2006) Cultivation of methanogens from shallow marine sediments at Hydrate Ridge, Oregon. Archaea, 2, 31–38.

Kenward, P.A., Goldstein, R.G., Gonzalez, L.A. and Roberts, J.A. (2009) Precipitation of low-temperature dolomite from an anaerobic microbial consortium: the role of methanogenic Archaea. Geobiology, 7, 556-565.

Khalil, M.A.K. and Rasmussen, R.A. (1990) Atmospheric methane: recent global trends.

Environmental Science and Technology, 24, 549–553.

Kitano, Y. (1962) The behavior of various inorganic ions in the separation of calcium carbonate from a bicarbonate solution. Bulletin of the Chemical Society of Japan, 35, 1973–1980.

Kluge, S. and Weston, J. (2005) Can a Hydroxide Ligand Trigger a Change in the Coordination Number of Magnesium Ions in Biological Systems? Biochemistry, 44, 4877–4885.

Kemper, M.A., Urrutia, M.M., Beveridge, T.J., Koch, A.L., and Doyle, R.J. (1993) Proton motive force may regulate cell wall-associated enzymes of Bacillus subtilis. Journal of Bacteriology, 175, 5690-5696.

Koch, A.L. (1986) The pH in the neighborhood of membranes generating a protonmotive force. Journal of Theoretical Biology, 120, 73-84.

Konhauser, K.O. and Ferris, F.G. (1996) Diversity of iron and silica precipitation by microbial mats in hydrothermal waters, Iceland: implications for Precambrian iron formations. Geology, 24, 323–326.

Konhauser, K.O., Pecoits, E., Lalonde, S.V., Papineau, D. Nisbet, E.G., Barley, M.E., Arndt, N.T., Zahnle, K. and Kamber, B.S. (2009) Oceanic nickel depletion and a methanogen famine before the Great Oxidation Event. Nature, 458, 750-753.

Kotsyurbenko, O.R., Nozhevnikova, A.N., Soloviova T.I, and. Zavarzin, G.A. (1996) Methanogenesis at low temperatures by microflora of tundra wetland soil. Antonie van Leeuwenhoek, 69, 75-86, 1996.

Kump, L.R. and Barley, M.E. (2007) Increased subaerial volcanism and the rise of atmospheric oxygen 2.5 billion years ago. Nature, 448, 1033-1036.

Labischinski, H., Barnickel, G., Leps, B., Bradaczek, H. and Giesbrecht, P. (1980) Initial data for the comparison of murein and pseudomurein conformations. Archaeal Microbiology, 127, 195-201.

Land, L.S. (1985) The origin of massive dolomite. Journal of Geological Education, 33, 112–125.

Land, L.S. (1998) Failure to precipitate dolomite at 25°C from dilute solution despite 1000-fold oversaturation after 32 years. Aquatic Geochemistry, 4, 361–368.

Land, L.S. and Hoops, G.K. (1973) Sodium in carbonate sediments and rocks: a possible index to the salinity of diagenetic solutions. Journal of Sedimentary Petrology, 43, 614–617.

Lay, J.J., Miyahara, T. and Noike, T. (1996) Methane release rate and methanogenic bacterial populations in lake sediments. Water Resources, 30, 901-908.

Leps, B., Barnickel, G. and Labischinski, H. (1984) Structural studies on the bacterial cell wall peptidoglycan pseudomurein. I. Conformational energy calculations on the glycan strands in Cl conformation and comparison with murein. Journal of Theorhetical Biology, 107, 85-114.

Leps, B., Labischinski, H., Barnickel, G., Bradaczek, H. and Giesbrecht, P. (1984) A new proposal for the primary and secondary structure of the glycan moiety of pseudomurein. Conformational energy calculations on the glycan strands with talosaminuronic acid in

1C conformation and comparison with murein. European Journal of Biochemistry, 144, 279-286.

Li, Y.Y., and Noike, T. (1992) Upgrading of anaerobic digestion of waste activated sludge by thermal pretreatment: Water Science Technology, v. 26, p. 857–866.

Lippmann F. (1973) Sedimentary Carbonate Minerals. Springer-Verlag.

Lovley, D.R. and Phillips, E.J.P. (1987) Competitive mechanisms for inhibition of sulfate reduction and methane production in the zone of ferric iron reduction in sediments. Applied and Environmental Microbiology, 53, 2636–2641.

Lovley, D.R., Coates, J.D., Saffarini, D. and Lonergan, D.J. (1997) Diversity of dissimilatory Fe (III)-reducing bacteria. In Iron and Related Transition Metals in Microbial Metabolism (eds. Winkelman, G. and Carrano, C.J.). Harwood Academic Publishers, Chur, Switzerland, 187–215.

Lovelock, J.E. (1979) Gaia: A new look at life on Earth. Oxford University Press, Oxford ; New York.

Lucia, J.F. (1997) Carbonate reservoir characterization. Springer-Verlag, Berlin Heidelberg Germany.

Lumsden, D.N. (1988) Characteristics of deep marine dolomite. Journal of Sedimentary Petrology, 58, 1023-1031.

Madigan, M.T. and Martinko, J.M. (2005) Brock Biology of Microorganisms, eleventh edn. Pearson Prentice Hall, Upper Saddle River, NJ.

Mazzullo, S.J. (1977) Diagenesis of the Skinner Ranch Formation (Permian), Glass Mountains (abs.). Geological Society of America Abstracts with Programs, 9, 63.

Mazullo, S.J. (2000) Organogenic dolomitization in peritidal to deep-sea sediments. Journal of Sedimentary Research, 70, 10-23.

Mazzullo, S.J. (2004) Overview of Porosity Evolution in Carbonate Reservoirs. Kansas Geological Society Bulletin, 79.

McKenzie, J.A. (1991) The dolomite problem: an outstanding controversy. In Controversies in Modern Geology. Evolution of Geological Theories in Sedimentology, Earth History and Tectonics (eds. Müller, D.W., Bernoulli, D., McKenzie, J.A. and Weissert, H.). Academic Press, London, pp. 37–54.

McNeill, D.F. (2005) Accumulation rates from well-dated late Neogene carbonate platforms and margins. Sedimentary Geology, 175, 73–87.

Middleburg, J.J., Lange, G.J.D. and Kreulen, R. (1990) Dolomite formation in anoxic sediments of Kau Bay, Indonesia. Geology, 18, 399–402.

Moore, T.S., Murray, R.W. Kurtz, A.C. and Schrag, D.P. (2004) Anaerobic methane oxidation and the formation of dolomite. Earth and Planetary Science Letters, 229,141-154.

Moreira, N.F., Walter, L.M., Vasconcelos, C., McKenzie, J.A. and McCall, P.J. (2004) Role of sulfide oxidation in dolomitization: sediment and pore-water geochemistry of a modern hypersaline lagoon system. Geology, 32, 701–704.

Morrow, D.W., and Ricketts, B.D. (1988) Experimental investigation of sulfate inhibition of dolomite and its mineral analogues. Society of Economical Paleontology Mineralogy, 43, 25-38.

Mualem, Y. (1976) A new model predicting the hydraulic conductivity of unsaturated porous media. Water Resources Research, 12, 513-522.

Müller, D.W., McKenzie, J.A. and Mueller, P.A. (1990) Abu Dhabi sabkha Persian Gulf revisited: application of strontium isotopes to test an early dolomitization model. Geology, 18, 618–621.

Murray, R.C., 1960, Origin or porosity in carbonate rocks: Journal of Sedimentary Research, v. 30, p. 59-84.

Murray, R.C. and Lucia, F.J. (1976) Cause and control of dolomite distribution by rock selectivity. Geological Society of America, 78, 21-36.

Nadson, G.A. (1928) Breitag zur kenntnis der bakteriogenen kalkablagerungen. Archiv fuer Hydrobiologie, 19, 154-164.

Nation, J.L. (1983) A new method using hexamethyldisilazane for preparation of soft insect tissues for scanning electron microscopy. Stain Technology, 58, 347–351.

Neher, J. (1959) Bakterien in tieferliegenden gesteinslagen. Eclogae Geologicae Helvetiae, 52, 619-625.

Nielsen, A.E. (1984) Electrolyte crystal-growth mechanisms. Journal of Crystal Growth, 67, 289-310.

Nisbet, E.G., and Walker, D. (1982) Komatiites and the structure of the Archaean mantle. Earth and Planetary Science Letters, 60, 105-116.

Newberry, C.J., Webster, G., Cragg, B.A., Parkes, J., Weightman, A.J., and Fry, J.C. (2004) Diversity of prokaryotes and methanogenesis in deep subsurface sediments from the Nankai Trough, Ocean Drilling Program Leg 190. Environmental Microbiology, 6, 274-287.

Ngwenya, B.T., Sutherland, T.W., Kennedy, L. (2002) Comparison of the acid-base behavior and metal adsorption characteristics of a gram-negative bacterium with other strains. Applied Geochemistry, 18, 527–538.

Noble, R.A. and Henk Jr. F.N. (1998) Hydrocarbon charge of a bacterial gas field by prolonged methanogenesis: an example from the East Java Sea, Indonesia. Organic Geochemistry, 29, 301-314.

Papineau, D., Mojzsis, S.J. and Schmitt, A.K. (2007) Multiple sulfur isotopes from Paleoproterozoic Huronian interglacial sediments and the rise of atmospheric oxygen. Earth and Planetary Science Letters, 255, 188–212.

Parkes, R. J., Cragg, B. A., Bale, S. J., Getlifff, J. M., Goodman, K., Rochelle, P. A., Fry, J. C., Weightman, A. J. and Harvey, S. M. (1994) Deep bacterial biosphere in Pacific Ocean sediments. Nature, 371, 410-413.

Pavlov, A.A. and Kasting, J.F. (2002) Mass-independent fractionation of sulfur: evidence for an anoxic Archean atmosphere. Astrobiology, 2, 27-41.

Pursar, B.H., Tucker, M.E., and Zenger, D.H., 1994. Problems, progress and future research concerning dolomites and dolomitization. In: Pursar, B., Tucker, M., and Zenger, D.(eds.) *Dolomites: a Volume in Honour of Dolomieu*. Publication of the International Association of Sedimentology, 21: 3-20.

Rancourt, D.G., Thibault, P.J., Mavrocordatos, D., and Lamarche, G. (2005) Hydrous ferrous oxide precipitation in the presence f nonmetabolizing bacteria: constraints on the mechanism of a biotic effect. Geochimica et Cosmochimica Acta, 69, 553-577.

Rao,V.P., Kessarkar, P.M., Krumbein, W.E., Krajewski, K.P. and Schneider, R.J. (2003) Microbial dolomite crusts from the carbonate platform off western India. Sedimentology, 50, 819–830.

Reed, D.W, Y. Fujita, M.E. Delwiche, D.B. Blackwelder, P.P. Sheridan, Takashi T. Uchida, and Colwell, F.S. (2002) Microbial Communities from Methane Hydrate-Bearing Deep Marine Sediments in a Forearc Basin. Applied and Environmental Microbiology, 69, 3759-3770.

Riding, R. (2006) Microbial carbonate abundance compared with fluctuations in metazoan diversity over geological time. Sedimentary Geology, 185, 229-238.

Rivadeneyra, M.A., Martín-Algarra, A., Sánchez-Navas, A. and Martín-Ramos, D. (2006) Carbonate and phosphate precipitation by *Chromohalobacter marismortui*. Geomicrobiology Journal 23, 89–101.

Roberts, J.A., Bennett, P.C., Gonzalez, L.A., Macpherson, G.L., and Milliken, K.L. (2004) Microbial precipitation of dolomite in methanogenic groundwater. Geology, 32, 277–280.

Roden, E.E. and Wetzel, R.G. (1996) Organic carbon oxidation and suppression of methane production by microbial Fe (III) oxide reduction in vegetated and unvegetated freshwater wetland sediments. Limnology and Oceanography, 41, 1733–1748.

Sánchez-Román, M., Vasconcelos, C., Schmid, T., Dittrich, M., McKenzie, J.A., Zenobi, R., Rivadeneyra, M.A. (2008) Aerobic microbial dolomite at the nanometer scale: implications for the geologic record. Geology, 36, 879–882.

Sánchez-Román, M., McKenzie, J.A., Wagener, A., Rivadeneyra, M.A. and Vasconcelos, C. (2009) Presence of sulfate does not inhibit low-temperature dolomite formation. Earth and Planetary Science Letters, 285, 131-139.

Sayles, F.L., and Fyfe, W.S., (1973) The crystallization of magnesite from aqueous solution. Geochimica Cosmochimica Acta 37, 87-99.

Schmoker, J.W., and Halley, R.B. (1982) Carbonate Porosity Versus Depth: A Predictable Relation for South Florida. American Association of Petroleum Geologists Bulletin, 66, 2561 – 2570.

Schmoker, J.W., Krystinik, K.B., and Halley, R.B. (1985) Selected characteristics of limestone and dolomite reservoirs in the United States. American Associations of Petroleum Geologists Bulletin, 69, 733-741.

Schönheit, P., Moll, J. and Thauer, R.K. (1979) Nickel, cobalt, and molybdenum requirement for growth of *Methanobacterium thermoautotrophicum*. Archives of Microbiology, 123, 105-107.

Schulz, S. Matsuyama, H., and Conrad, R. (1997) Temperature dependence of methane production from different precursors in a profundal sediment (Lake Constance). FEMS Microbiology Ecology, 22, 207-213.

Schultze-Lam, S., Fortin, D., Davis, B.S., Beveridge, T.J. (1996) Mineralization of bacterial surfaces. Chemical Geology, 132, 171–181.

Scott, C. Lyons, T.W., Bekker, A., Shen, Y., Poulton, S.W., Chu, X. and A. D. Anbar, A.D. (2008) Tracing the stepwise oxygenation of the Proterozoic ocean. Nature, 452, 456–459.

Sibley, D.F., Dedoes, R.E., and Bartlett, T.R. (1987) The kinetics of dolomitization. Geology, 15, 1112-1114.

Siegel, F.R. (1961) Factors influencing the precipitation of dolomite. Kansas Geological Survey Bulletin, 152, 127-158.

Skolasiska, K. (2006) Clogging microstructures in the vadose zone-laboratory and field studies. Hydrogeology Journal, 14, 1005-1017.

Slaughter, M. and Hill, R.J. (1991) The influence of organic matter in organogenic dolomitization. Journal of Sedimentary Petrology, 61, 296–303.

Sleytr, U.B. and Messner, P. (1988) Crystalline Surface Layers in Procaryotes. Journal Of Bacteriology, 170, 2891-2897.

Sleep, N.H., Meibom, A., Fridriksson, Th., Coleman, R.G. and D. K. Bird, D.K., (2005) H_2-rich fluids from serpentinization: Geochemical and biotic implications. Proceedings of the National Academy of Science, 101, 12818–12823.

Sleep, N.H., and Bird, D.K. (2008) Evolutionary ecology during the rise of dioxygen in the Earth's atmosphere. Philosophical Transactions of the Royal Society of London B Biological Sciences, 363, 2651-2664.

Smith, K.A., Ball, T., Conen, F., Dobbie, K.E., Massheder, J. and Rey, A. (2003) Exchange of greenhouse gases between soil and atmosphere: interactions of soil physical factors and biological processes. European Journal of Soil Science, 54, 779-791.

Sokolov, I., Smith, D.S., Henderson, G.S., Gorby, Y.A. and Ferris, F.G. (2001) Cell surface electrochemical heterogeneity of the Fe(III)-reducing bacteria *Shewanella putrefaciens*. Environmental Science and Technology, 35, 341–347.

Sowers, K. and Anderson, K. (2007) Molecular genetics of Archaea. In Archaea: molecular and cellular biology (ed. Cavicchioli, R.). ASM Press, Washington D.C.

Speece, R.E., Parkin, G.F., and Gallagher, D. (1983) Nickel stimulation of anaerobic digestion. Water Research, 17, 677-683.

Stephenson, A.E., DeYoreo, J.J., Wu, L., Wu, K.J., Hoyer, J. and Dove, P.M. (2008) Peptides enhance magnesium signature in calcite: Insights into origins of vital effects. Science, 322, 724–727.

Stookey, L.L. (1970) Ferrozine-A new spectrophotometric reagent for iron. Analytical Chemistry 42, 779–781.

Suess, E., Torres, M.E., Bohrmann, G., Collier, R.W., Rickert, D., Goldfinger, C., Linke, P., Heuser, A., Sahling, H., Heeschen, K., Jung, C., Nakamura, K., Greinert, J., Pfannkuche, O., Trehu, A., Klinkhammer, G., Whiticar, M.J., Eisenhauer, A., Teichert, B., and Elvert, M. (2001) Sea floor methane hydrates at Hydrate Ridge, Cascadia Margin. In Natural Gas Hydrates: Occurrence, Distribution, and Detection (eds. Paul, C.K. and Dillon, W.P.). American Geophysical Union, Geophysical Monograph Series, v. 124.

Summons, R.E., Jahnke, L.L., Hope, J.M., and Logan, G.A. (1999) 2-Methylhopanoids as biomarkers for cyanobacterial oxygenic photosynthesis. Letters to Nature, 400, 554-557.

Sun, R., and Duan, Z. (2005) Prediction of CH_4 and CO_2 hydrate phase equilibrium and cage occupancy from ab initio intermolecular potentials. Geochimica et Cosmochimic Acta, 69, 4411-4424.

Takeshi, Y., Hiromasa, K. and Kazue, T. (2000) Crystal growth of calcite in microbial mats in hot springs is controlled by microorganisms. Journal of the Geological Society of Japan, 106, 548–559.

Thauer, R.K. (1998) Biochemistry of methanogenesis: a tribute to Marjory Stephenson. Microbiology, 144, 2377–2406.

Tian, F., Toon, O.B., Pavlov A.A. and De Sterck, H. (2005) A Hydrogen-Rich Early Earth Atmosphere. Science, 308, 1014-1017.

Tian, F., Toon, O.B. and Pavlov A.A. (2006) Response to Comment on "A Hydrogen-Rich Early Earth Atmosphere". Science, 311, 38

Tommaso, D.D. and de Leeuw, N.H. (2008) The Onset of Calcium Carbonate Nucleation: A Density Functional Theory Molecular Dynamics and Hybrid Microsolvation/Continuum Study. Journal of Physical Chemistry B, 112, 6965–6975.

Turner, B.F. and Fein, J.B. (2006) Protofit: A program for determining surface protonation constants from titration data. Computers and Geosciences, 32, 1344-1356.

van Genuchten, M.T. (1980) A closed-form equation for predicting the hydraulic conductivity of unsaturated soils. Soil Science Society of America Journal, 44, 892-898.

van Lith, Y., Wathmann, R., Vasconcelos, C. and McKenzie, J.A. (2002) Microbial fossilization in carbonate sediments: a result of the bacterial surface involvement in dolomite precipitation. Sedimentology, 50, 237–245.

van Lith, Y., Warthmann, R., Vasconcelos, C., and McKenzie, J.A. (2003) Sulphate-reducing bacteria induce low-temperature Ca-dolomite and high Mg-calcite formation. Geobiology, 1, 71-79.

Vandevivere, P. and Bevaye, P. (1993) Improved preservation of bacterial exopolymers for scanning electron microscopy. Journal of Microscopy, 167, 323–330.

Vargas, M., Kashefi, K., Blunt-Harris, E.L. and Lovley, D.R. (1998) Microbiological evidence for Fe (III) reduction on early Earth. Nature, 395, 65–67.

Vasconcelos, C., McKenzie, J.A., Warthmann, R. and Bernasconi, S.M. (2005) Calibration of the $\delta^{18}O$ paleothermometer for dolomite precipitated in microbial cultures and natural environments. Geology, 33, 317–320.

Vasconcelos, C. and McKenzie, J.A. (1997) Microbial mediation of modern dolomite precipitation and diagenesis under anoxic conditions, Lagoa Vermelha, Rio de Janeiro, Brazil. Journal of Sedimentary Research, 67, 378–390.

Vasconcelos, C., McKenzie, J.A., Bernasconi, S., Grujic, D., and Tien, A.J. (1995) Microbial mediation as a possible mechanism for natural dolomite formation at low temperatures. Nature, 377, 220–222.

Warthmann, R., van Lith, Y., Vasconcelos, C., McKenzie, J.A. and Karpoff, A.M. (2000) Bacterially induced dolomite precipitation in anoxic culture experiments. Geology, 28, 1091–1094.

Wellsbury, P., Mather, I. and Parkes, R.J. (2002) Geomicrobiology of deep, low organic carbon sediments in the Woodlark Basin, Pacific Ocean. FEMS Microbiology Ecology, 42, 59–70.

Whipkey, C.E., Capo, R.C., Hsieh, J.C.C. and Chadwick, O.A. (2002) Development of magnesian carbonates in Quaternary soils on the Island of Hawaii. Journal of Sedimentary Research, 72, 158–165.

Whiticar, M.J., Faber, E. and Schoell. M. (1986) Biogenic methane formation in marine and freshwater environments: CO2 reduction vs. acetate fermentation—isotope evidence. Geochimica et Cosmochimica Acta, 50, 693-709.

Wood, J.R., and Hewett, T.A. (1982) Fluid convection and mass transfer in porous sandstones-a theoretical model. Geochimica et Cosmochimica Acta, 46, 1707-1713.

Wright, D. (1999) The role of sulfate-reducing bacteria and cyanobacteria in dolomite formation in distal ephemeral lakes of the Coorong region, South Australia. Sedimentary Geology, 126, 147–157.

Wright, D.T. and Wacey, D. (2004) Sedimentary dolomite – a reality check. In The Geometry and Petrogenesis of Dolomite Hydrocarbon Reservoirs (eds. Braithwaite, C.J.R., Rizzi, G. and Darke G). Geological Society Special Publication, 235, 65–74.

Wright D.T. and Wacey, D. (2005) Precipitation of dolomite using sulphate-reducing bacteria from the Coorong Region, South Australia: significance and implications. Sedimentology, 28, 987–1008

YongSheng, M.A, TongLou, G., XueFeng, Z. and XunYu, C. (2008) The formation mechanism of high-quality dolomite reservoir in the deep of Puguang Gas Field. Science in China Series D: Earth Sciences, 51, 53-64.

Yu, W., Dodds, W.K., Banks, K., Skalsky, J. and Strauss, E.A. (1995) Optimal staining and sample storage time for direct microscopic enumeration of total and active bacteria in soil with two fluorescent dyes. Applied and Environmental Microbiology, 61, 3367-3372.

Zahnle, K.J., Claire, M.W. and Catling, D.C. (2006) The loss of mass-independent fractionation of sulfur due to a Paleoproterozoic collapse of atmospheric methane. Geobiology 4, 271–283.

Zeikus, J.G. and Wolfe. R.S. (1973) Fine structure of Methanobacterium thermoautotrophicum:

effect of growth temperature on morphology and ultrastructure. Journal of Bacteriology, 113,461-467.

Zhang, X., Song, C., Duan, Y.Q., Li, X., Ma, L. and Zhang, M. (2005) Methanogenic pathway of the Quaternary biogenic gases in the Qaidam Basin, China. Geochemical Journal, 39, 411-416.

Zhong, S. and Mucci, A. (1989) Calcite and aragonite precipitation from seawater solutions of various salinities: precipitation rates and overgrowth compositions. Chemical Geology, 78, 283-299.

APPENDICES

APPENDIX A

CHARACTERIZATION AND POTENTIAL MECHANISM OF FORMATION FOR PLATY CRYSTAL AGGREGATES (PCAs) OF BIOGENIC DOLOMITE

In the study by Kenward *et al.* 2009, microbially induced precipitation of ordered dolomite crystals were observed in direct association with the individual cells and their putative EPS (Chapter 2, Figure 4). However the precipitation of thin (0.1-0.2 μm thick), rhombohedral plates that grew together to form widespread aggregates (25-50 μm) coating basalt grains was the predominant morphology in these reactor experiments (Appendix Figure C1-C4). This section describes this morphology and proposes a mechanism of formation for these important high surface area dolomites that may act as nucleation sites for further growth of massive dolomites. The scanning electron micrographs in this section were acquired from reactor vessels designed using 40 mL of anaerobic groundwater from the petroleum-contaminated aquifer near Bemidji, MN. These microcosms contained the native microbial consortium extracted from 10 g of aquifer sediment consisting of dissimilatory iron reducers, fermenting bacteria and methanogenic Archaea (Bekins *et al.,* 2009). SEM images were acquired from those samples that had already started forming dolomite (after 90 days).

Using powdered X-ray diffraction (XRD) we determined that dolomite was present in these systems containing the platy crystal aggregates PCAs. In order to verify that these aggregates are the dolomites detected we used energy dispersive spectroscopy (EDS) to generate elemental maps of the scanning electron micrograph seen in Appendix Figure C1. The SEM image in Appendix Figure C1 depicts the edges of two basalt grains coated in PCAs of dolomite (flat raised areas) and ringed by EPS. In the space between the two grains are several microorganisms of the consortium. Elemental scans for carbon, oxygen, calcium and magnesium were conducted to determine if the PCAs possessed the necessary chemistry to be dolomite. The scans for carbon and oxygen were ubiquitously distributed amongst the PCAs, microbes and their EPS. Appendix Figure C2 and C3 show the same field of view as C1 with areas of high densities of calcium (blue) and magnesium (yellow) respectively. EDS scans for calcium (Appendix Figure C2) show highest concentration of calcium concentrated in the areas of PCAs and sparsely amongst the microbes. Magnesium is also most concentrated along the PCAs, but is more ubiquitously distributed amongst the biomass (Appendix Figure C3). While this meets the criterion for dolomite, $CaMg(CO_3)_2$, additional elemental scans were run for iron and silica to determine if the aggregates were perhaps silicates or ferroan dolomite. Appendix Figure C4 shows that silicon is not associated with the PCAs on the basalt surface and are not simply Mg and Ca rich platy silicates. The absence of iron (yellow) associated with the PCAs (Appendix Figure C5) confirms that this Mg-bearing carbonate is not ferroan. The iron and silica in the system, not associated with the basalt, appears to be bound up by the cell walls of the microbes and their EPS.

The thin dolomite rhombohedra growing together in Figure 4 of Kenward *et al.* 2009 and in Appendix Figure C1 to C5 illustrate a mature surface of the PCAs. Those observed in Appendix Figure C6 represent an earlier stage while maturation is in progress. Appendix Figure C1 depicts a small circular surface (~2 μm in diameter) and a ring of desiccated (EPS) enclosing it (A). This early stage formation of PCA can be identified as immature by two features: microporosity visible in the core of the aggregate (B) and early crystal-crystal contacts (C). The circled area illustrates an example of crystal ripening, where the microporous core contacts well ripened rhombohedra. Ripening occurs from the perimeter inwards until well formed rhombohedra are seen growing into contact with each other (C).

The size of the PCA in Appendix Figure C1 is controlled by the size of the basalt grain on which the microorganisms were colonizing. Appendix Figure C7 identifies two much larger surfaces showing ripened PCAs coating larger basalt grains. Examples of these dolomite coated basalt surfaces are common in the reaction vessels and range in size from 2 to 50 μm in length. Note the significant mass of microorganisms dominating the lower right hand corner of the SEM image. This, along with the desiccated EPS surrounding and coating the sides (Chapter 2, Figure 4) of these dolomite coated surfaces, reinforces the biogenic origin of these PCAs. It is also likely that the platy morphology, a result of growth in two planes only, was also controlled by the colonies of microorganisms.

Appendix Figure E4 is a model diagram of how the PCA forms in contact with the consortium of microbes populating the basalt grains. In the first stage microbes populate the basalt grain and secrete EPS to coat the grain surface completely (A). This is followed by the precipitation of dolomite on the cell walls and other organic surfaces (EPS) with high carboxyl functional group densities (B). Over time through continued mineralization and replacement a thin layer of microporous dolomite forms. This is followed by the continued colonization of the mineral surface and further deposition of EPS over the microporous dolomite (C). The final phase is the ripening step which leads to the formation of thin rhombohedra of dolomite which grow together to form PCAs (D). The last image (E) is what these surfaces look like after desiccation during preservation for SEM, when the EPS has retracted to the edges of the mineral.

The formation of the PCAs of dolomite provides a high surface area to volume crystals of ordered dolomite. These areas, when precipitated over a large area, can serve as seed crystals for the abiotic precipitation of massive dolomites.

APPENDIX B

Media Recipes

Recipe B1: *Bacillus subtilis*: Tryptic Soy Broth (TSB)

Ingredients:

Yeast extract…….5g

TSB (powder)…….30g

Distilled deionized water…….1L

Mix all the ingredients except and autoclave for 15 minutes

Recipe B2: *Shewenella putrefaciens*: Tryptic Soy Broth (TSB)

Ingredients:

Yeast extract…….5g

TSB (powder)…….30g

Distilled deionized water…….1L

Mix all the ingredients except and autoclave for 15 minutes

Recipe B3: *Methanobacterium formicicum*: ATCC medium1045

Mineral Solution 1:

K_2HPO_4 .....6.0 g

Distilled water.....1.0 L

Mineral Solution 2:

KH_2PO_4 .....6.0 g

$(NH_4)_2SO_4$.....6.0 g

NaCl.....12.0 g

$MgSO_4$ $7H_2O$ .....2.4 g

$CaCl_2$ $2H_2O$ .....1.6 g

Distilled water.....1.0 L

Sodium Carbonate Solution:

Na_2CO_3 .....8.0 g

Distilled water.....100.0 ml

Reducing Agent:

Add 300 mg L-Cysteine HCl to 10 ml of water and 300 mg Na_2S $9H_2O$ to a second 10 ml of water: tube under nitrogen gas. After autoclaving at 121C for 15 minutes under fast exhaust and allowing it to cool, mix equal amounts of the cysteine and the sodium sulfide (under nitrogen). The mixture should be clear and can be kept for up to two weeks. Prepare the complete medium by mixing the above components in the following proportions:

83.5 parts of distilled water

5.0 parts of Mineral Solution 2

2.5 parts of Mineral Solution 1

5.0 parts of 8.0% Na_2CO_3 Solution

1.0 part of Wolfe's Mineral Solution (see below)

1.0 part of Wolfe's Vitamin Solution (see below)

2.0 parts of Cysteine-Sulfide Reducing Agent

Wolfe's Mineral Solution:

Nitrilotriacetic acid.....1.5 g

$MgSO_4$ $7H_2O$ .....3.0 g

$MnSO_4$ H_2O .....0.5 g

NaCl.....1.0 g

$FeSO_4$ $7H_2O$ .....0.1 g

$CoCl_2$ $6H_2O$ .....0.1 g

$CaCl_2$ .....0.1 g

$ZnSO_4$ $7H_2O$ .....0.1 g

$CuSO_4$ $5H_2O$ .....0.01 g

$AlK(SO_4)_2$ $12H_2O$.....0.01 g

H_3BO_3.....0.01 g

Na_2MoO_4 $2H_2O$….....0.01 g

Distilled water.....1.0 L

Wolfe's Vitamin Solution

Biotin.....2.0 mg

Folic acid.....2.0 mg

Pyridoxine hydrochloride.....10.0 mg

Thiamine HCl….....5.0 mg

Riboflavin.....5.0 mg

Nicotinic acid.....5.0 mg

Calcium D-(+)-pantothenat.....5.0 mg

Vitamin B12.....0.1 mg

p-Aminobenzoic acid.....5.0 mg

Thioctic acid.....5.0 mg

Distilled water.....1.0 L

Mix all the ingredients except the Wolfe's Vitamin and Cysteine/Na_2S Solutions. After autoclaving for 15 minutes, allow the solution to cool under 80% N_2, 20% CO_2. Then add the sterile Wolfe's Vitamin Solution, then Cysteine/Na_2S Solution (via filter syringe). Adjust pH to 7.2 if necessary and tube anaerobically, aseptically.

Recipe B4: *Haloferax sulfurifontis*: ATCC medium

Recipe B5: *Methanobacterium thermoautotrophicus*: ATCC medium

Mineral Solution 1:

K_2HPO_4 .....6.0 g

Distilled water.....1.0 L

Mineral Solution 2:

KH_2PO_4 .....6.0 g

$(NH_4)_2SO_4$.....6.0 g

NaCl.....12.0 g

$MgSO_4$ $7H_2O$ .....2.4 g

$CaCl_2$ $2H_2O$ .....1.6 g

Distilled water.....1.0 L

Sodium Carbonate Solution:

Na_2CO_3 .....8.0 g

Distilled water.....100.0 ml

Reducing Agent:

Add 300 mg L-Cysteine HCl to 10 ml of water and 300 mg Na_2S $9H_2O$ to a second 10 ml of water: tube under nitrogen gas. After autoclaving at 121C for 15 minutes under fast exhaust and allowing it to cool, mix equal amounts of the cysteine and the sodium sulfide (under nitrogen). The mixture should be clear and can be kept for up to two weeks. Prepare the complete medium by mixing the above components in the following proportions:

83.5 parts of distilled water

5.0 parts of Mineral Solution 2

2.5 parts of Mineral Solution 1

5.0 parts of 8.0% Na_2CO_3 Solution

1.0 part of Trace Elements Solution (see below)

1.0 part of Wolfe's Vitamin Solution (see below)

2.0 parts of Cysteine-Sulfide Reducing Agent

Wolfe's Vitamin Solution

Biotin.....2.0 mg

Folic acid.....2.0 mg

Pyridoxine hydrochloride.....10.0 mg

Thiamine HCl.….....5.0 mg

Riboflavin.....5.0 mg

Nicotinic acid.....5.0 mg

Calcium D-(+)-pantothenat.....5.0 mg

Vitamin B12.....0.1 mg

p-Aminobenzoic acid.....5.0 mg

Thioctic acid.....5.0 mg

Distilled water.....1.0 L

Trace Elements Solution:

Nitrilotriacetic acid.....12.8 g

$FeCl_3$ $6H_2O$….....1.35 g

$MnCl_3$ $4H_2O$ ….....0.1 g

$CaCl_2$ $2H_2O$ .....0.1 g

$ZnCl_2$.....0.1 g

H_3BO_3 .....0.01 g

NaCl.....1.0 g

$NiCl_2$ $6H_2O$ .....0.15 g

$AlCl_3$ $6H_2O$ .....0.05 g

$CoCl_2$ $6H_2O$ .....24.0 mg

$CuCl_2$ $2H_2O$ .....25.0 mg

Na_2MoO_4 $2H_2O$.....24.0 mg

Na2SeO4 6H2O.....26.0 mg

Distilled water.....1.0 L

Mix all the ingredients except the Wolfe's Vitamin and Cysteine/Na_2S Solutions. After autoclaving for 15 minutes, allow the solution to cool under 80% N_2, 20% CO_2. Then add the sterile Wolfe's Vitamin Solution, then Cysteine/Na_2S Solution (via filter syringe). Adjust pH to 7.2 if necessary and tube anaerobically, aseptically.

APPENDIX C

SEM IMAGES

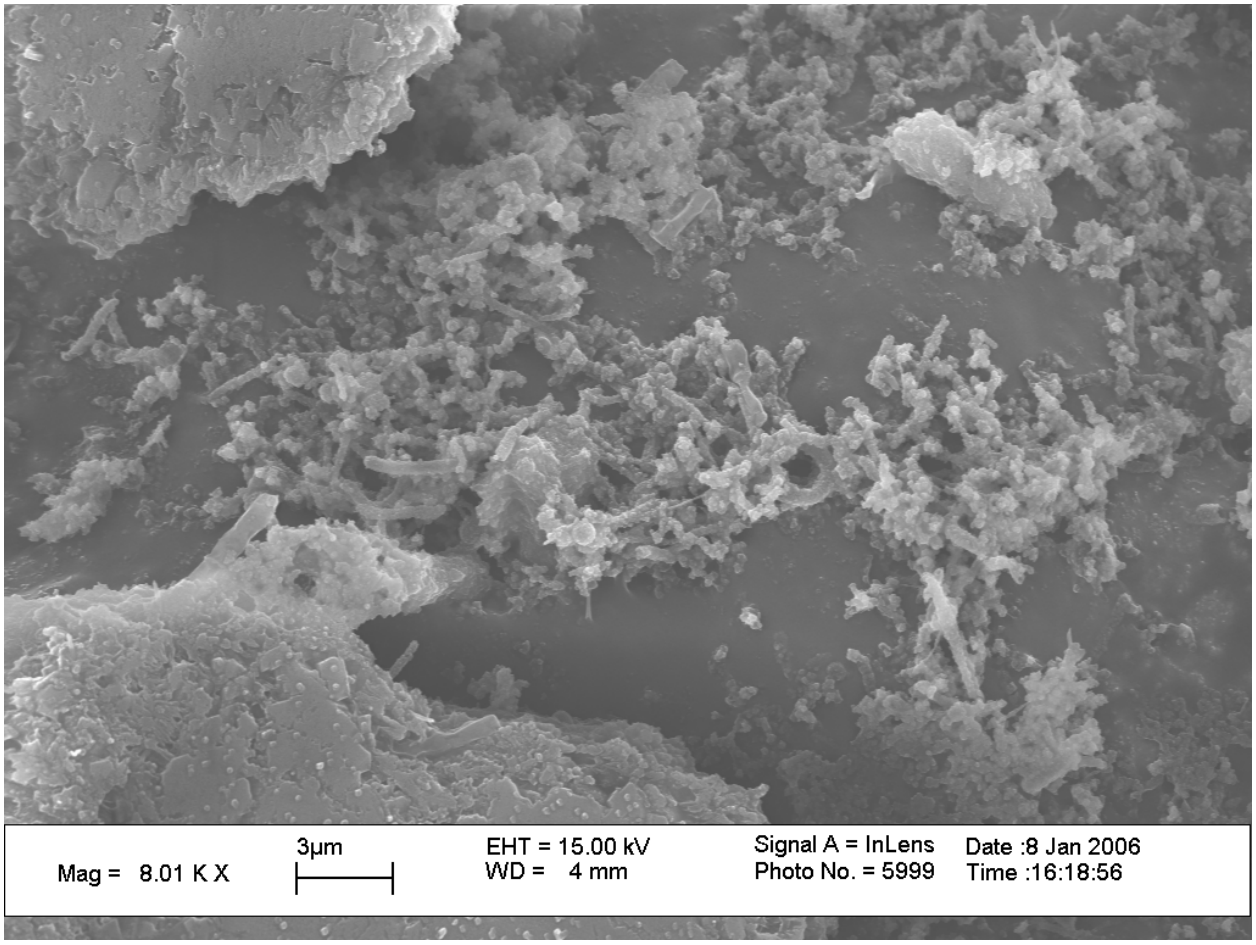

Figure C1: Scanning electron micrograph of the area used for elemental mapping (Figures C2, C3, C4 and C5). Platy aggregates of dolomite crystals have developed on the basalt grains in the top left and lower left corners. A consortium of microorganisms occupies the space between the crystal aggregates. Sample was taken from the Bemidji consortium batch experiments (Chapter 2).

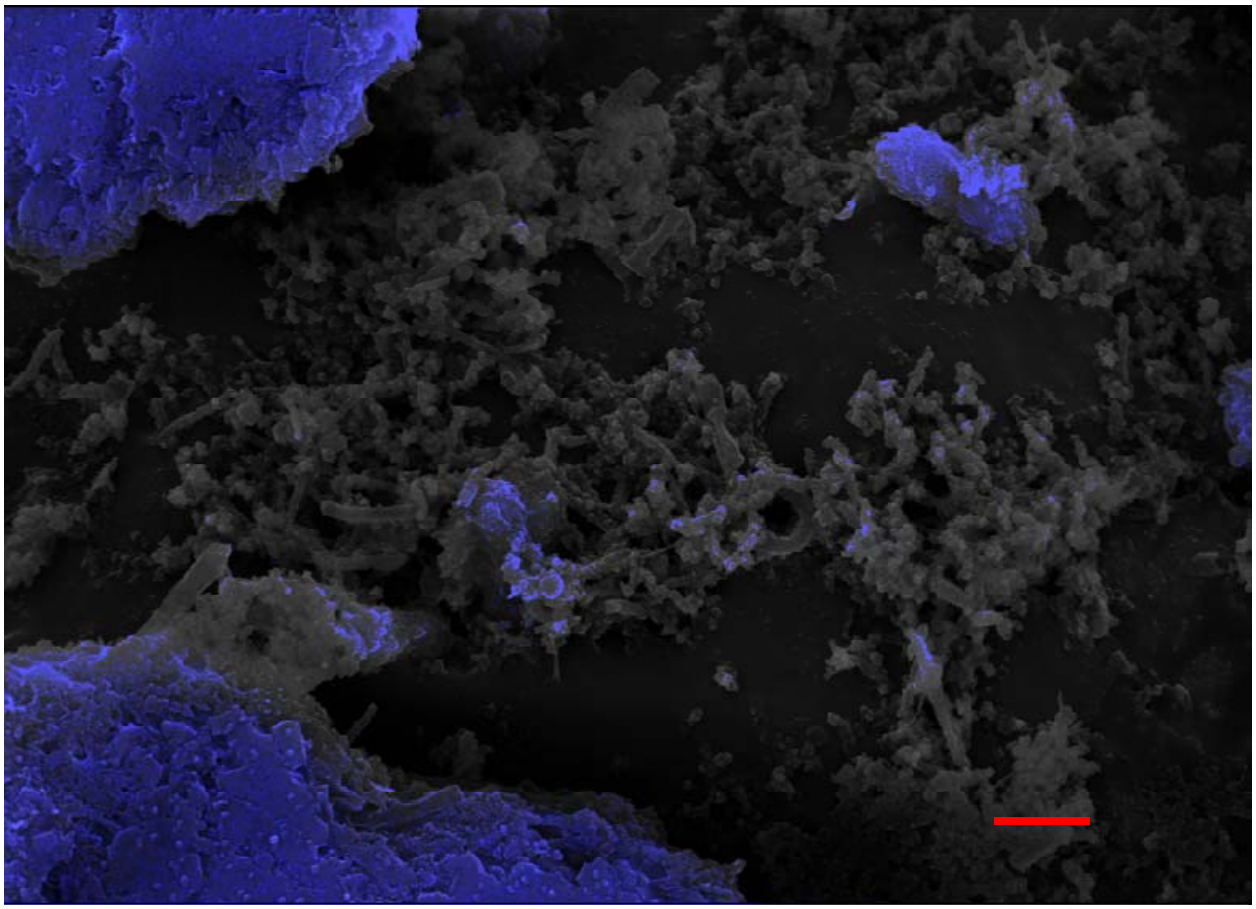

Figure C2: Scanning electron micrograph of the area from Figure C1 after being analyzed using EDS mapping technique. Blue areas identify areas rich in calcium. Scale bar is 3 μm.

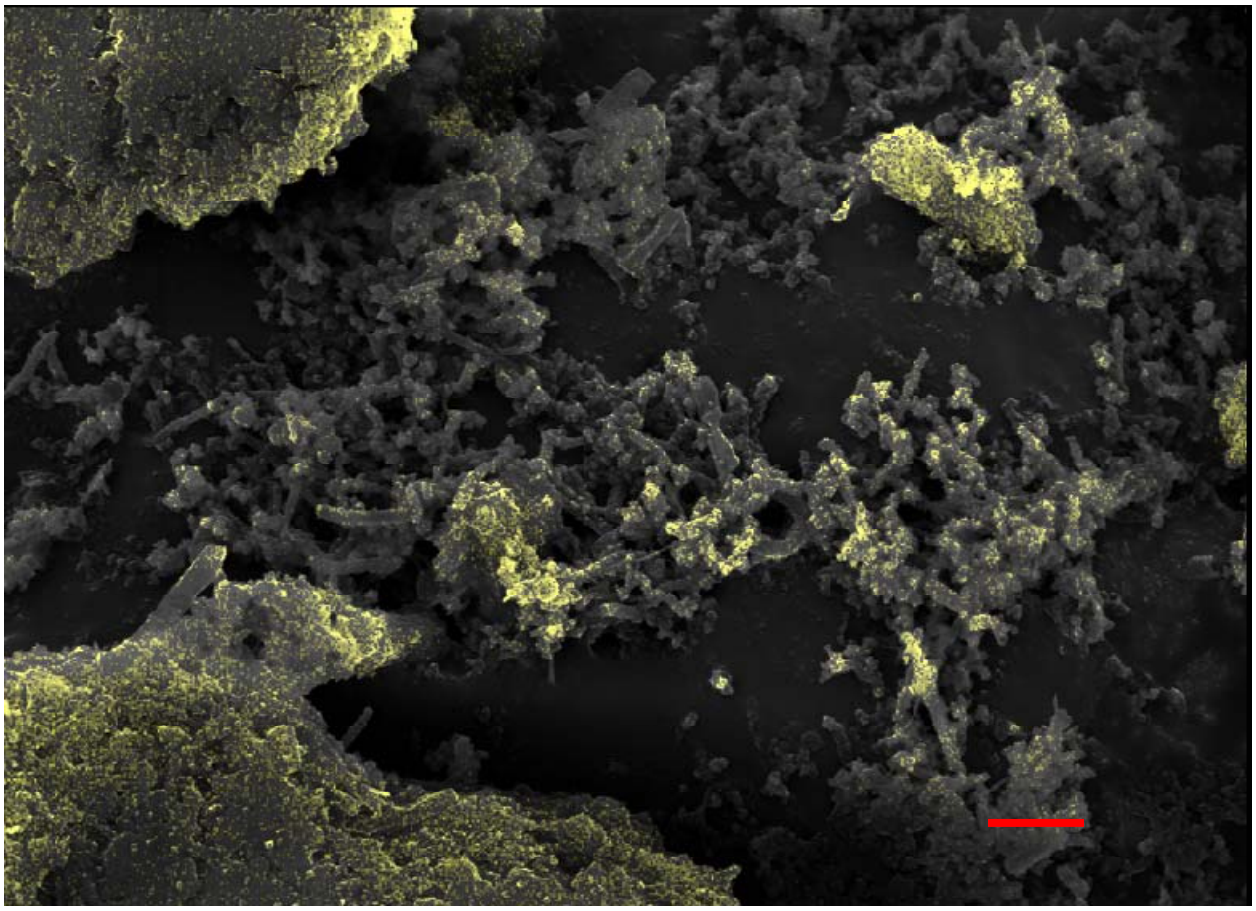

Figure C3: Scanning electron micrograph of the area from Figure C1 after being analyzed using EDS mapping technique. Yellow areas identify areas rich in magnesium. Scale bar is 3 μm.

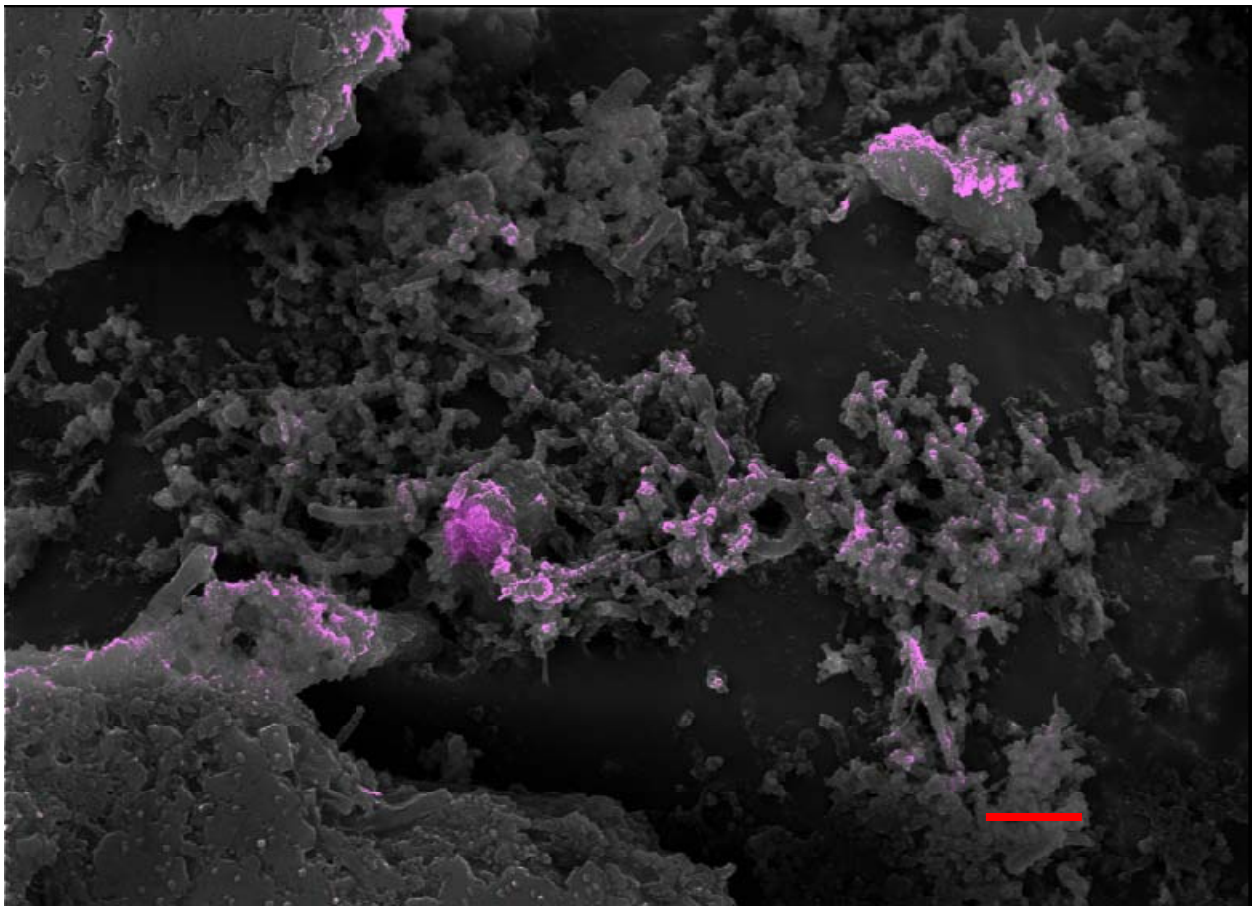

Figure C4: Scanning electron micrograph of the area from Figure C1 after being analyzed using EDS mapping technique. Pink areas identify areas rich in silicon. Scale bar is 3 μm.

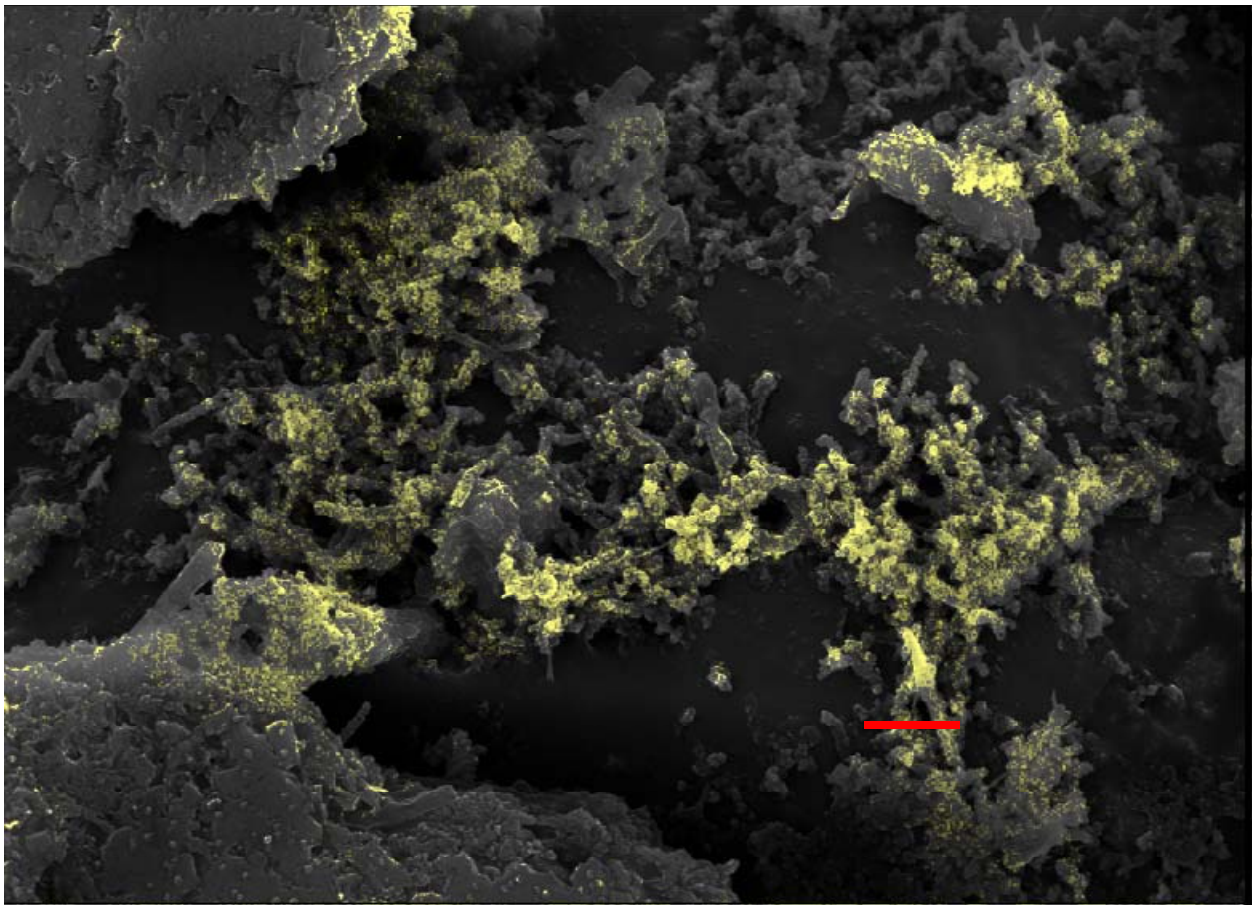

Figure C5: Scanning electron micrograph of the area from Figure C1 after being analyzed using EDS mapping technique. Yellow areas identify areas rich in iron. Scale bar is 3 μm.

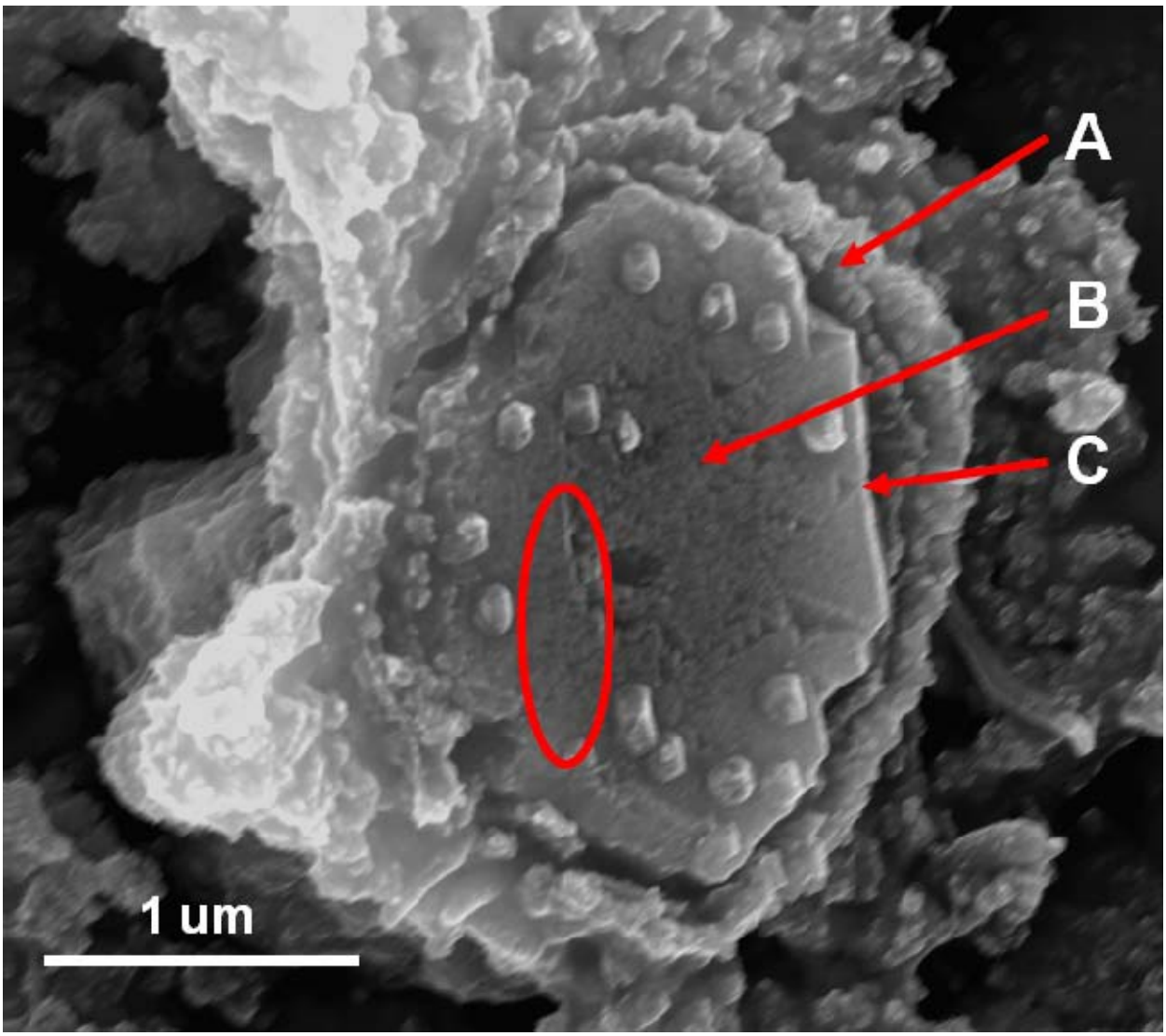

Figure C6: Platy crystal aggregates of dolomite forming on the surface of a basalt grain and in direct contact with a ring of biofilm (A). Microporosity is shown at the center of the crystal aggregate (B) and loss of microporosity due to ripening is shown in the circle. Well ripened crystals are seen in contact as the individual plates grow into each other (C). Scale bar is 1 μm.

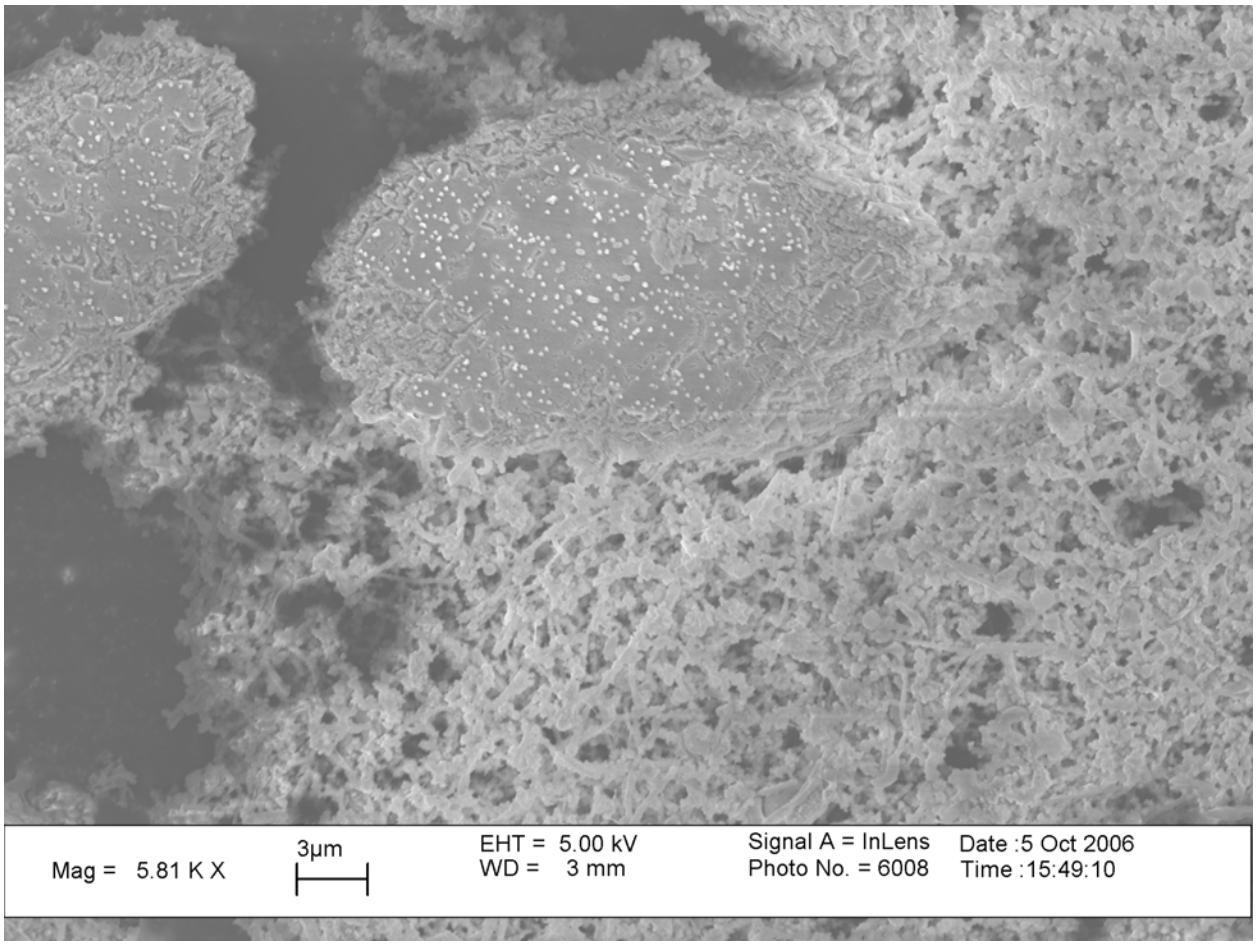

Figure C7: Scanning electron micrograph of a consortium of microorganisms (mass of short rods primarily in the lower right) and large grains of basalt coated in platy crystal aggregates of dolomite (similar to those seen in Figure C1 and in Chapter 2). Scale bar is 3 µm.

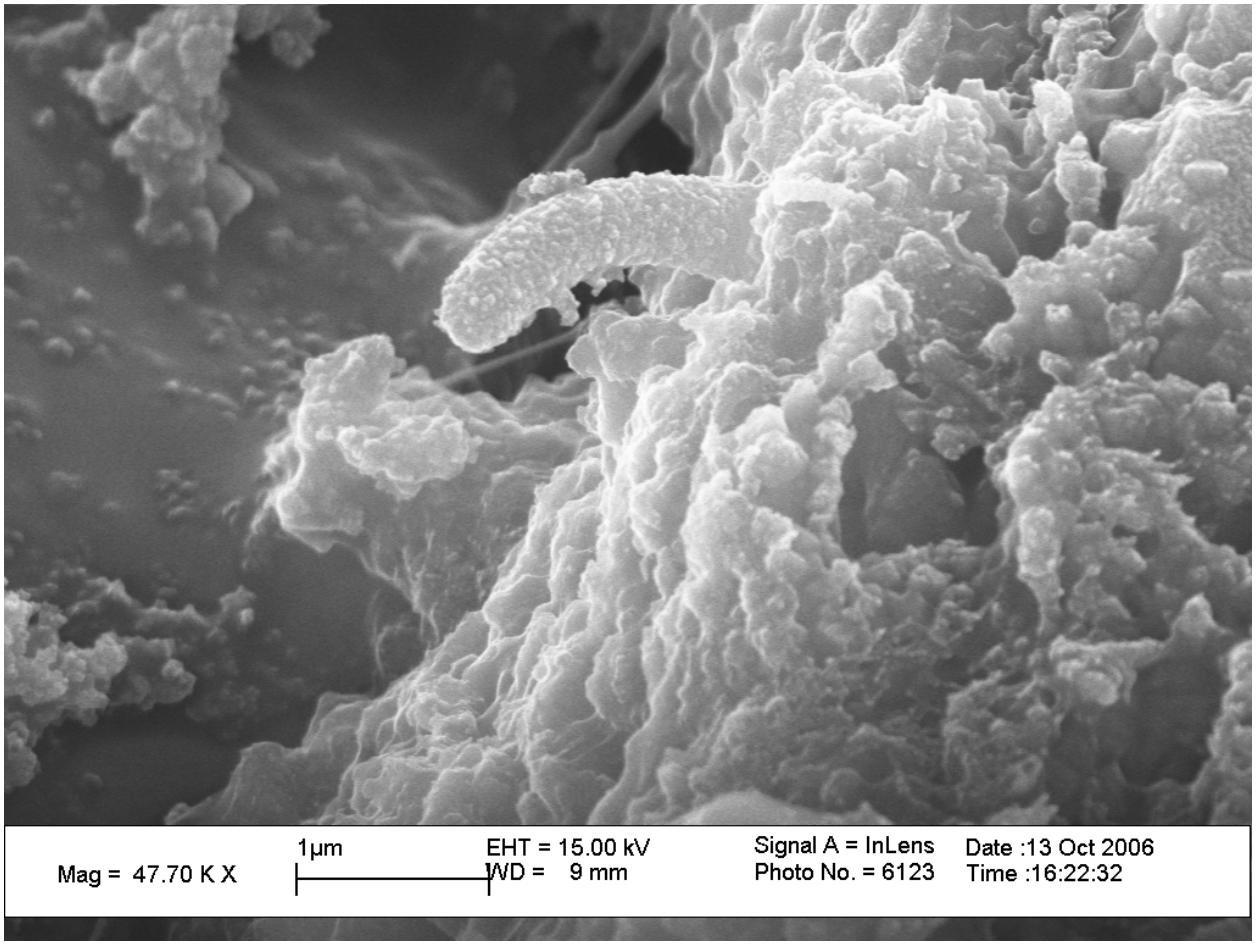

Figure C8: Scanning electron micrograph of an encrusted microbe. The sample was taken from the Bemidji consortium batch reactor after 166 days (Chapter 2). The microbe is bound to the EPS coating a grain of basalt. Scale bar is 1 µm.

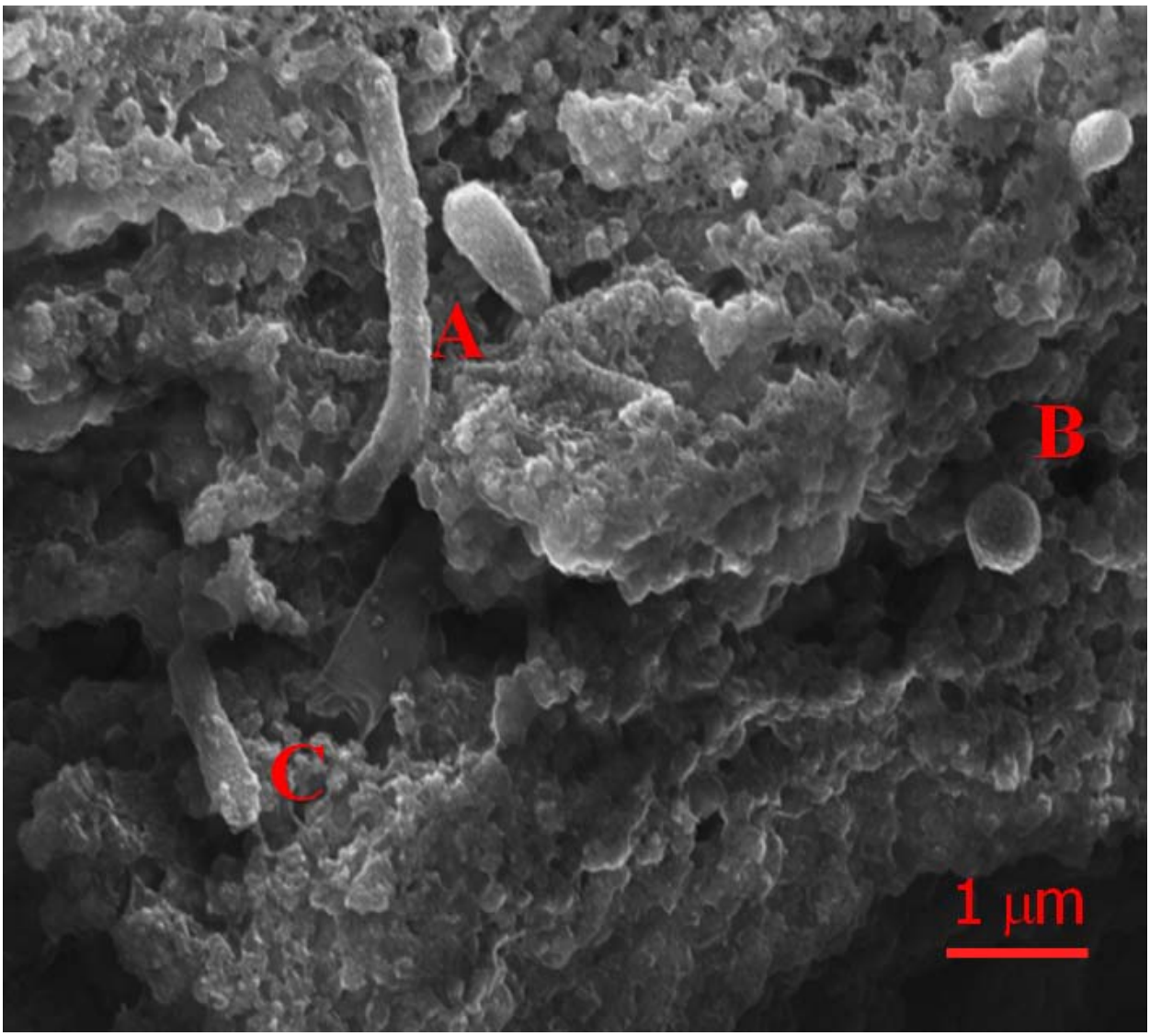

Figure C9: Scanning electron micrograph of a variety of encrusted microbes. The sample was taken from the Bemidji consortium batch reactor after 90 days (Chapter 2). This illustrates the diversity of microbial morphologies present in the consortium including rods (A), spheres (B) and blunt end rods (C, whole and collapsed). Scale bar is 1 μm.

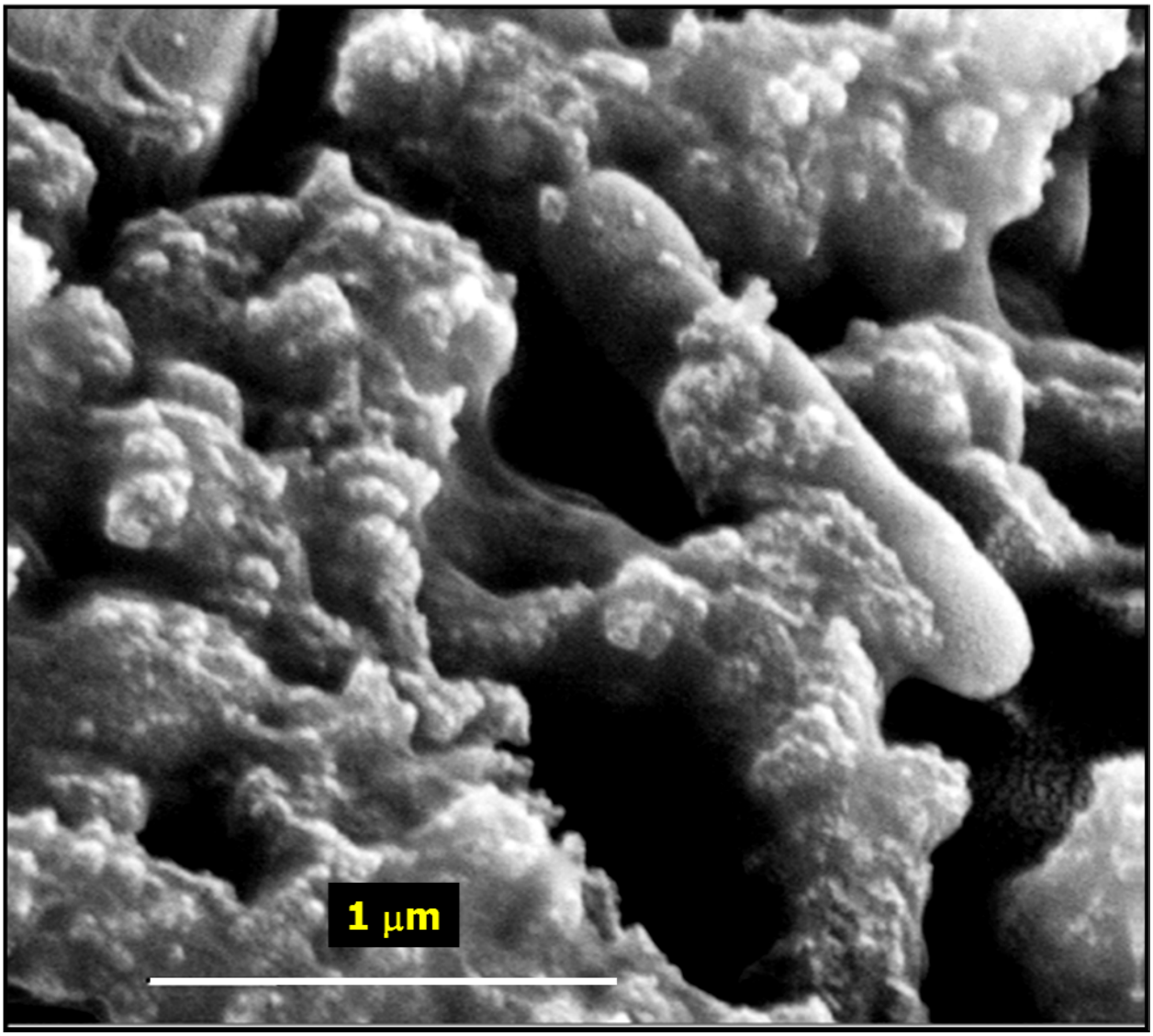

Figure C10: Scanning electron micrograph of a microbe and biofilm of an autoclaved control reactor vessel from Kenward *et al.*, 2009. No dolomite was detected in these reactor vessels and no PCAs were observed.

APPENDIX D

TEM

The following transmission electron micrographs are of the consortium of methanogenic Archaea and fermenting bacteria taken from experimental reactors from Chapter 2: Precipitation of low-temperature dolomite from an anaerobic microbial consortium: the role of methanogenic Archaea. Please see the methods of this section for all sampling and imaging techniques.

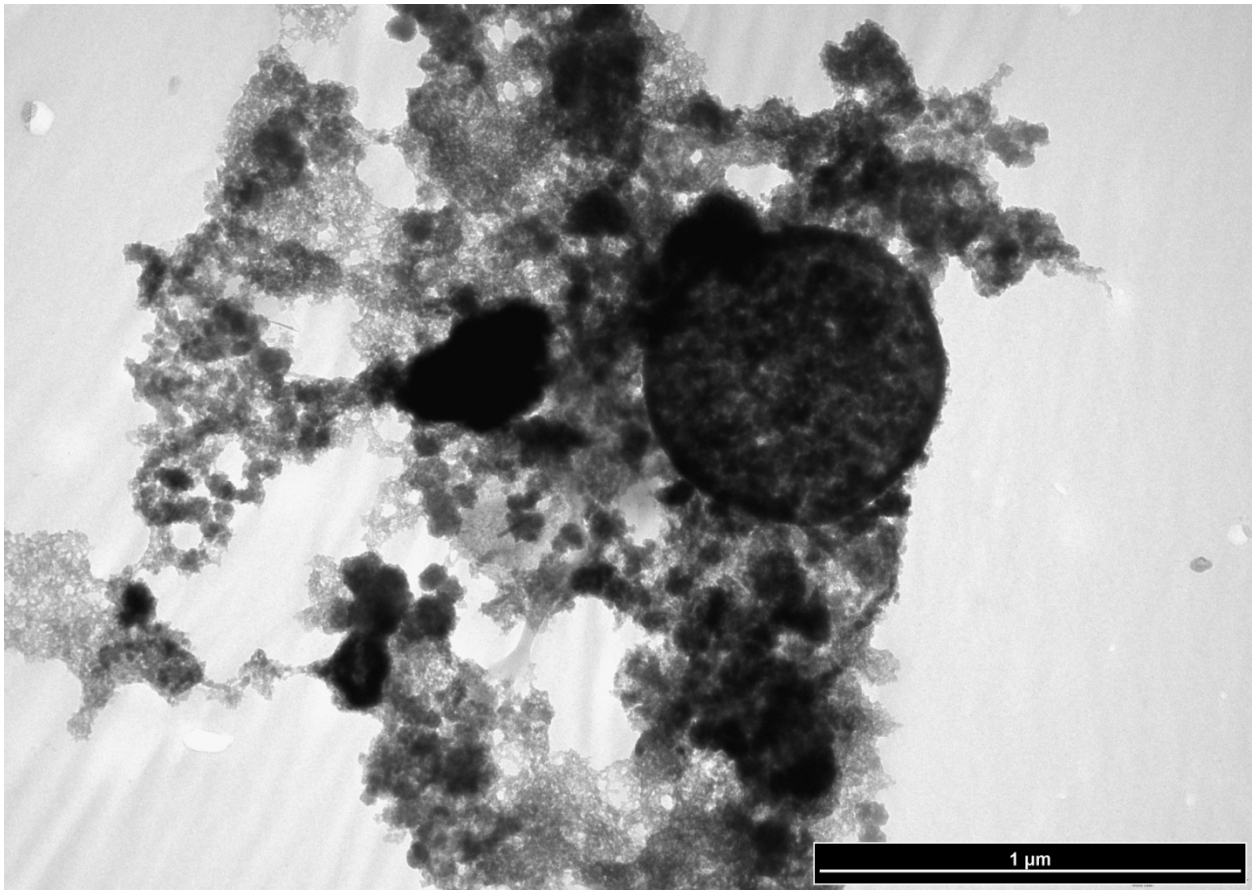

Figure D1

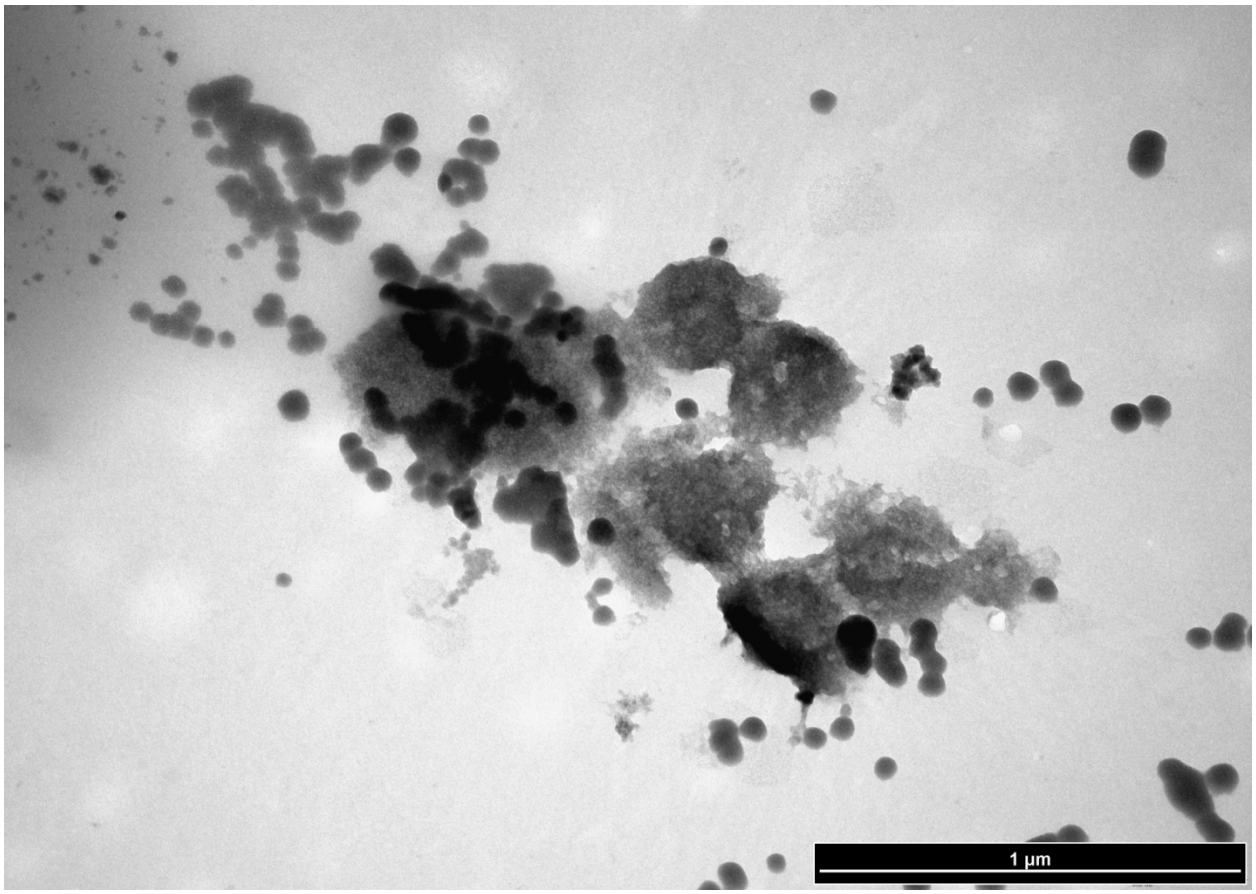

Figure D2

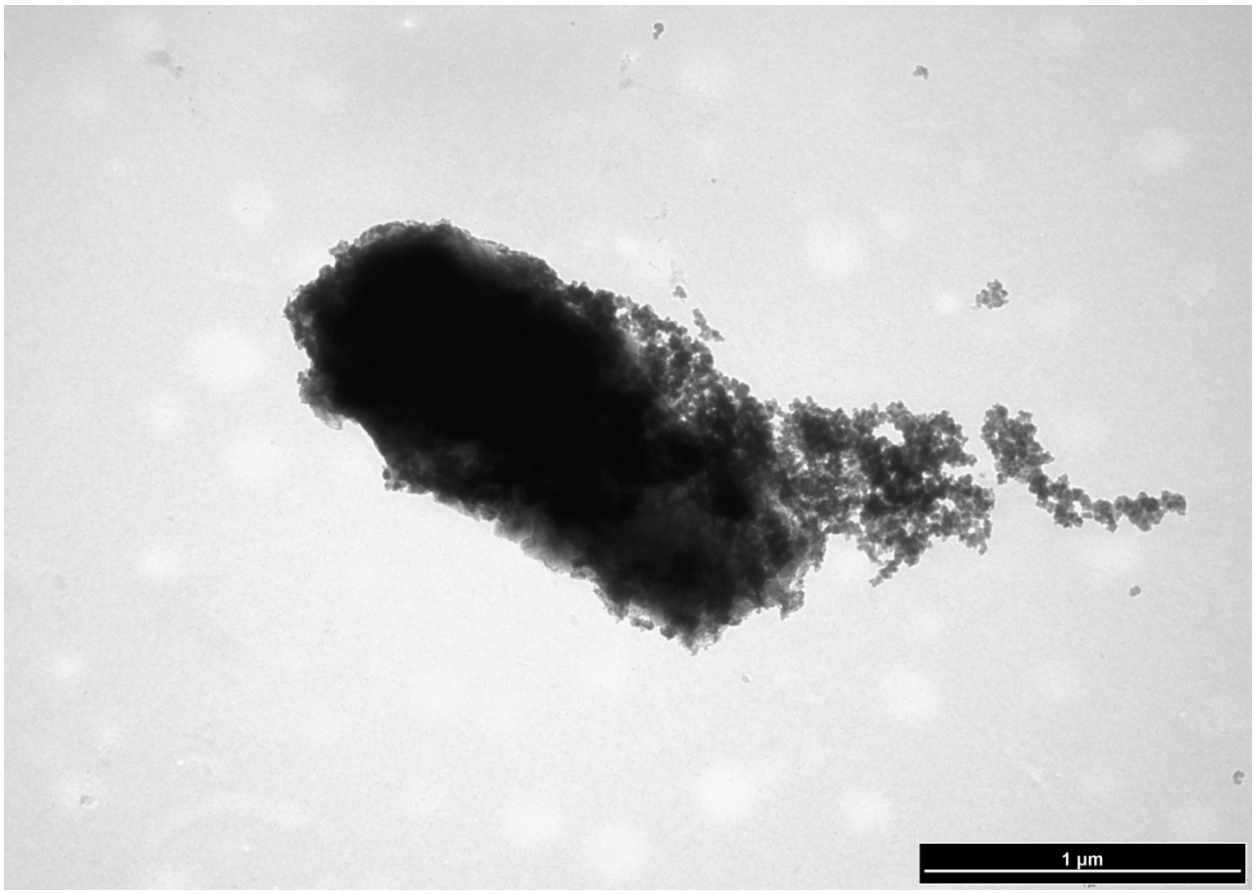

Figure D3

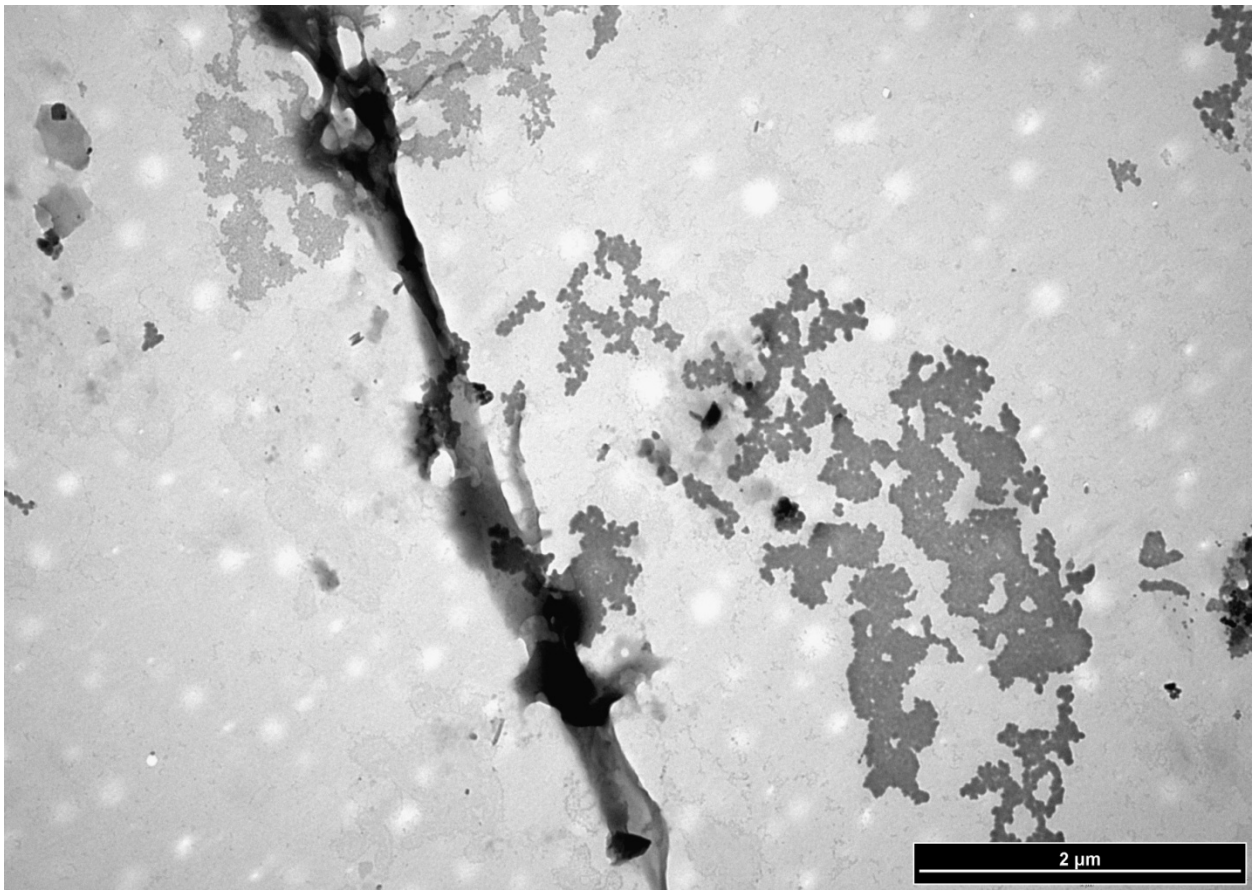

Figure D4

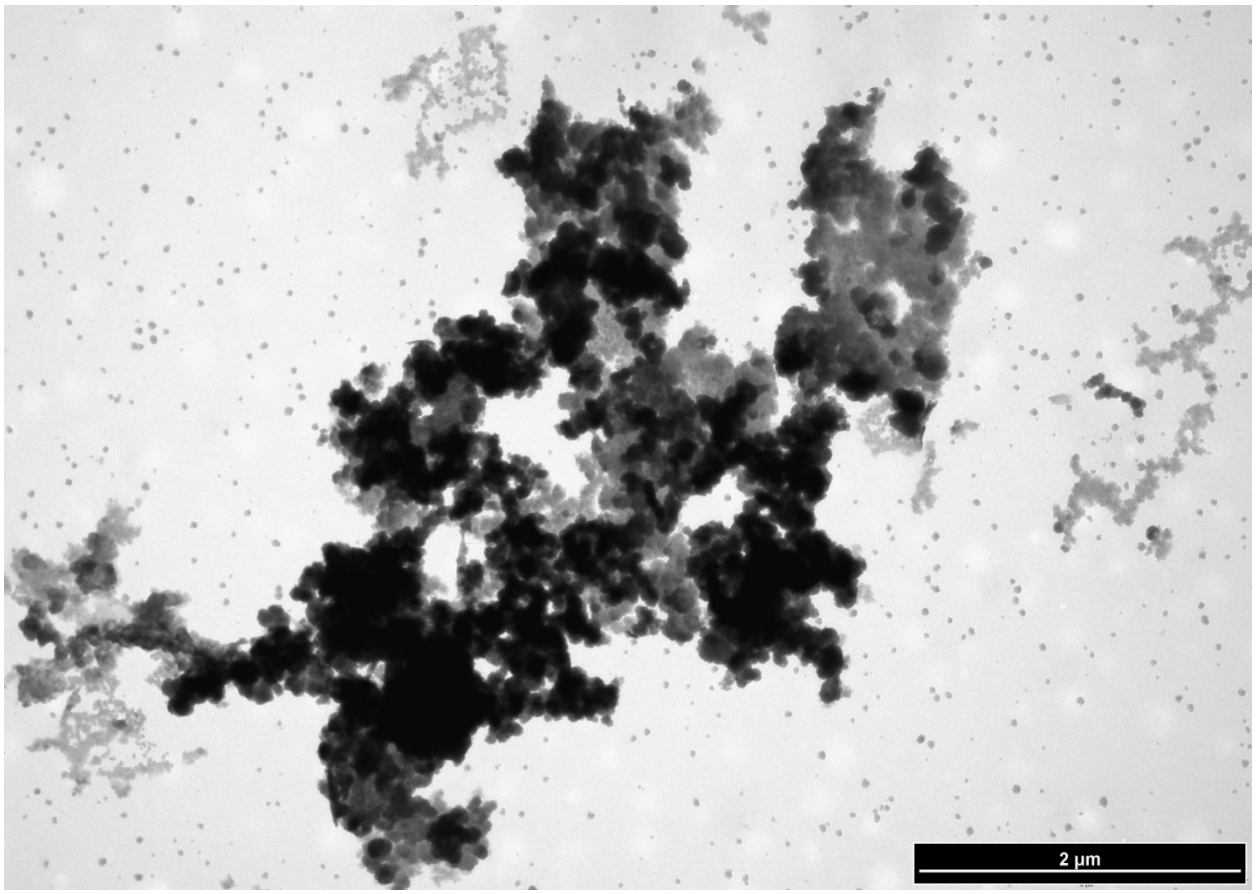

Figure D5

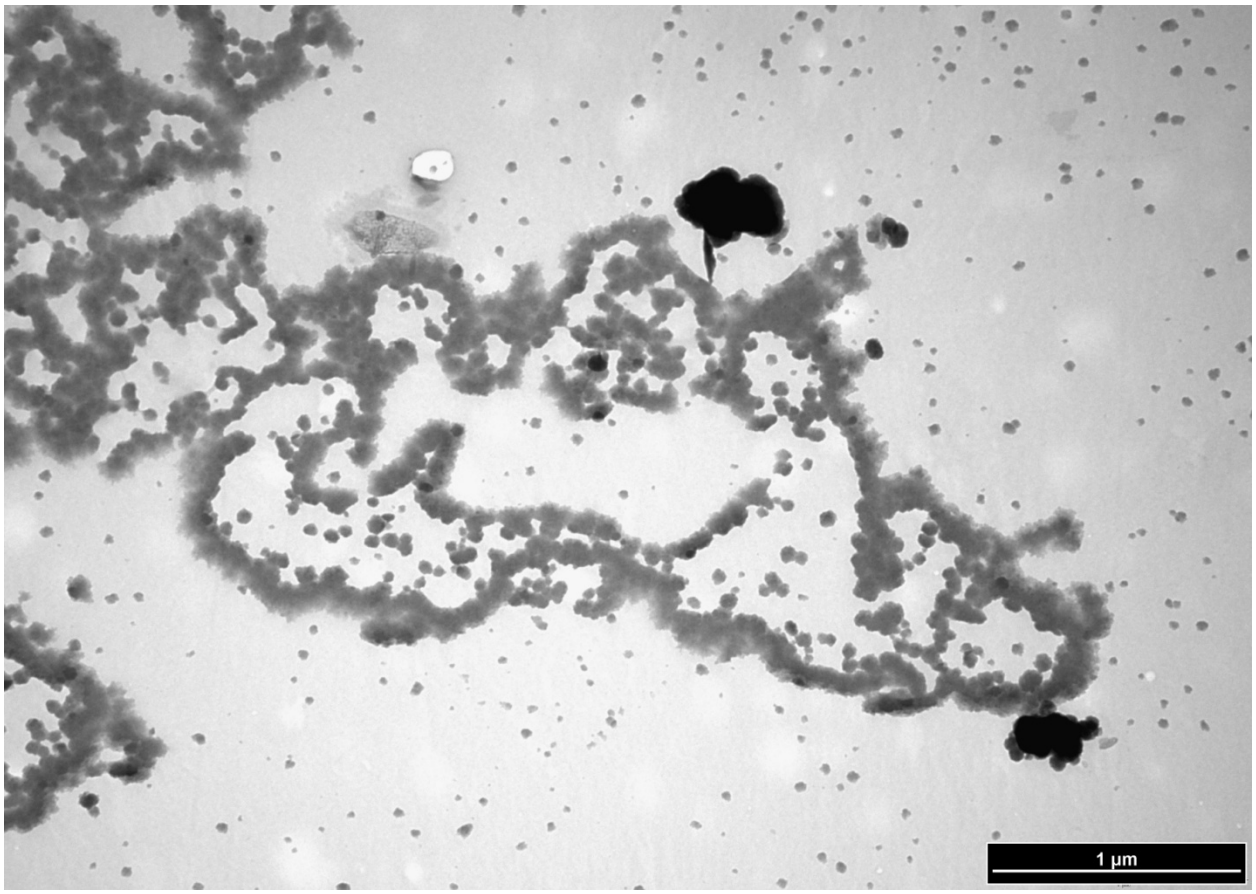

Figure D6

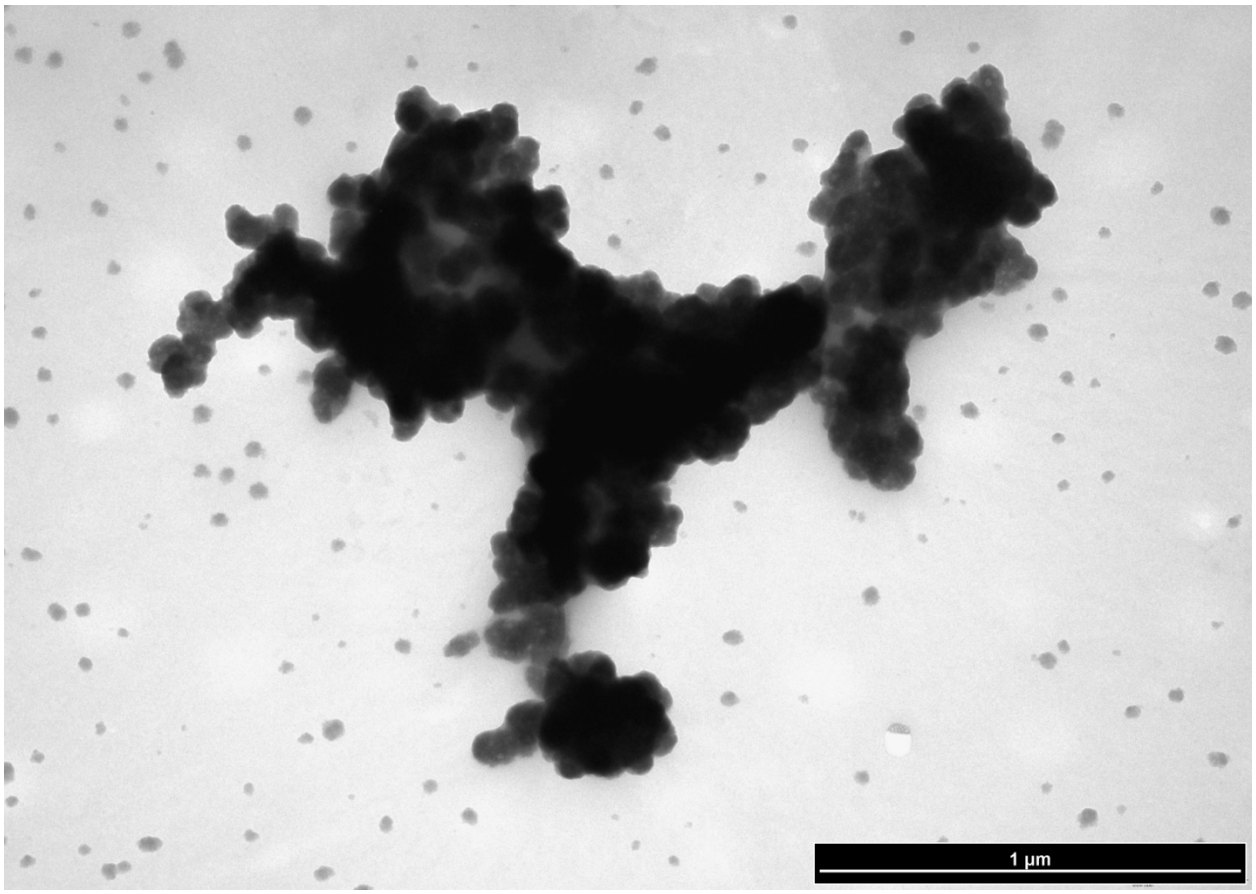

Figure D7

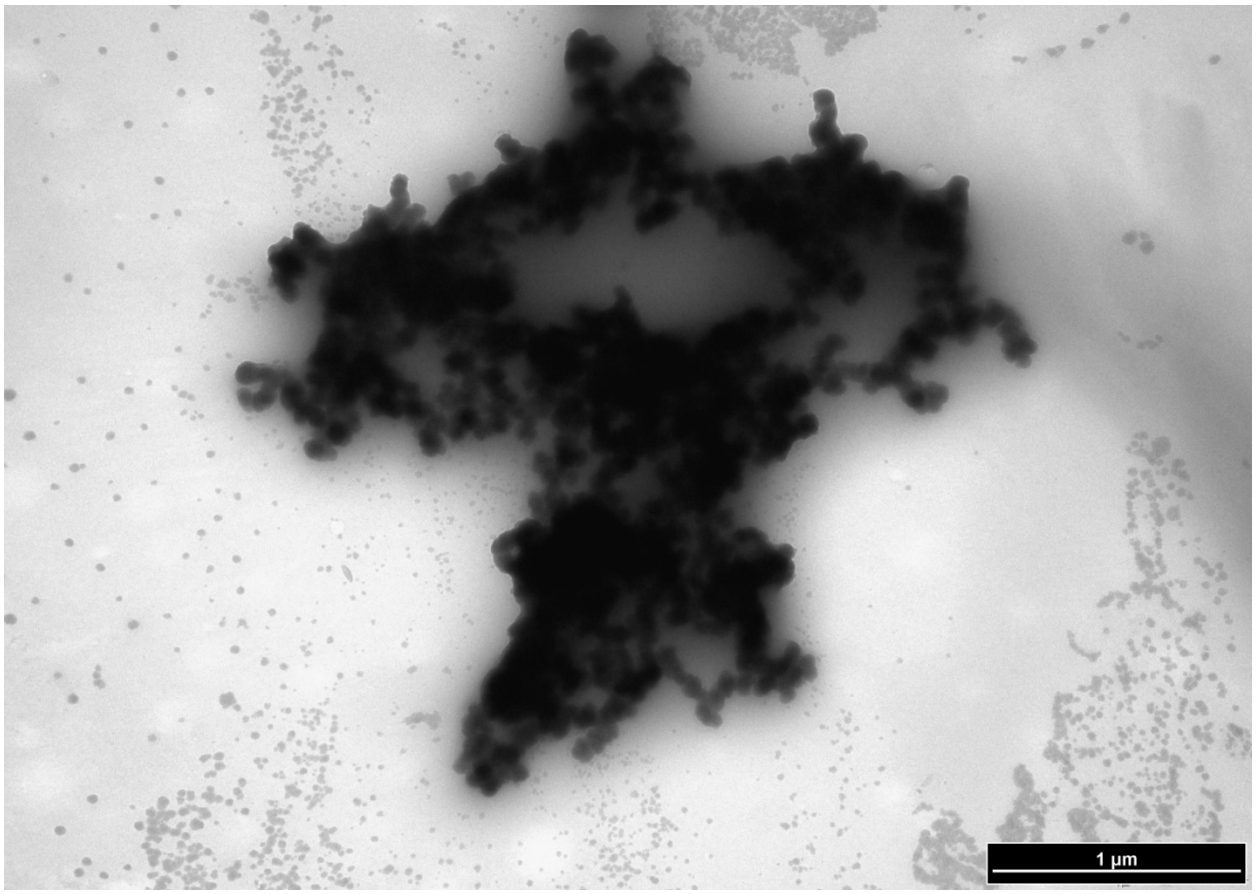

Figure D8

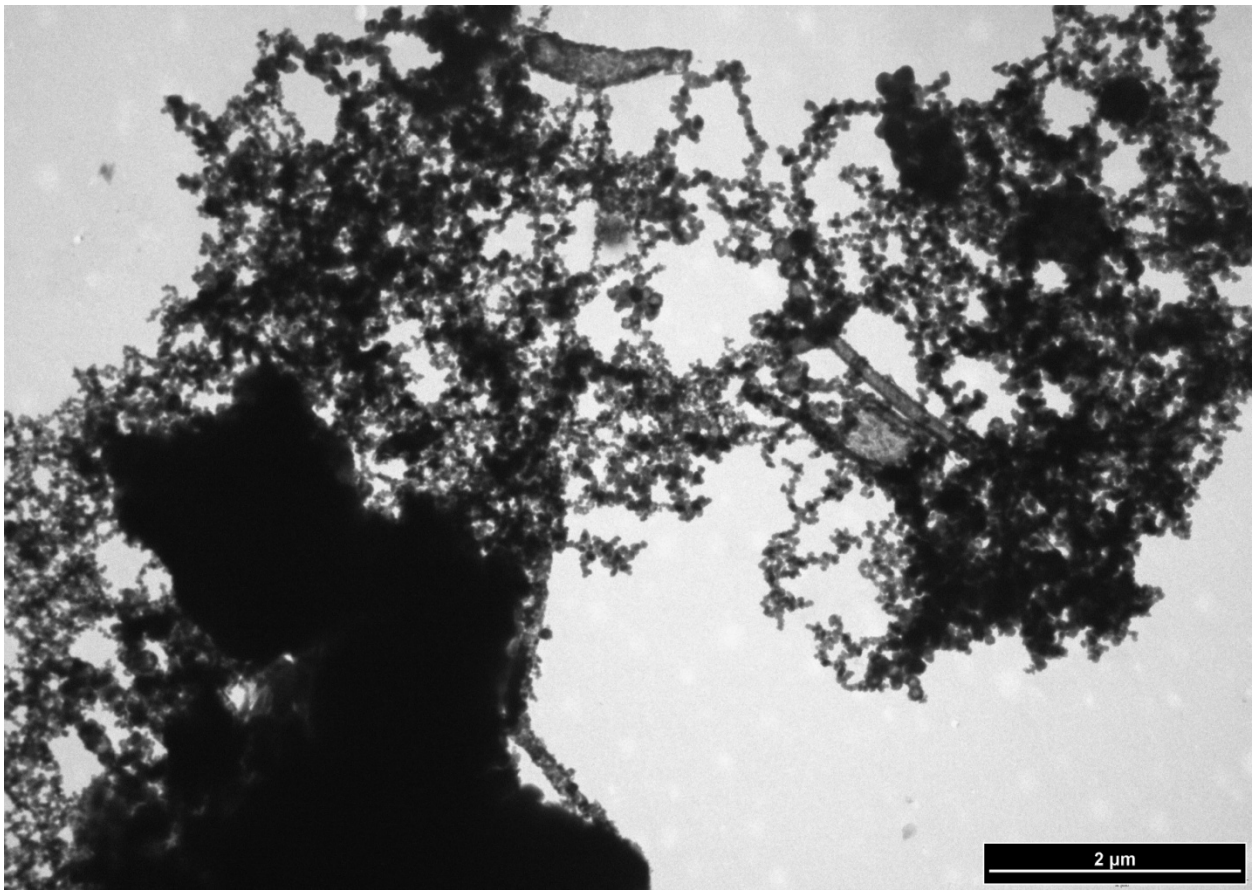

Figure D9

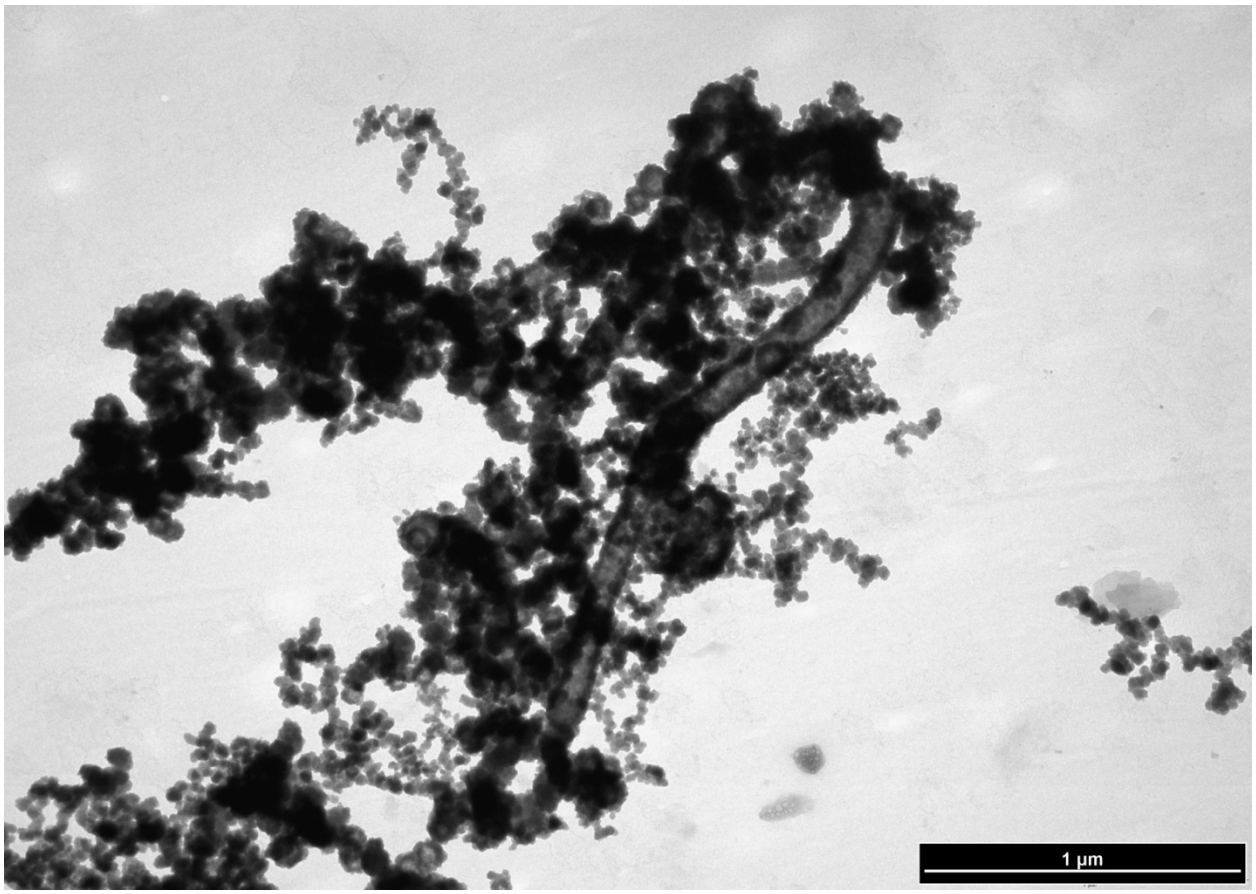

Figure D10

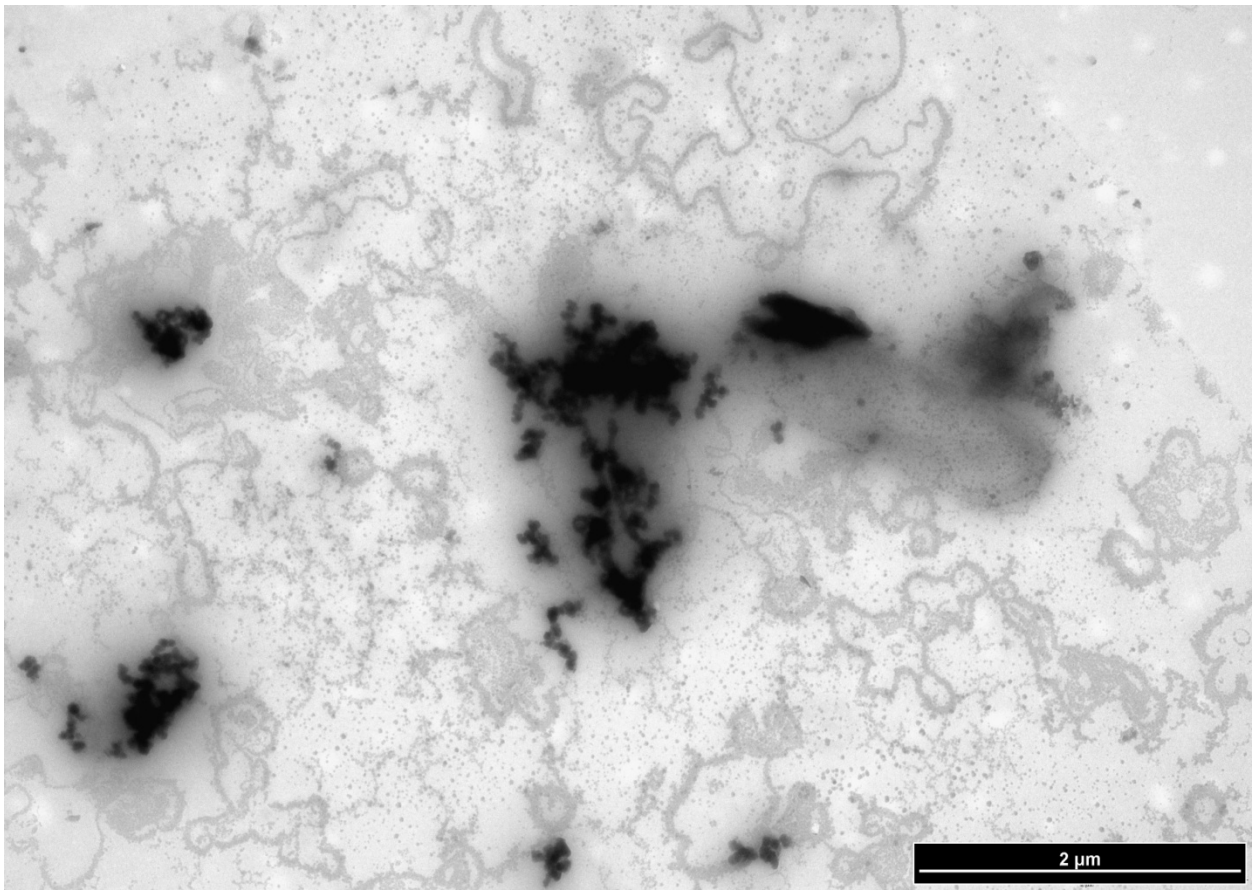

Figure D11

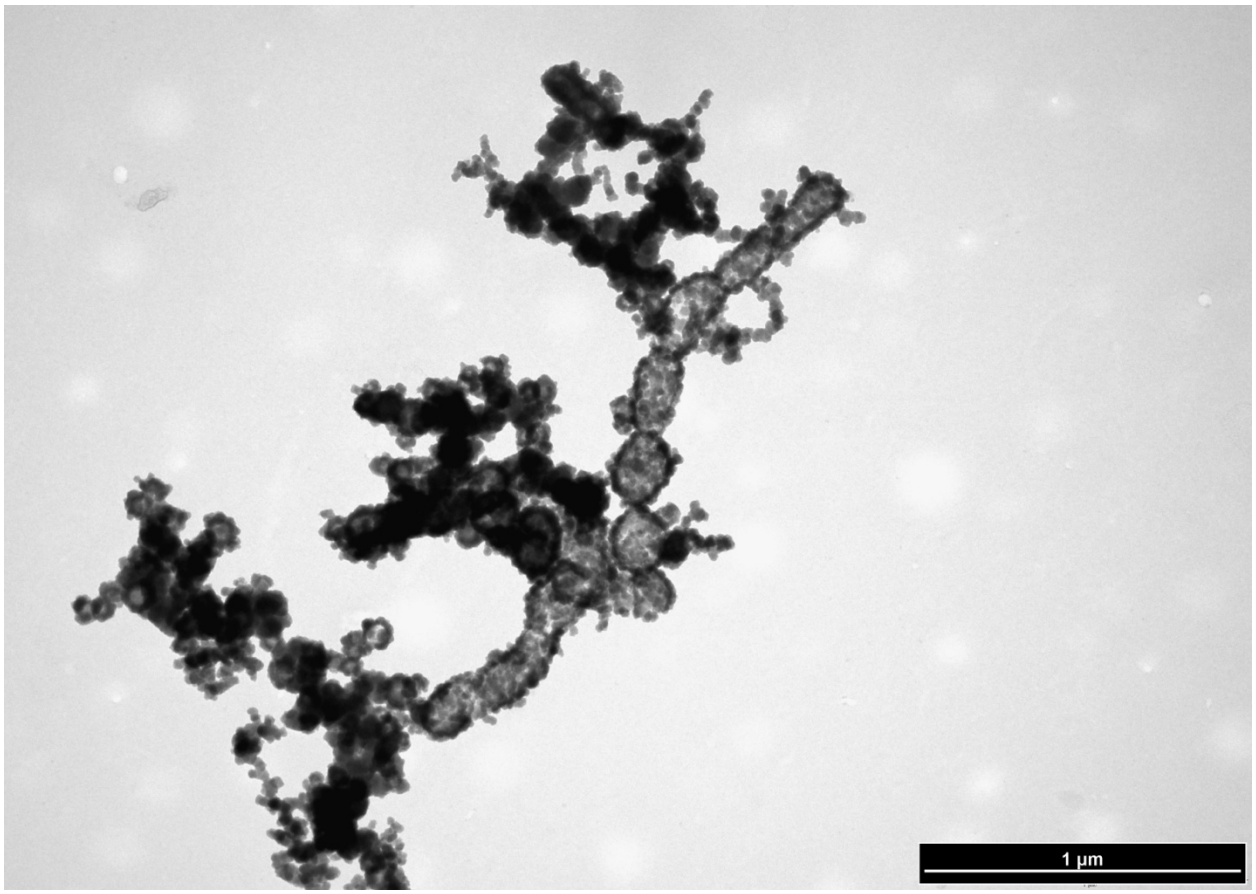

Figure D12

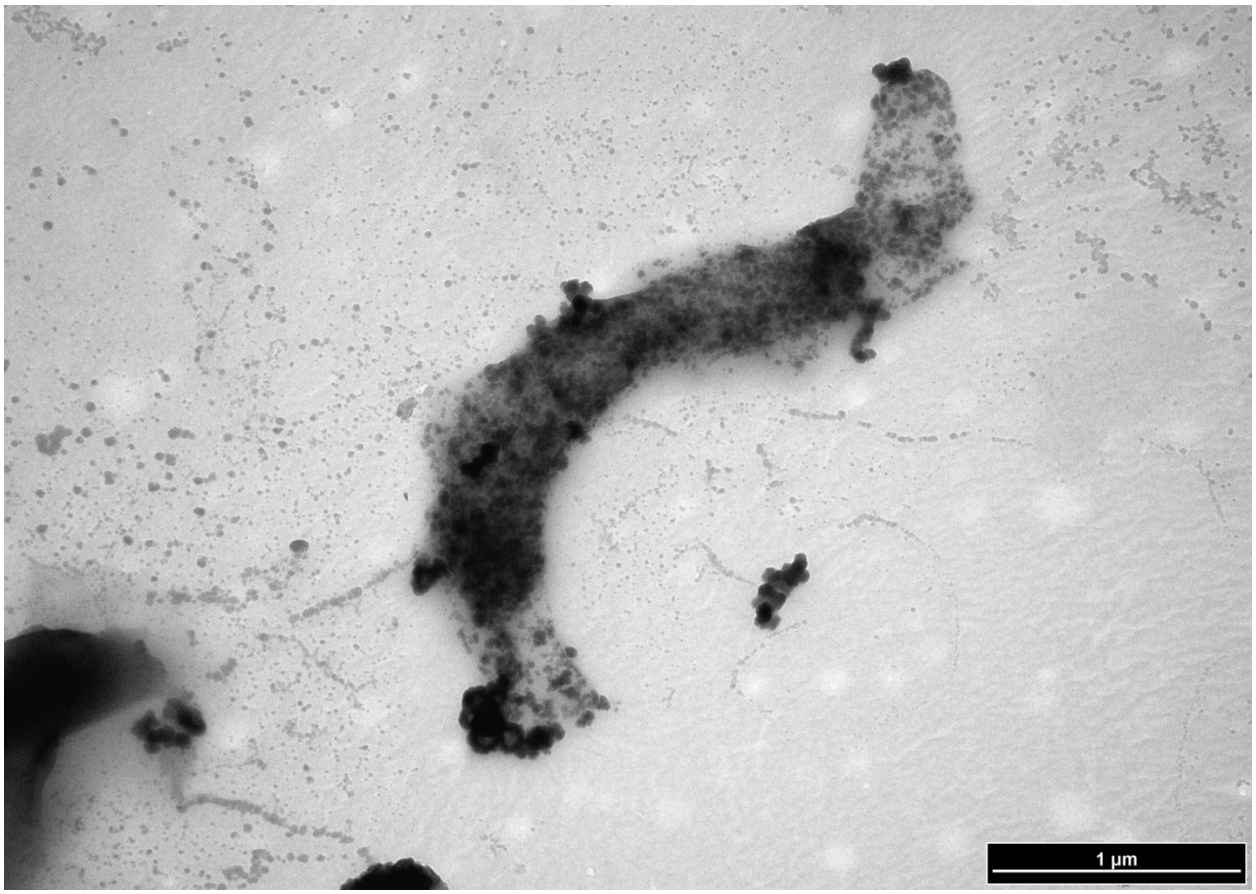

Figure D13

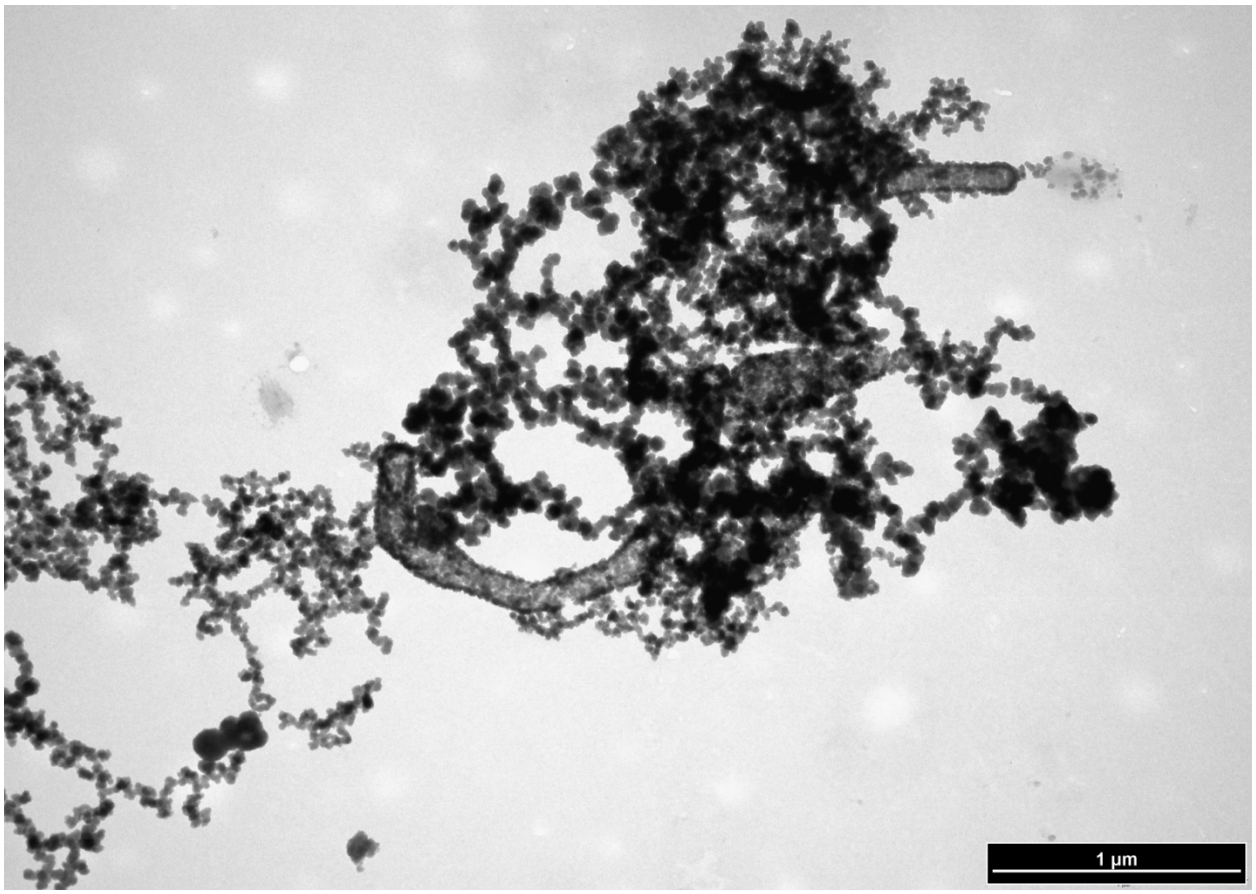

Figure D14

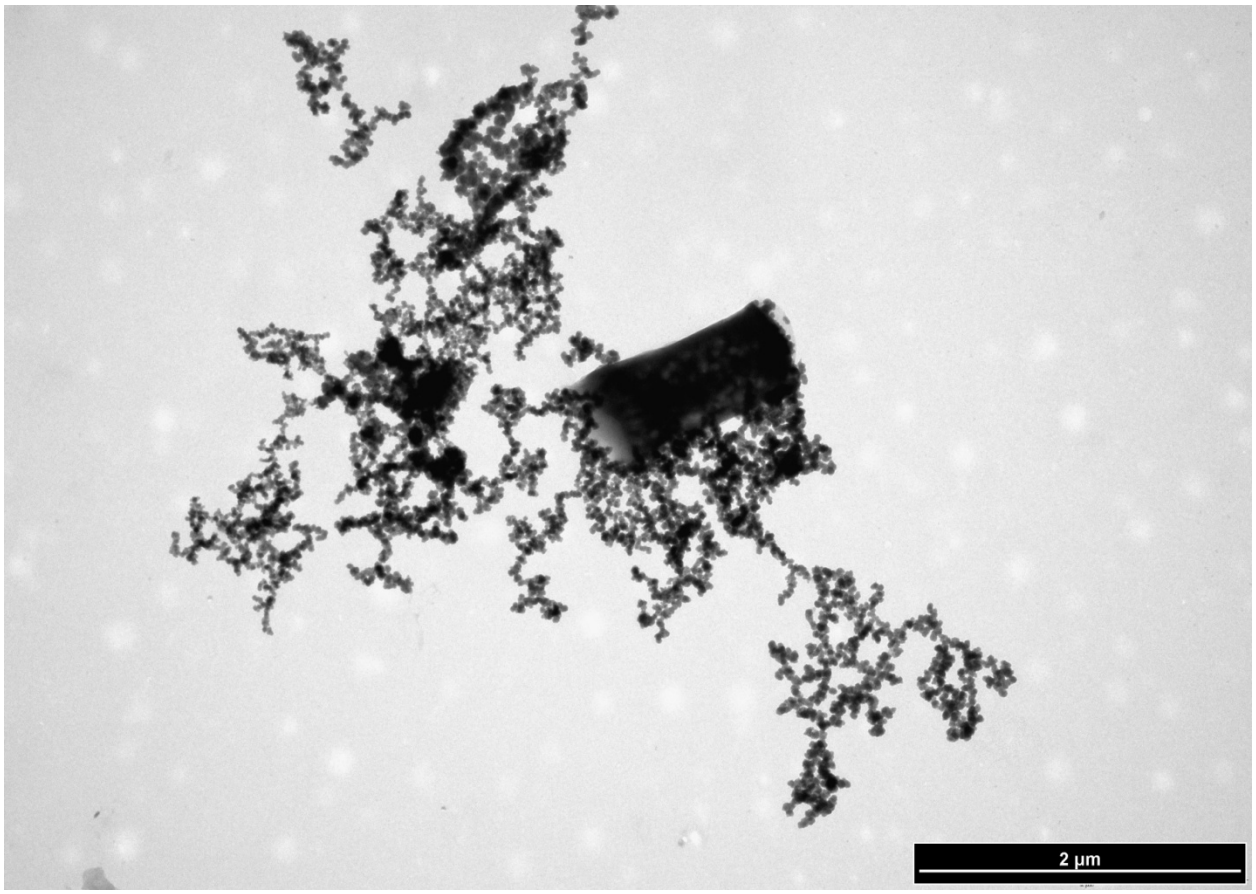

Figure D15

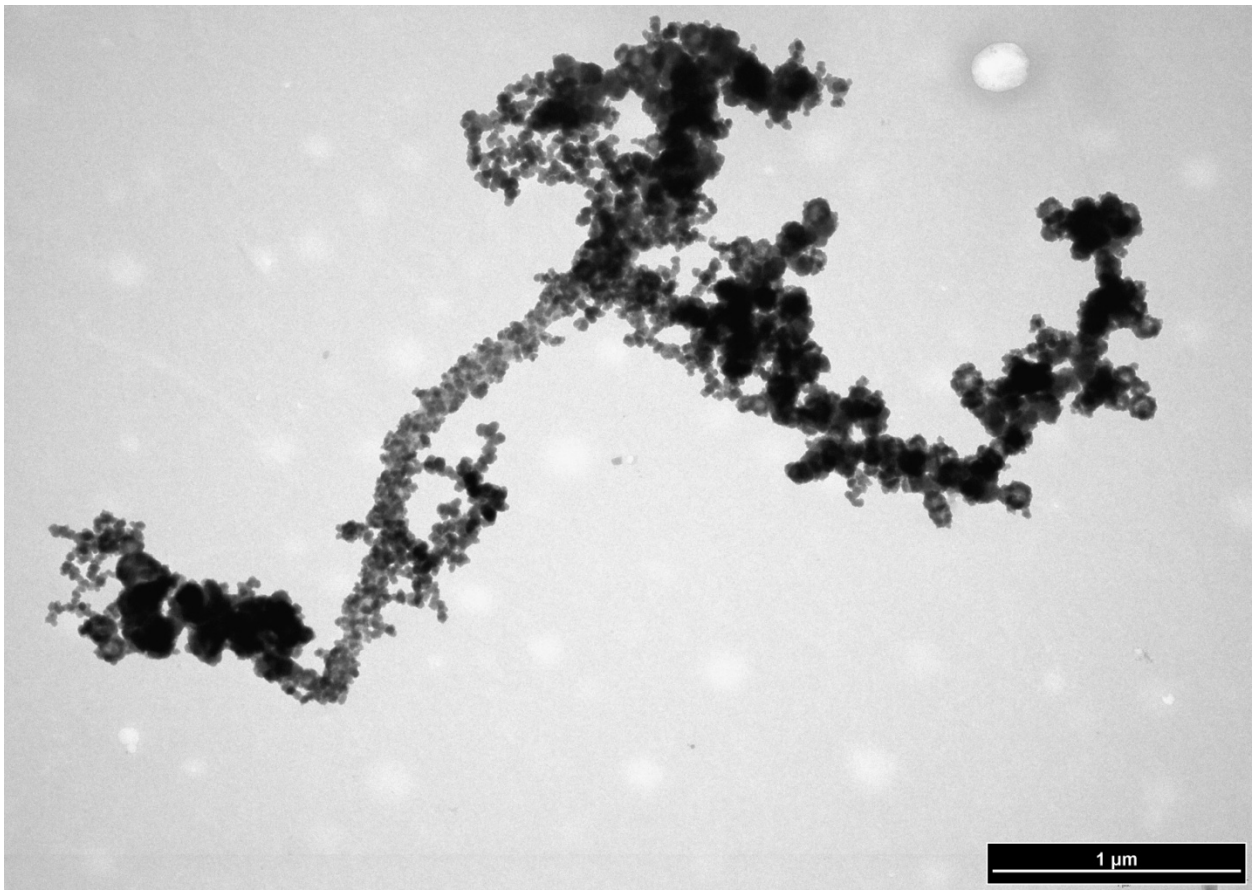

Figure D16

Figure D17

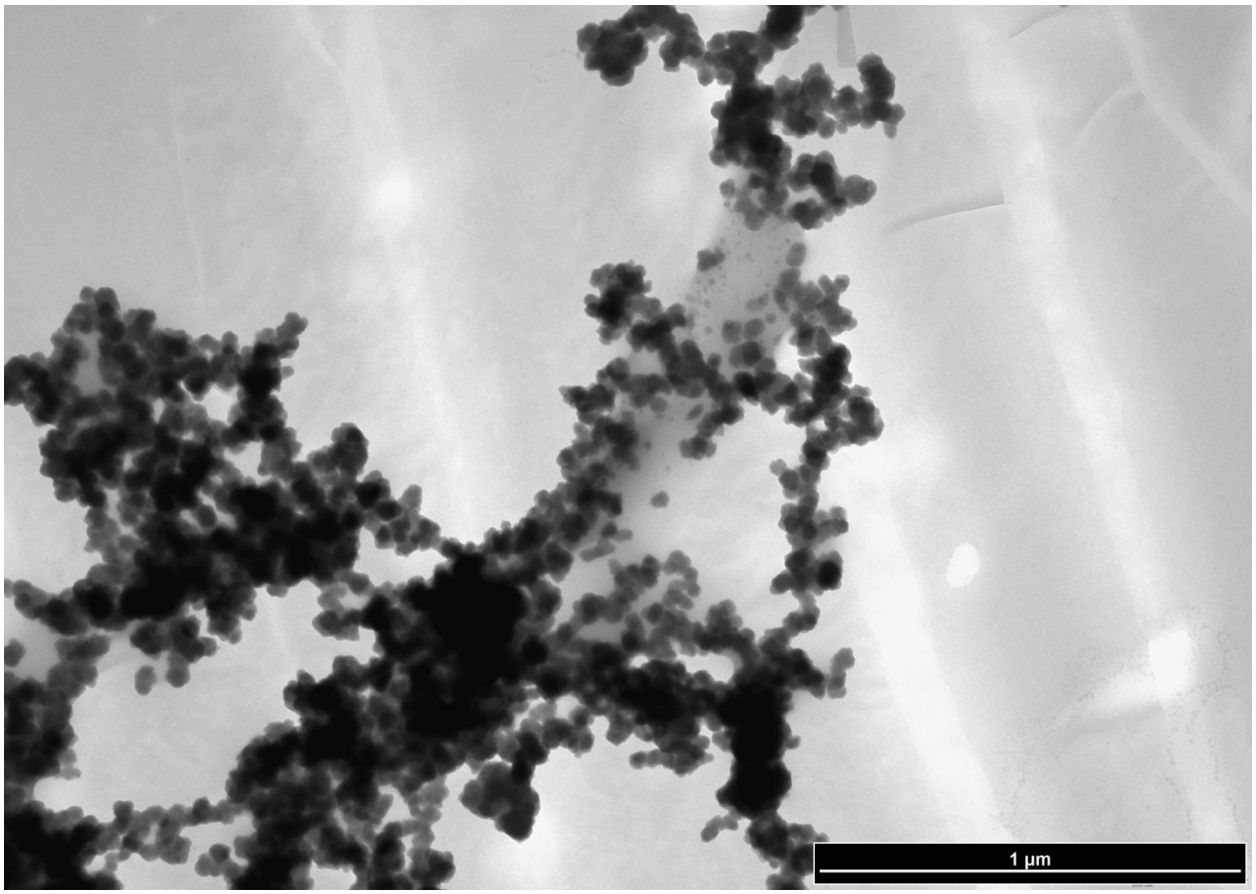

Figure D18

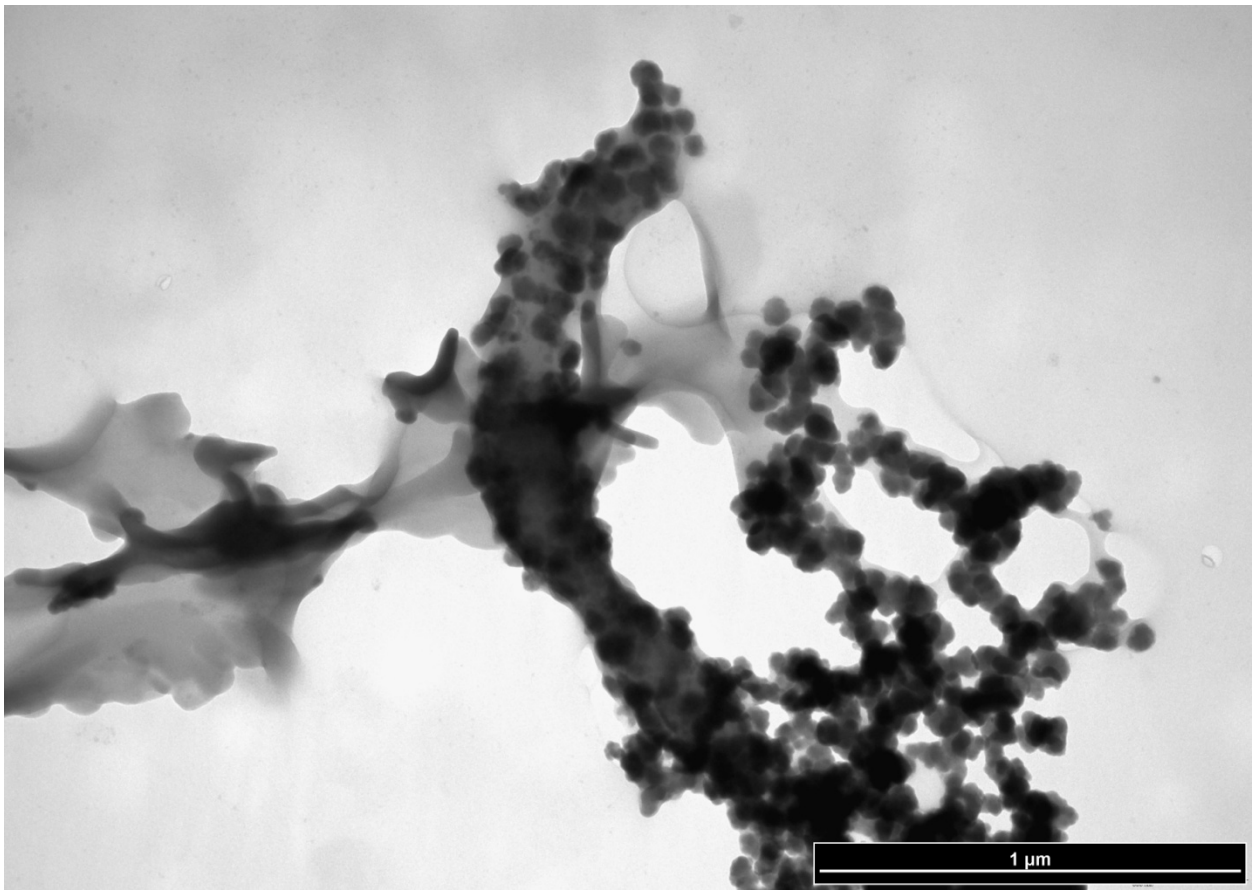

Figure D19

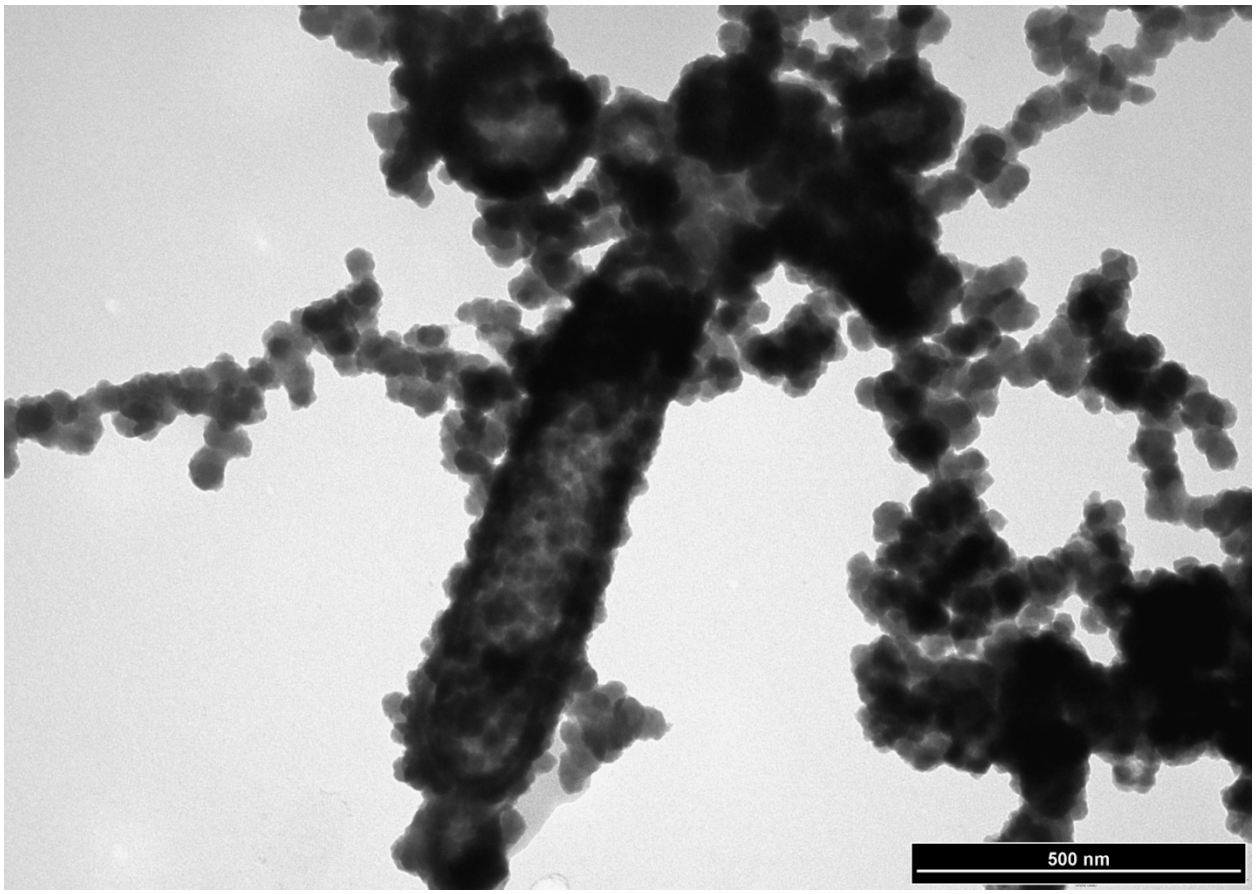

Figure D20

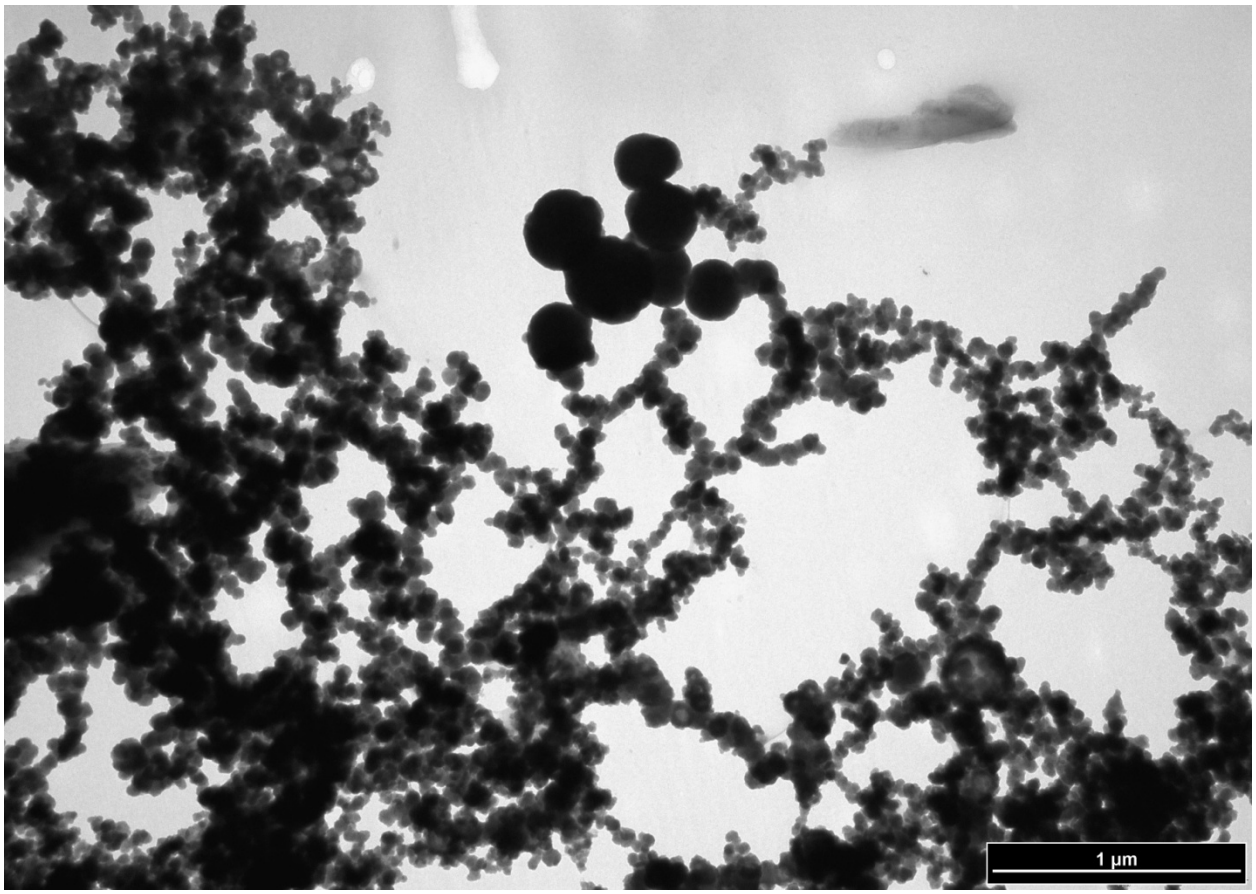

Figure D21

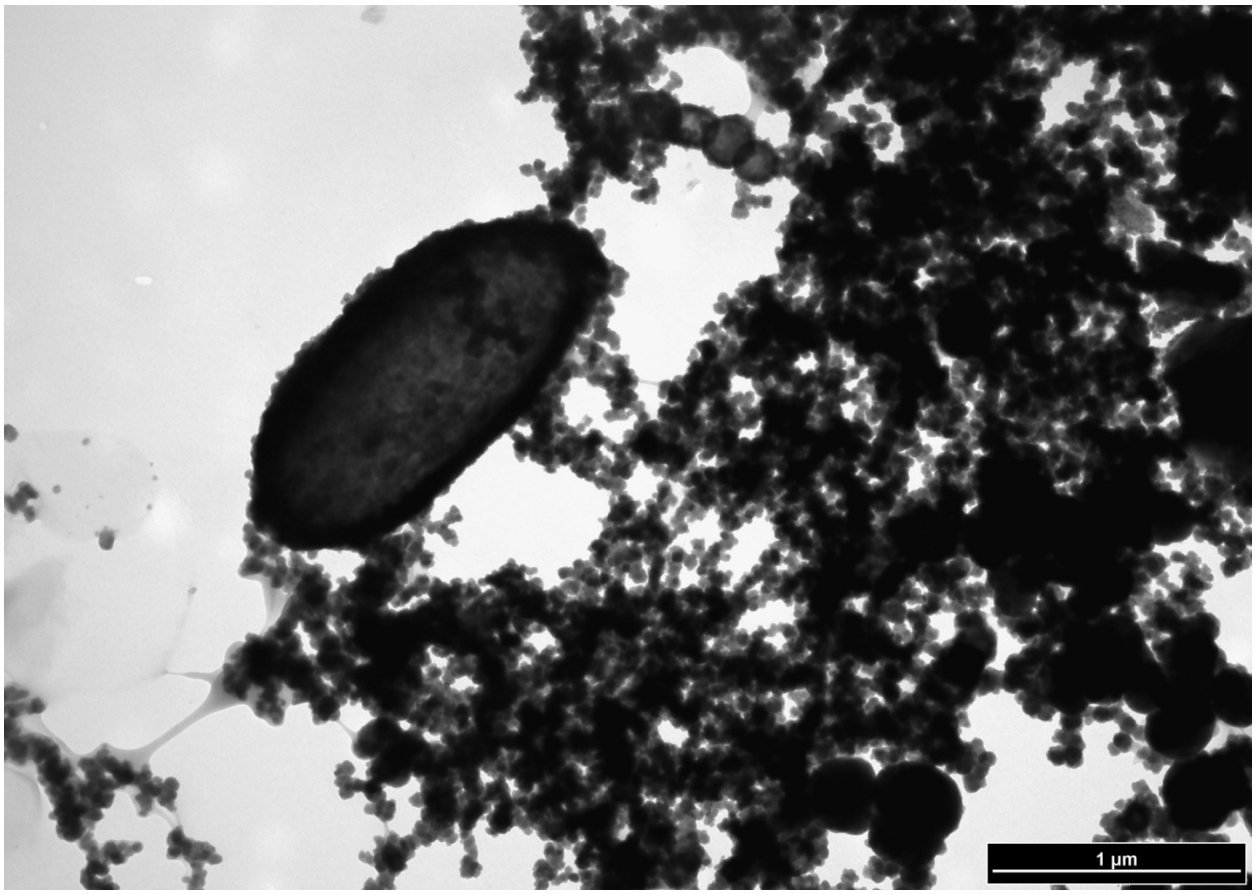

Figure D22

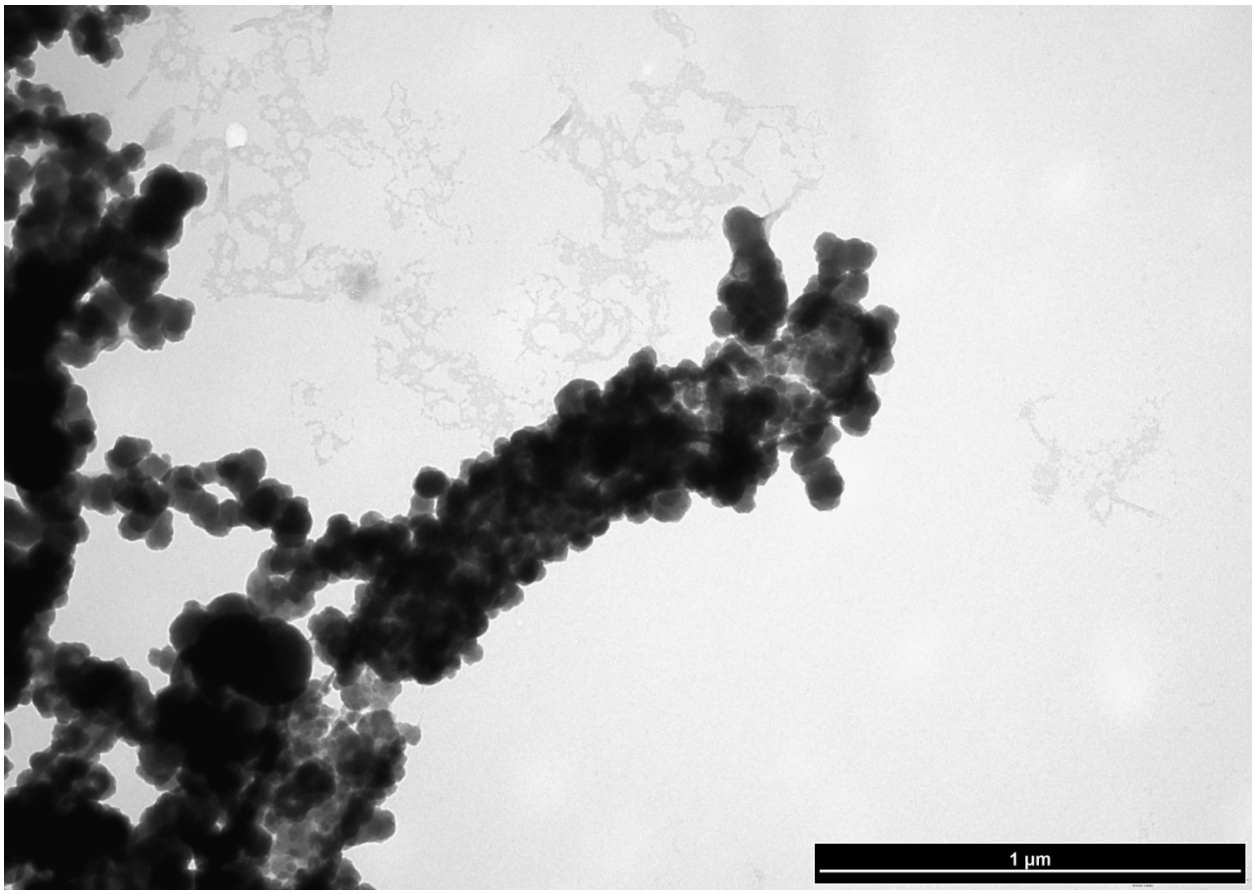

Figure D23

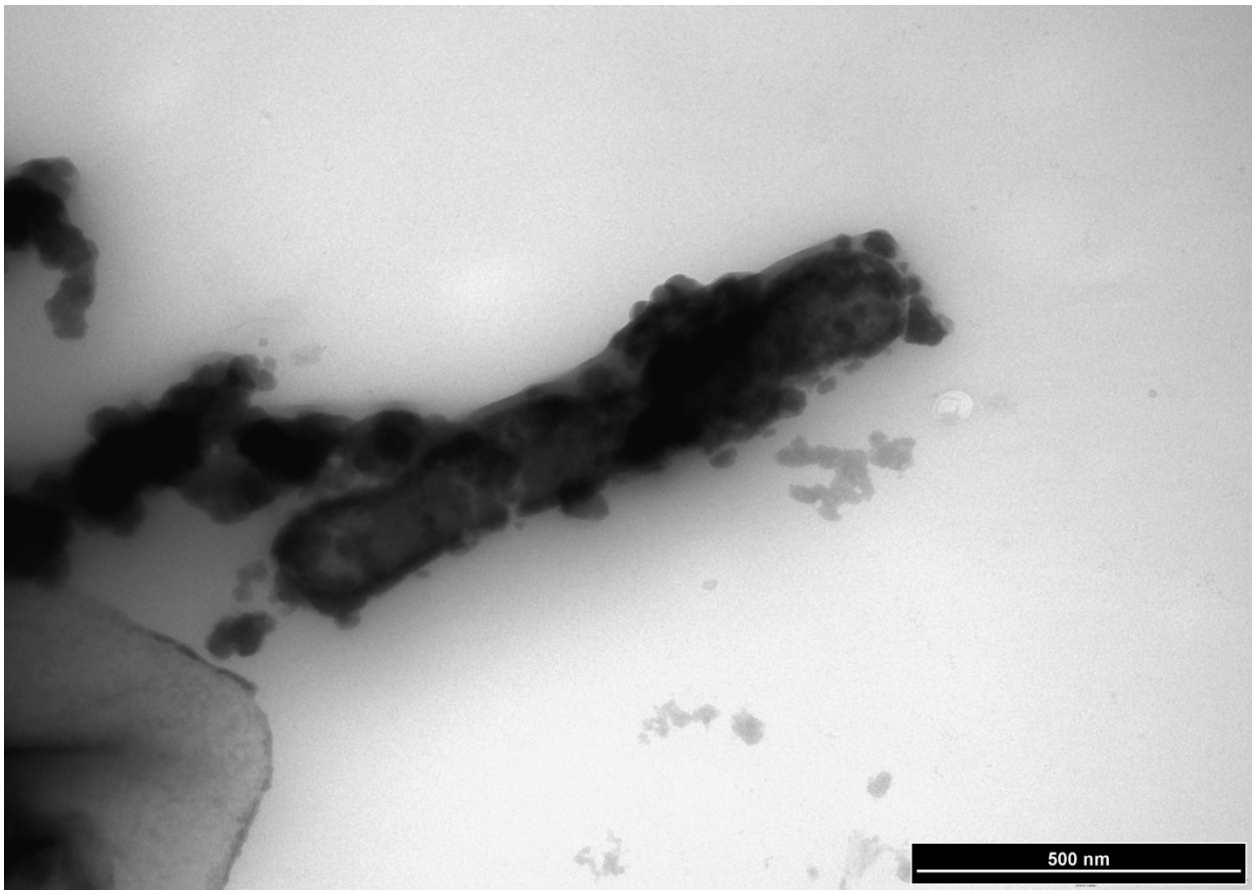

Figure D24

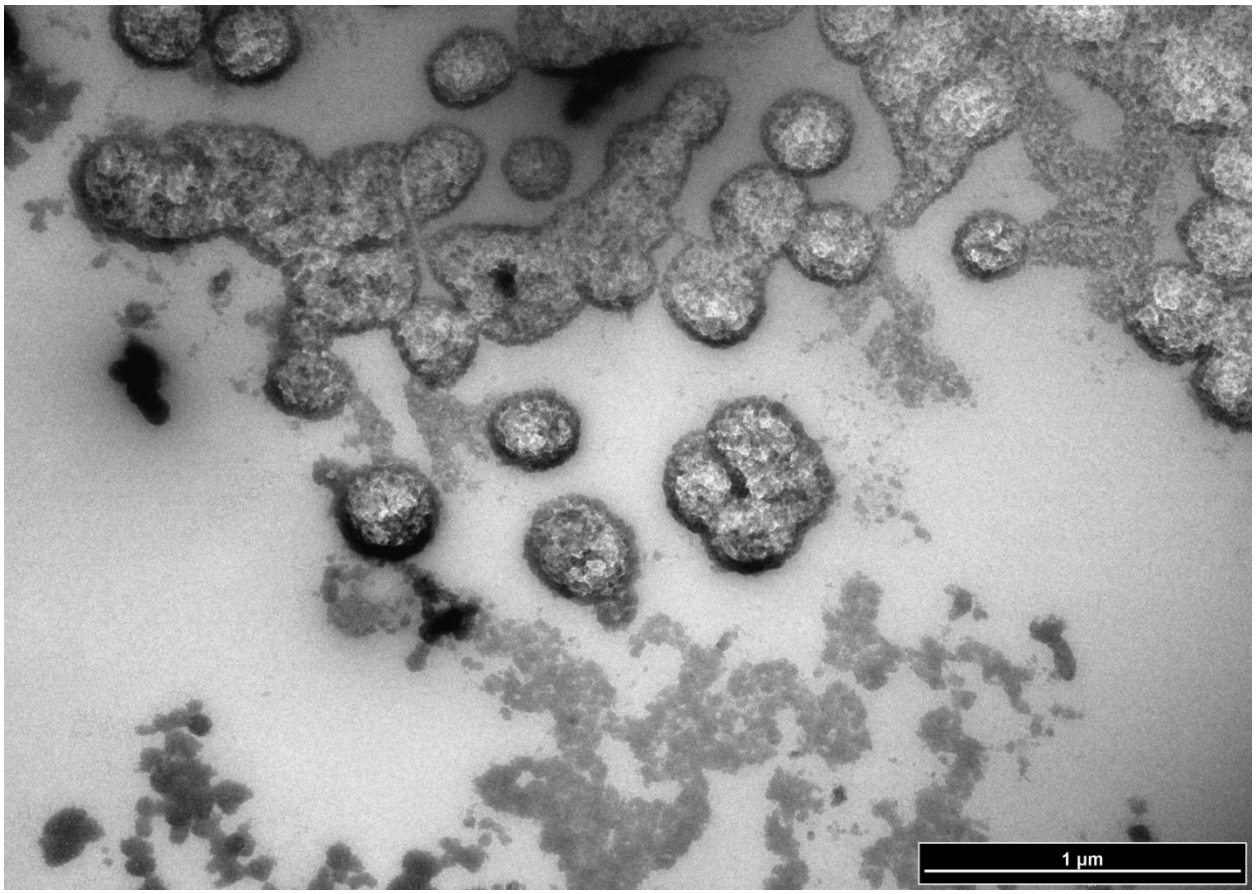

Figure D25

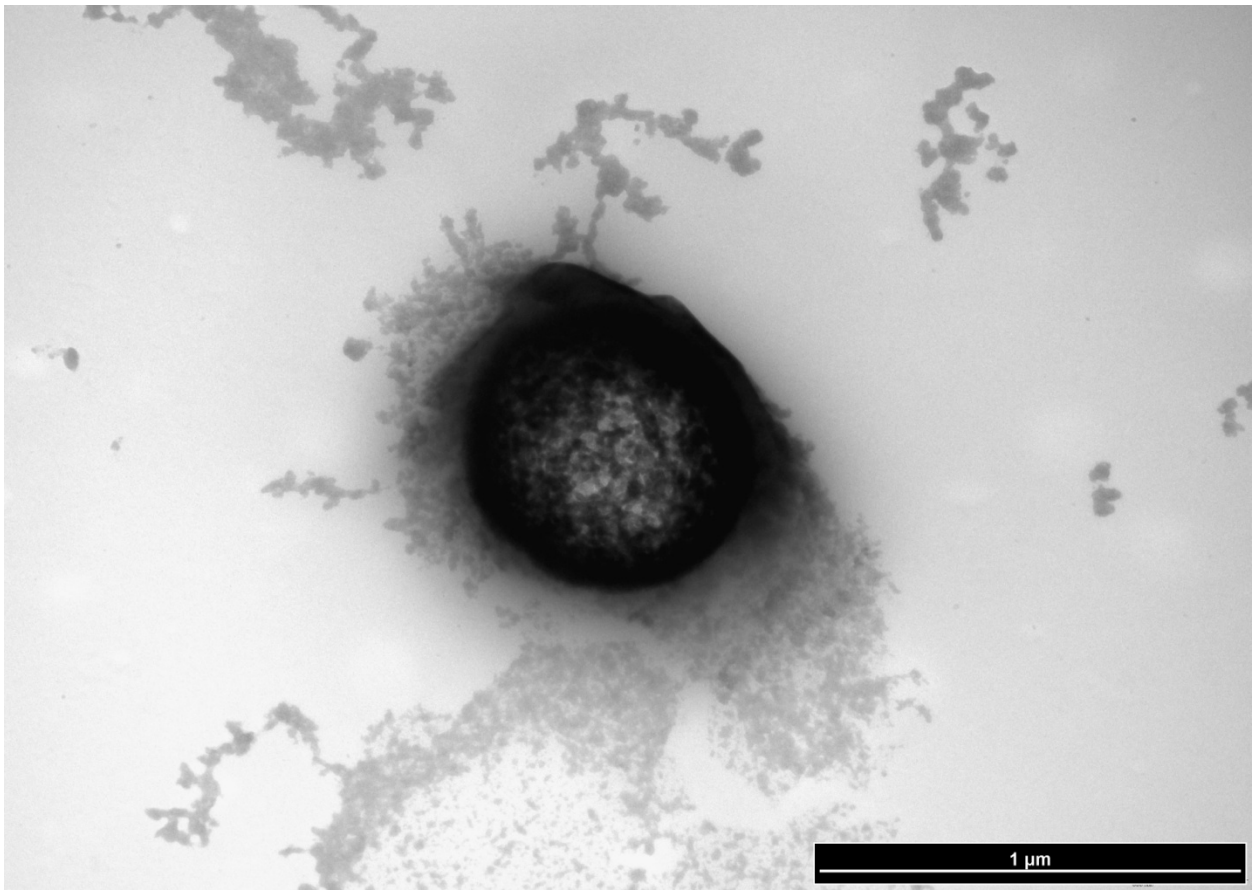

Figure D26

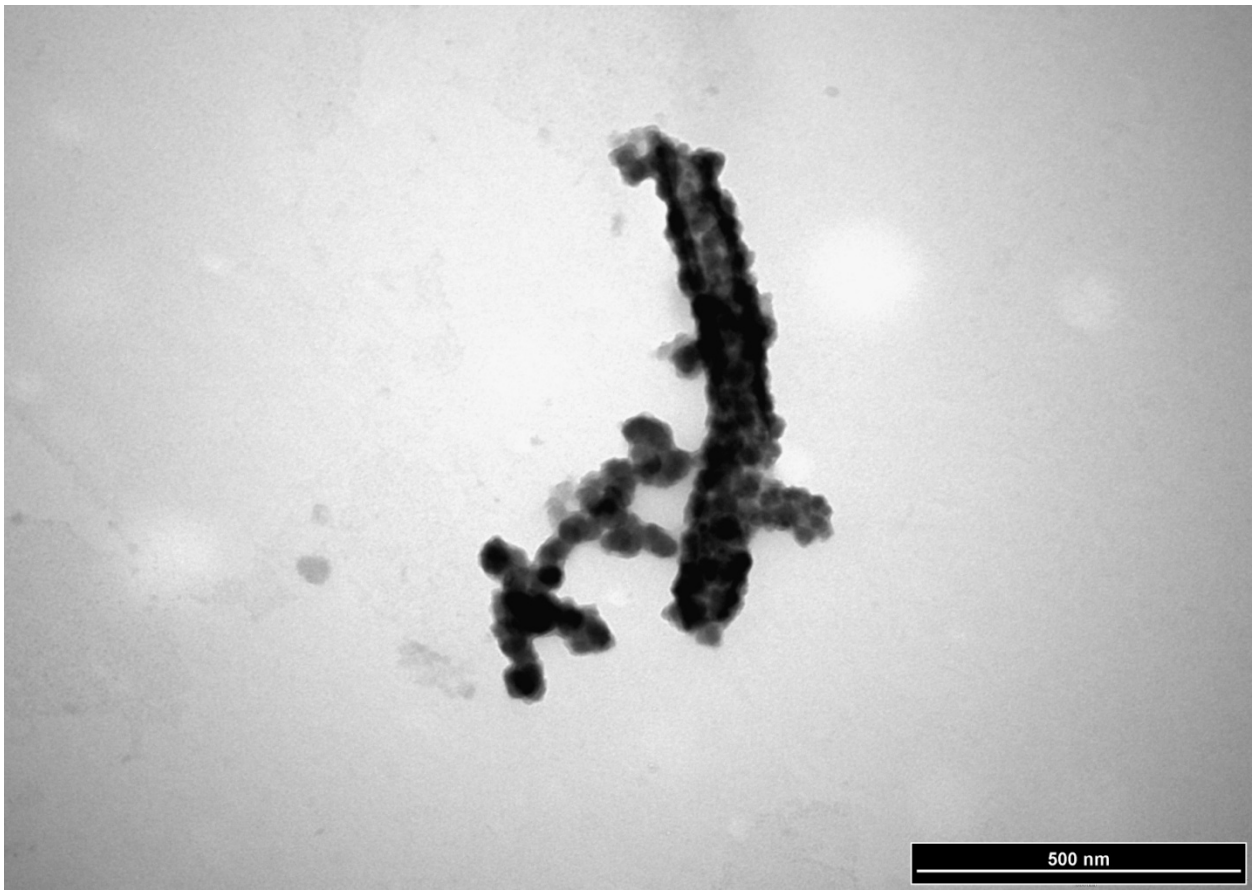

Figure D27

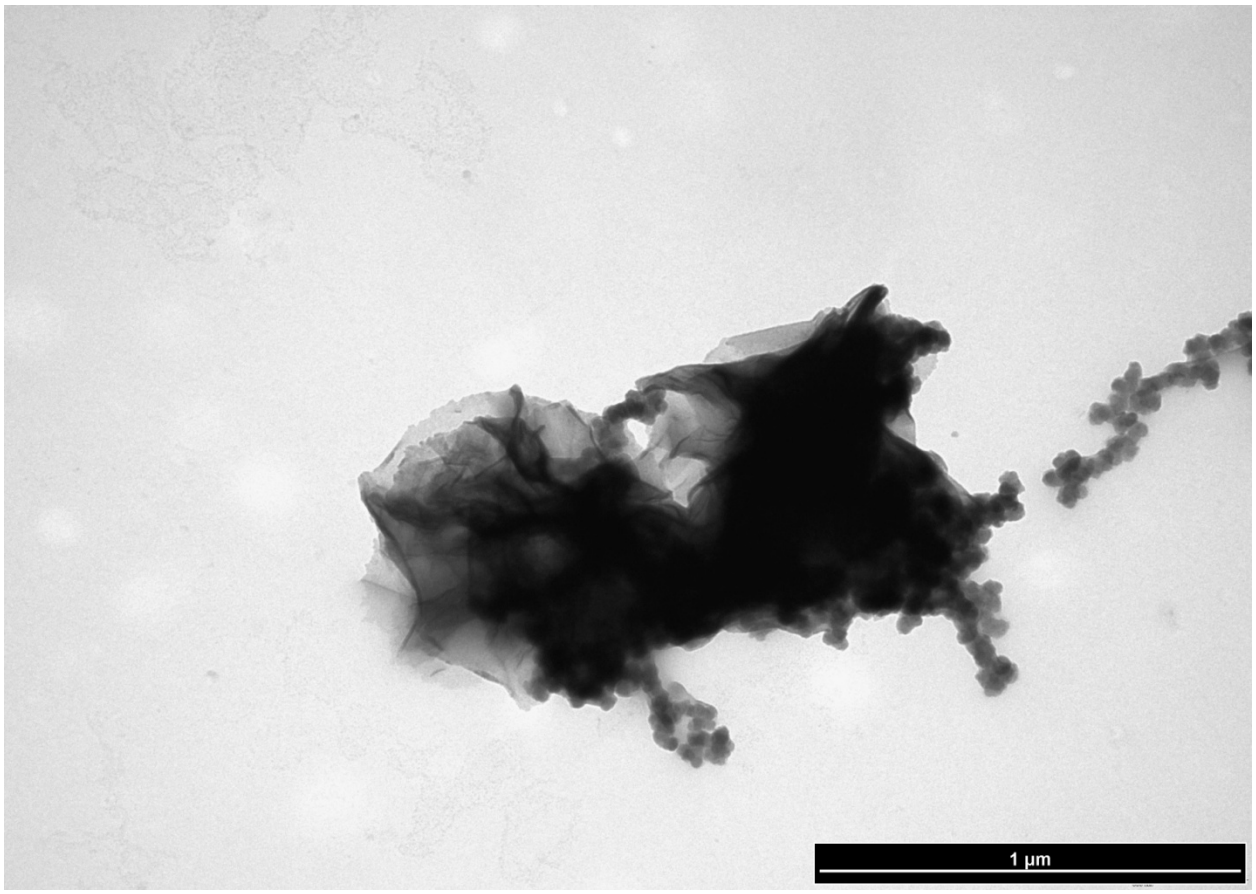

Figure D28

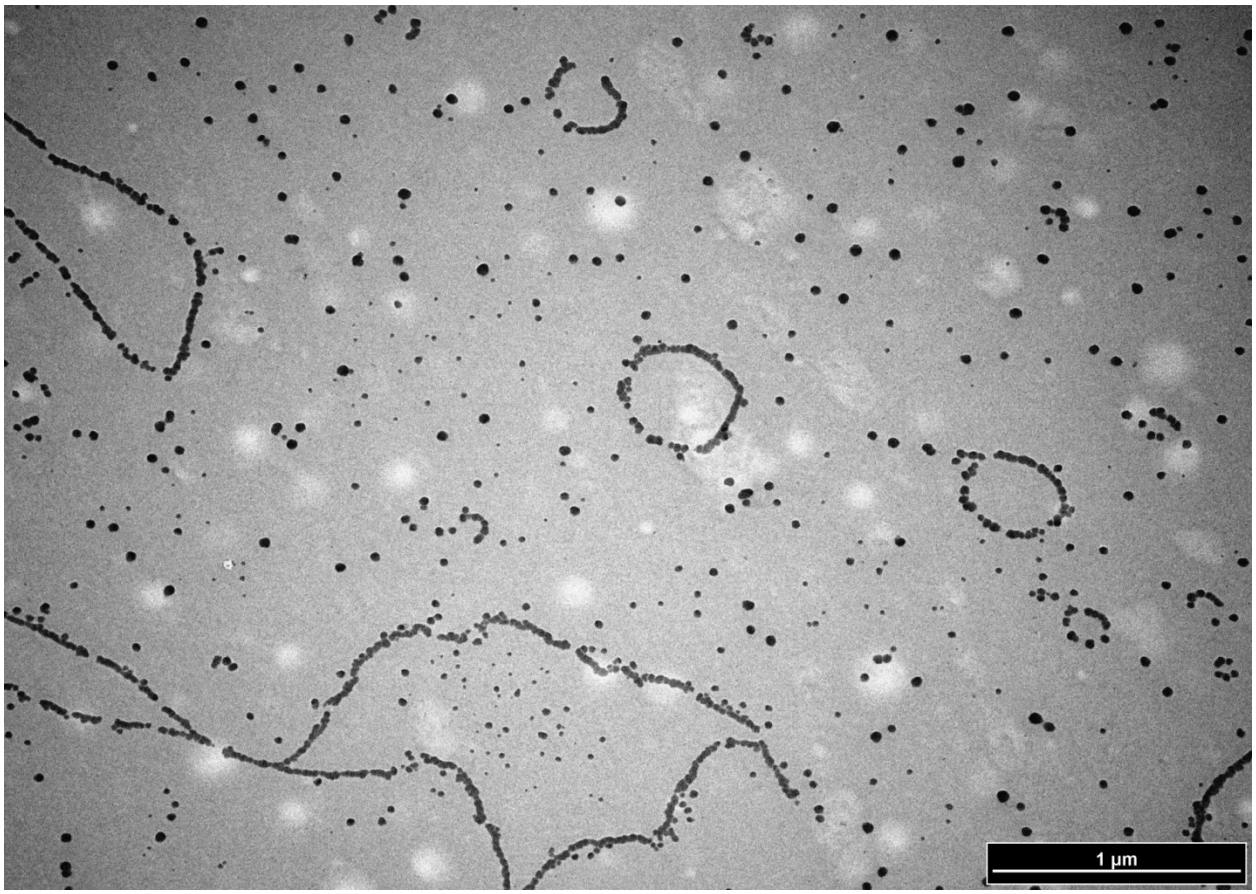

Figure D29

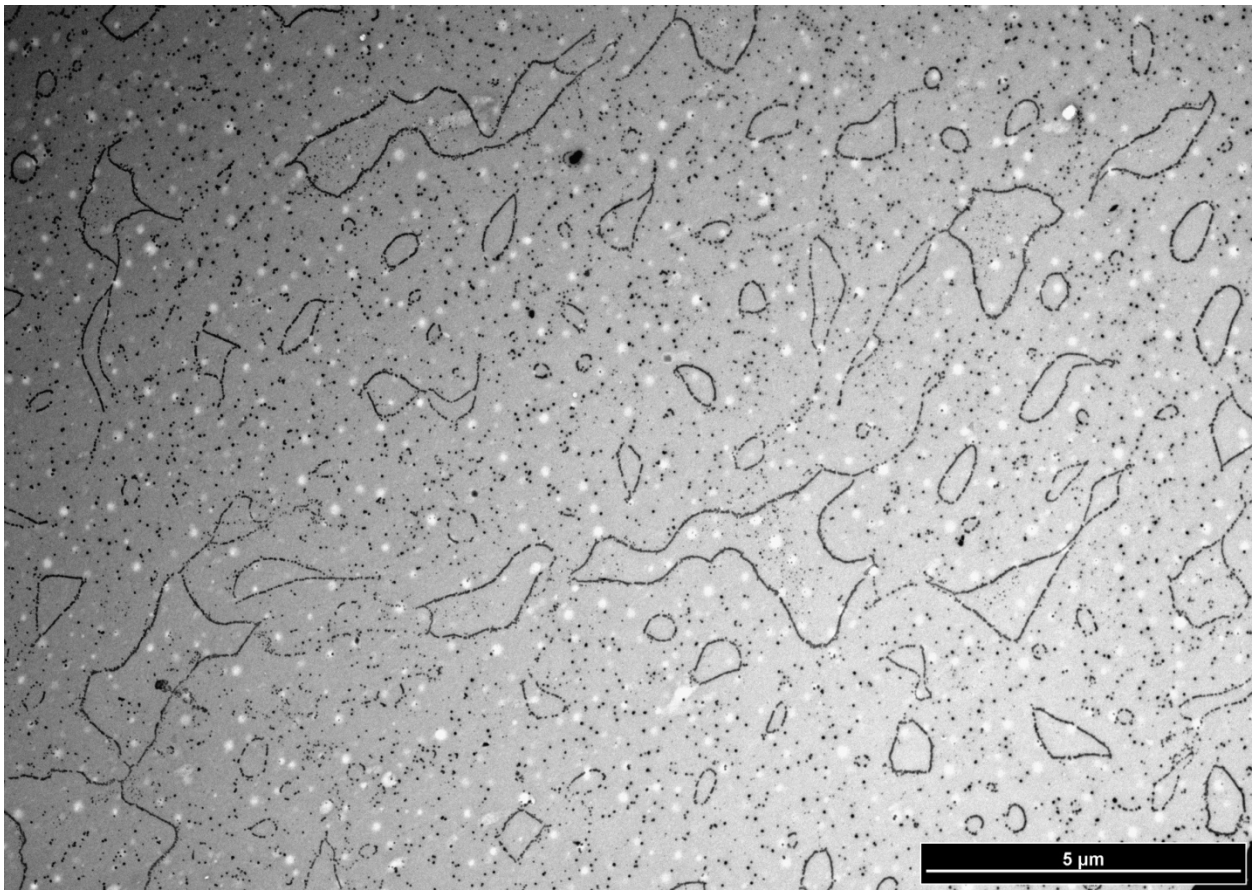

Figure D30

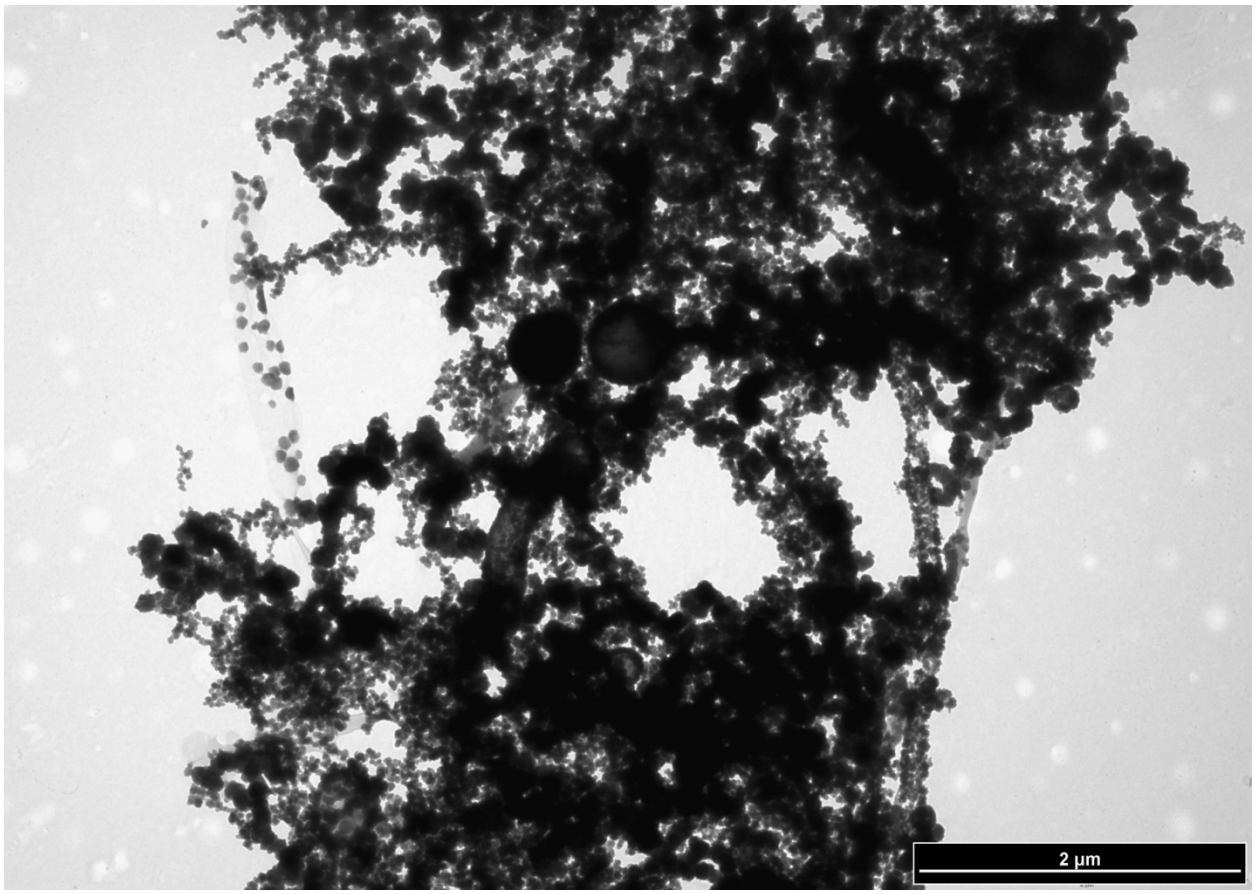

Figure D31

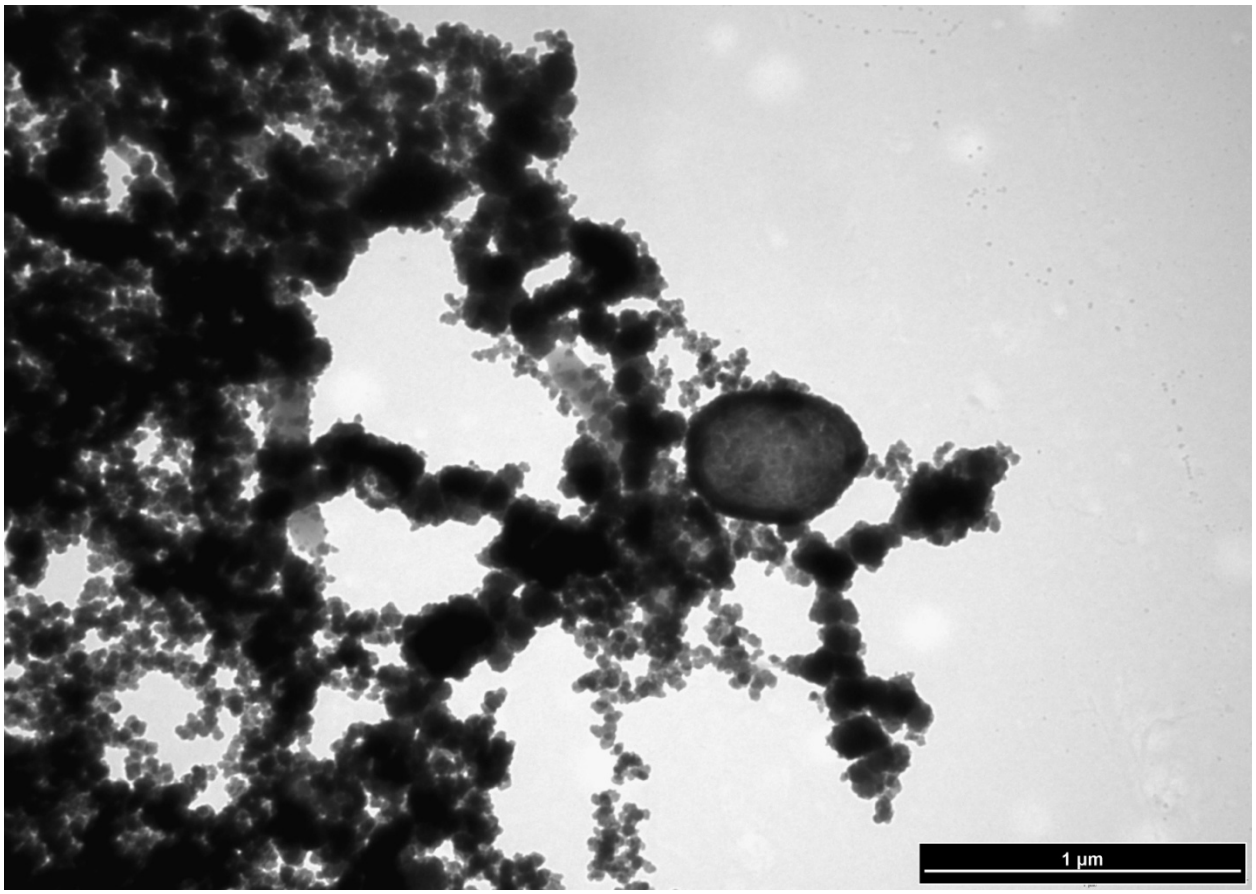

Figure D32

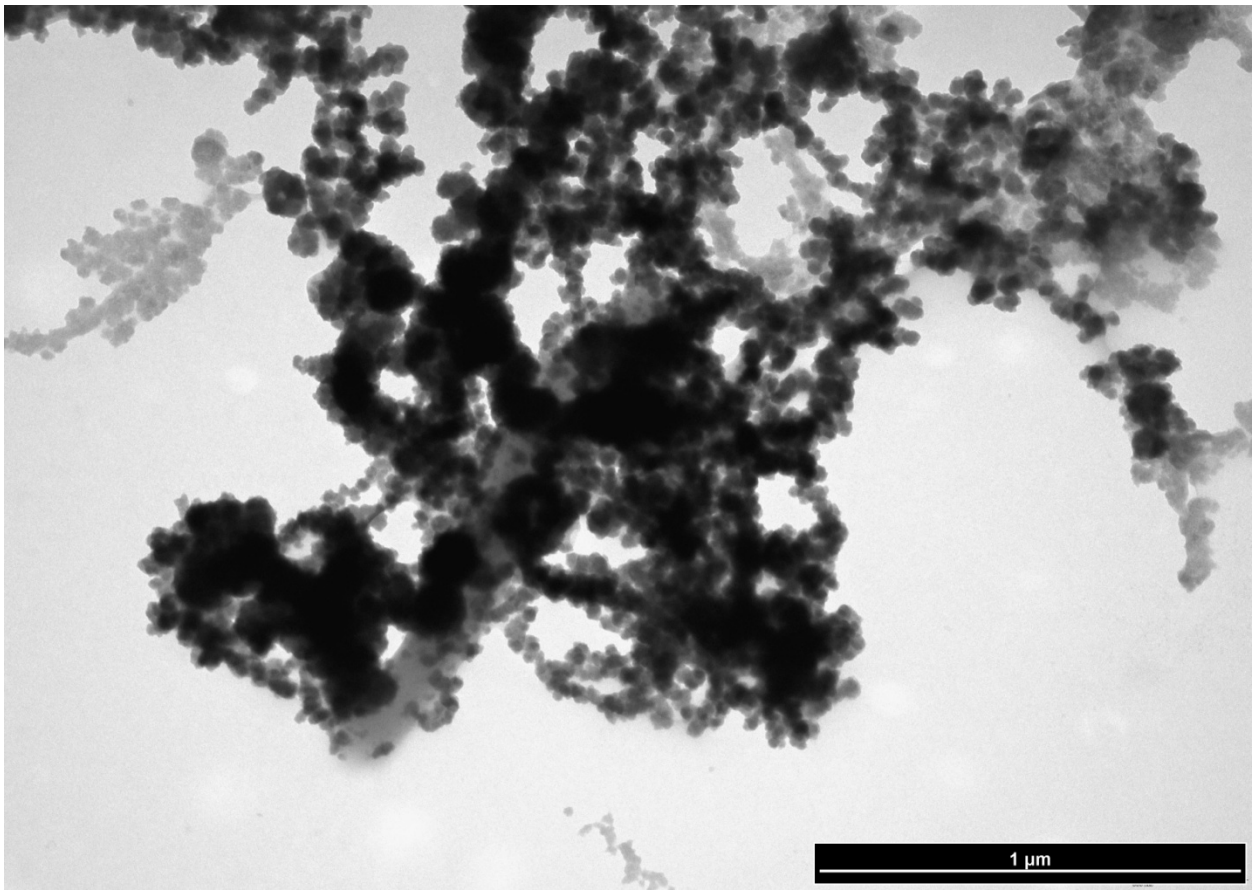

Figure D33

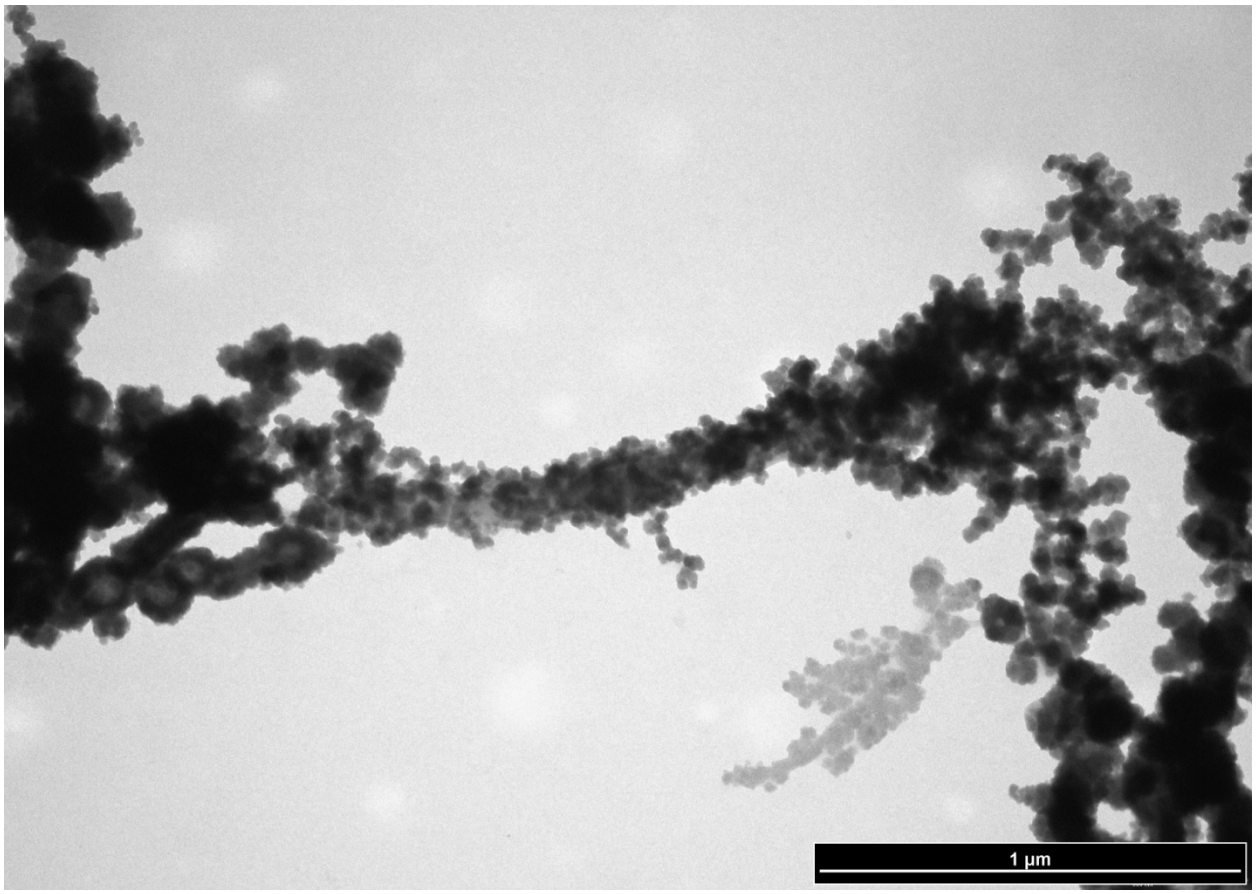

Figure D34

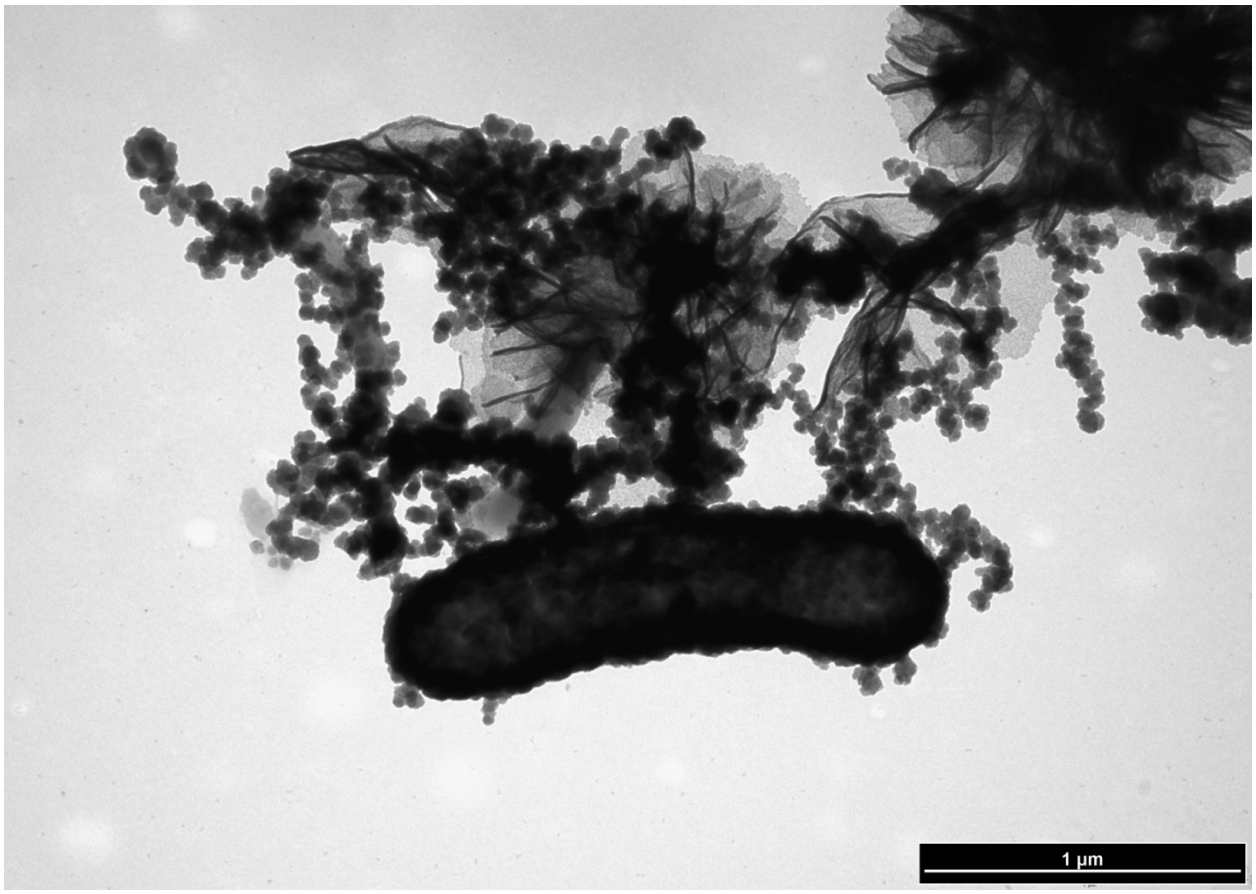

Figure D35

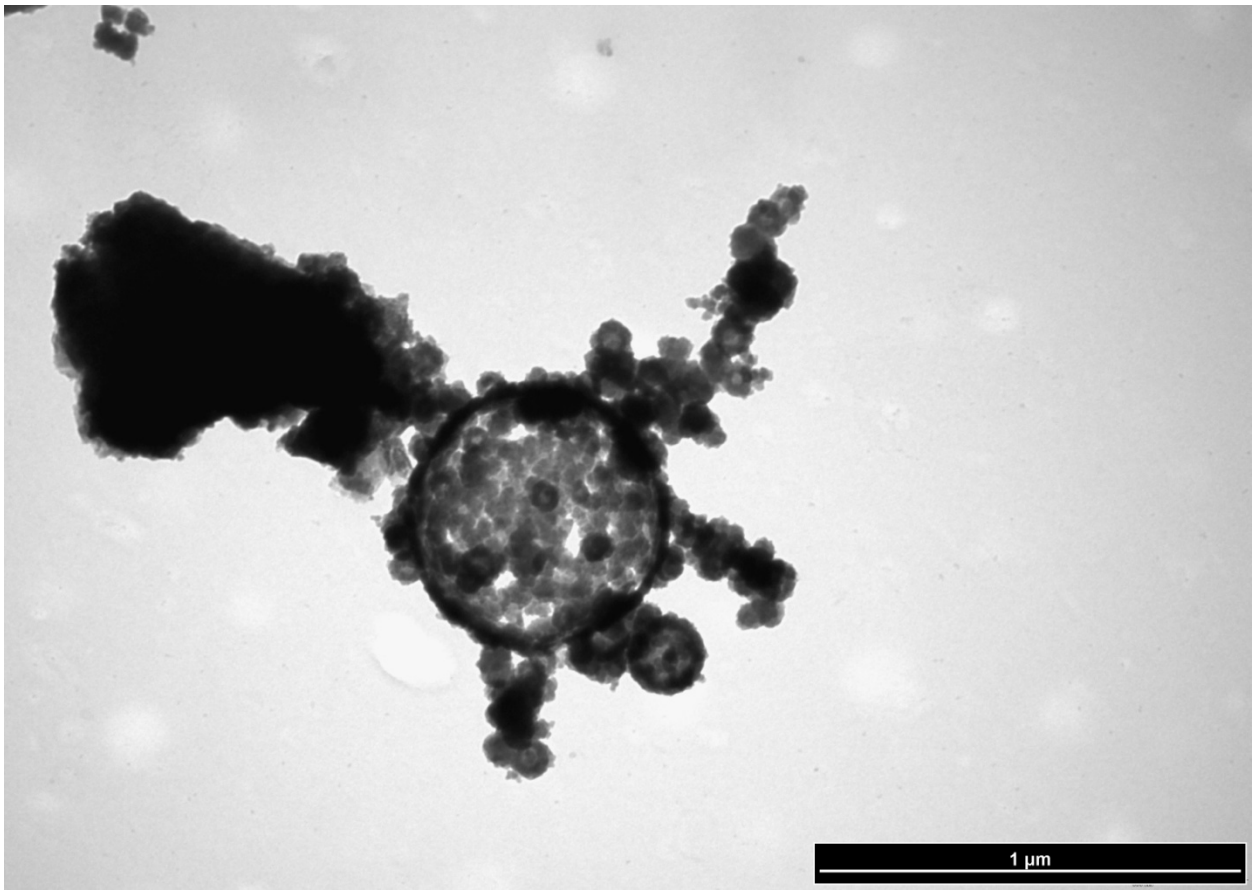

Figure D36

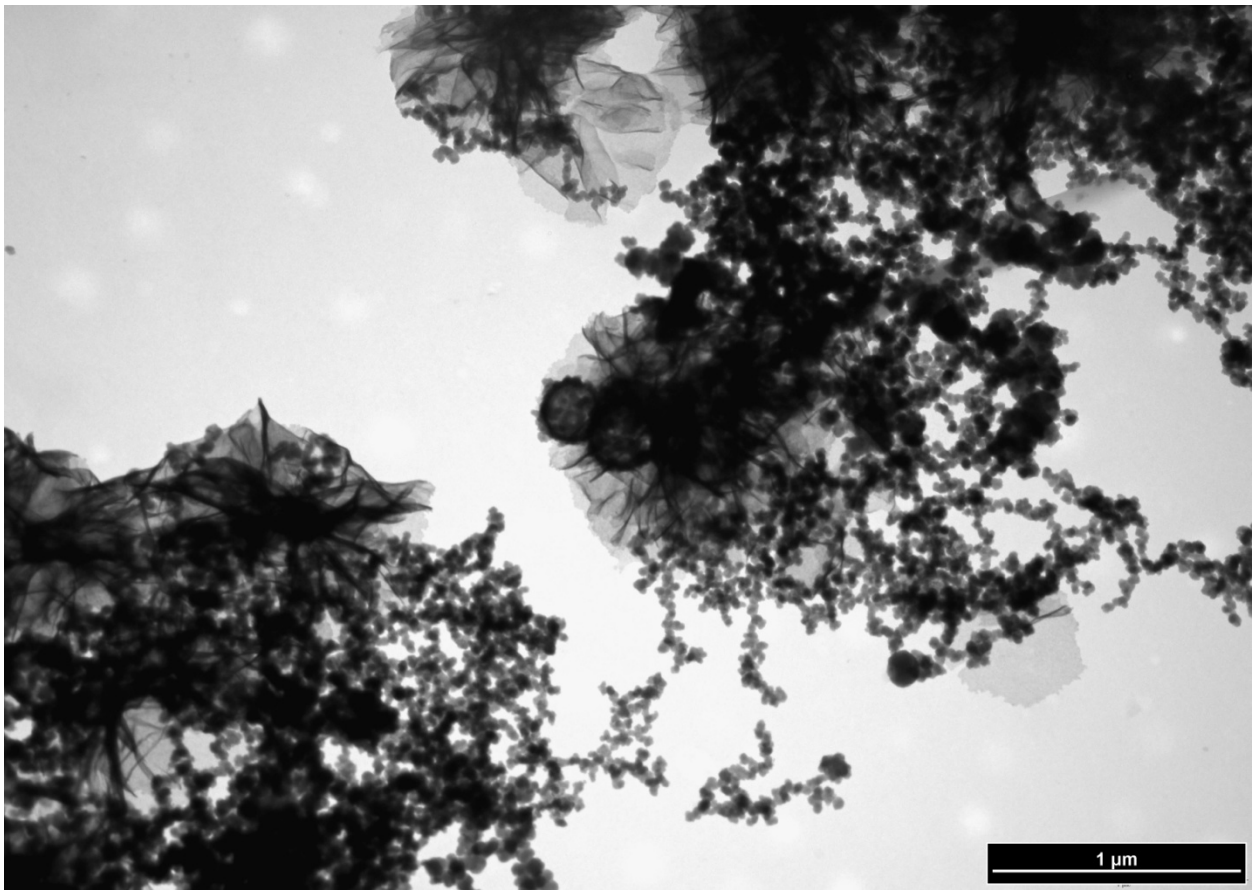

Figure D37

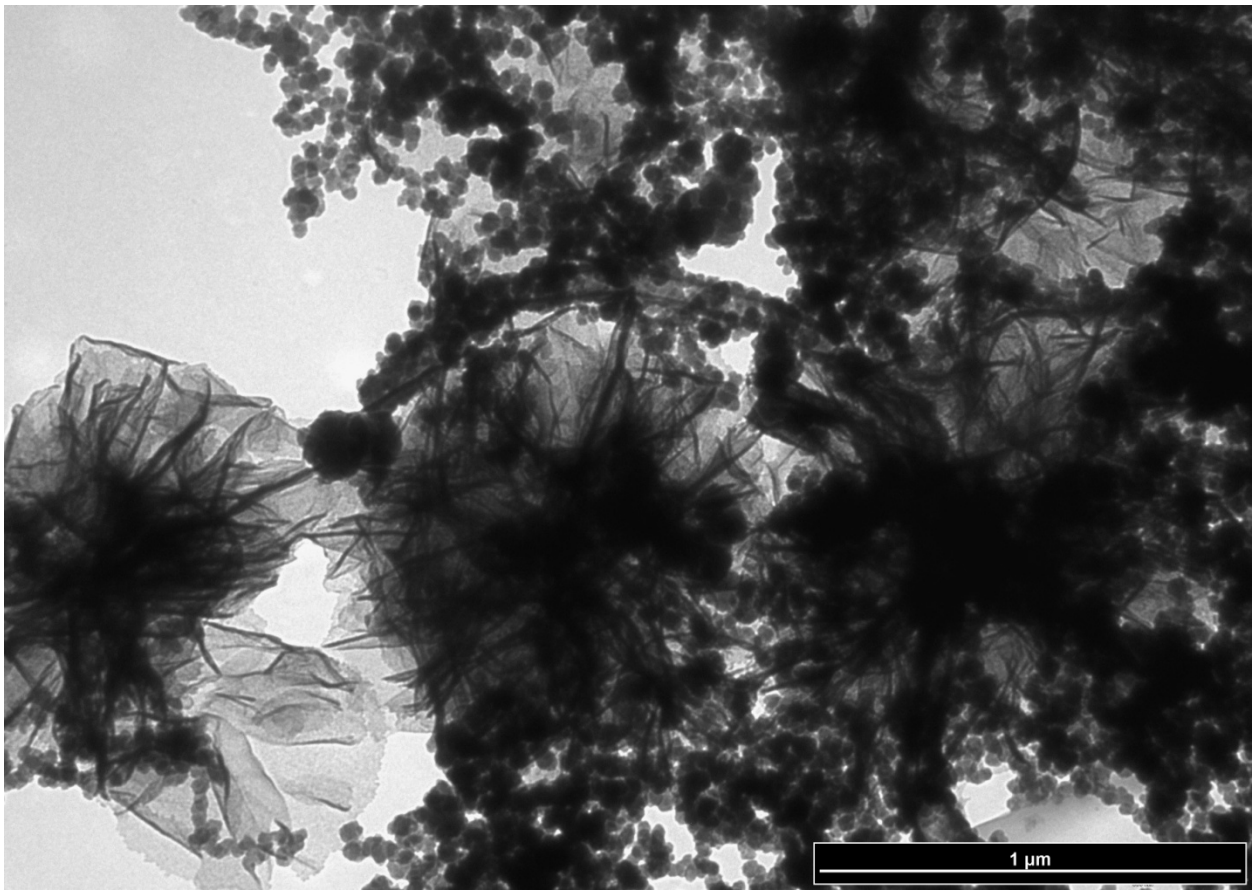

Figure D38

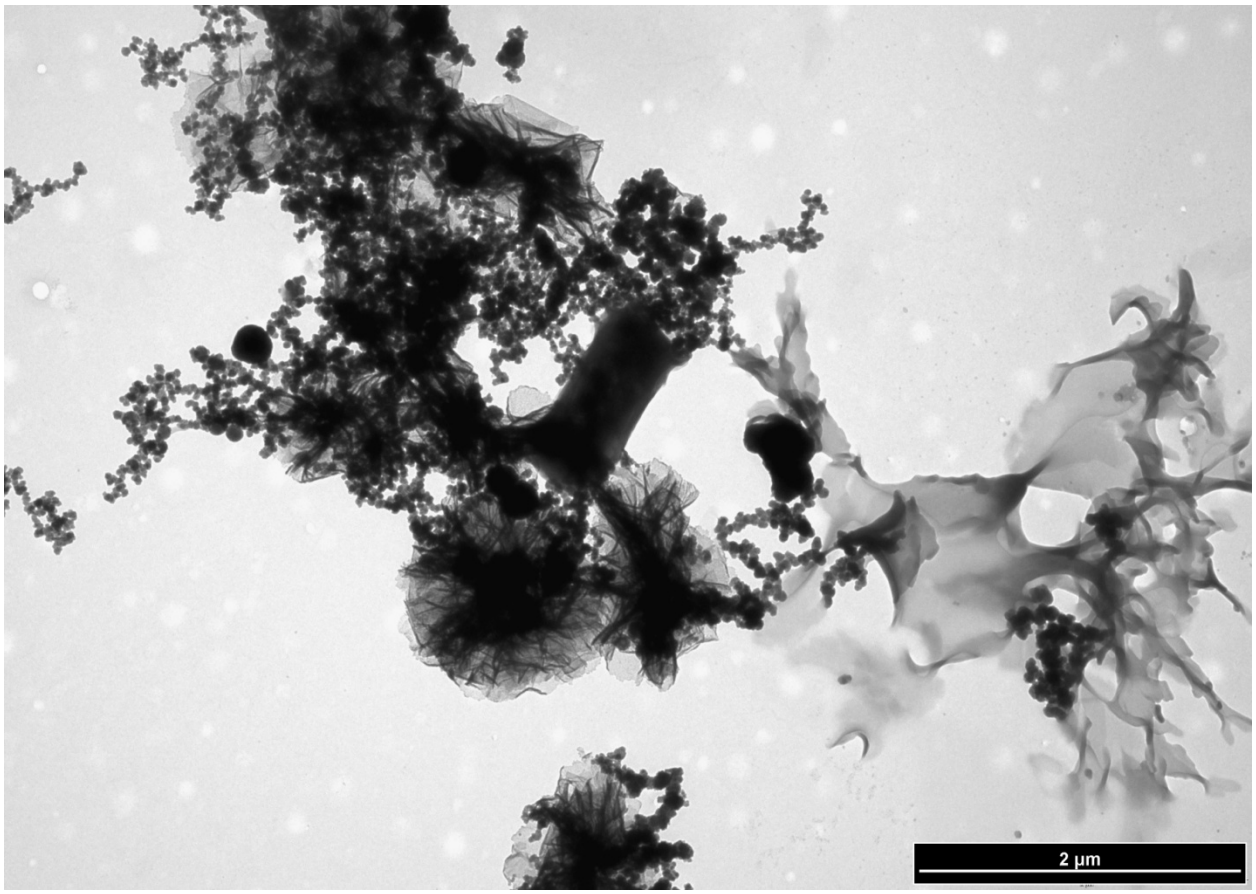

Figure D39

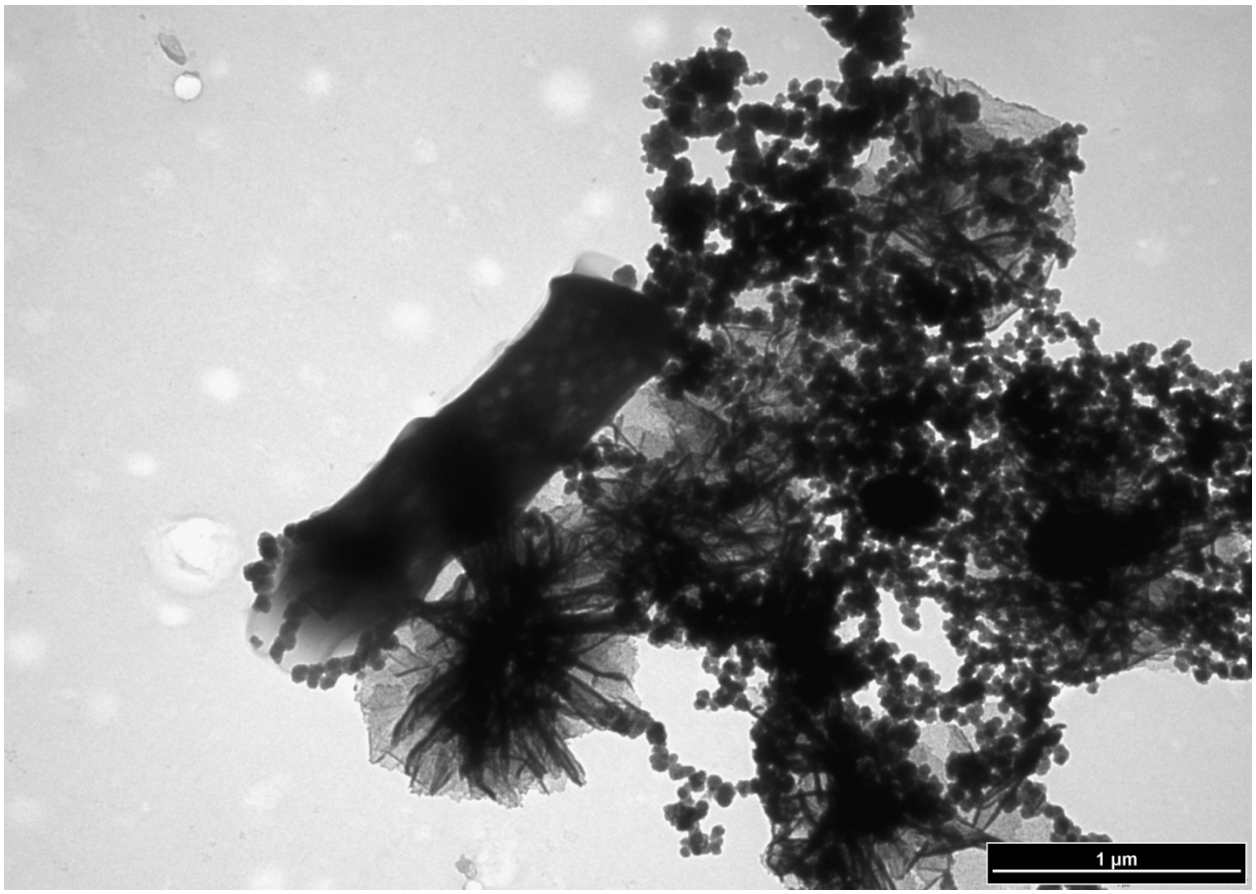

Figure D40

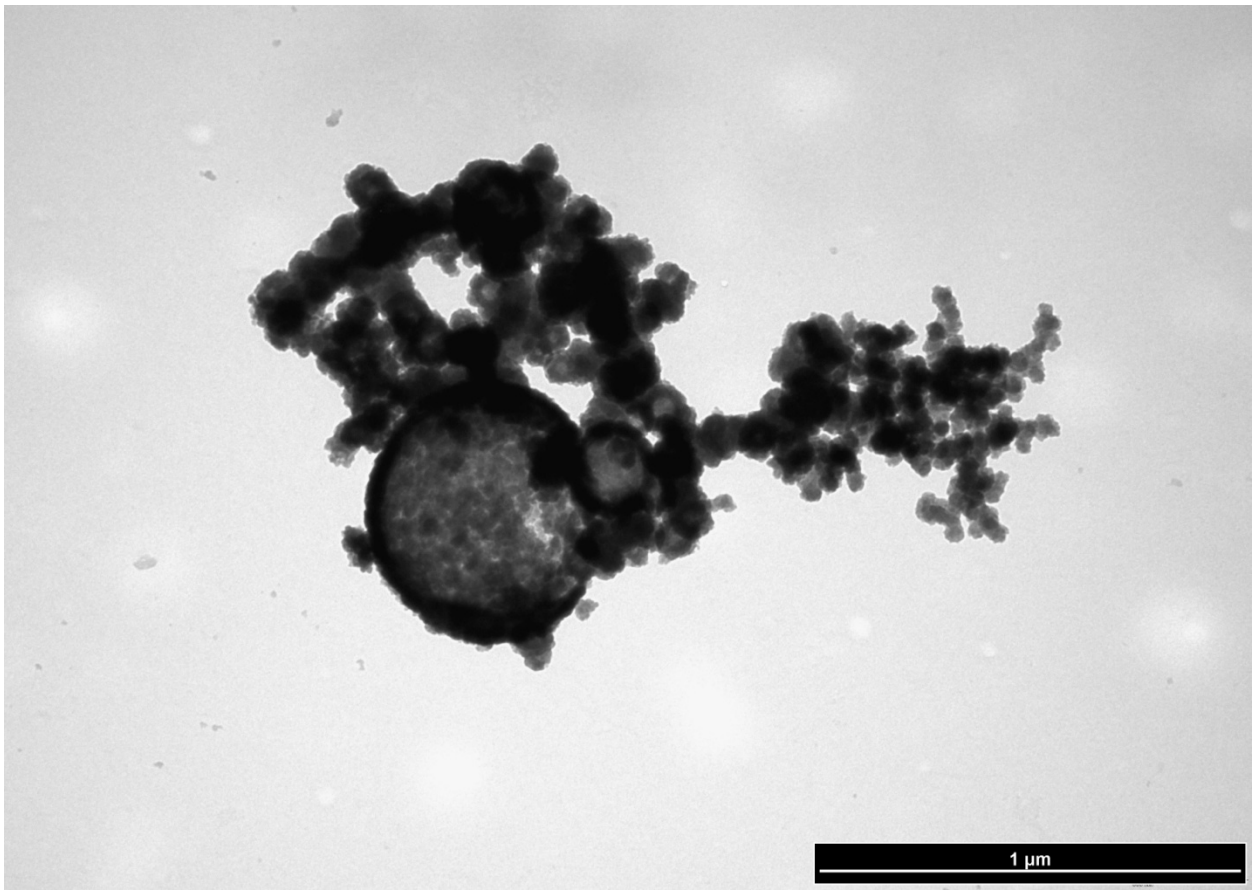

Figure D41

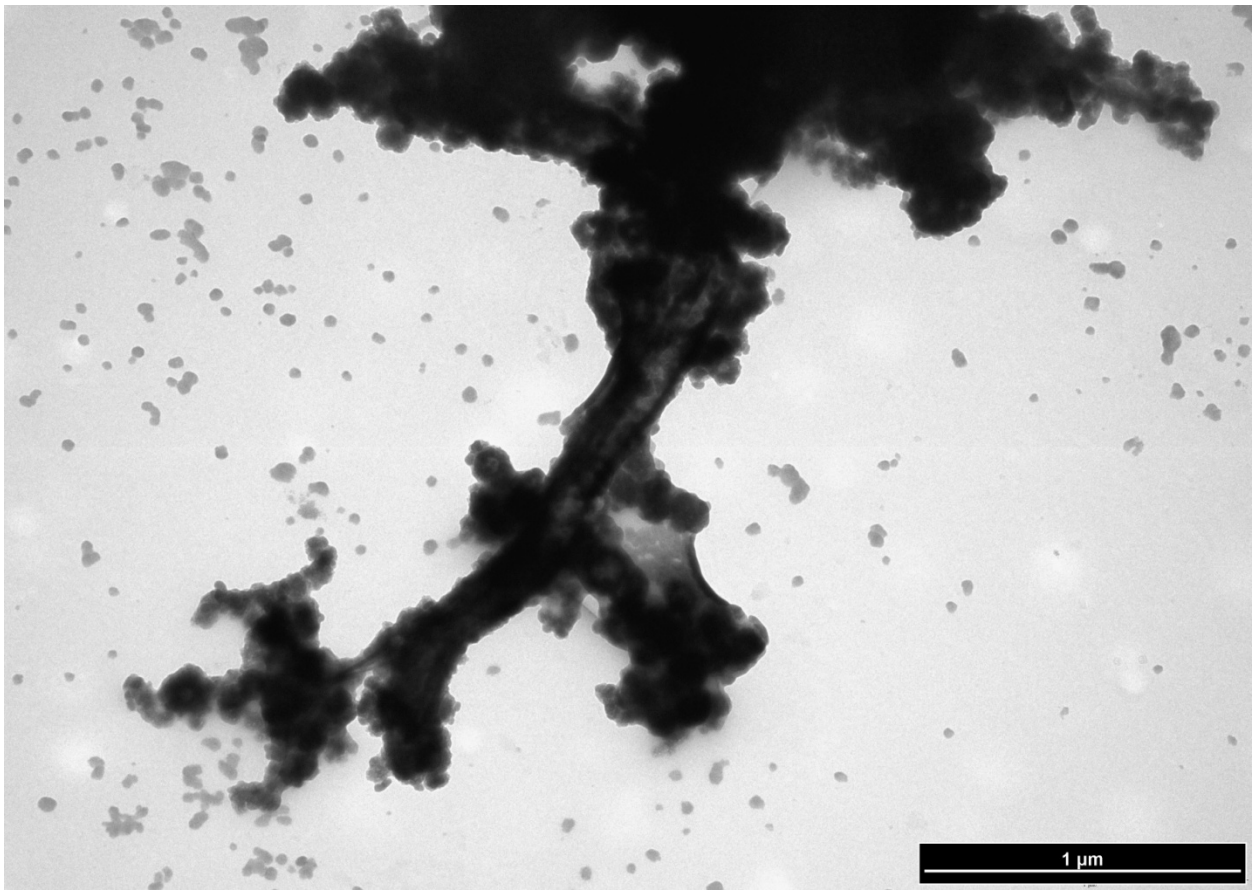

Figure D42

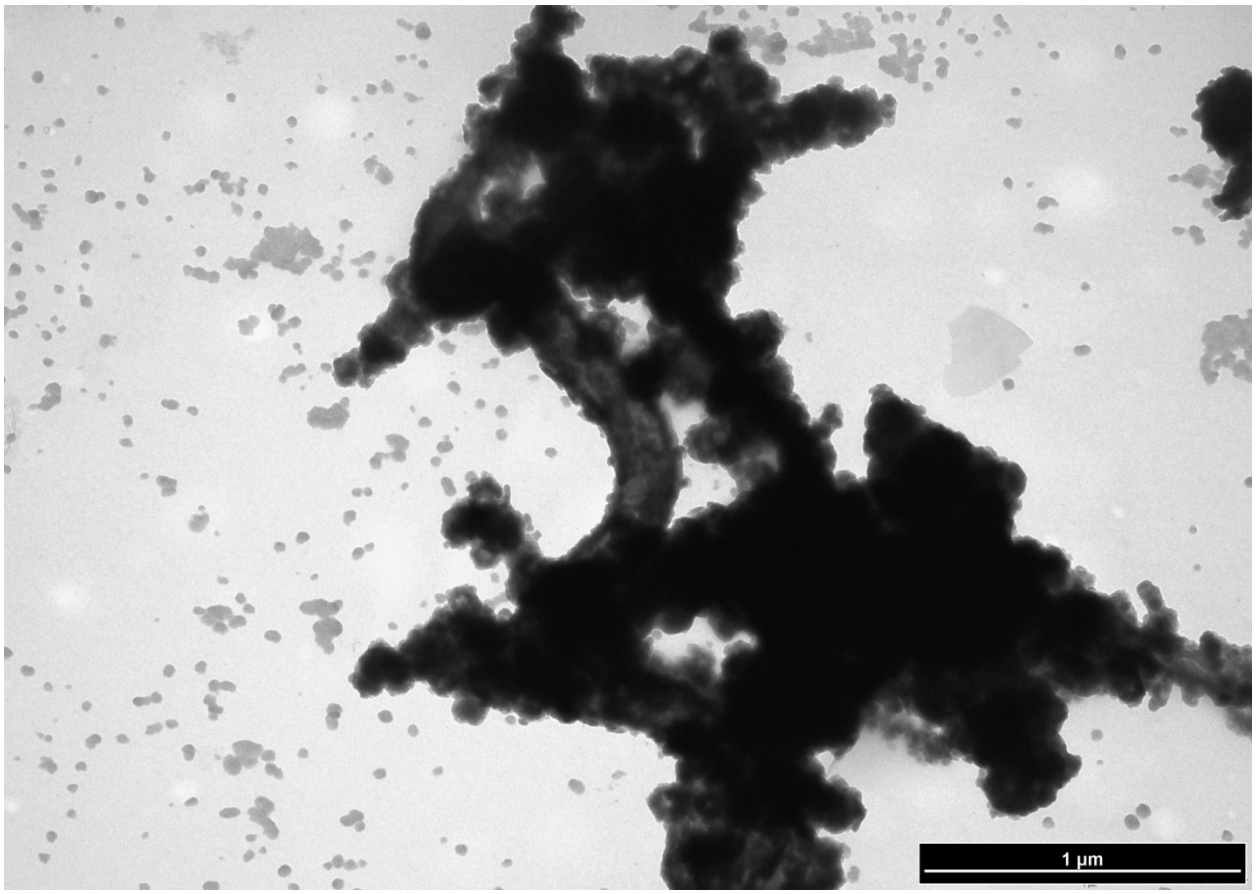

Figure D43

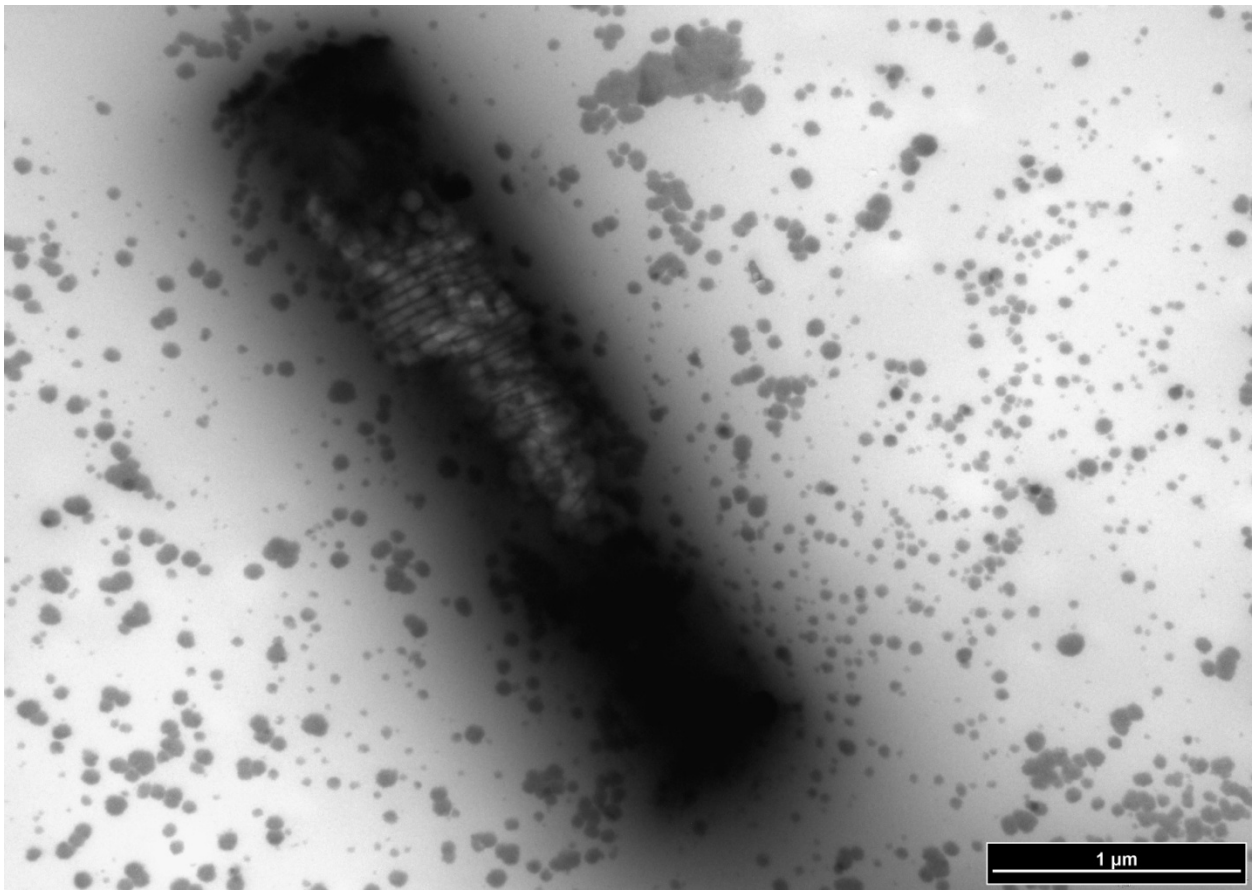

Figure D44

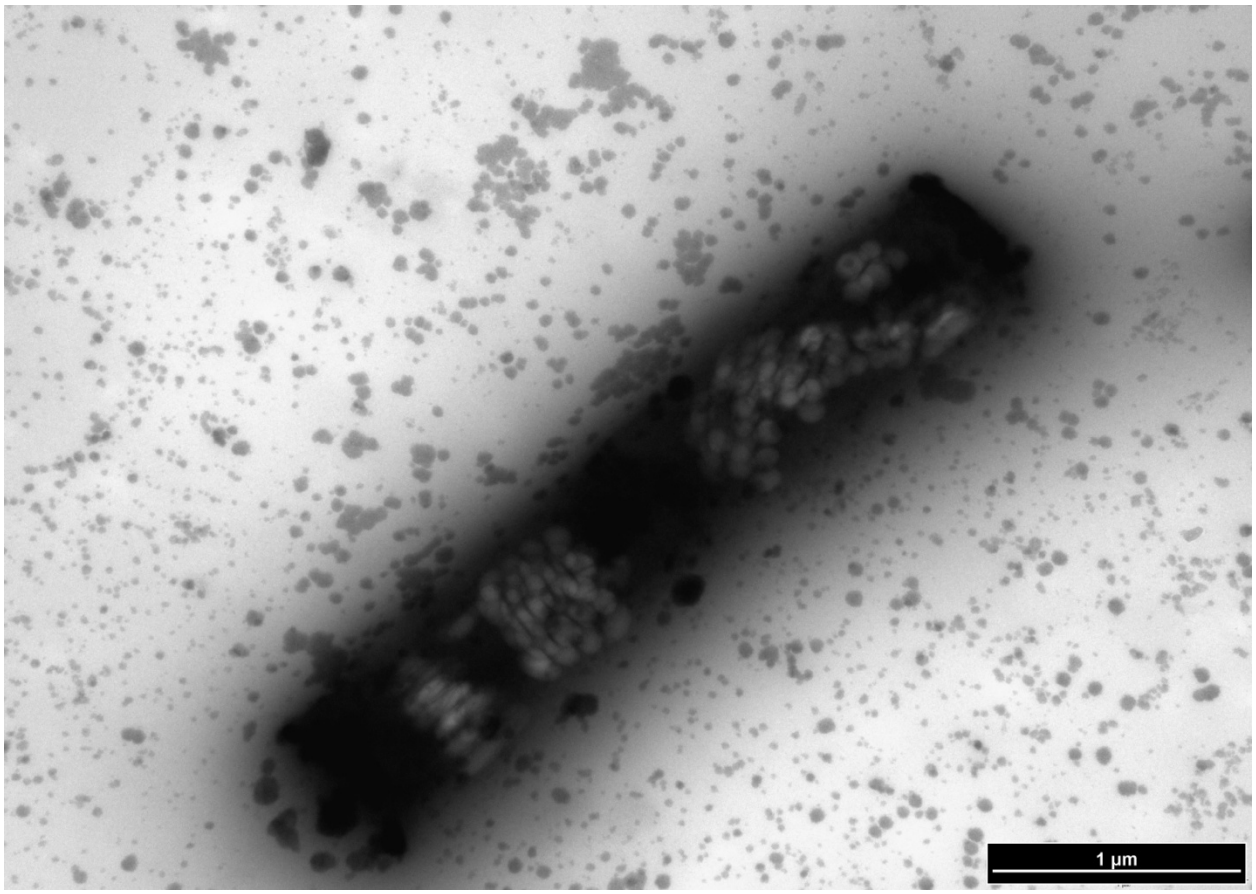

Figure D45

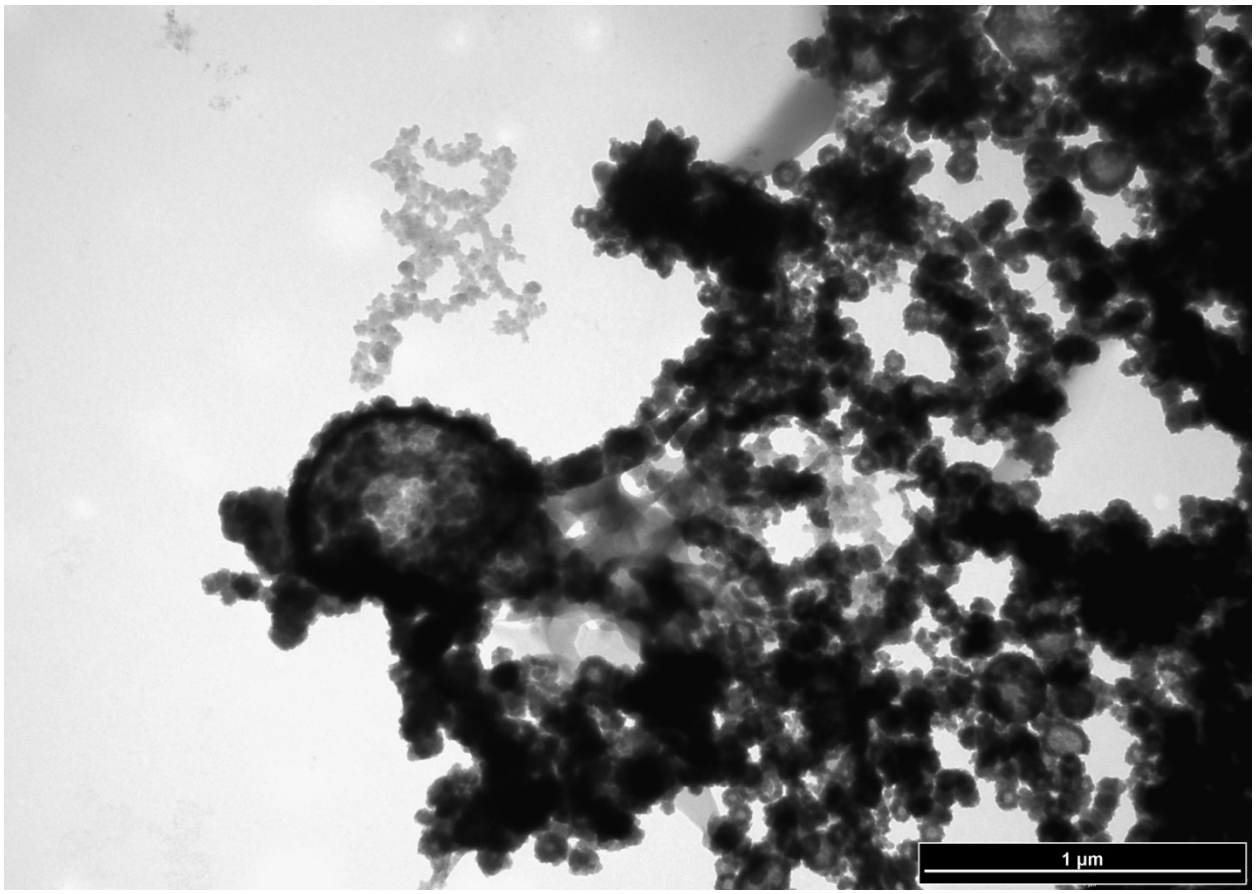

Figure D46

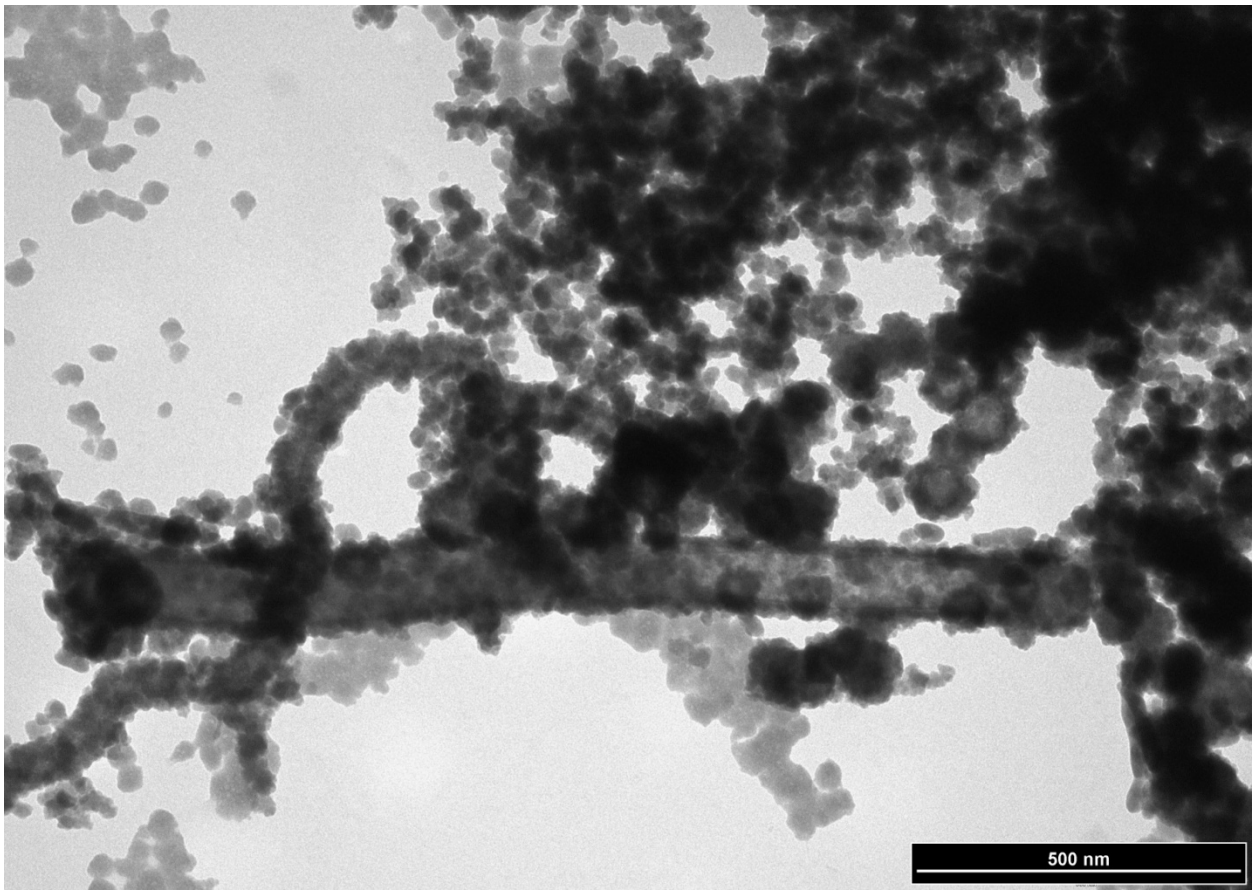

Figure D47

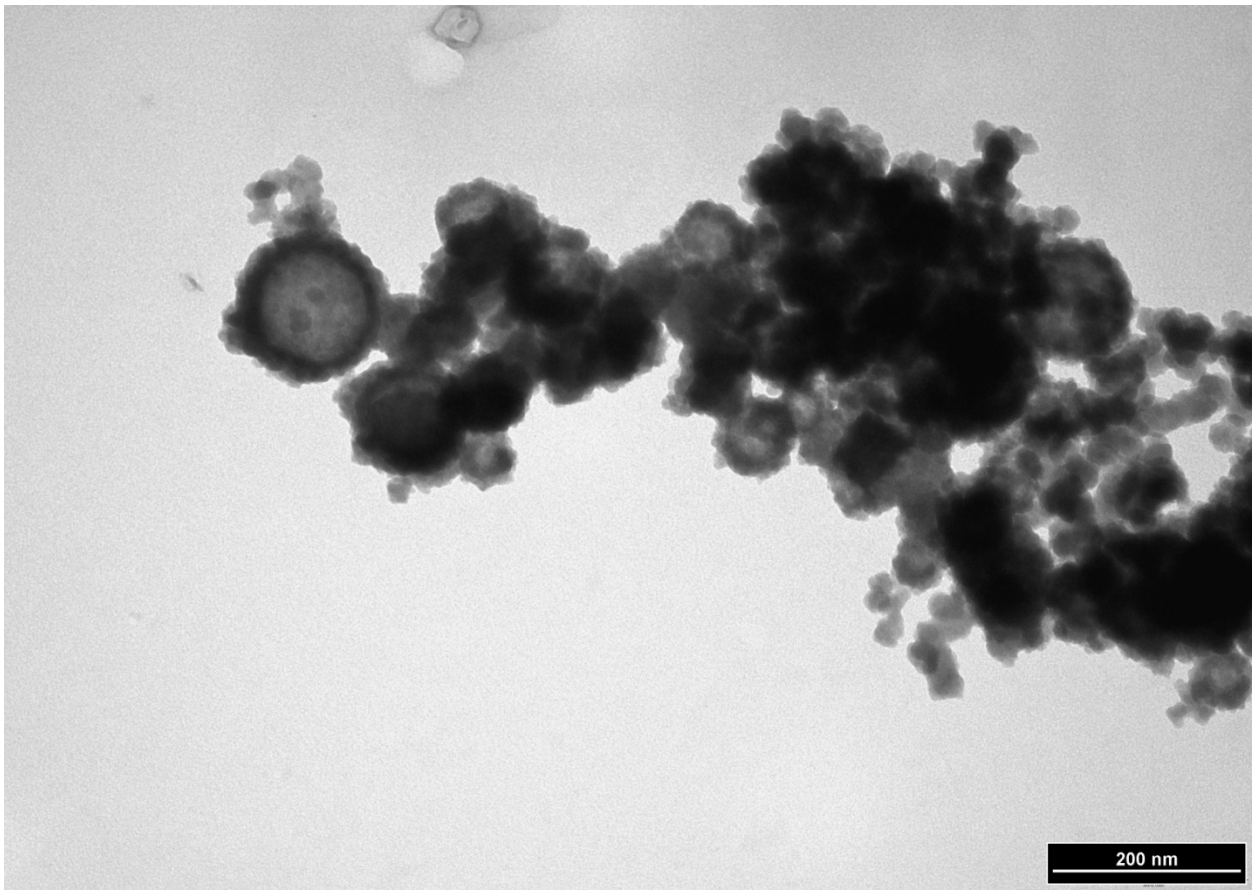

Figure D48

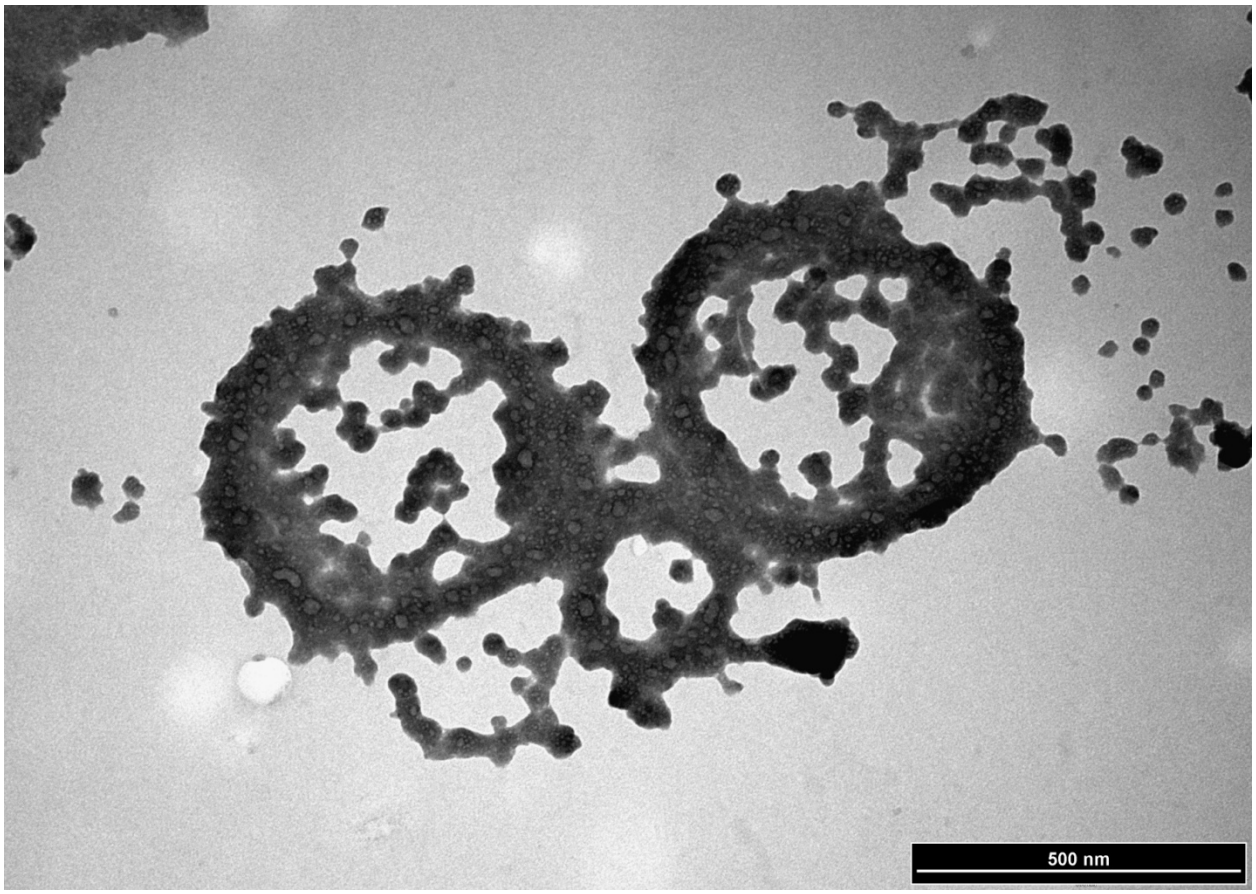

Figure D49

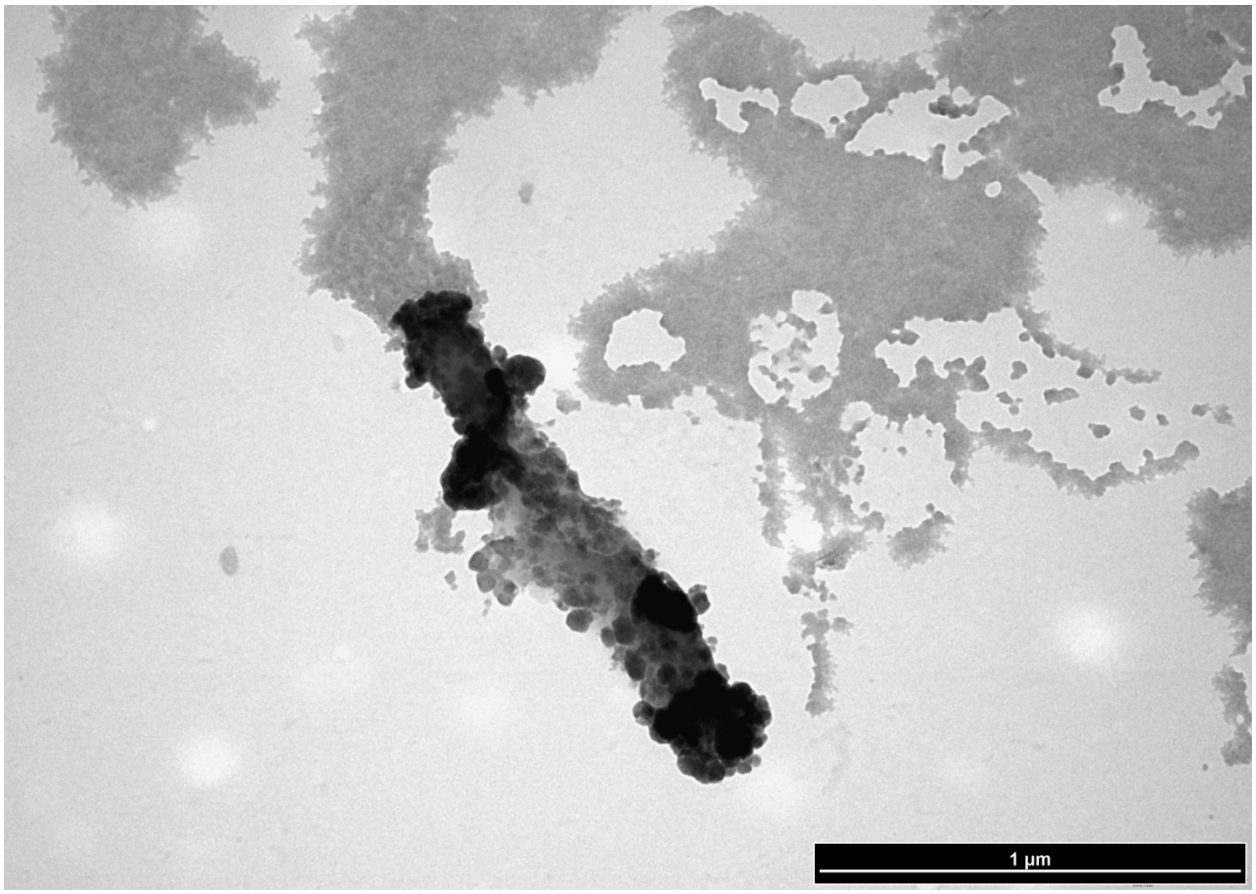

Figure D50

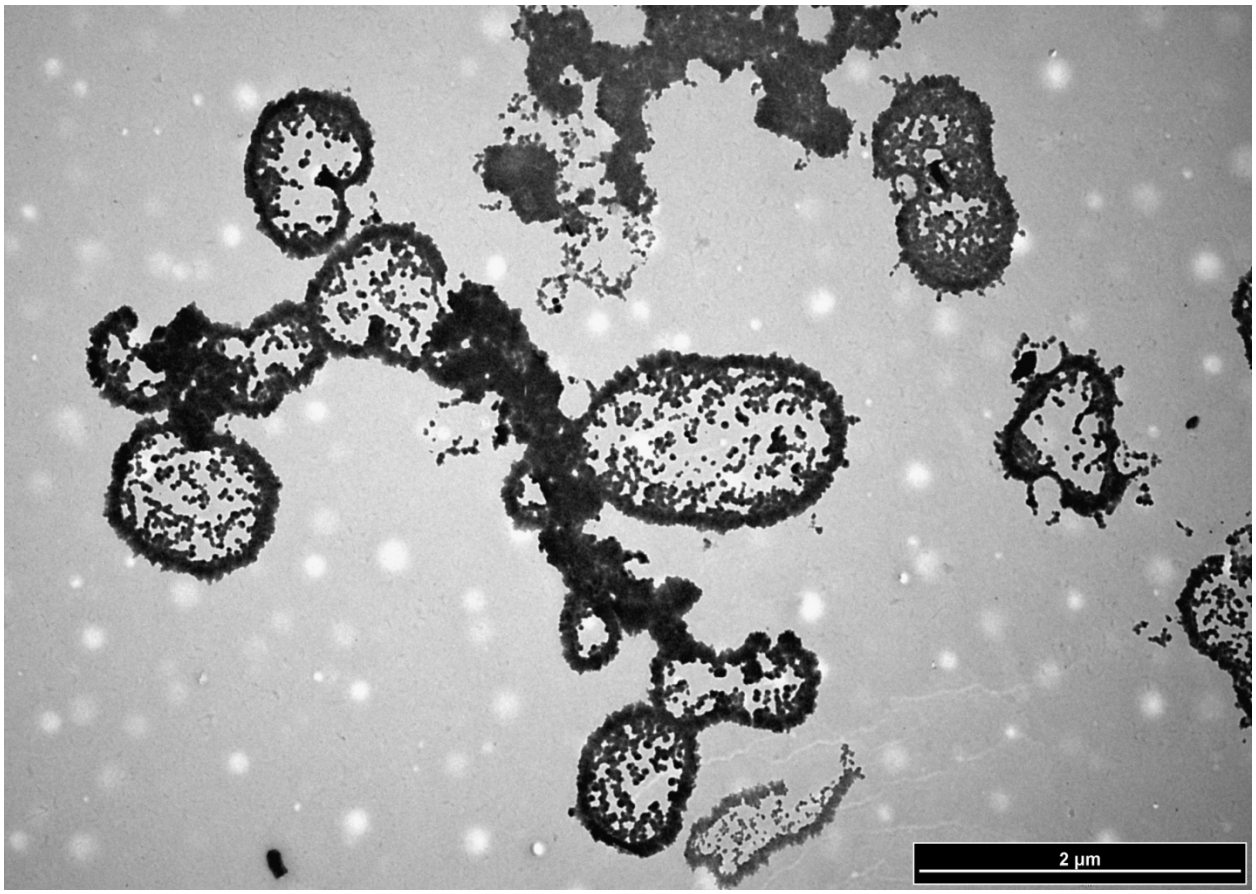

Figure D51

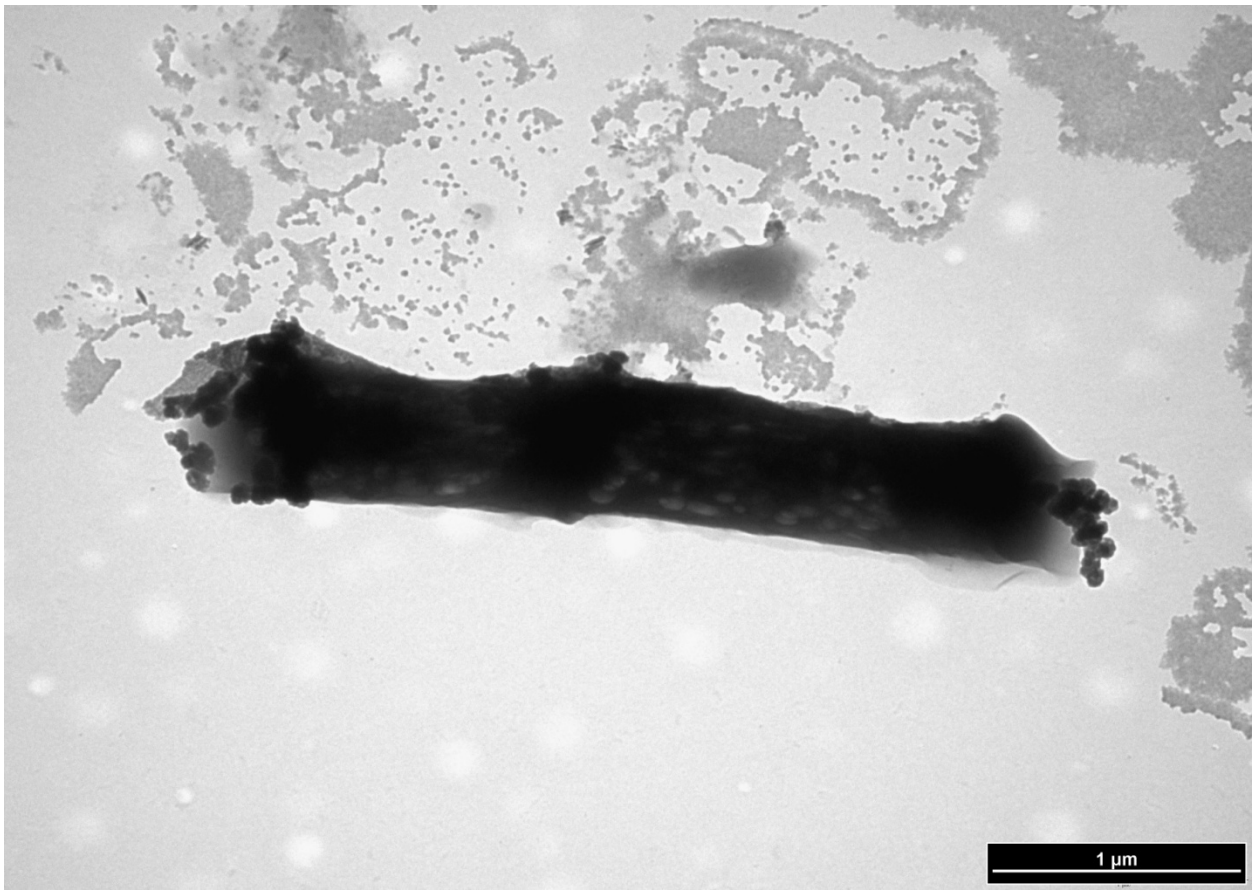

Figure D52

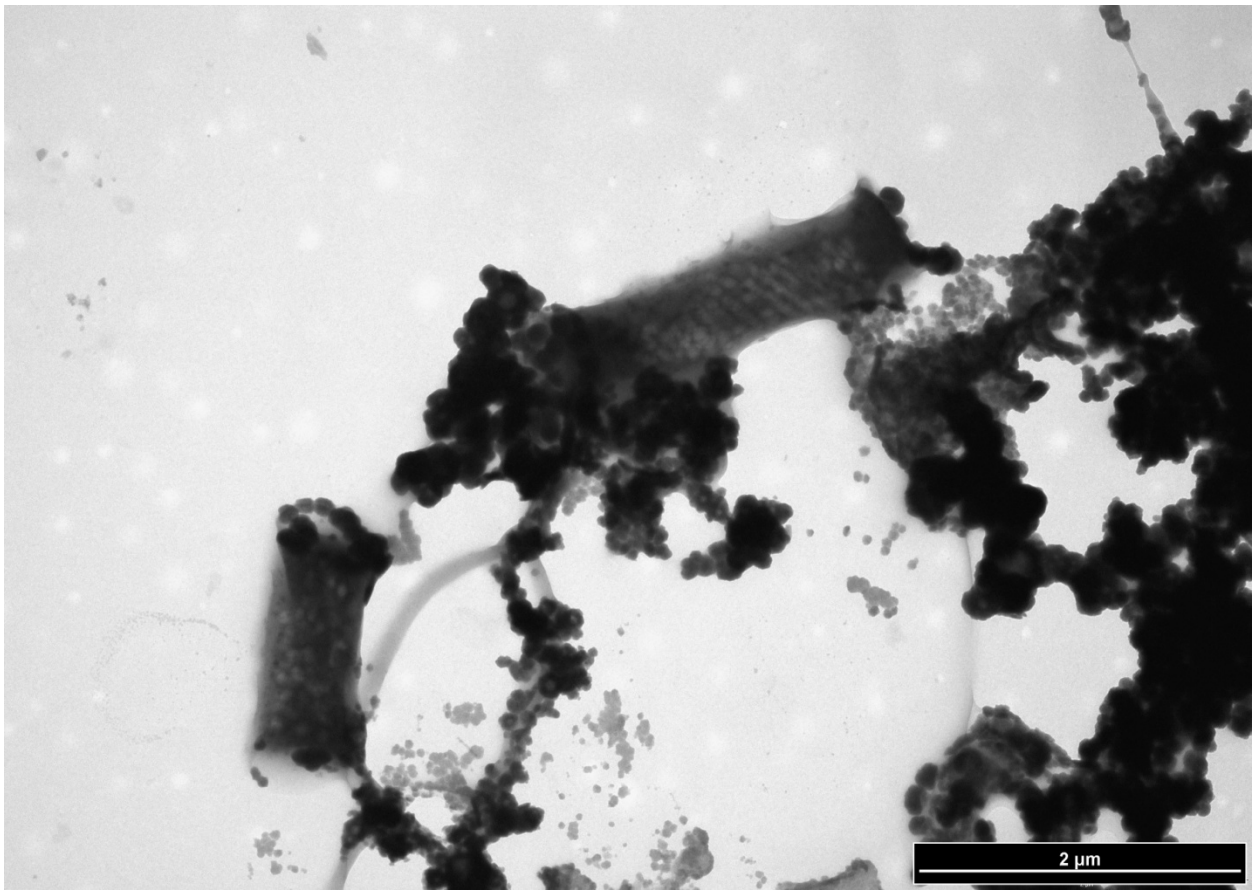

Figure D53

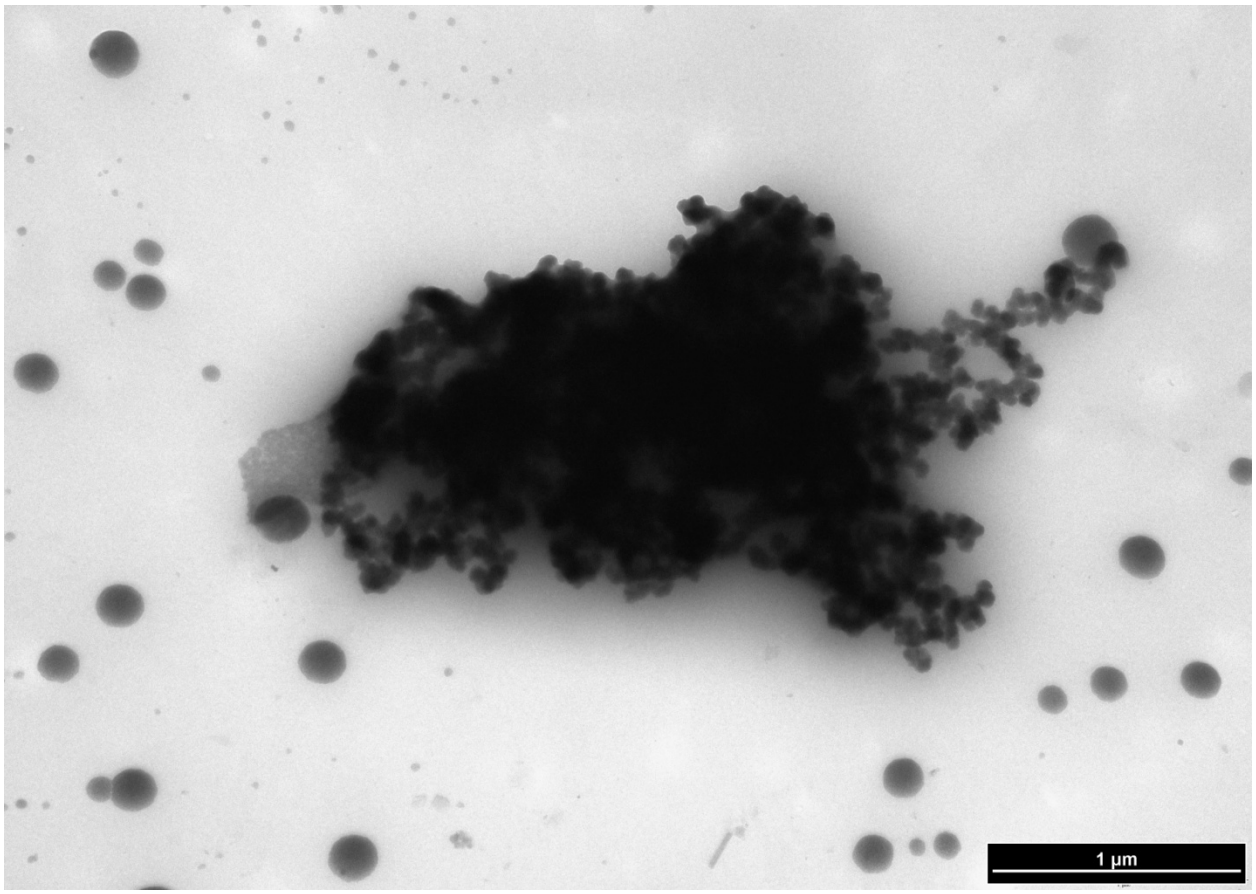

Figure D54

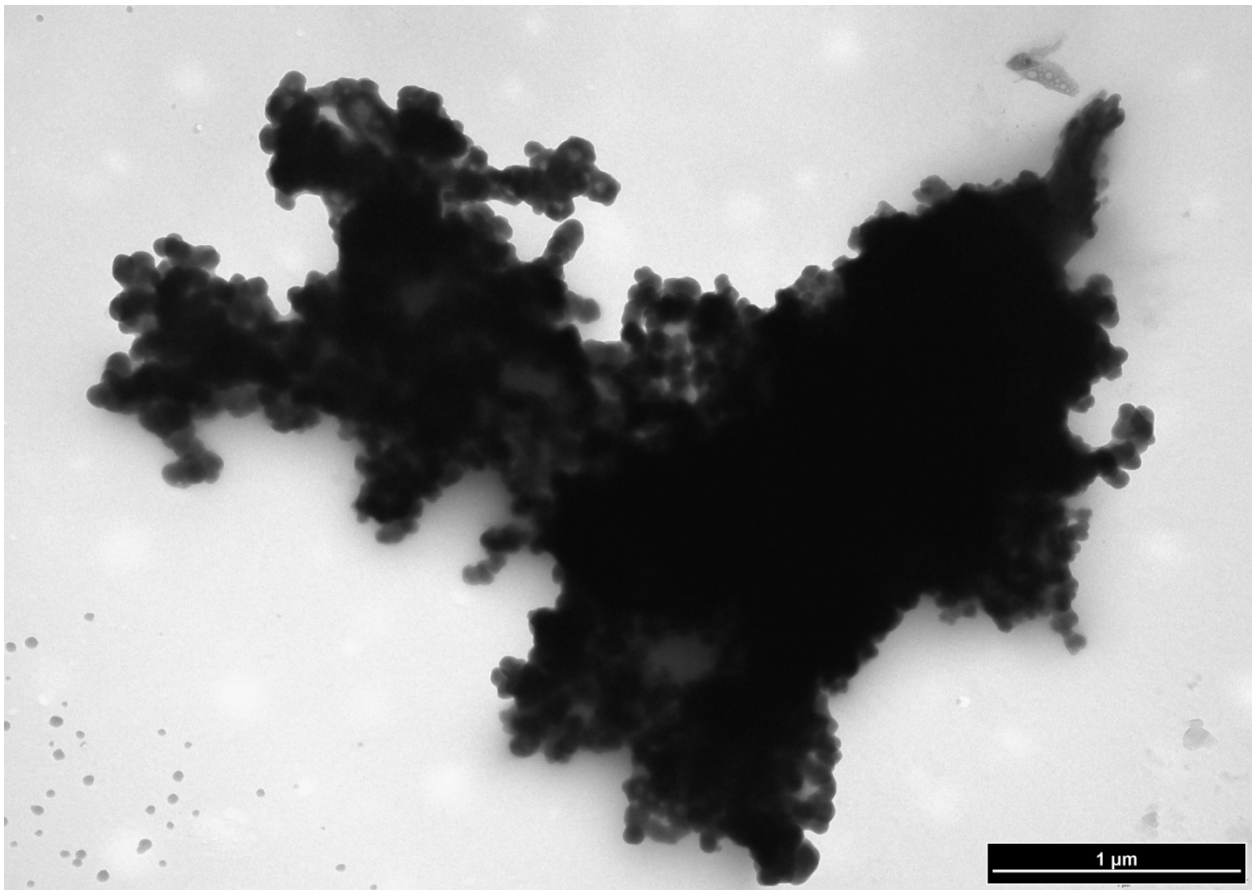

Figure D55

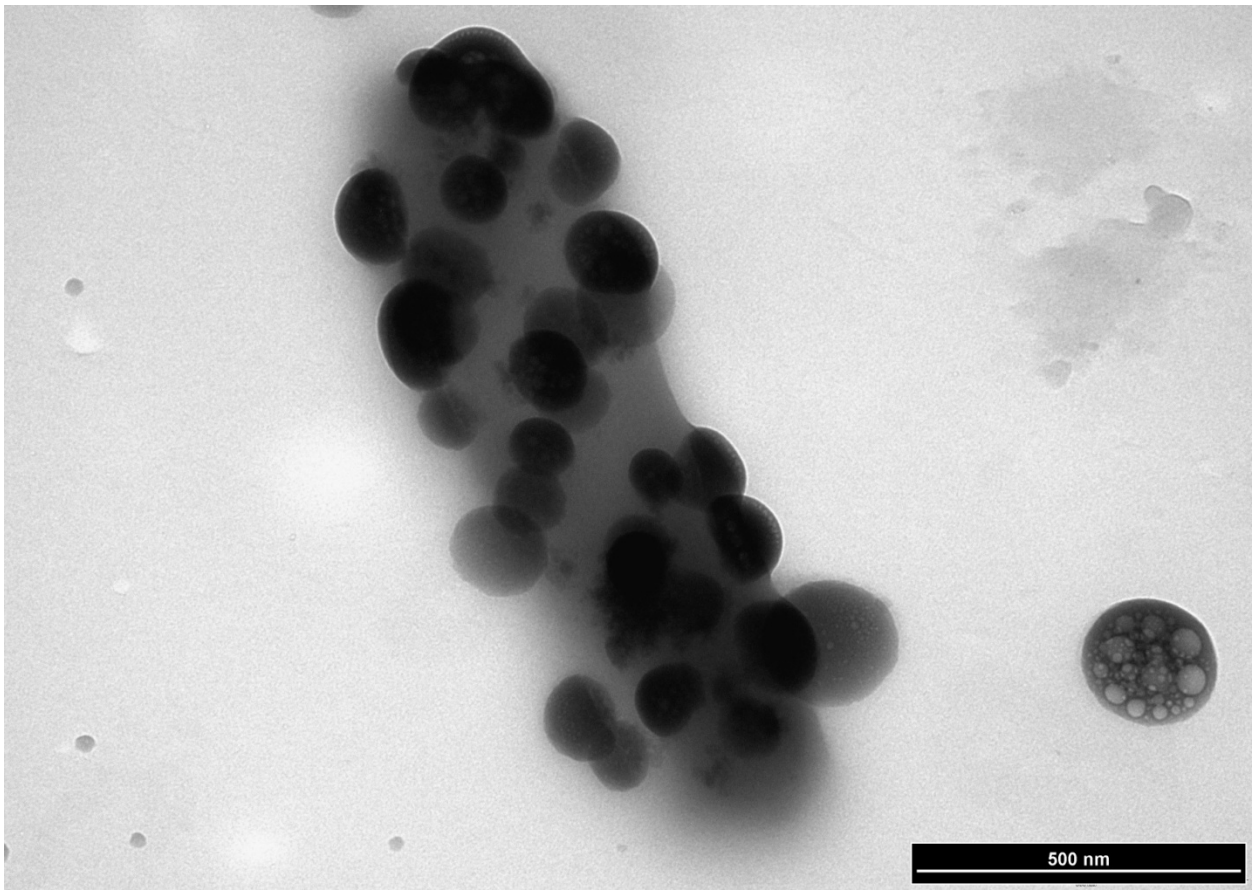

Figure D56

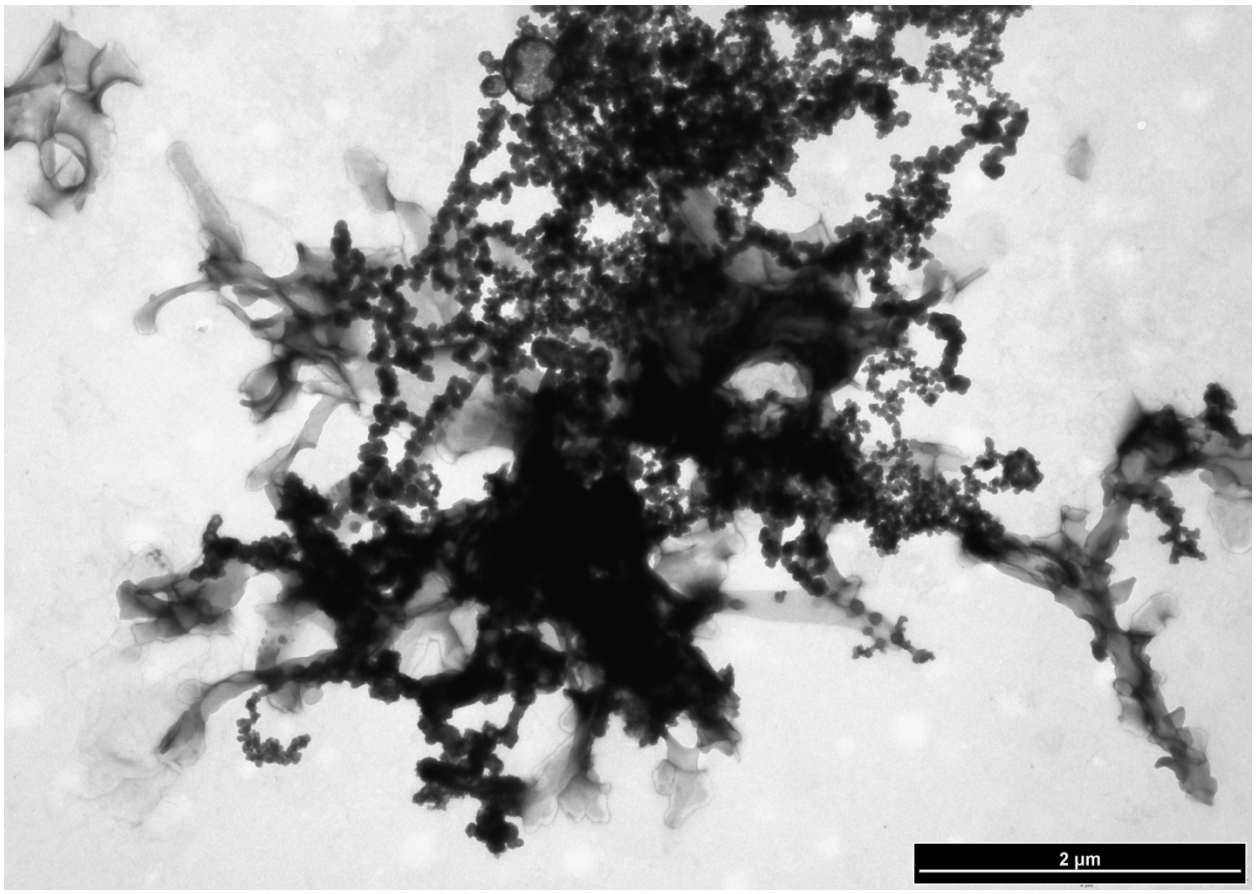

Figure D57

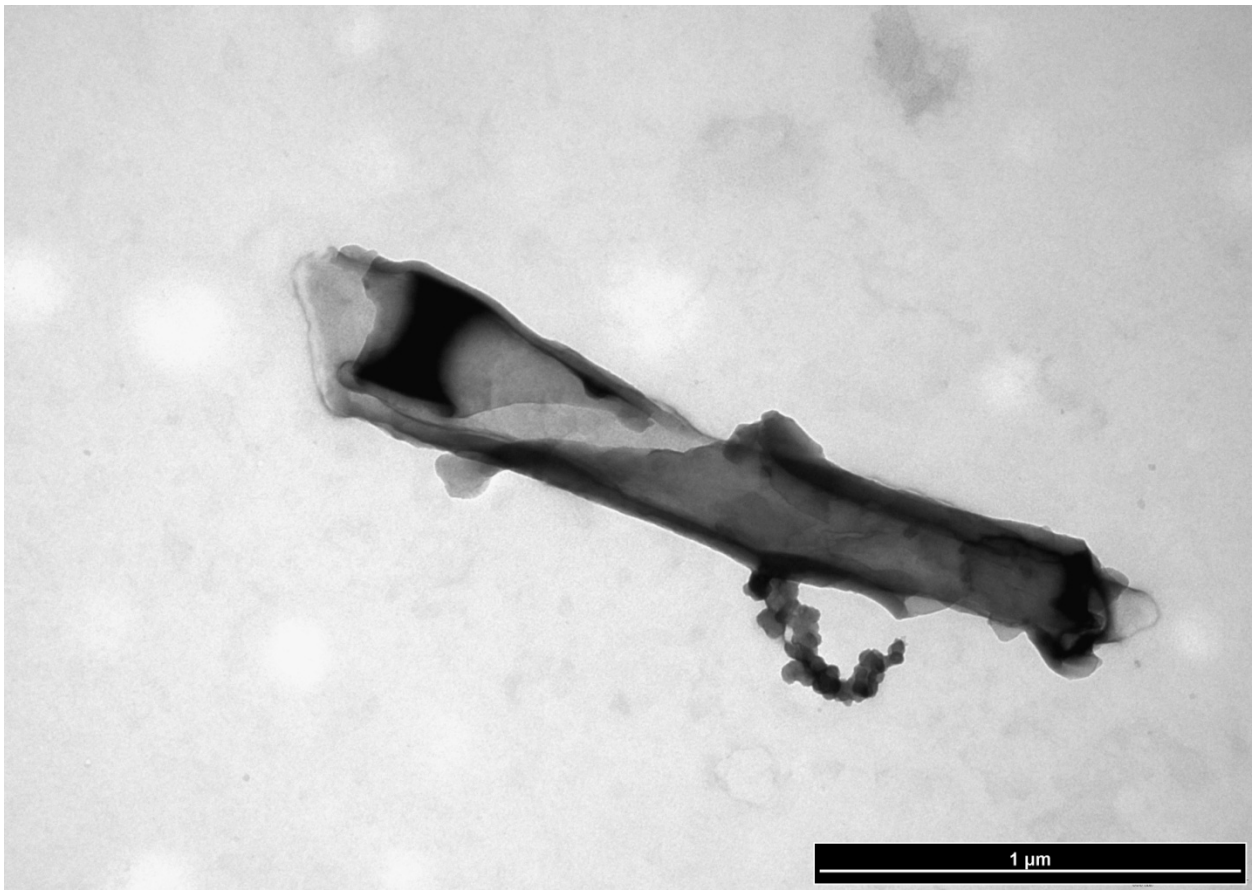

Figure D58

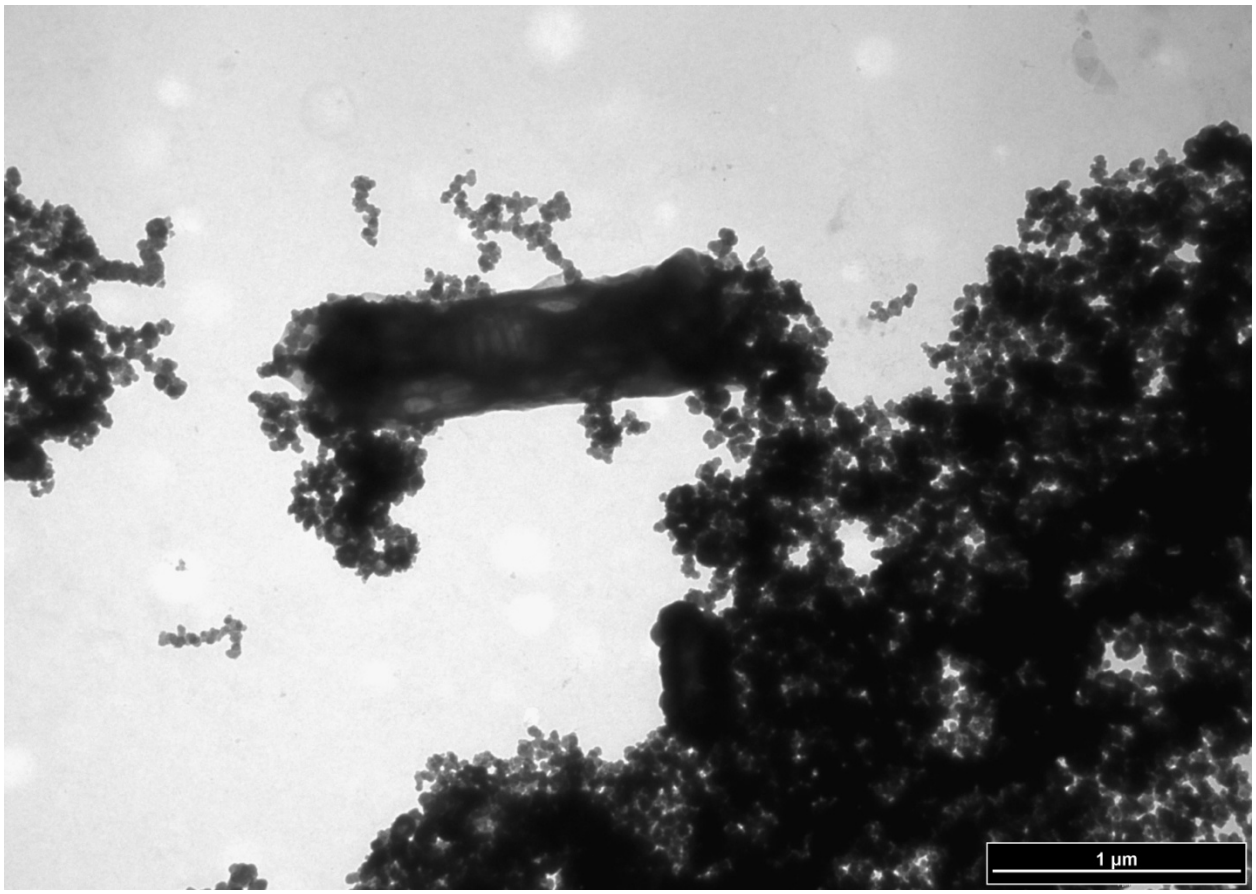

Figure D59

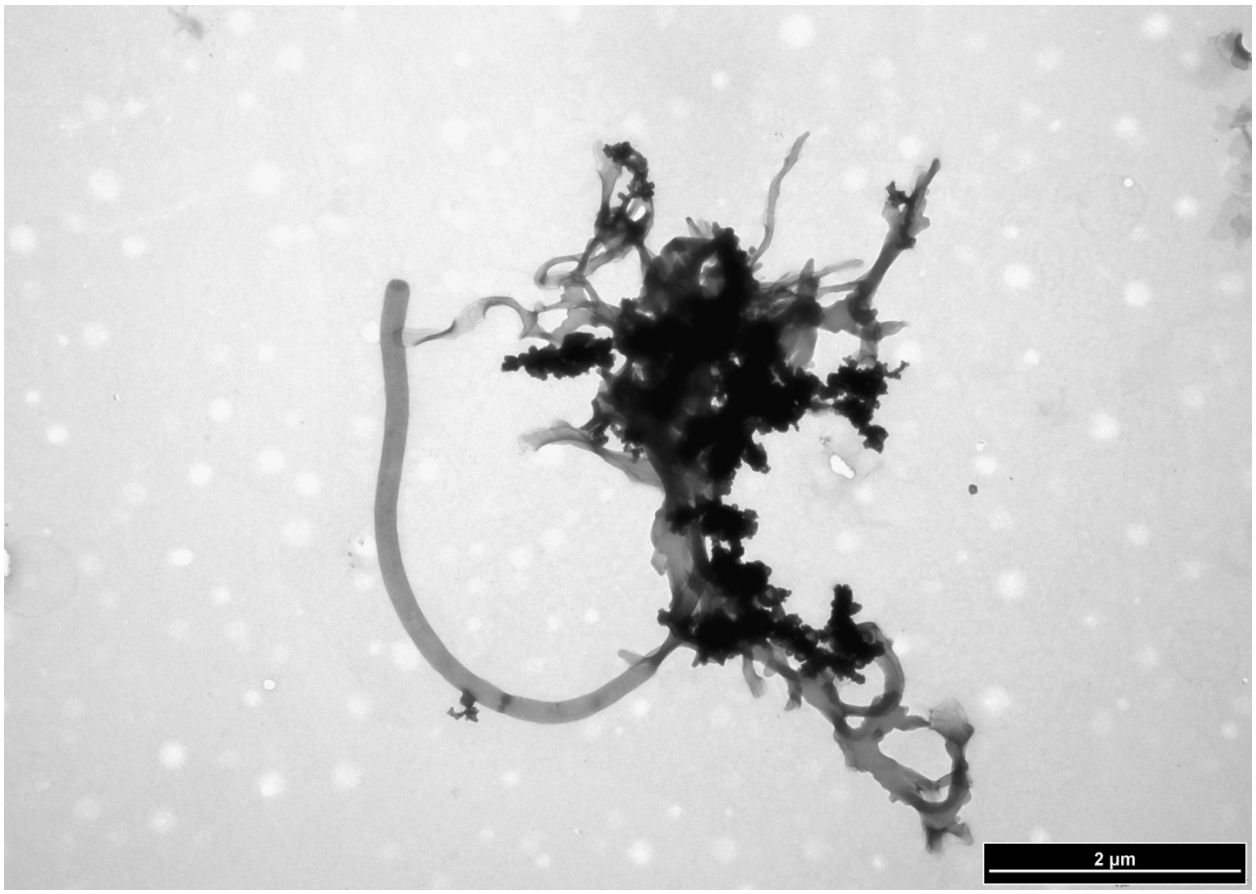

Figure D60

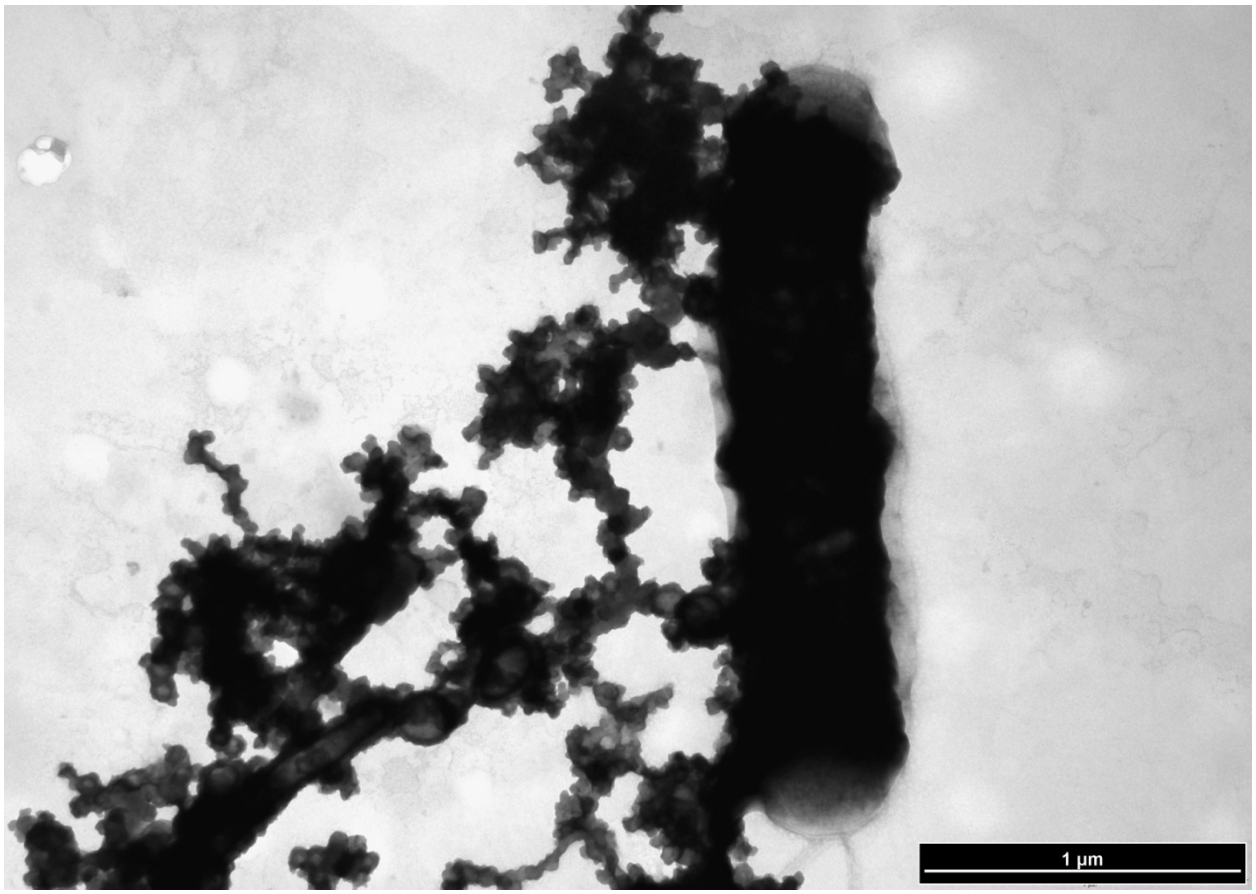

Figure D61

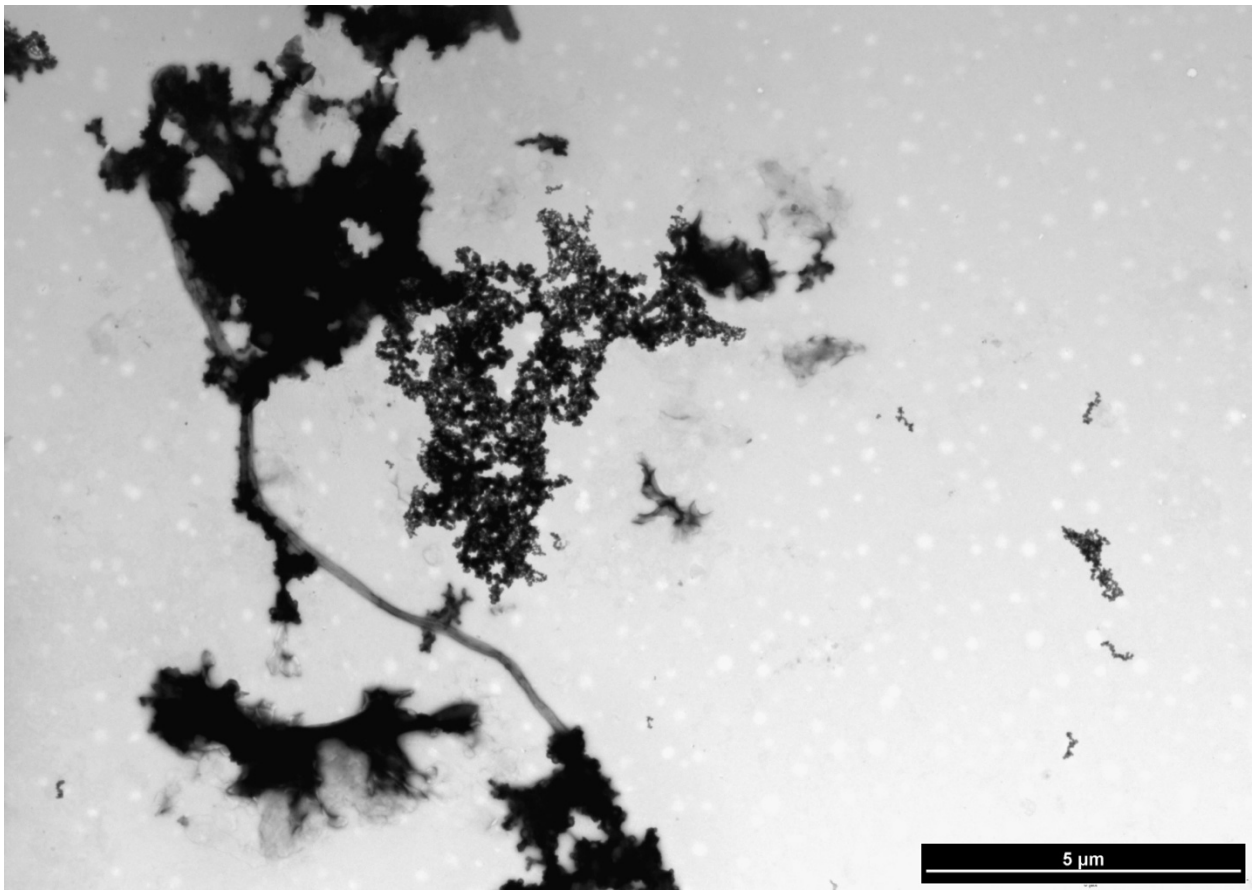

Figure D62

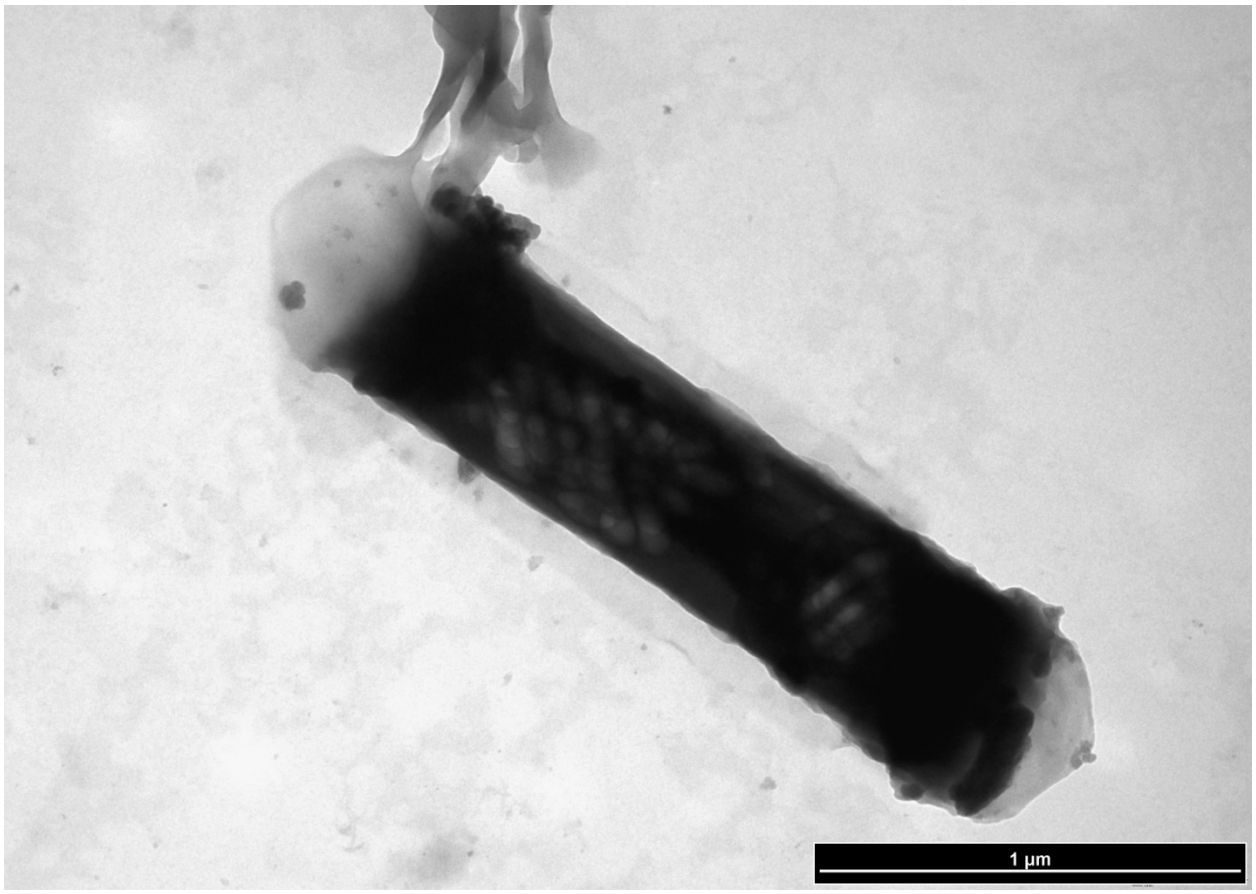

Figure D63

The following transmission electron micrographs are of *Methanobacterium formicicum* taken from experimental reactors from Chapter 3: Archaeal cell walls form ordered dolomite at Low-temperature due to high density of surface functional groups. Circles in images D64, D66, D68 and D70 are followed by the Energy-dispersive X-ray spectroscopy (EDS) spectra for these circled areas (D65, D67, D69 and D71 respectively). Please see the methods of this section for all sampling and imaging techniques.

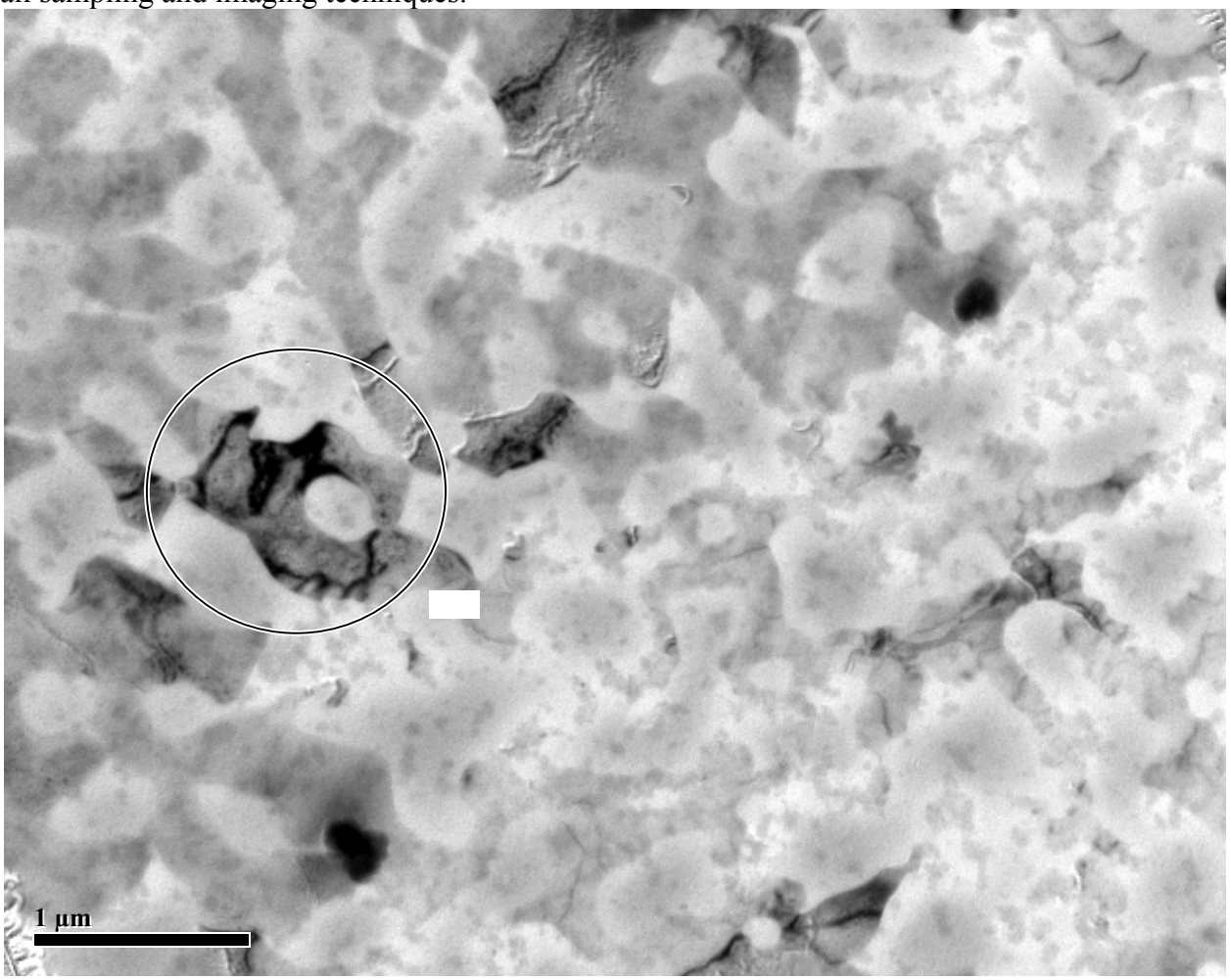

Figure D64

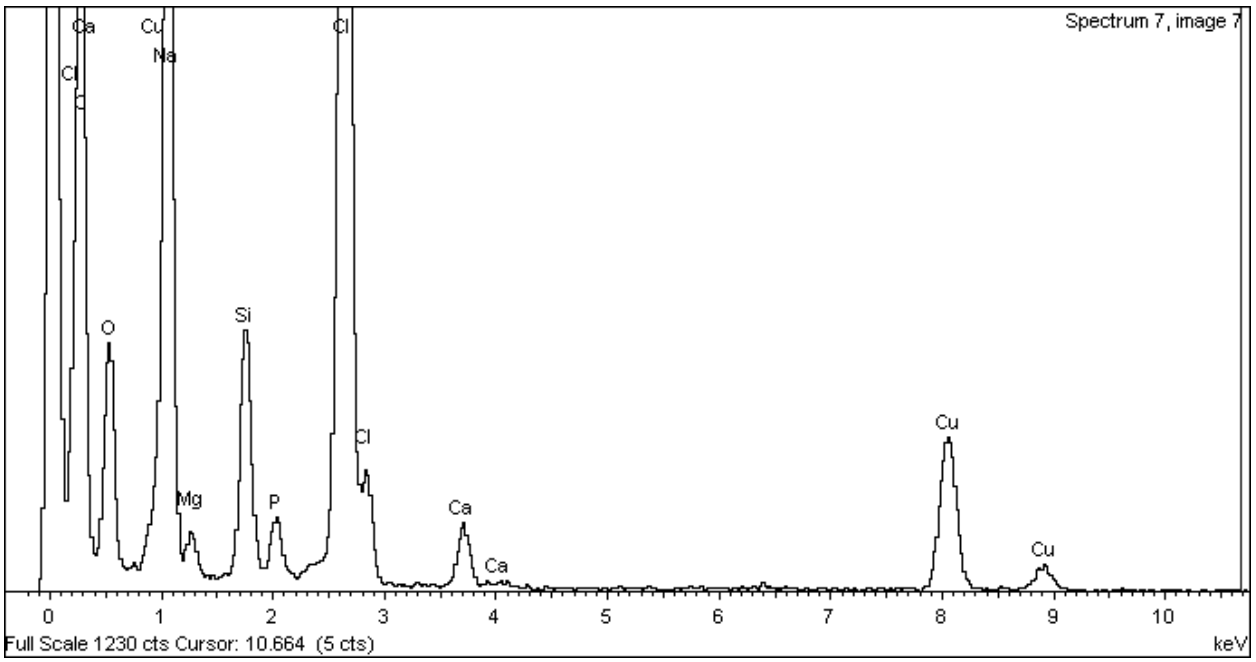
Spectrum 7, image 7
Ca
Cu
Na
Cl
Cl
C
O
Si
Cl
Mg
P
Cl
Ca
Ca
Cu
Cu
0
1
2
3
4
5
6
7
8
9
10
Full Scale 1230 cts Cursor: 10.664 (5 cts)
keV
Figure D65

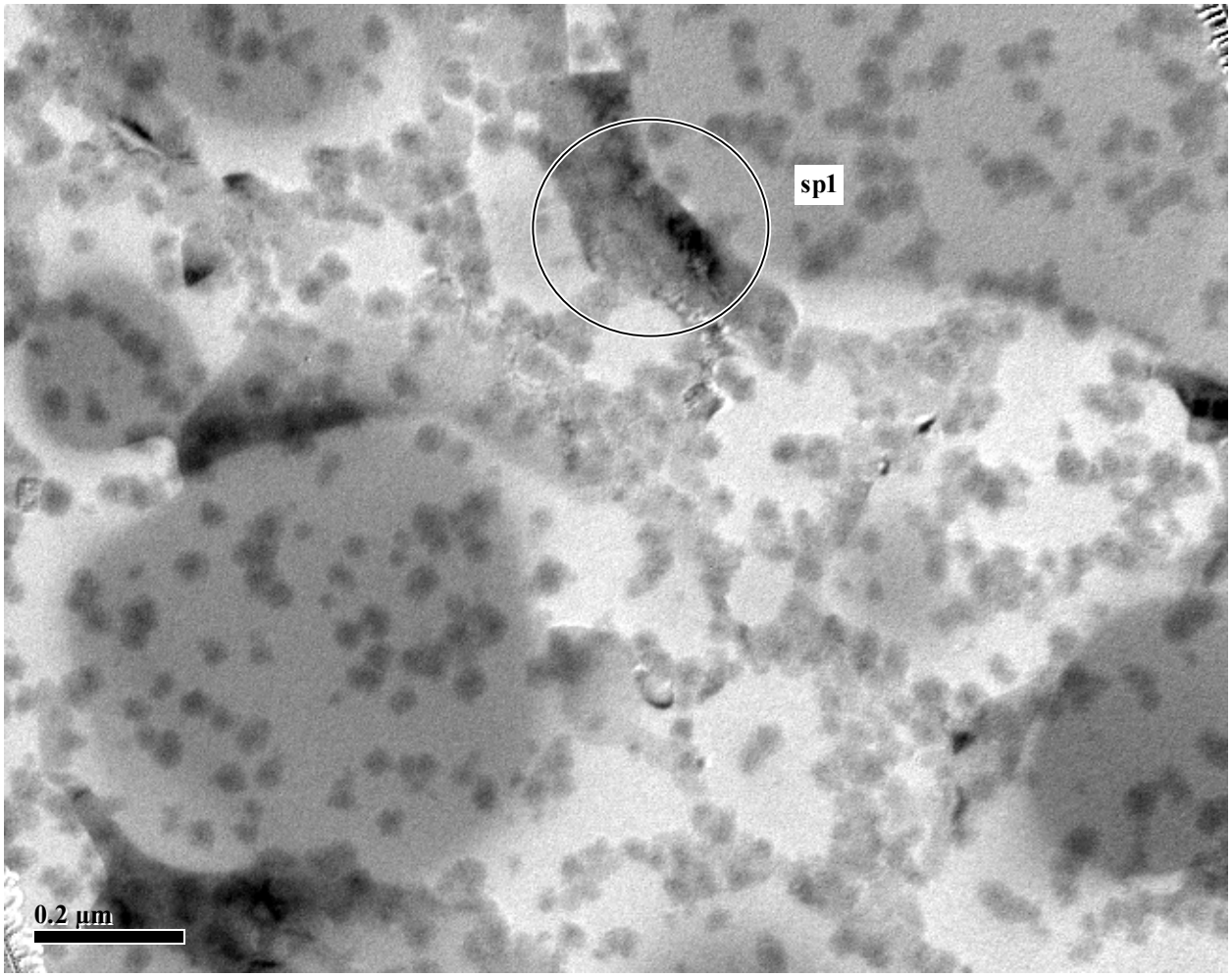

Figure D66

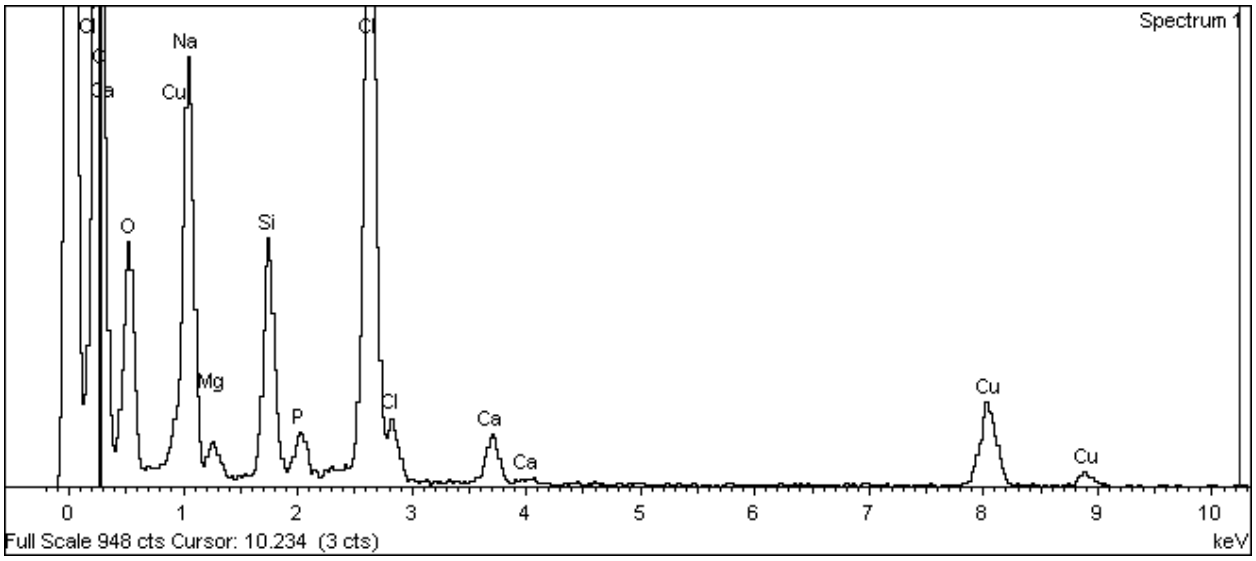
Spectrum 1
Cl
C
Ca
Na
Cu
O
Si
Mg
P
Cl
Cl
Ca
Ca
Cu
Cu
0
1
2
3
4
5
6
7
8
9
10
Full Scale 948 cts Cursor: 10.234 (3 cts)
keV
Figure D67

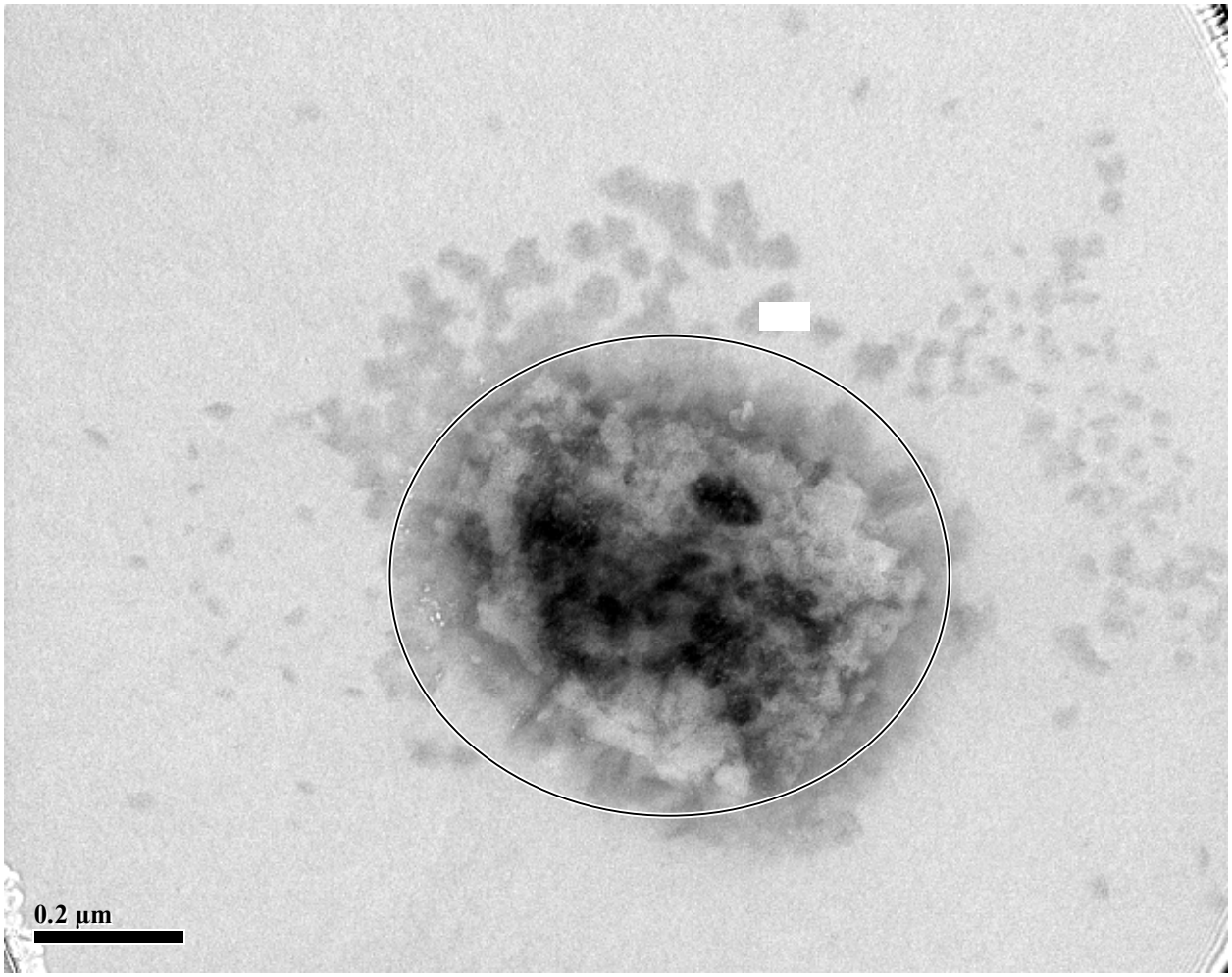

Figure D68

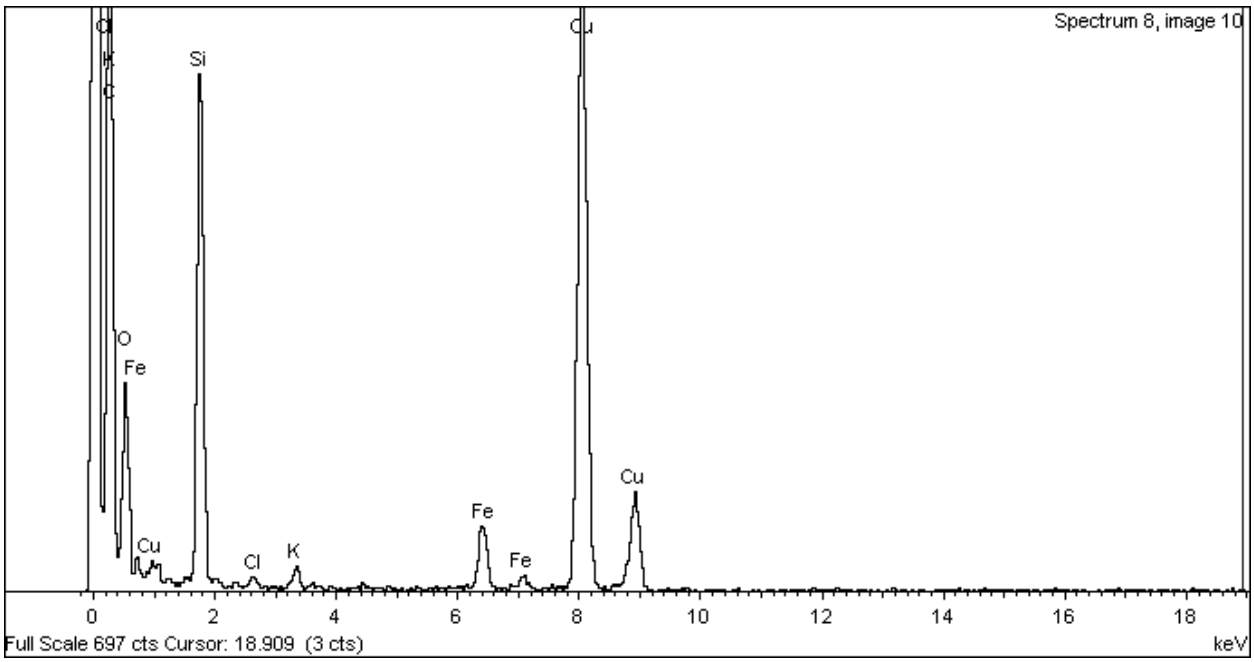
Spectrum 8, image 10
O
Si
Fe
Cu
Cl
K
Fe
Fe
Cu
0
2
4
6
8
10
12
14
16
18
Full Scale 697 cts Cursor: 18.909 (3 cts)
keV
Figure D69

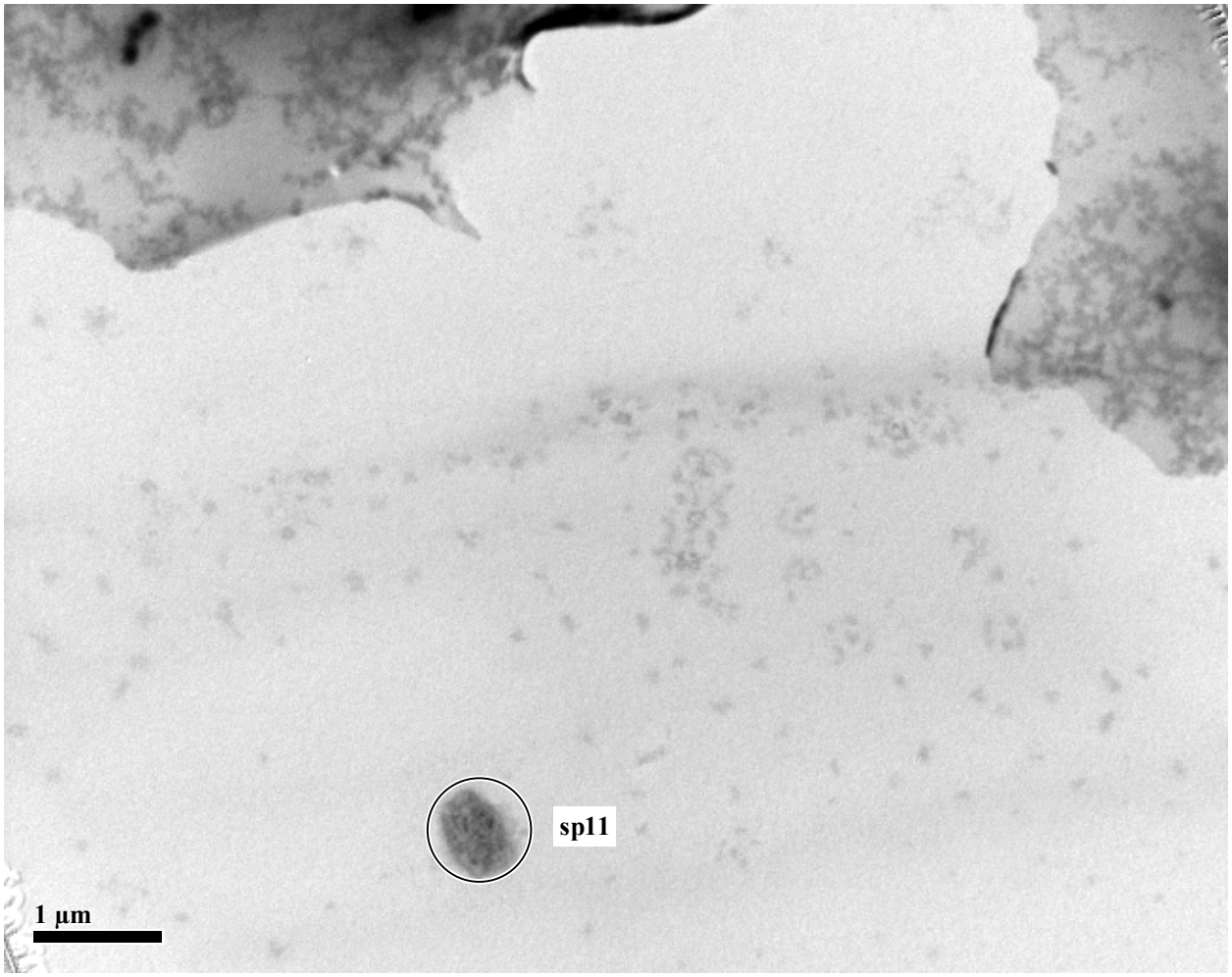

Figure D70

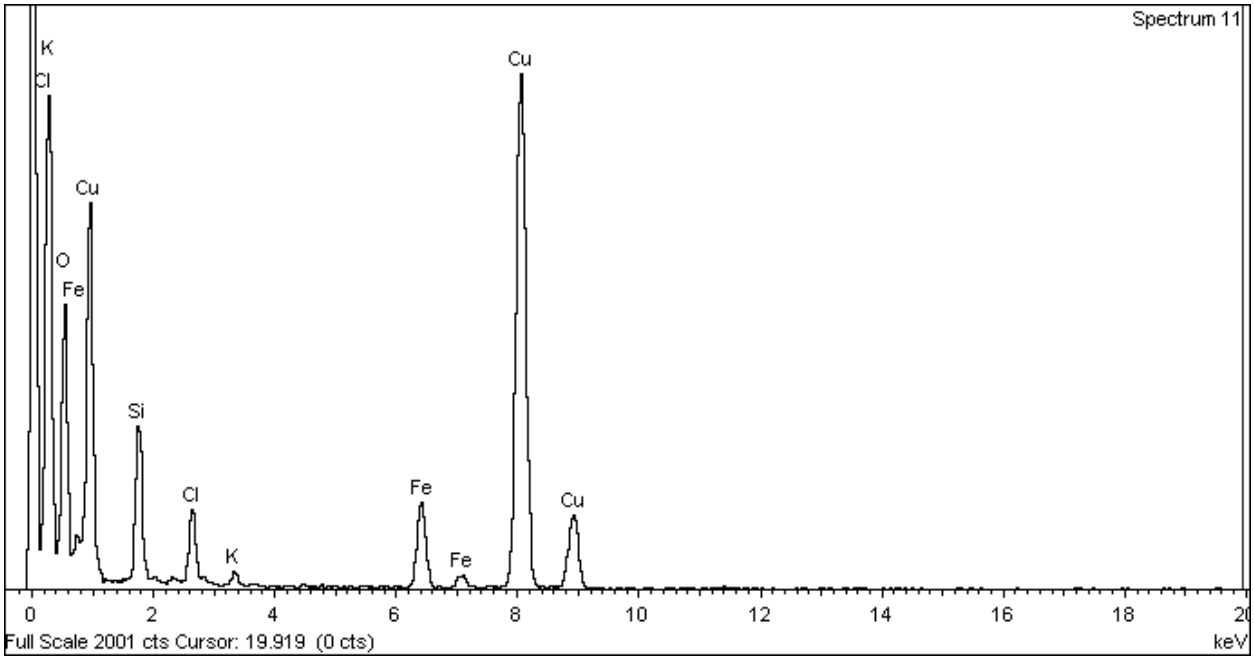
Spectrum 11
K
Cl
Cu
O
Fe
Si
Cl
K
Fe
Fe
Cu
Cu
0
2
4
6
8
10
12
14
16
18
20
Full Scale 2001 cts Cursor: 19.919 (0 cts)
keV
Figure D71

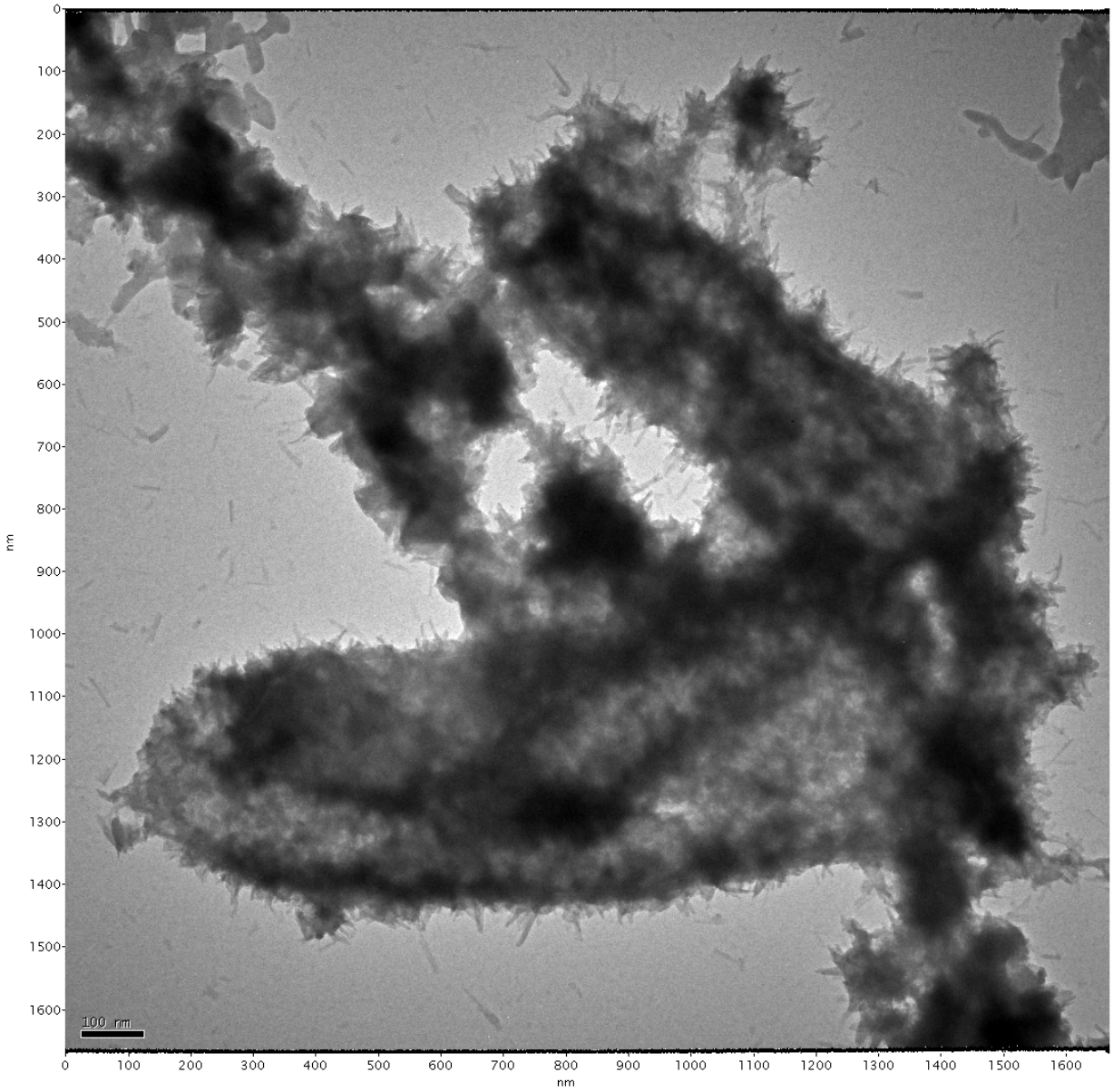
0
100
200
300
400
500
600
700
800
900
1000
1100
1200
1300
1400
1500
1600
nm
100 nm
0
100
200
300
400
500
600
700
800
900
1000
1100
1200
1300
1400
1500
1600
nm

Figure D72

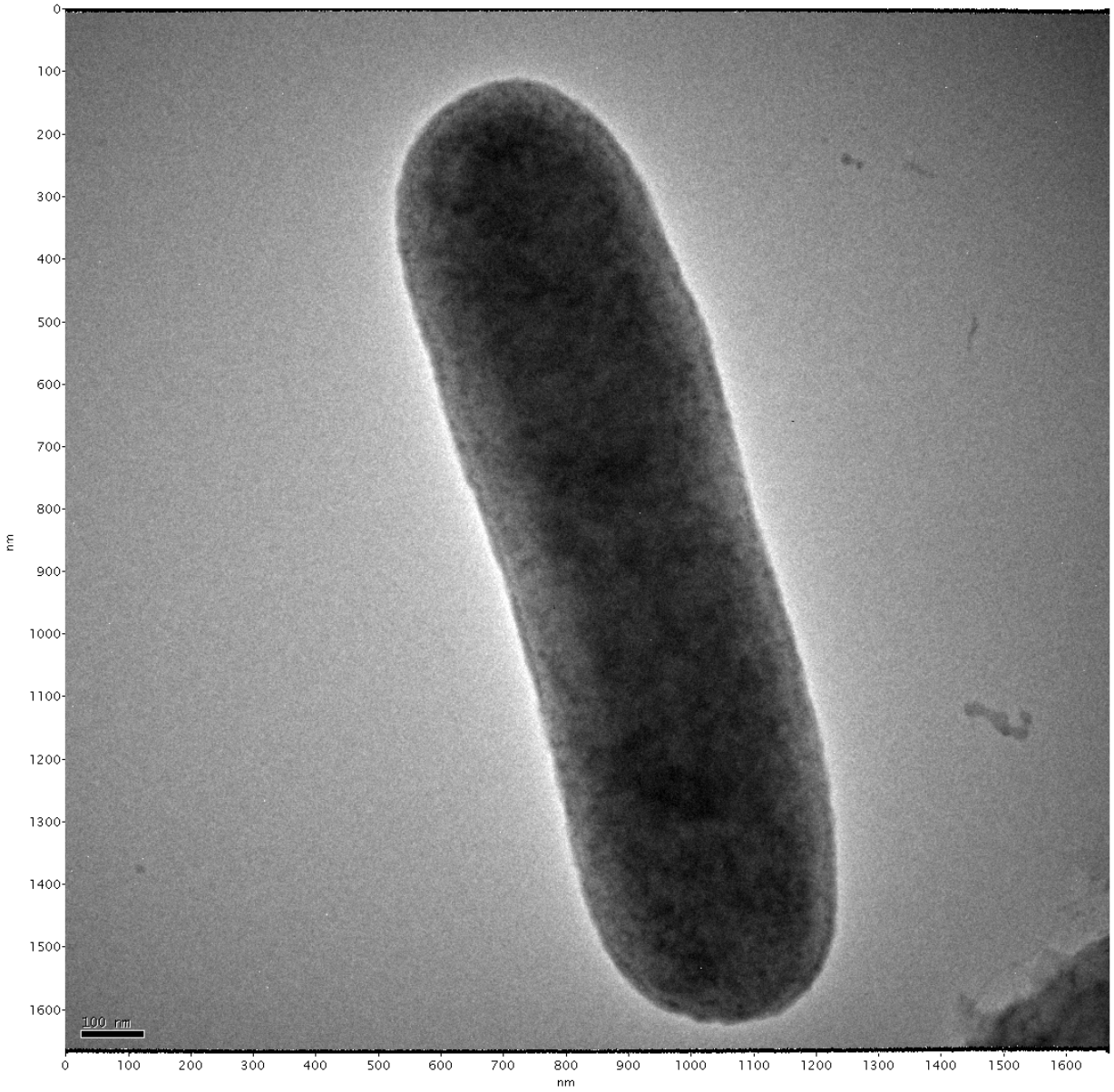
0
100
200
300
400
500
600
700
800
900
1000
1100
1200
1300
1400
1500
1600
nm
100 nm
0
100
200
300
400
500
600
700
800
900
1000
1100
1200
1300
1400
1500
1600
nm

Figure D73

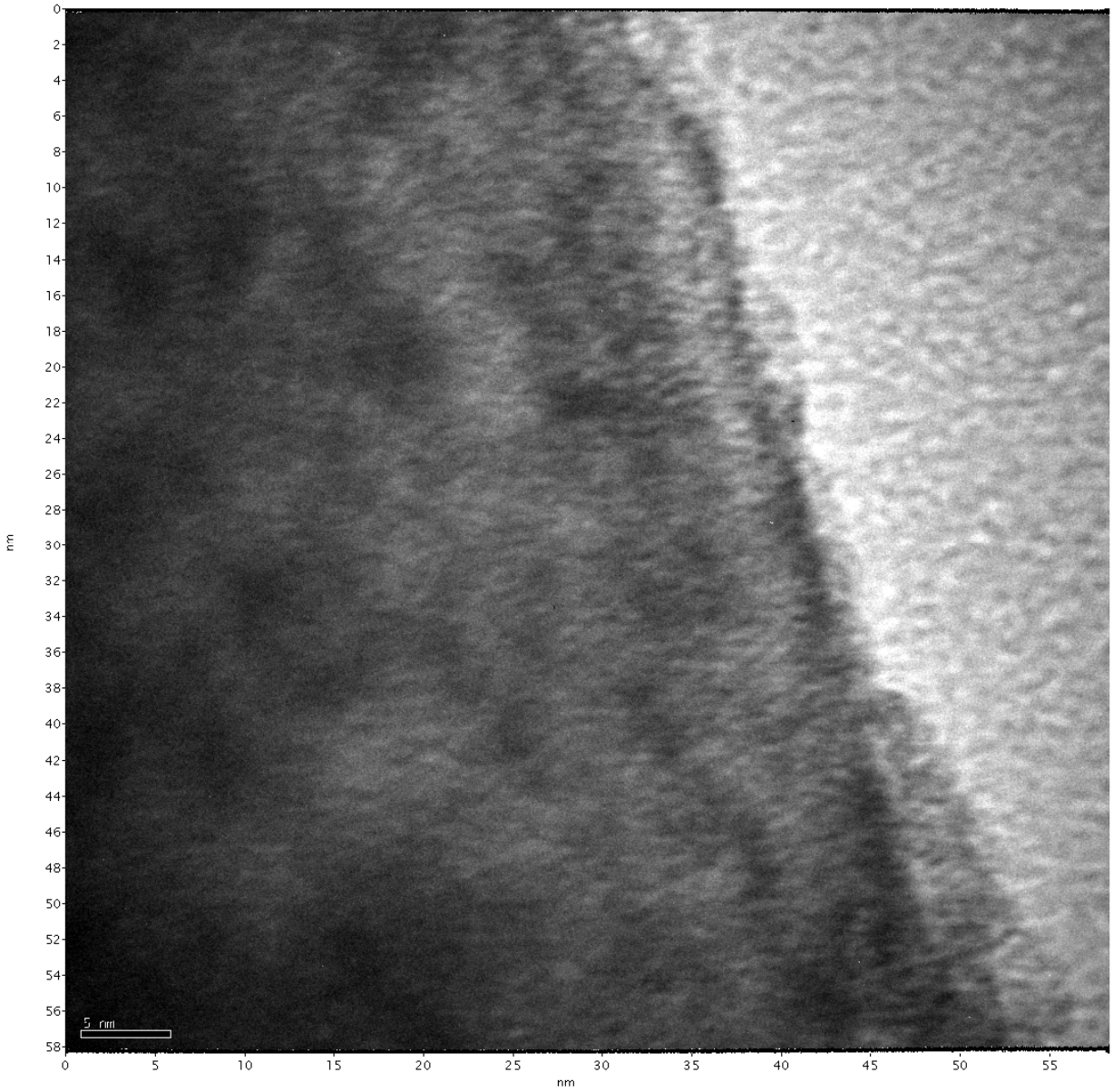
nm
0
2
4
6
8
10
12
14
16
18
20
22
24
26
28
30
32
34
36
38
40
42
44
46
48
50
52
54
56
58
5 nm
0
5
10
15
20
25
30
35
40
45
50
55
nm
Figure D74

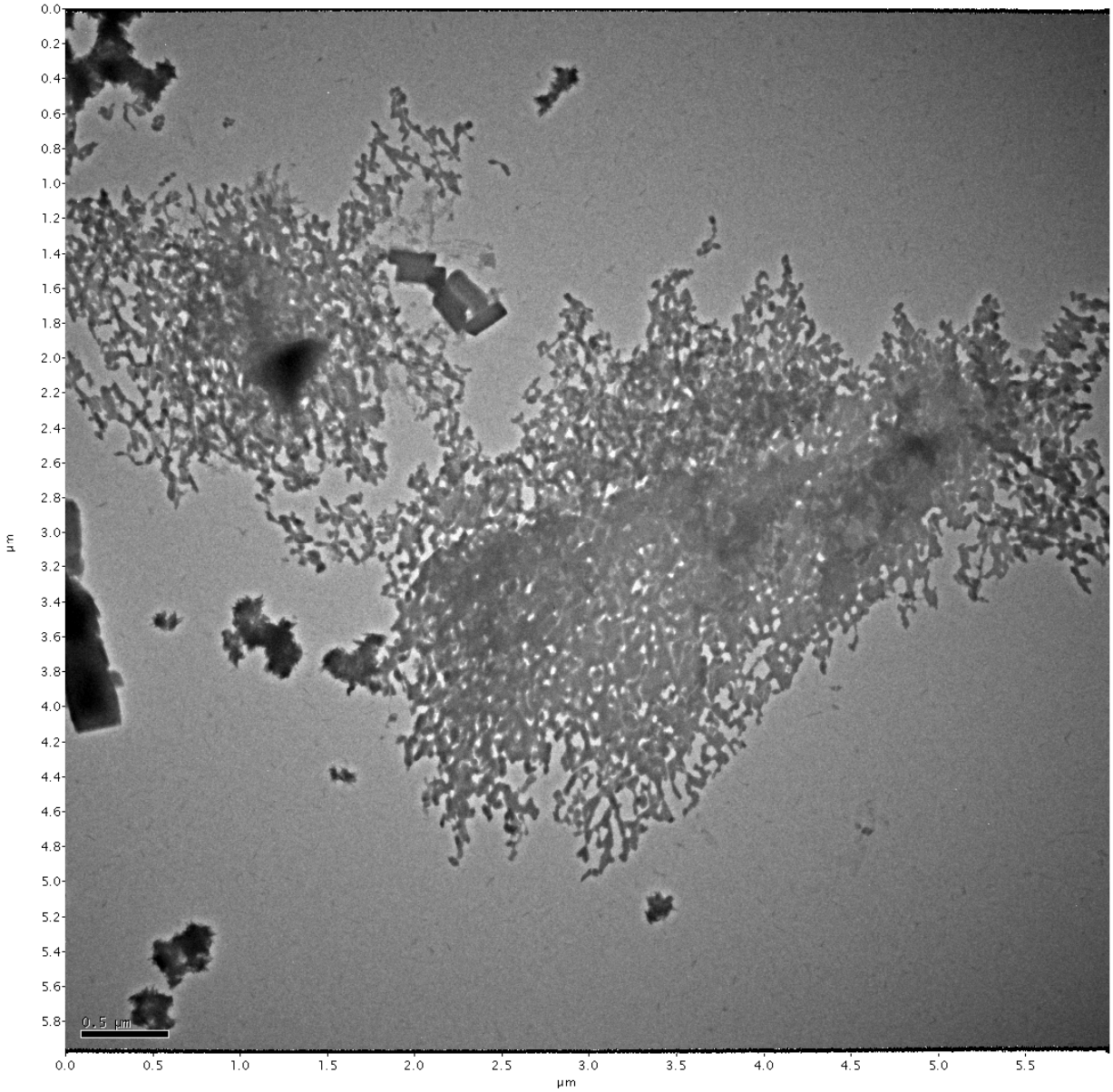
0.0
0.2
0.4
0.6
0.8
1.0
1.2
1.4
1.6
1.8
2.0
2.2
2.4
2.6
2.8
3.0
3.2
3.4
3.6
3.8
4.0
4.2
4.4
4.6
4.8
5.0
5.2
5.4
5.6
5.8
µm
0.5 µm
0.0
0.5
1.0
1.5
2.0
2.5
3.0
3.5
4.0
4.5
5.0
5.5
µm
Figure D75

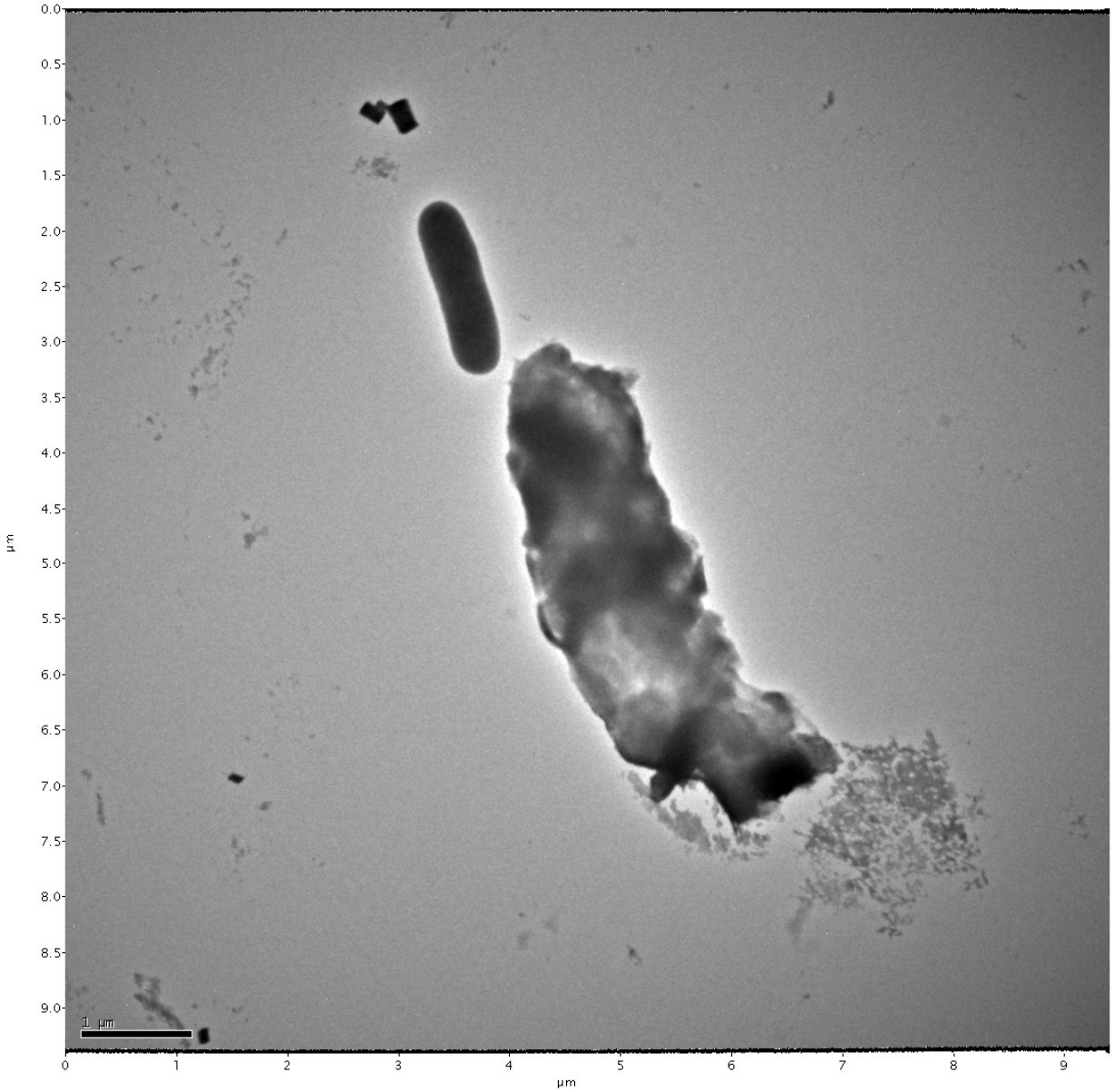
0.0
0.5
1.0
1.5
2.0
2.5
3.0
3.5
4.0
4.5
5.0
5.5
6.0
6.5
7.0
7.5
8.0
8.5
9.0
µm
1 µm
0
1
2
3
4
5
6
7
8
9
µm
Figure D76

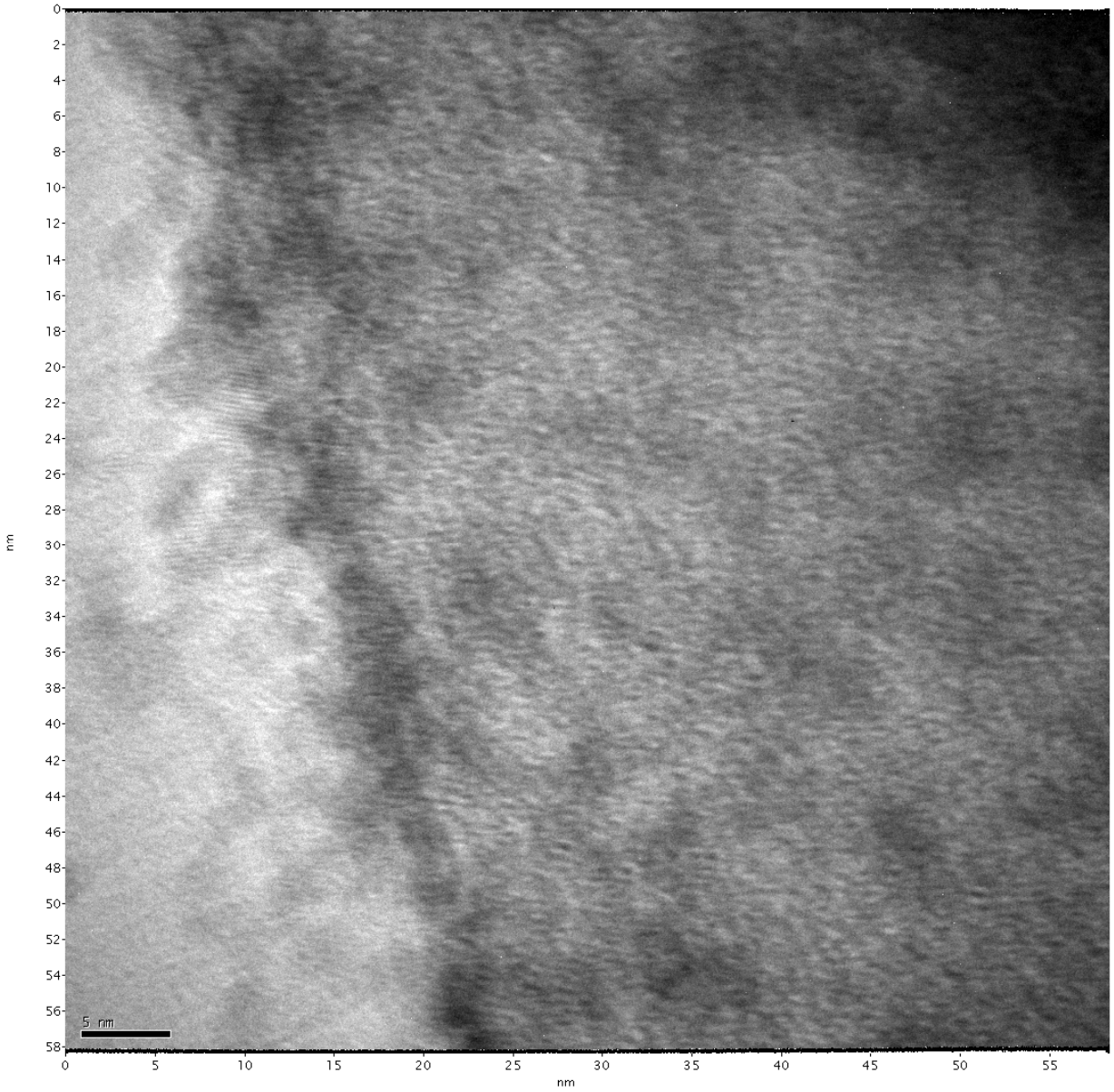
nm
0
2
4
6
8
10
12
14
16
18
20
22
24
26
28
30
32
34
36
38
40
42
44
46
48
50
52
54
56
58
5 nm
0
5
10
15
20
25
30
35
40
45
50
55
nm

Figure D77

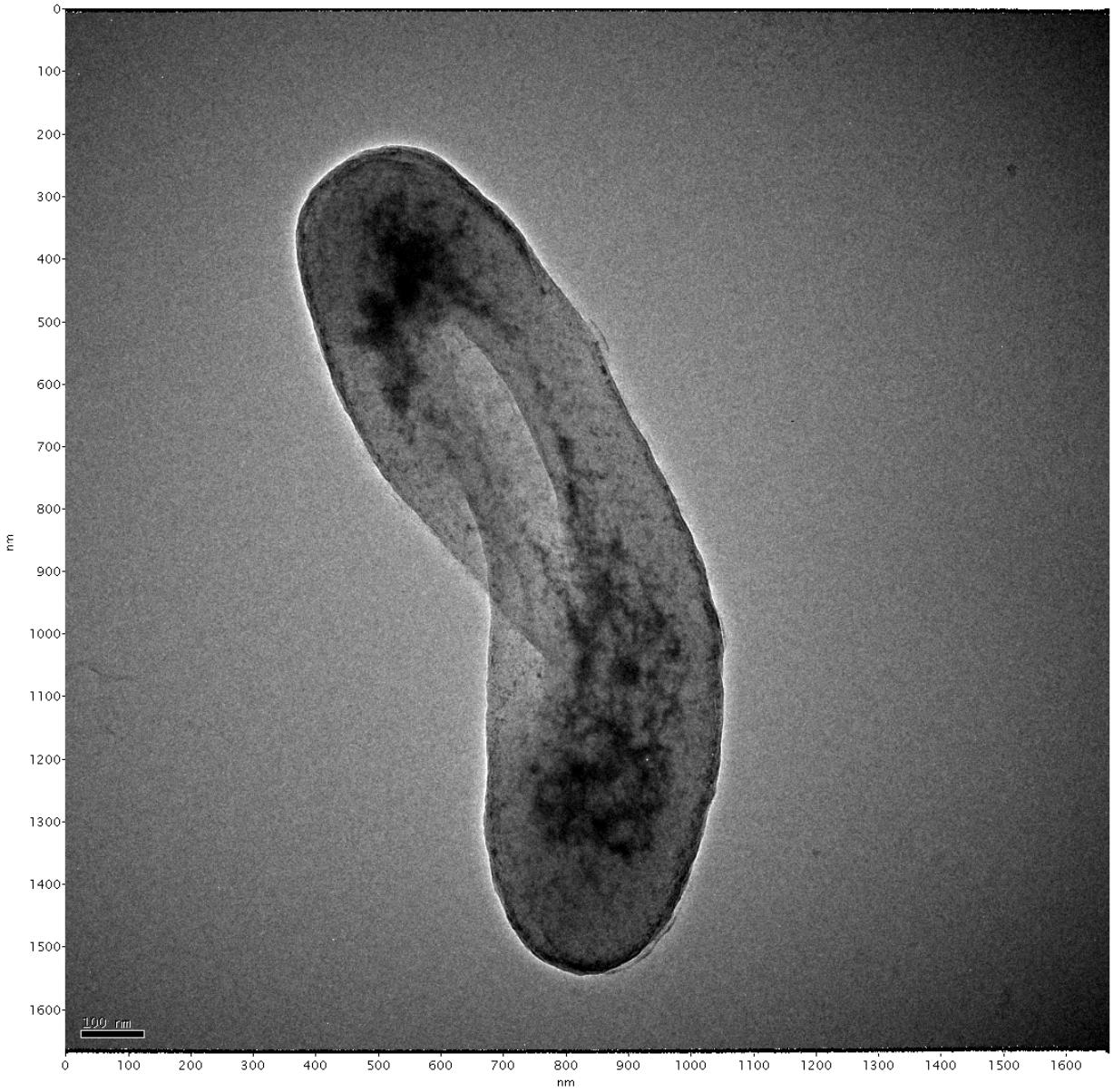
0
100
200
300
400
500
600
700
800
900
1000
1100
1200
1300
1400
1500
1600
nm
100 nm
0
100
200
300
400
500
600
700
800
900
1000
1100
1200
1300
1400
1500
1600
nm
Figure D78

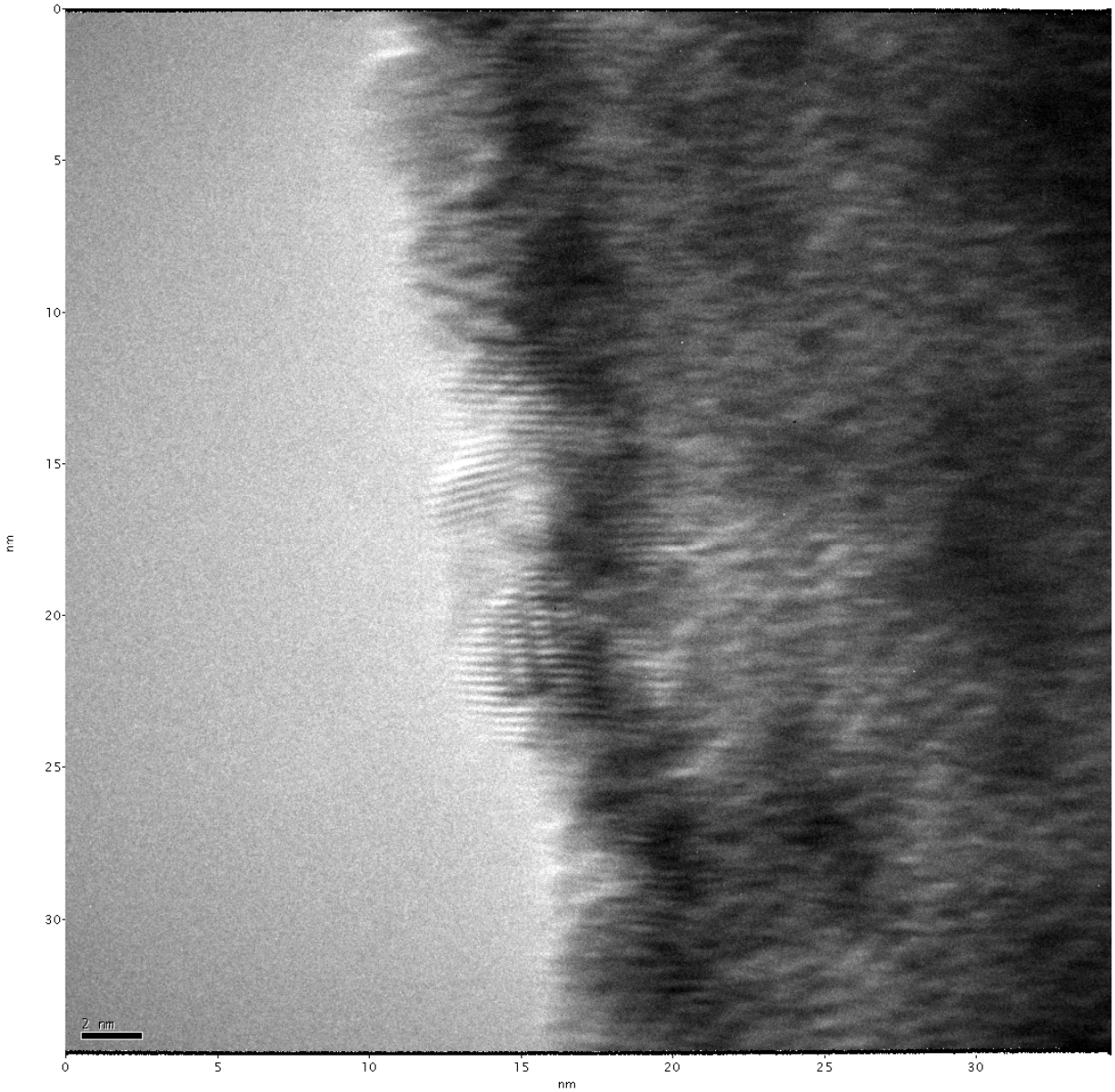

Figure D79

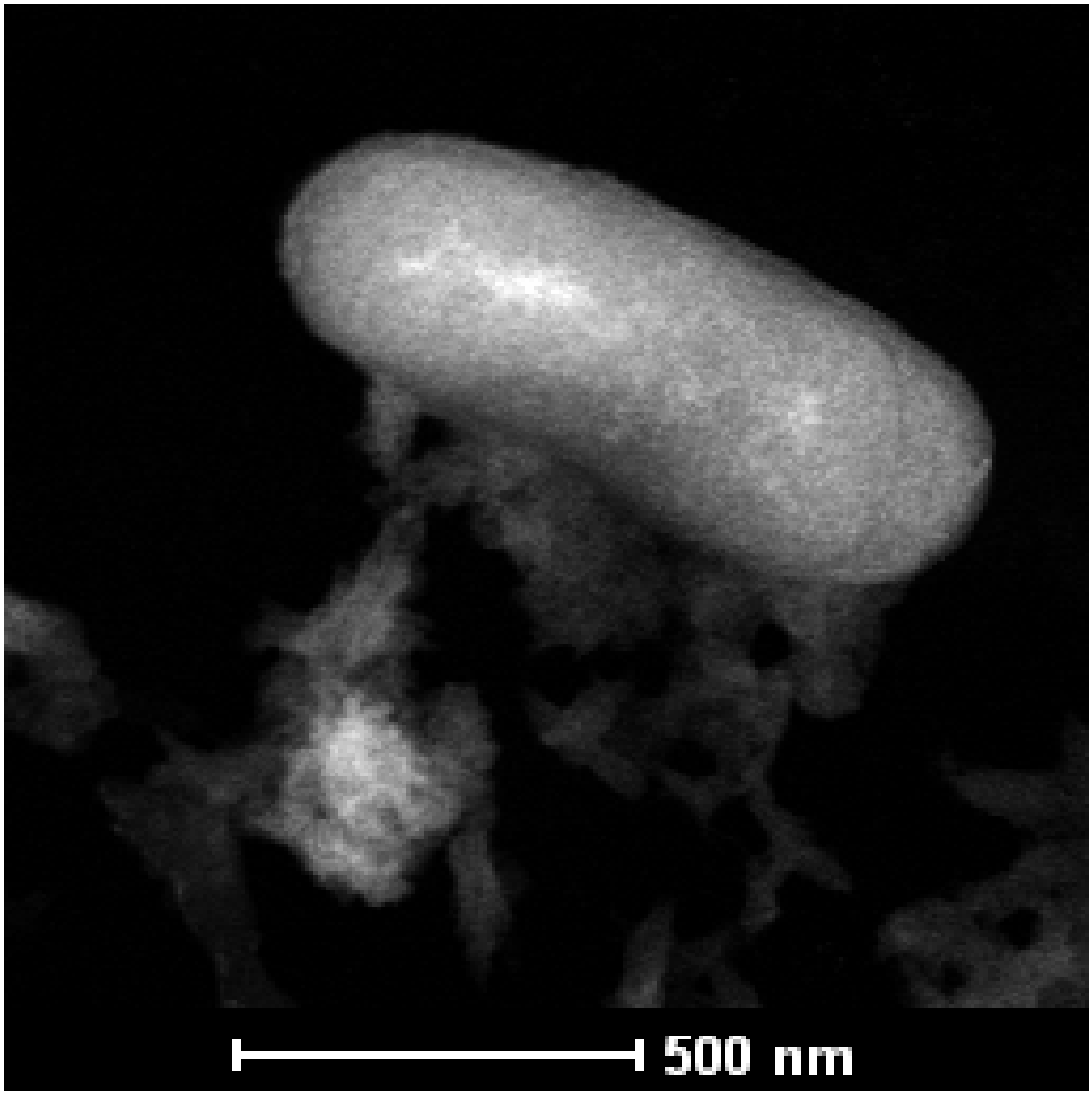

Figure D80

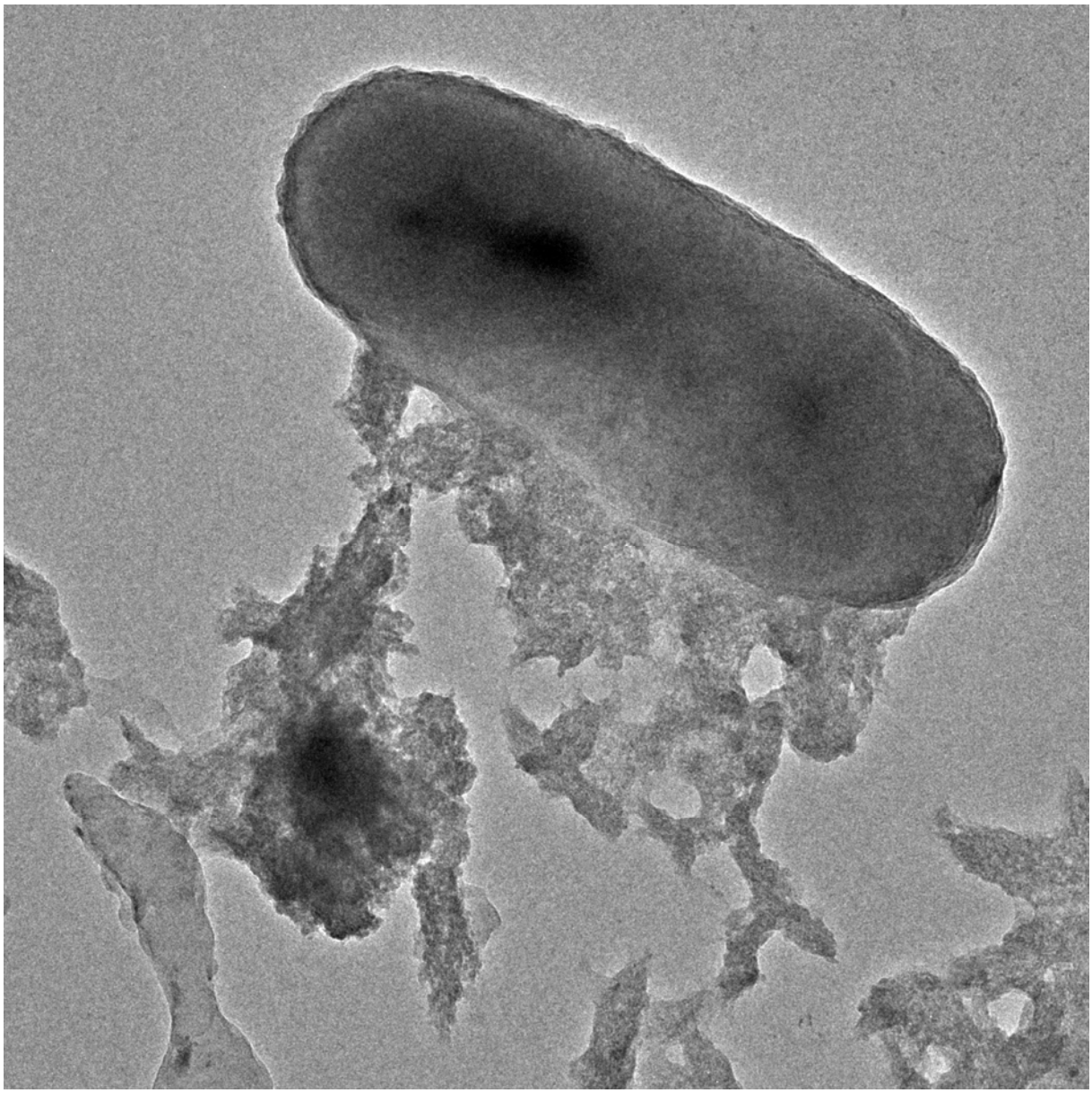

Figure D81

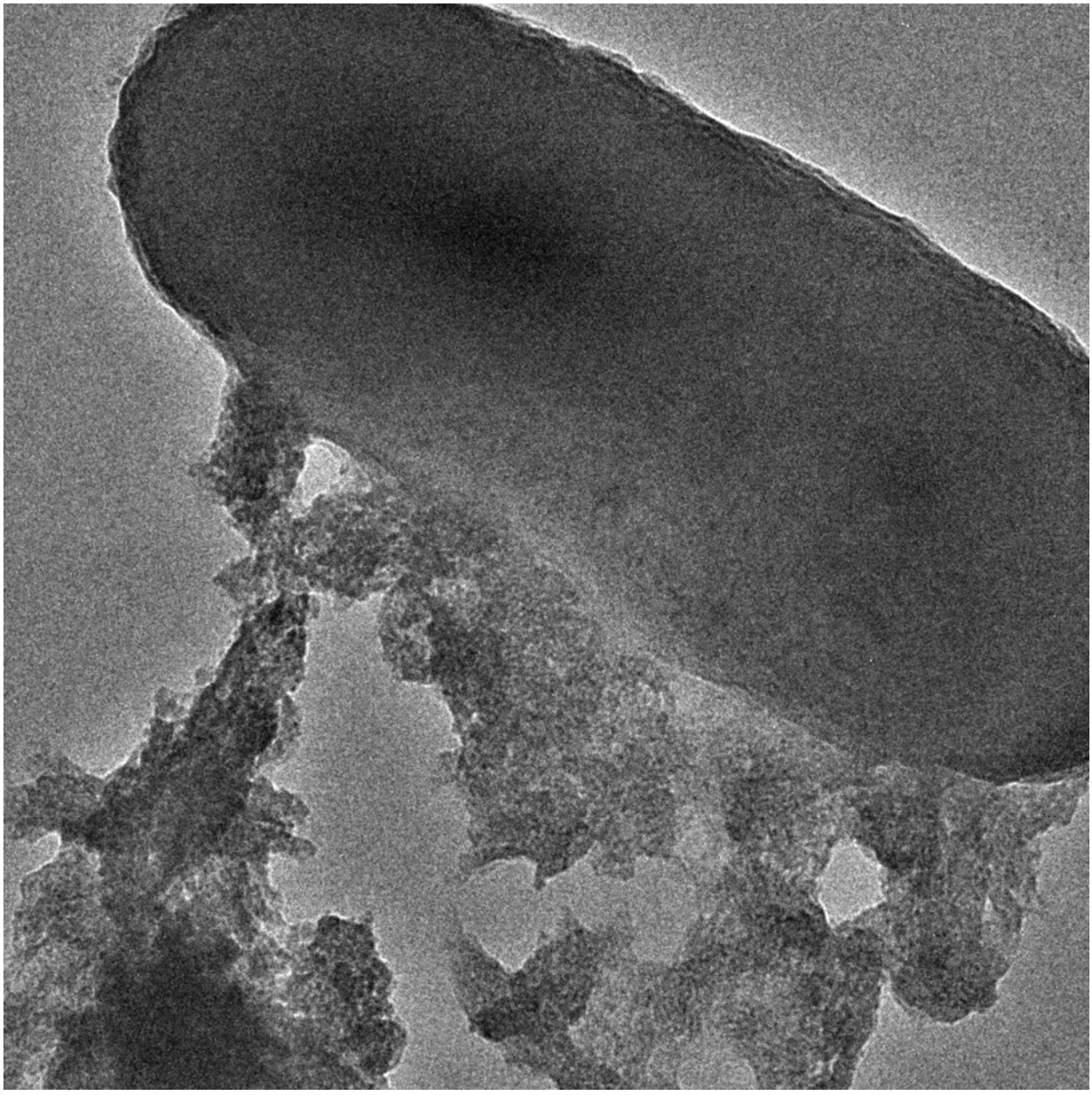

Figure D82

The following transmission electron micrographs are of *Haloferax sulfurifontis* taken from experimental reactors from Chapter 3: Archaeal cell walls form ordered dolomite at low-temperature due to high density of surface functional groups. Please see the methods of this section for all sampling and imaging techniques.

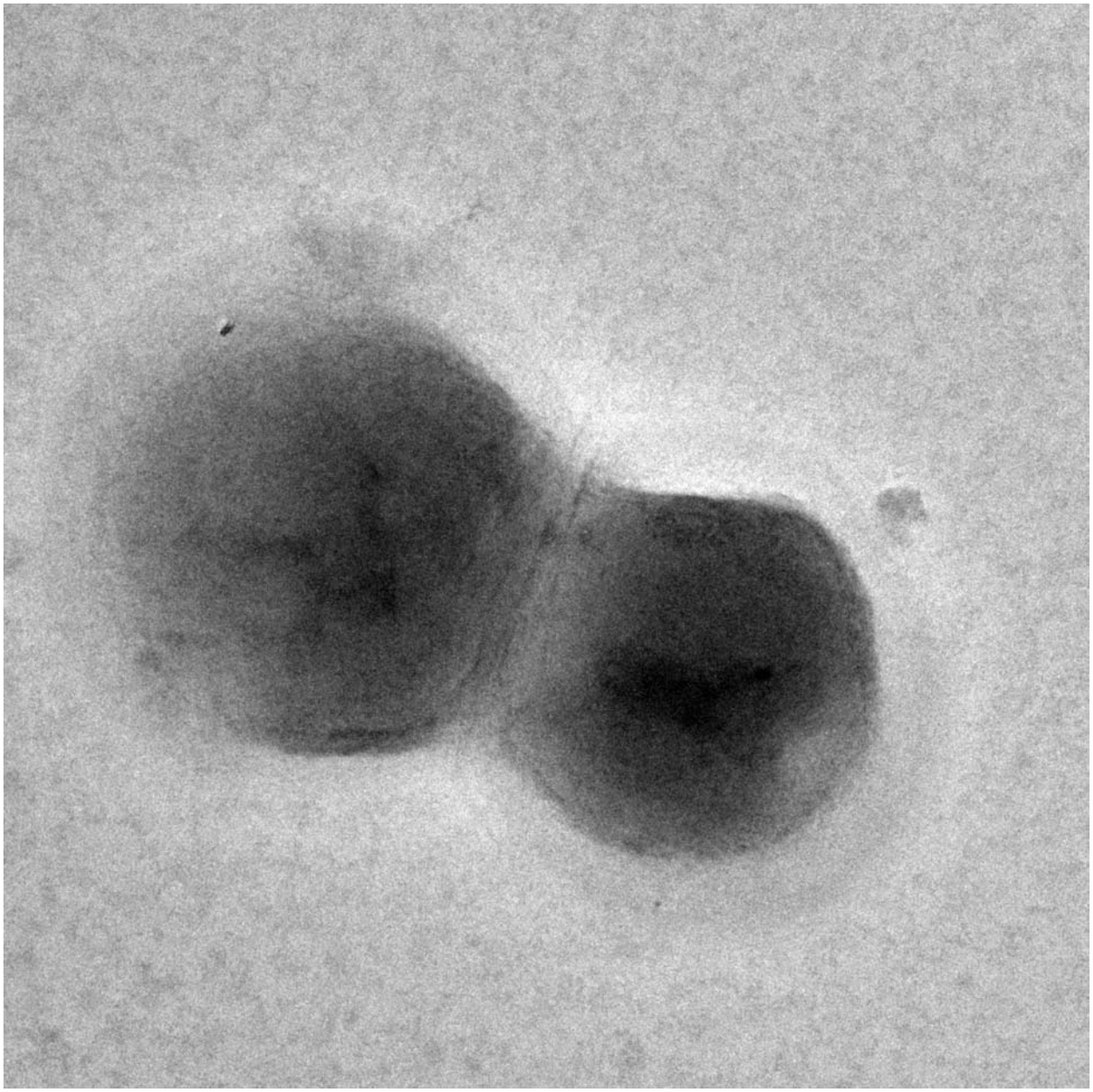

Figure D83

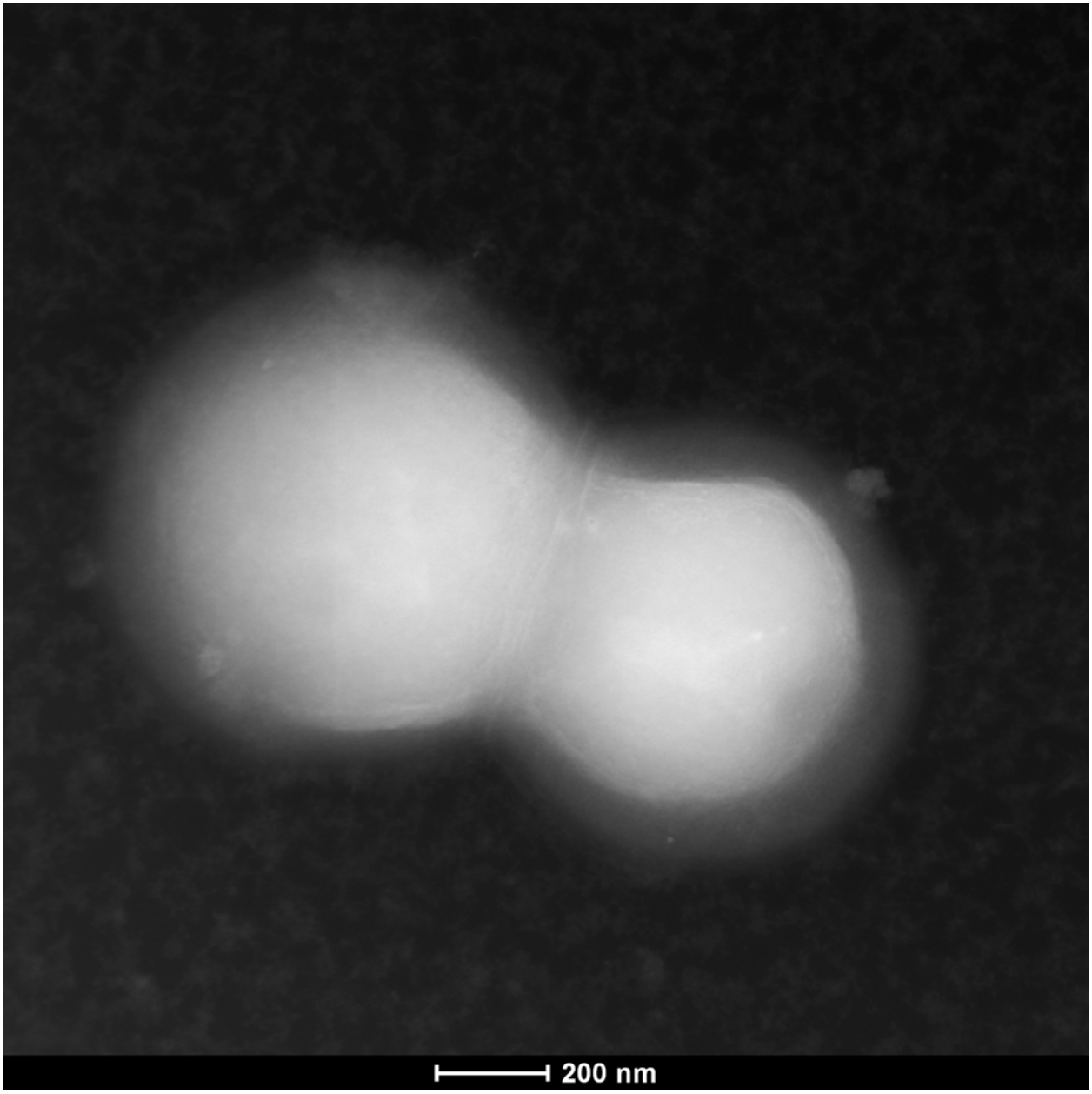

Figure D84

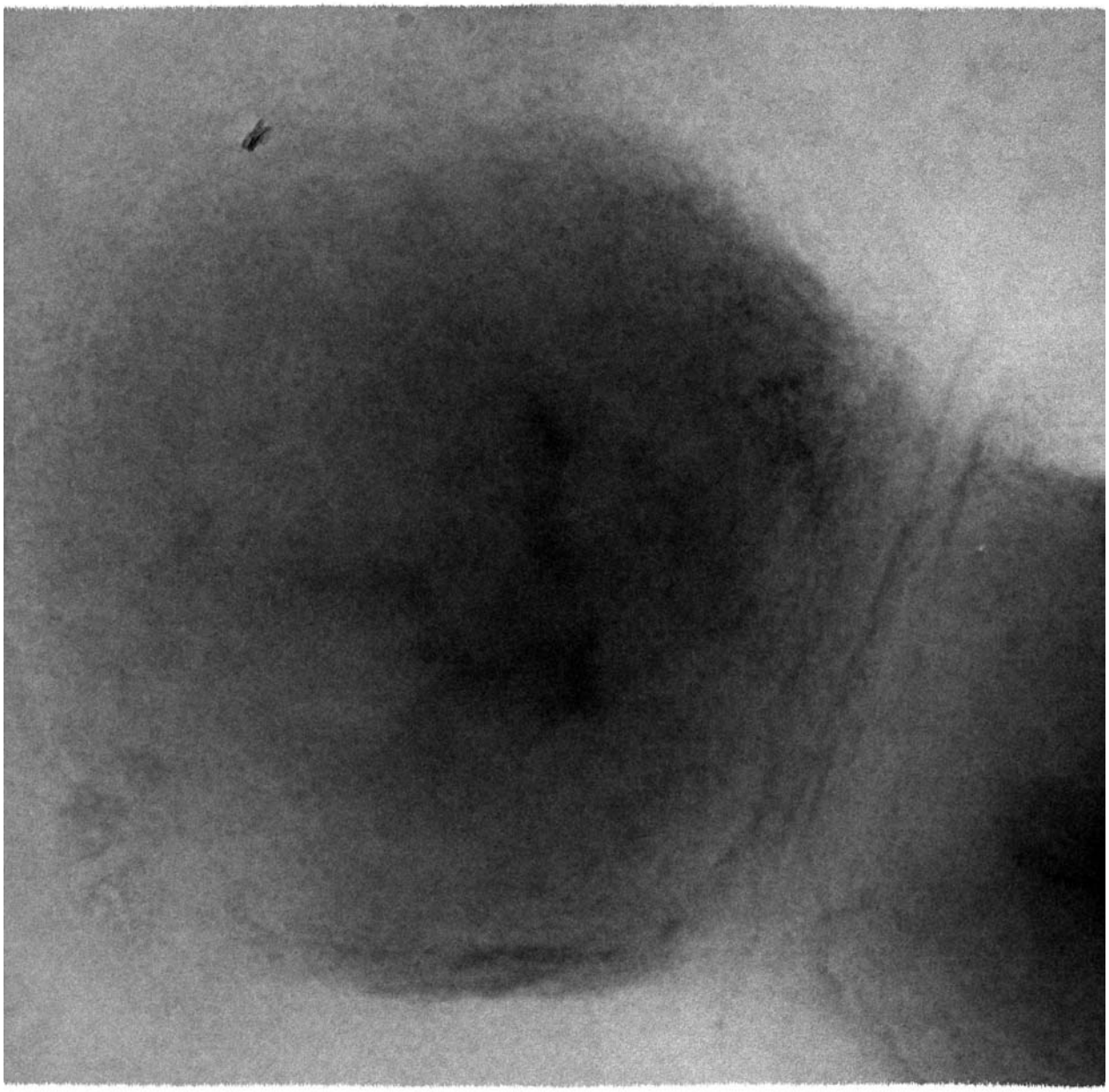

Figure D85

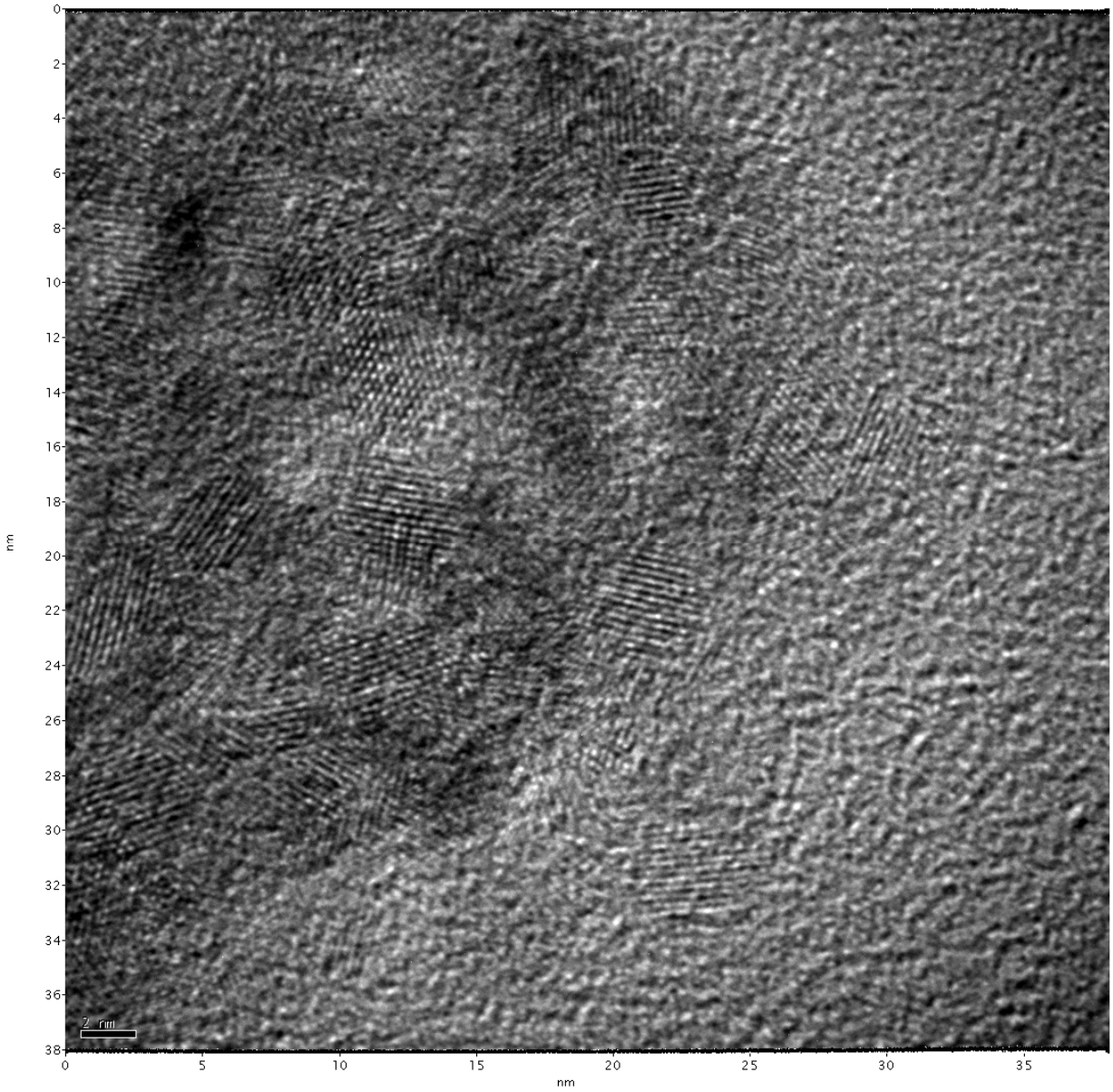
nm
0
2
4
6
8
10
12
14
16
18
20
22
24
26
28
30
32
34
36
38
2 nm
0
5
10
15
20
25
30
35
nm
Figure D86

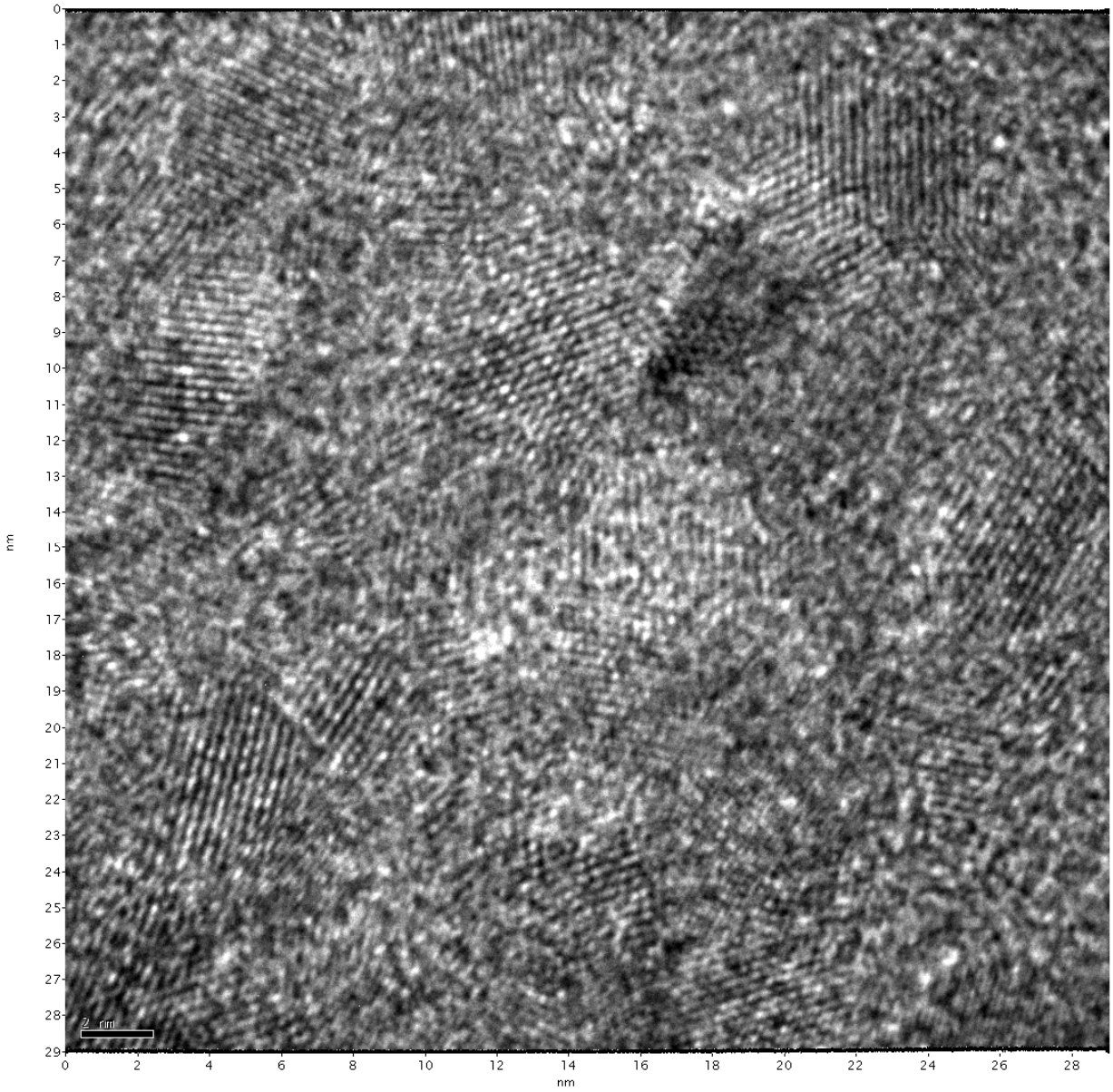

Figure D87

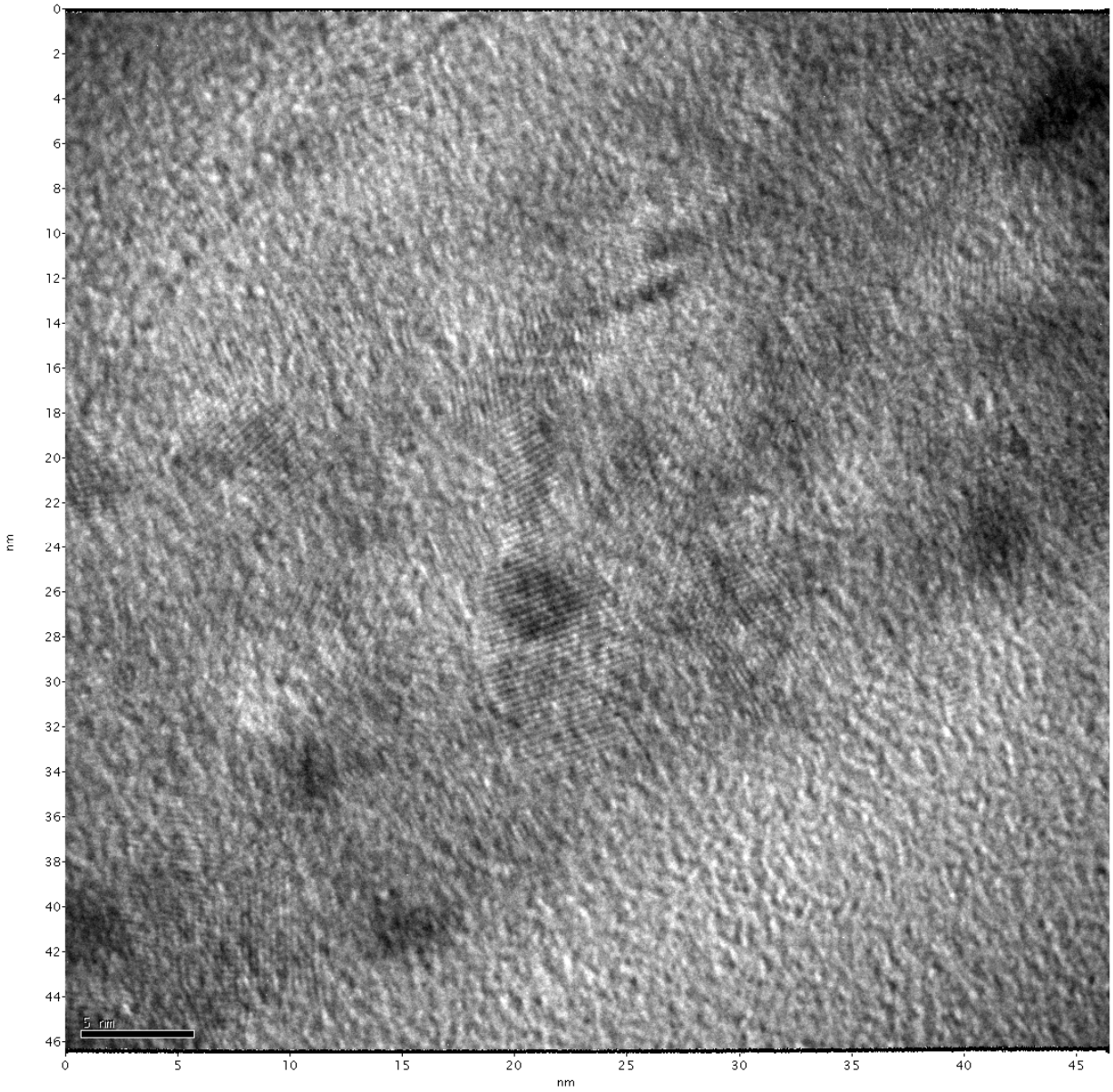
nm
0
2
4
6
8
10
12
14
16
18
20
22
24
26
28
30
32
34
36
38
40
42
44
46
5 nm
0
5
10
15
20
25
30
35
40
45
nm

Figure D88

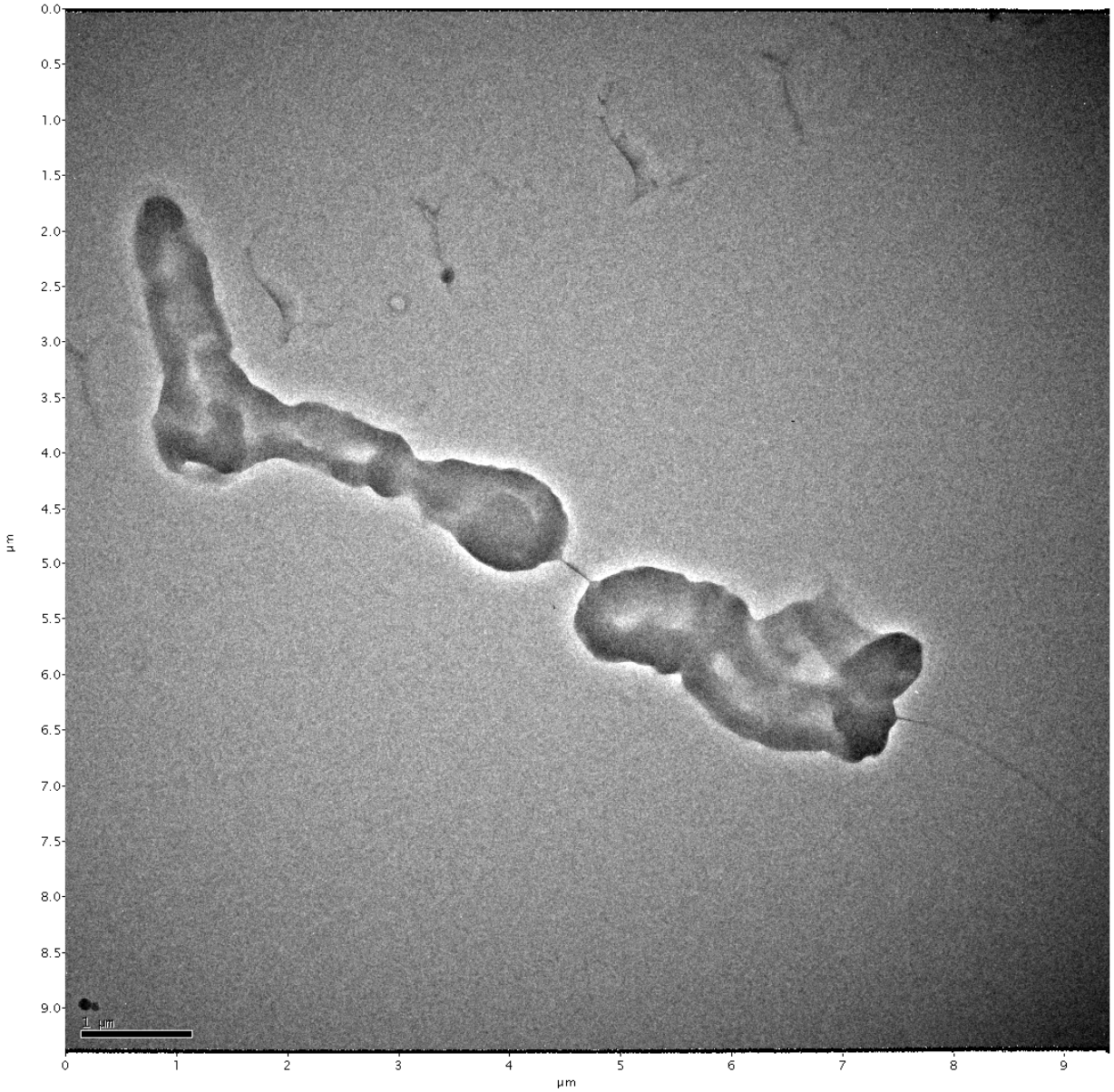
0.0
0.5
1.0
1.5
2.0
2.5
3.0
3.5
4.0
4.5
5.0
5.5
6.0
6.5
7.0
7.5
8.0
8.5
9.0
µm
1 µm
0
1
2
3
4
5
6
7
8
9
µm

Figure D89

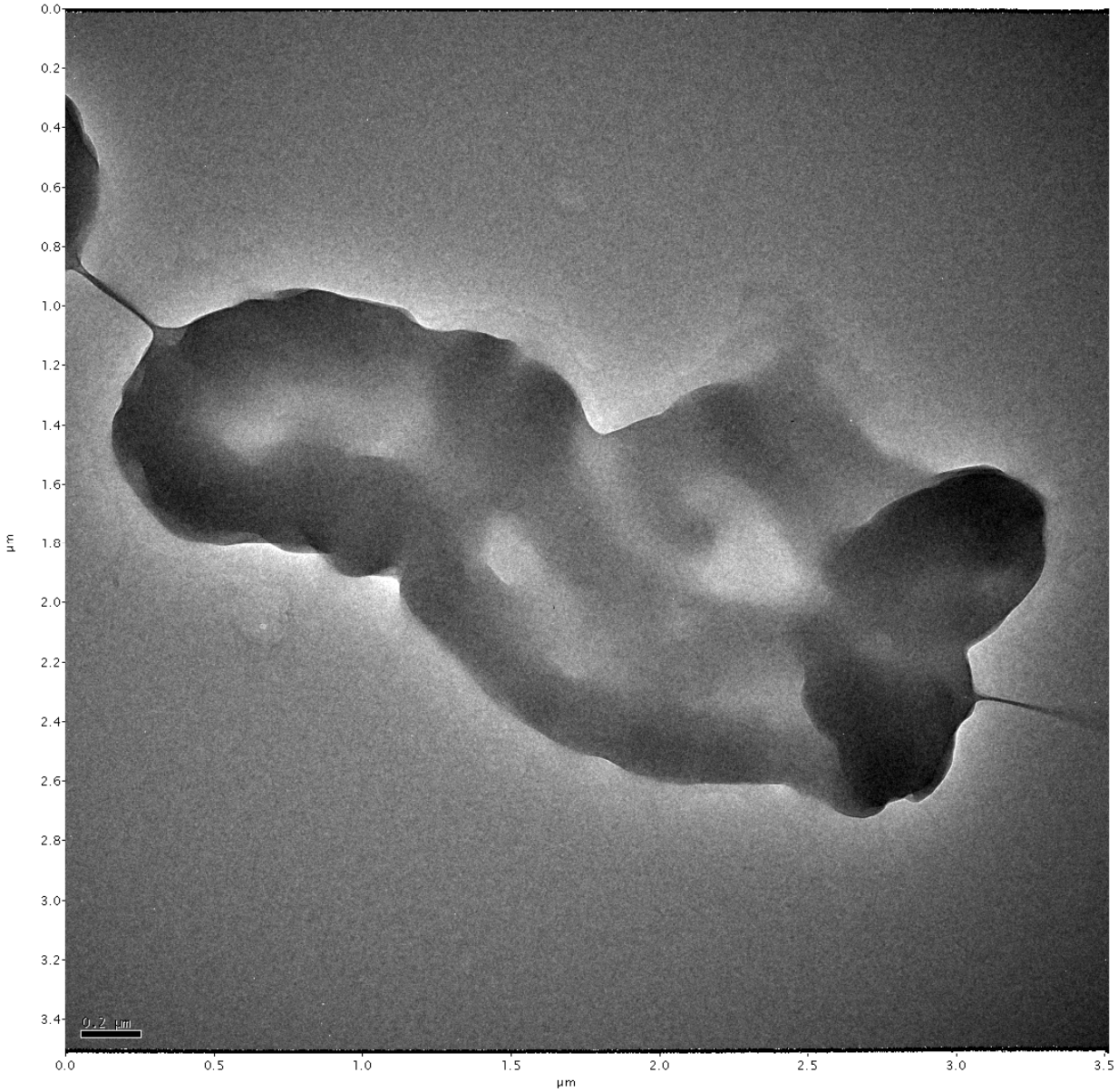
0.0
0.2
0.4
0.6
0.8
1.0
1.2
1.4
1.6
1.8
2.0
2.2
2.4
2.6
2.8
3.0
3.2
3.4
µm
0.2 µm
0.0
0.5
1.0
1.5
2.0
2.5
3.0
3.5
µm
Figure D90

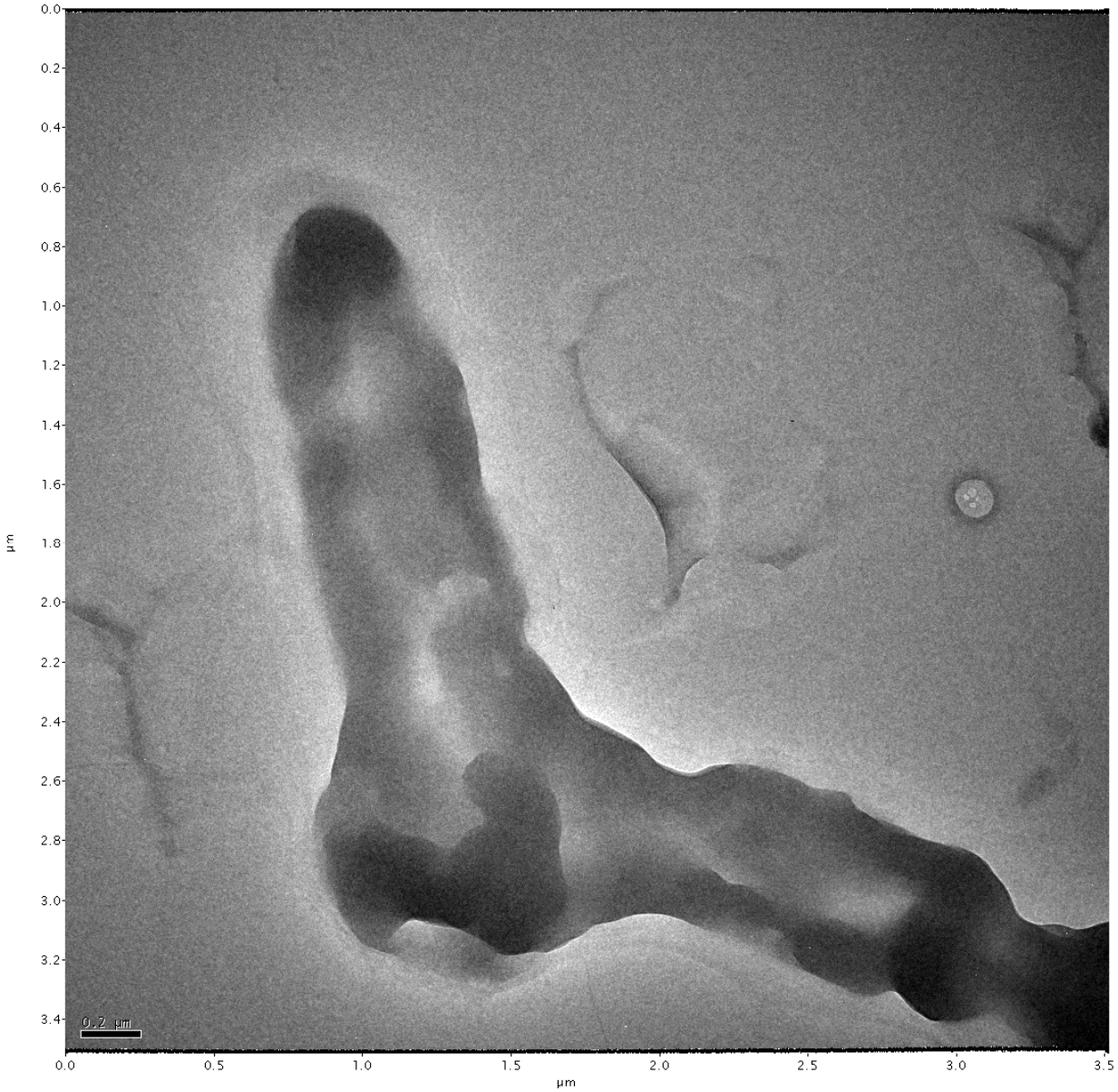
0.0
0.2
0.4
0.6
0.8
1.0
1.2
1.4
1.6
1.8
2.0
2.2
2.4
2.6
2.8
3.0
3.2
3.4
µm
0,2 µm
0.0
0.5
1.0
1.5
2.0
2.5
3.0
3.5
µm
Figure D91

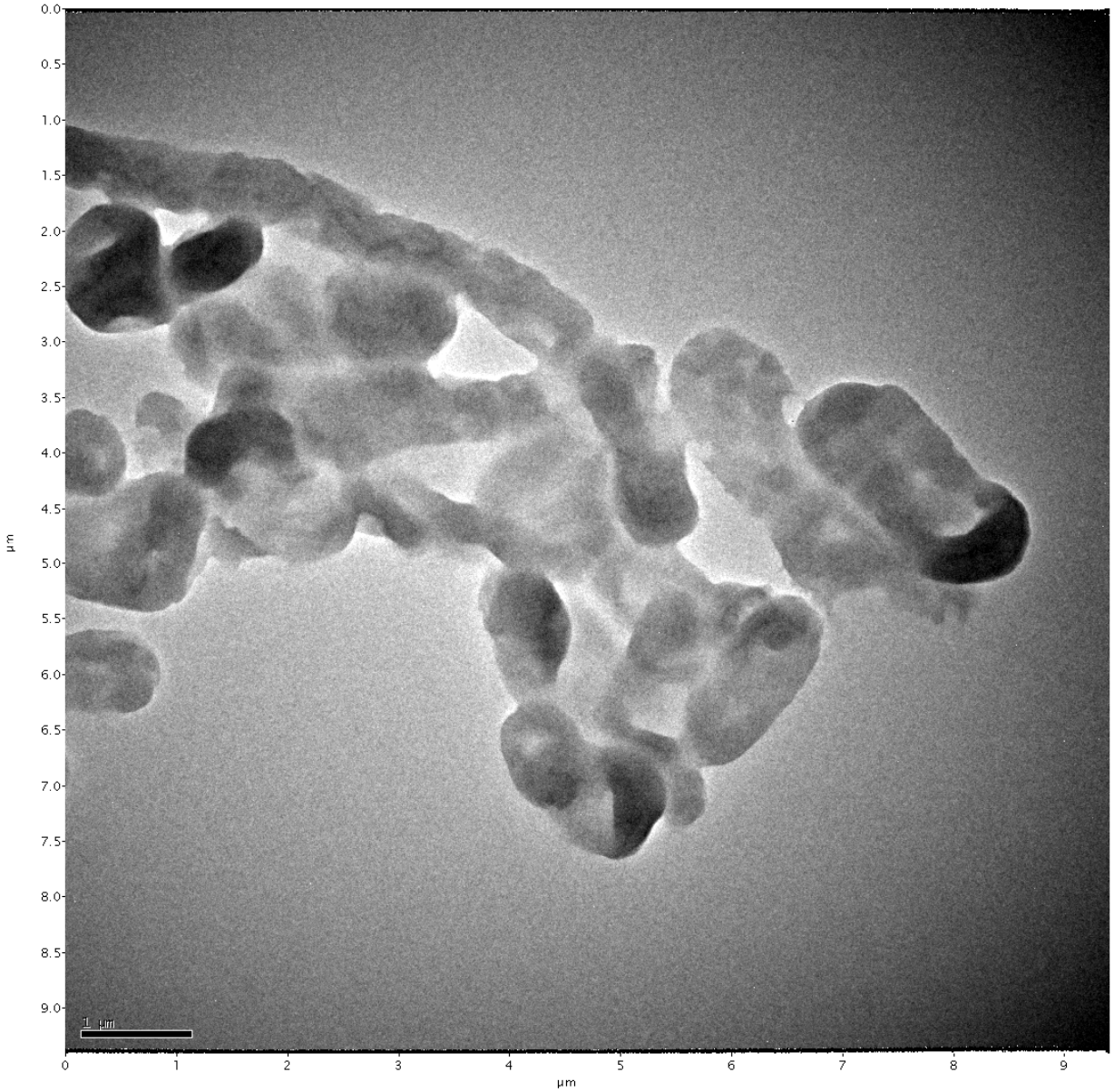
0.0
0.5
1.0
1.5
2.0
2.5
3.0
3.5
4.0
4.5
5.0
5.5
6.0
6.5
7.0
7.5
8.0
8.5
9.0
µm
1 µm
0
1
2
3
4
5
6
7
8
9
µm

Figure D92

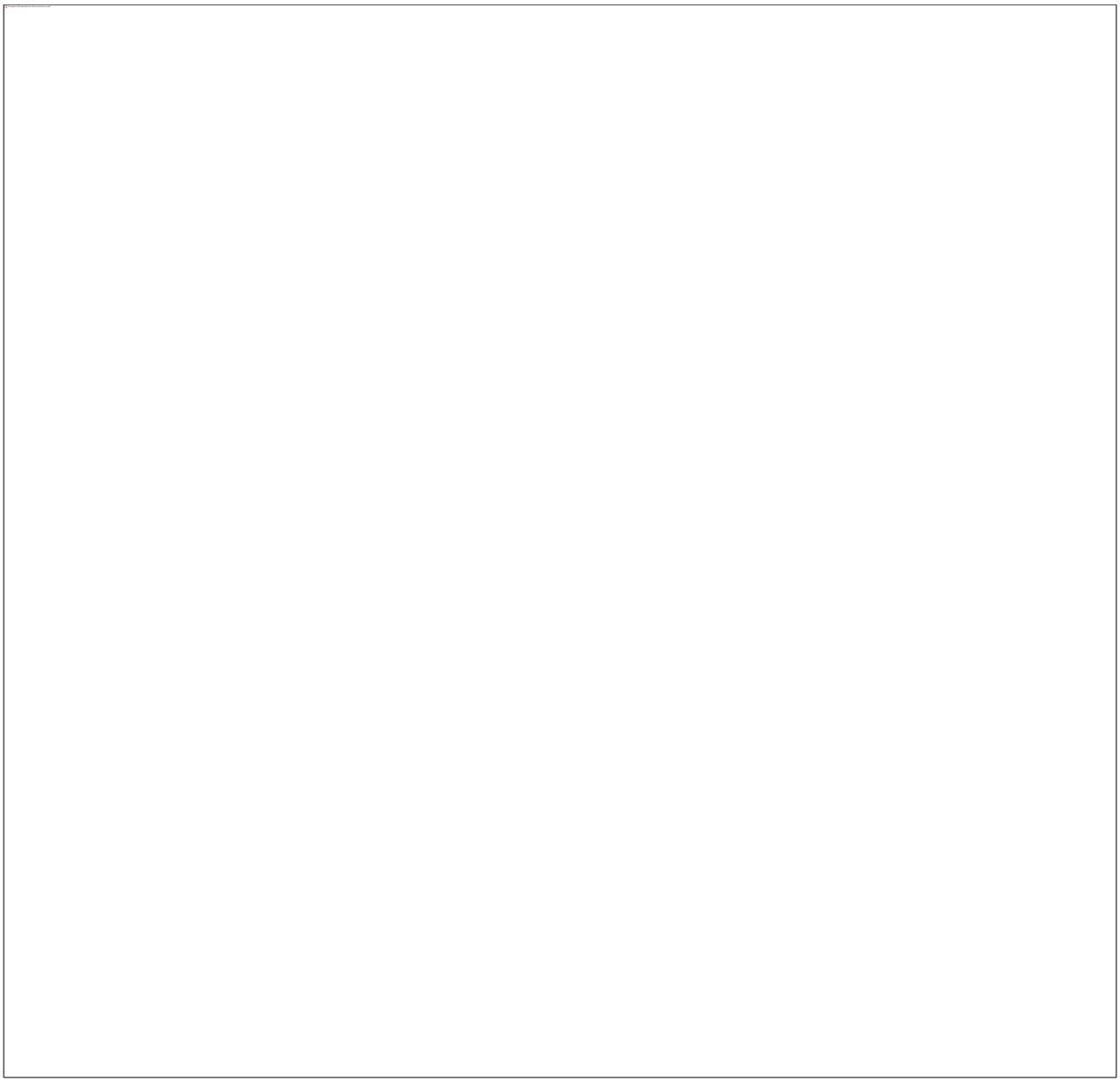

Figure D93

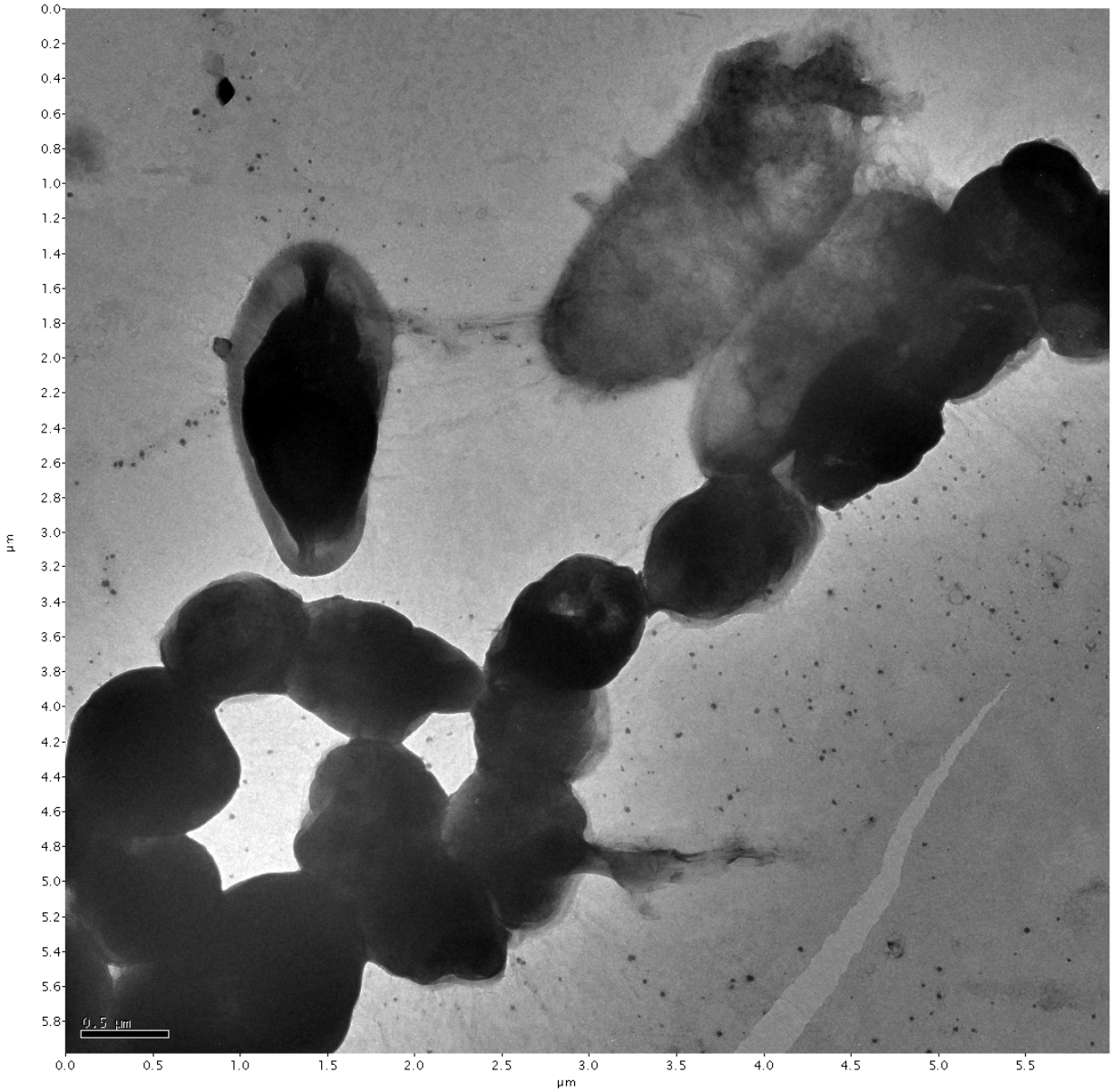

Figure D94

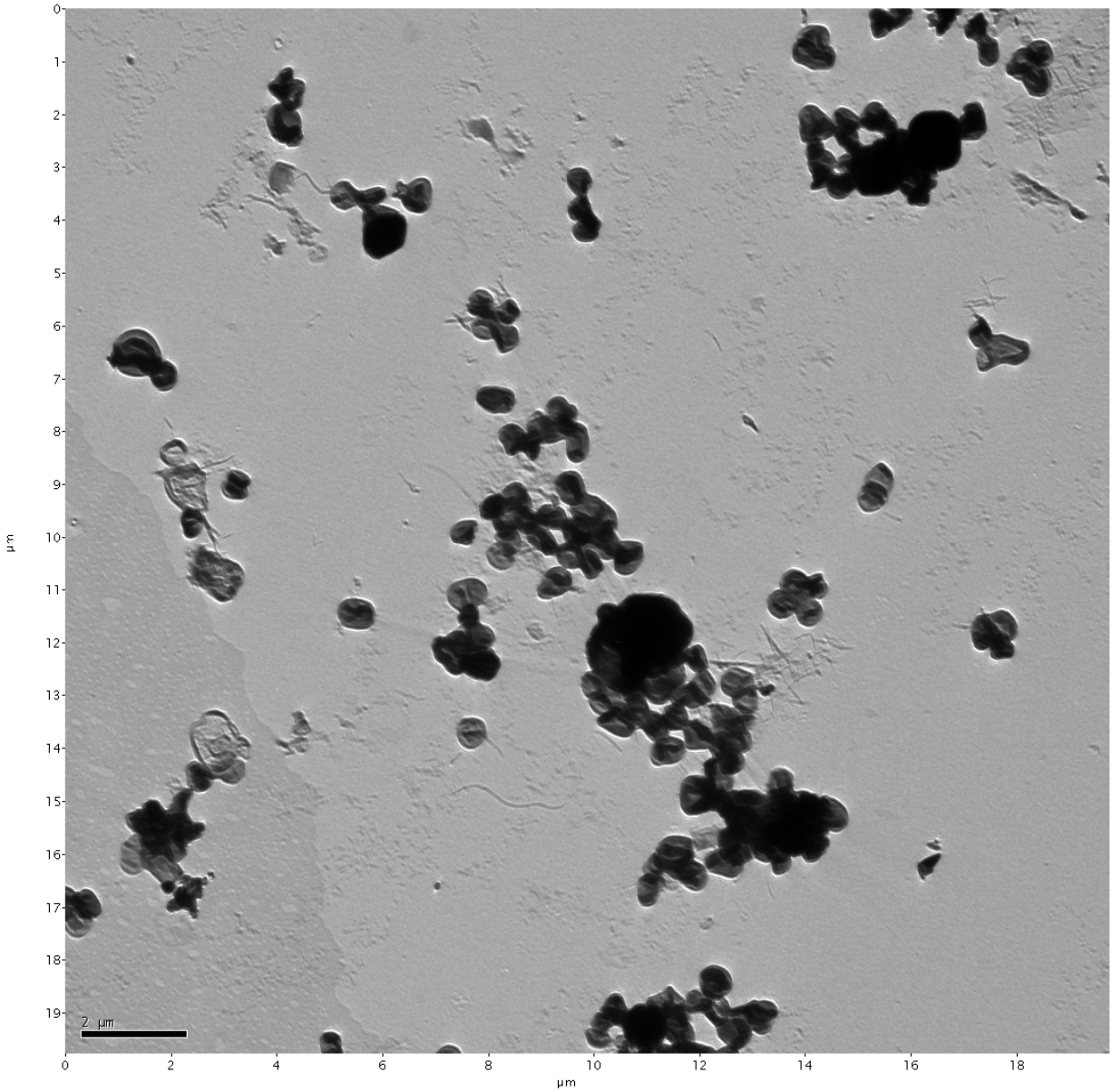

Figure D95

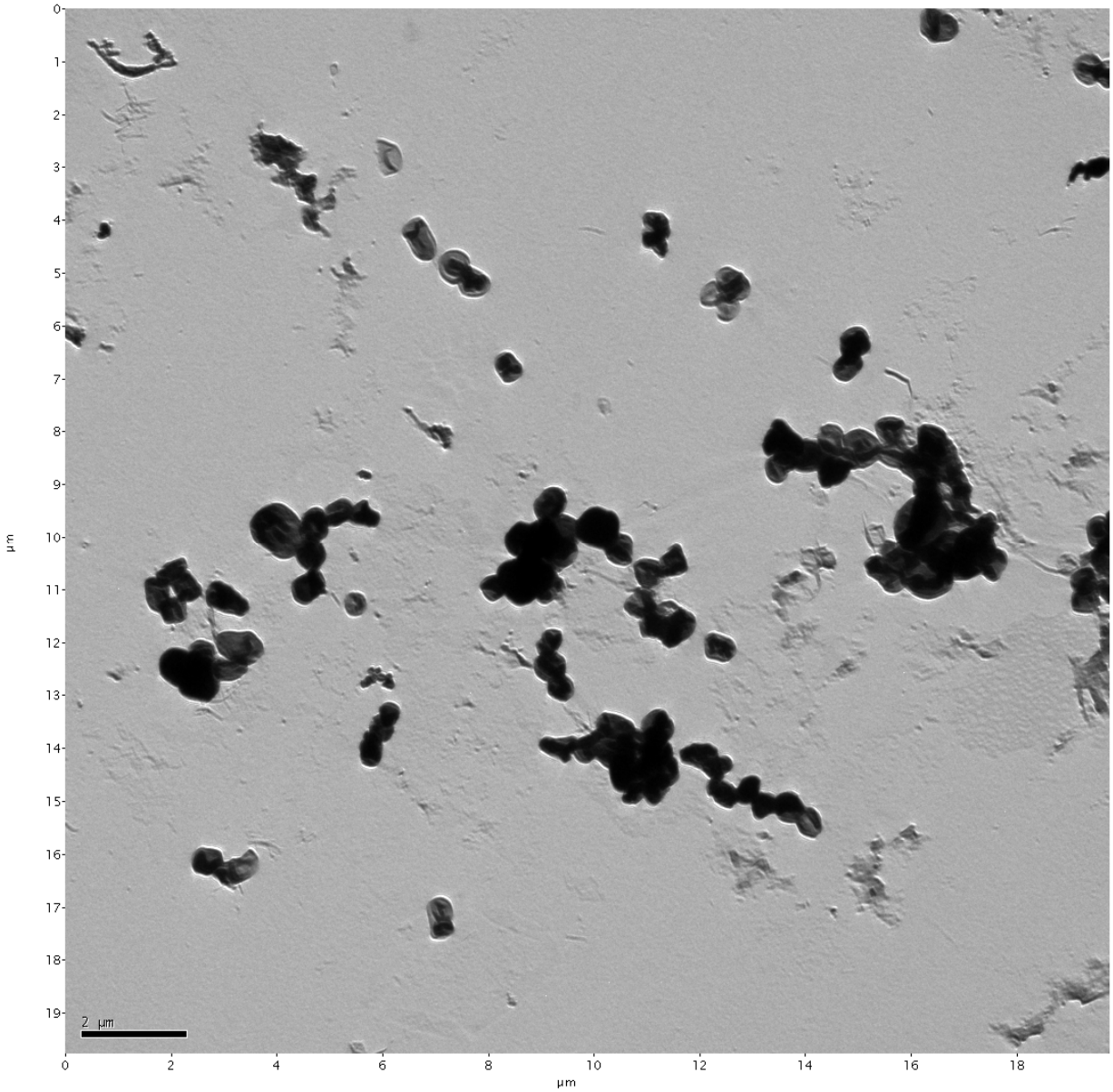

Figure D96

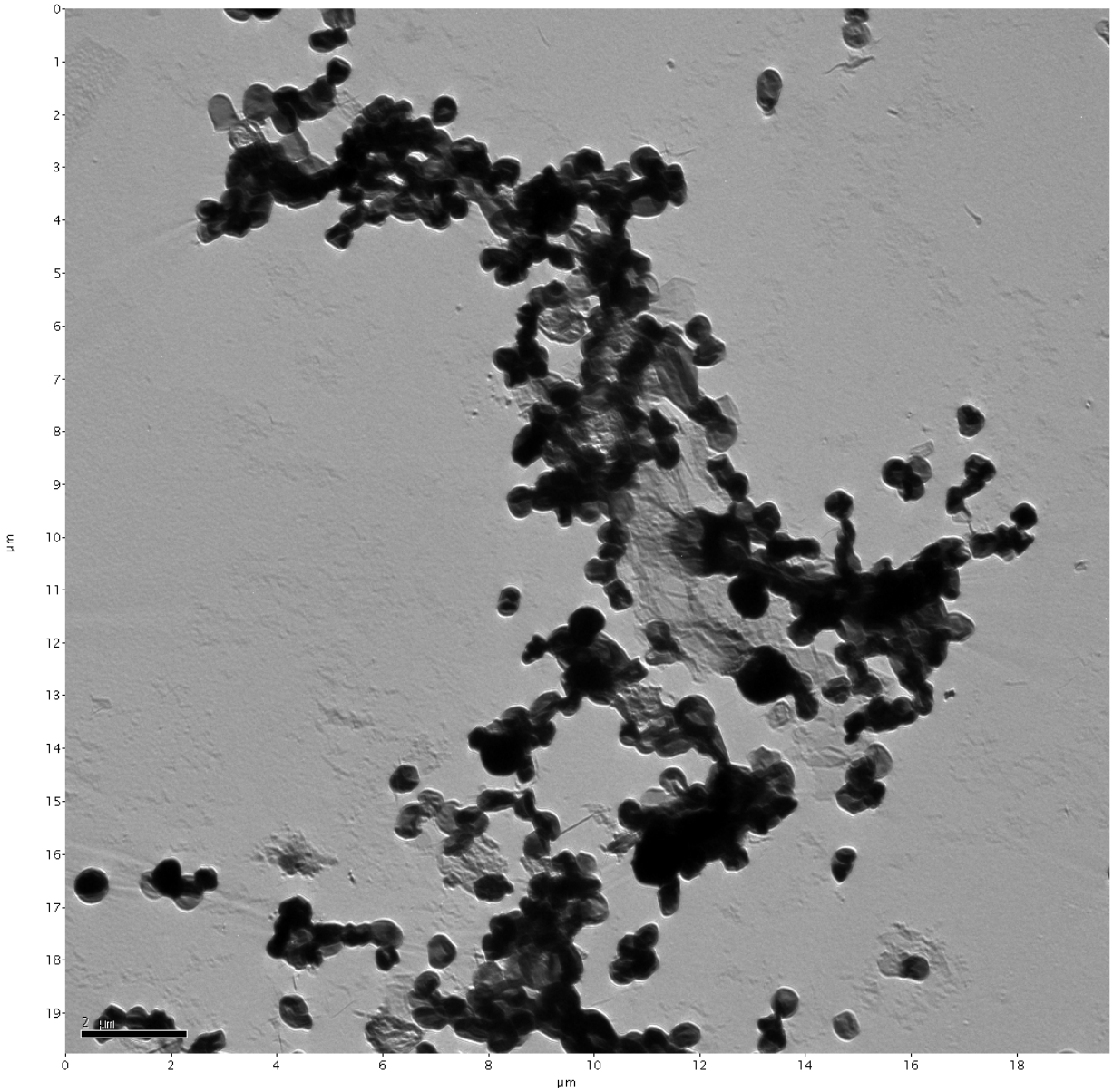
0
1
2
3
4
5
6
7
8
9
10
11
12
13
14
15
16
17
18
19
µm
2 µm
0
2
4
6
8
10
12
14
16
18
µm
Figure D97

APPENDIX E

SUPPLEMENTAL FIGURES

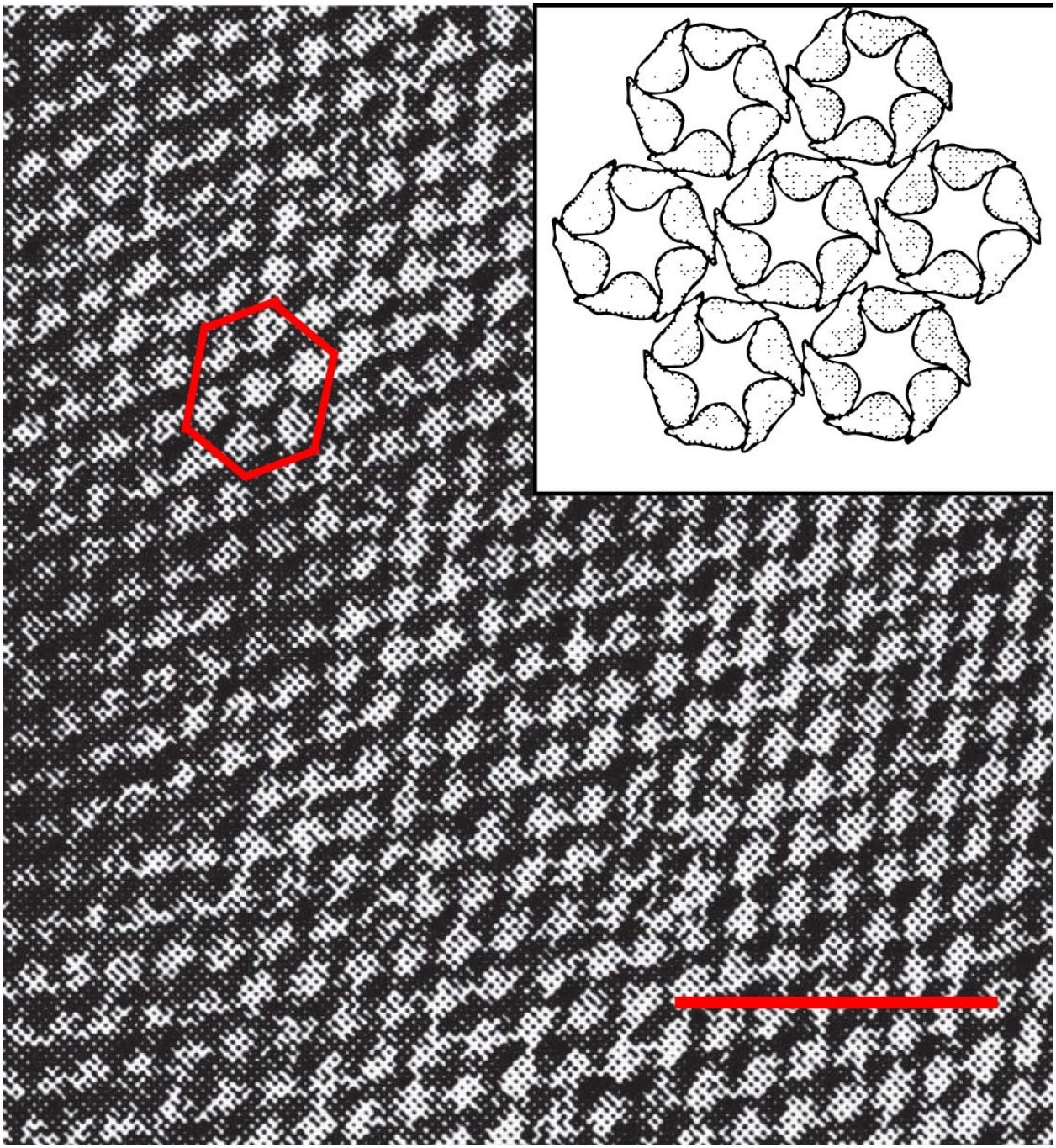

Figure E1: Transmission electron micrograph of a freeze-etched cell wall of *Thermoanaerobacter thermohydrosulfuricus* showing hexagonal (p6) symmetry (red outline and upper right inset). Scale bar is 100nm. Modifed from Sleytr et al., (1996).

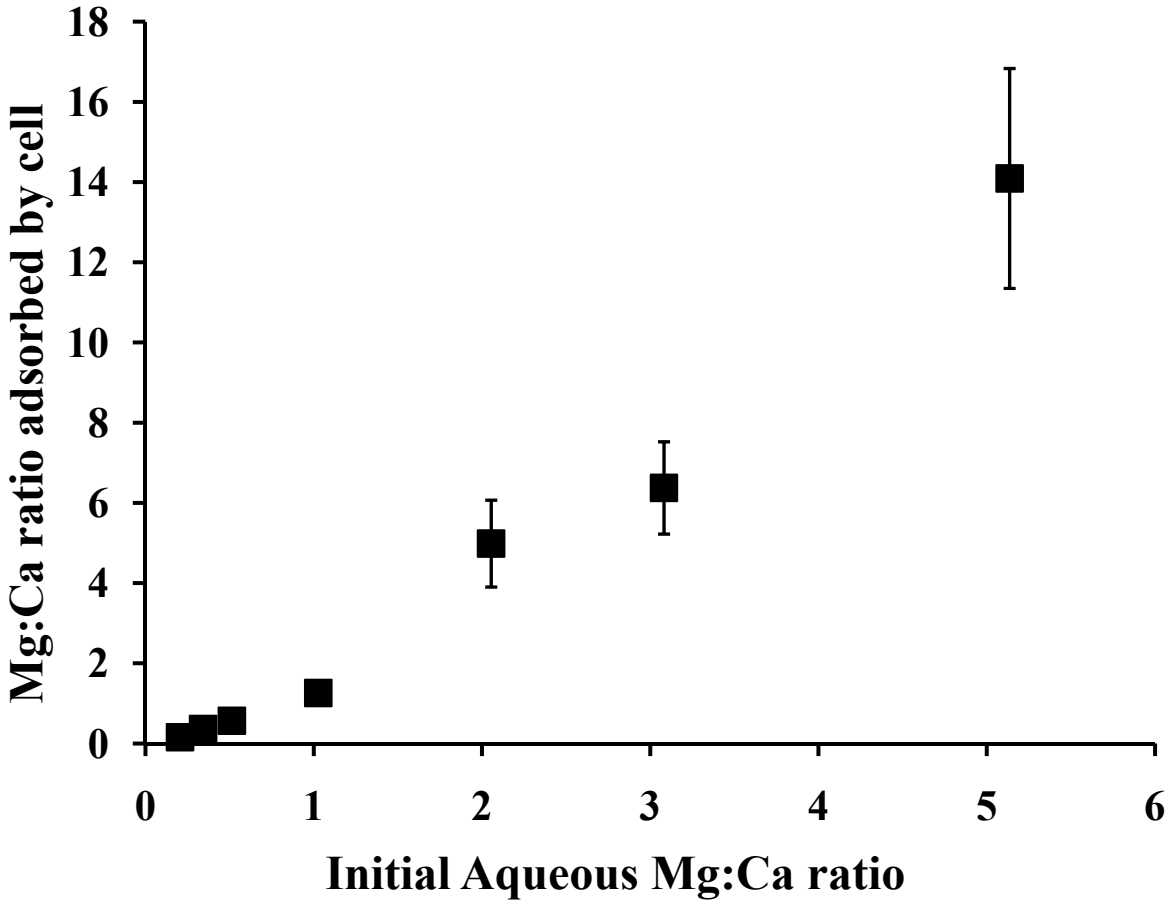

Figure E2: Ratio of Mg to Ca adsorbed to the cell surfaces of *Methanobacterium formicicum* (squares) as a function of the initial aqueous Mg:Ca ratio. Adsorption occurred over a two hour period at 25^{o}C.

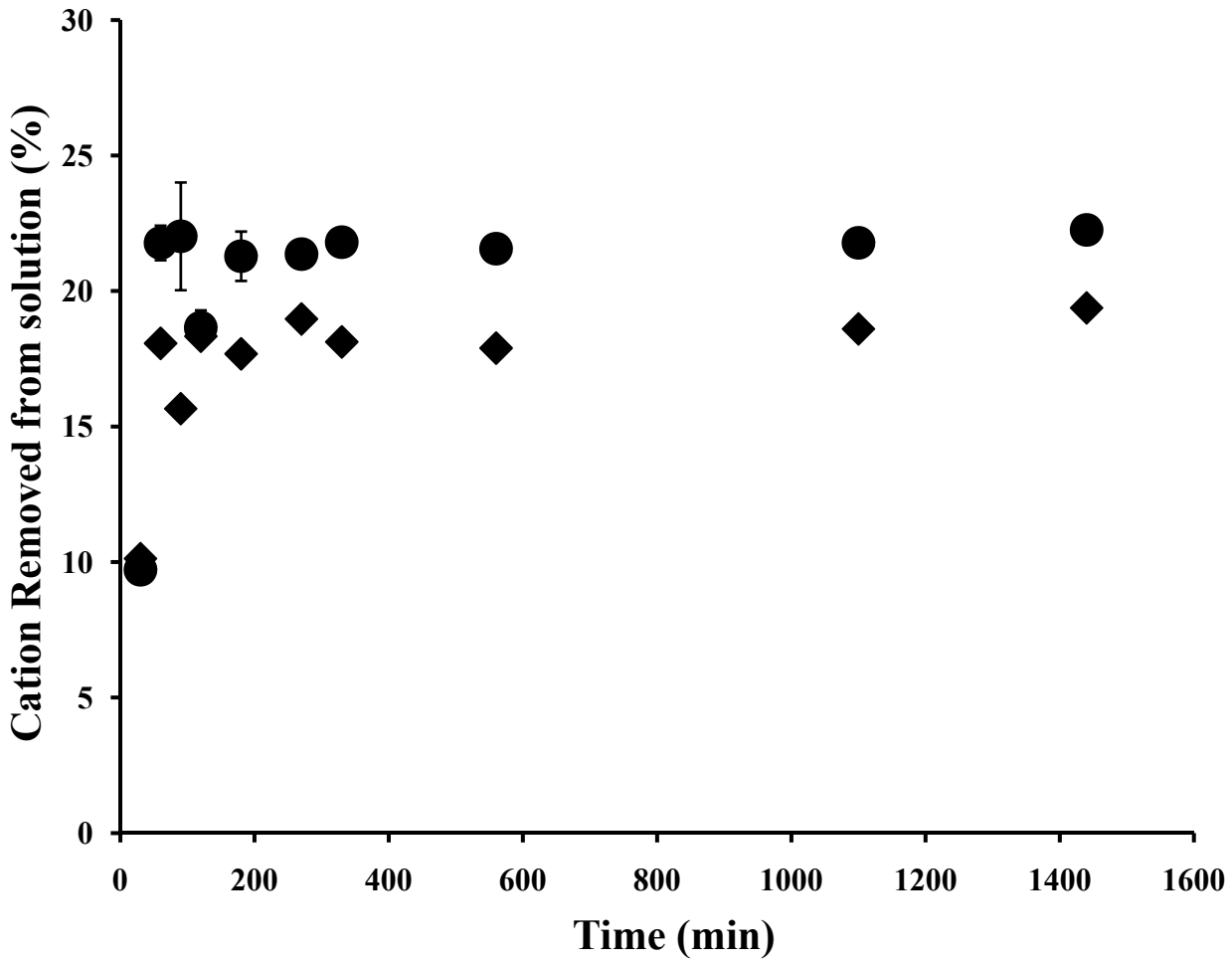

Figure E3: The percent of Mg (circles) and Ca (diamonds) adsorbed to the cell surfaces of *Methanobacterium formicicum* as a function of time. Equilibrium values were reached for both after 2 hours at 18% for calcium and 23% for magnesium.

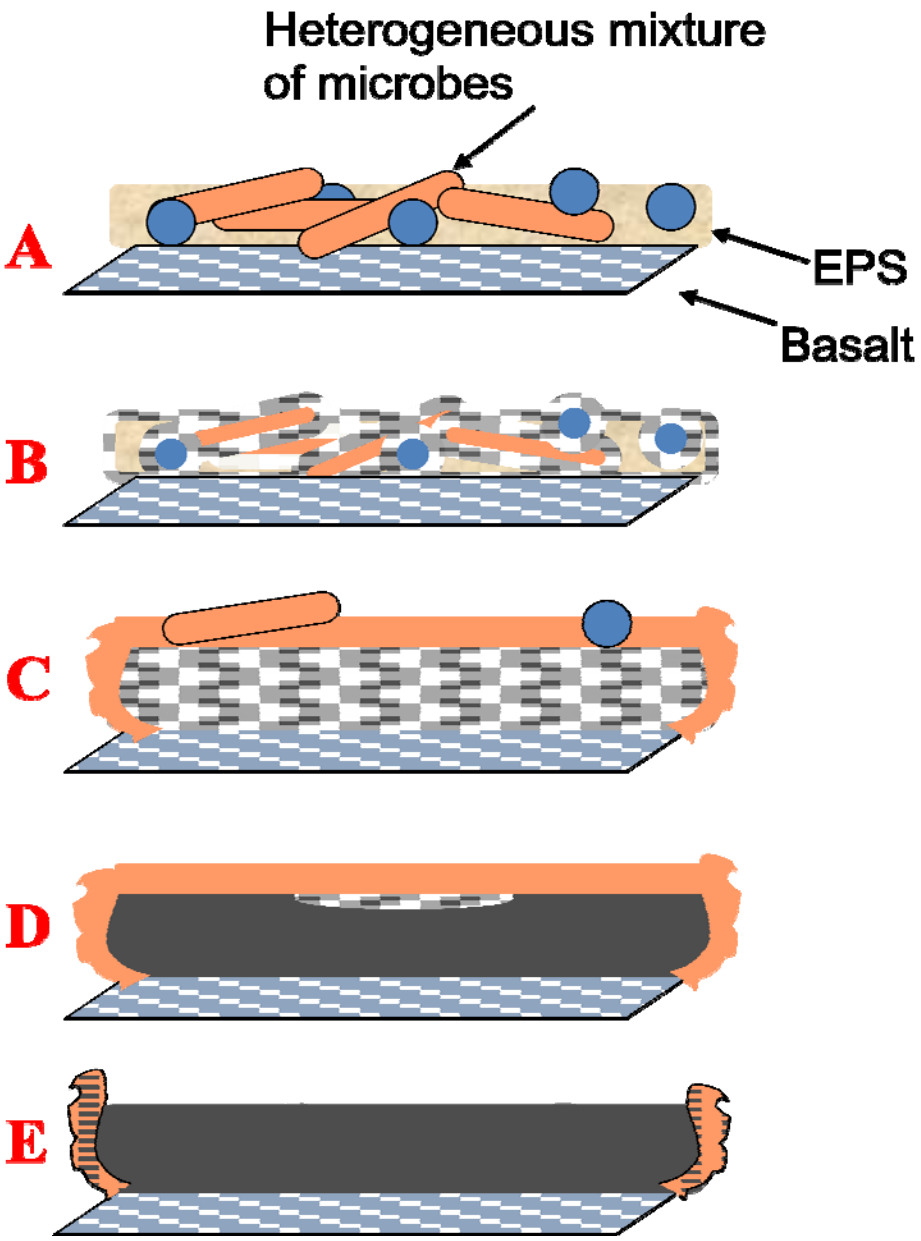

Figure E4: Sequence of events for the formation and growth of platy crystal aggregates (PCAs) developed in the reactor vessels from Kenward *et al.*, 2009. The process begins with the initial colonization of a hypothetical (2 μm in diameter) basalt grain by a consortium of fermenting bacteria and the subsequent deposition of EPS (A). This is followed by the precipitation of dolomite on organic surfaces with high carboxyl functional group densities, including cell walls and EPS (B). This proceeds to the formation of microporous dolomite and further colonization and EPS deposition coating the microporous dolomite (C). The final phase is the ripening step which leads to the formation of thin rhombohedra of dolomite which grow together to form PCAs. The last image (E) is what these surfaces look like after desiccation during preservation for SEM, when the EPS has retracted to the edges of the mineral.